Geochemistry of selected South African group I, group II and transitional kimberlites located on and off the Kaapvaal craton

Megan Coetzee

Thesis submitted in fulfilment of the requirements for the degree of Master of Science

Department of Geological Sciences
University of Cape Town
November 2004

ABSTRACT

Eighteen Jurassic to Cretaceous South African kimberlites representative of group I, group II and transitional varieties that have been emplaced through both the Archean Kaapvaal craton (on-craton) and Proterozoic Namaqua-Natal belt (off-craton), have been selected for a comparative study aimed at characterising their geochemistry and source region compositions, as well as understanding the petrogenetic processes that have affected them.

The petrography of the analysed kimberlites is similar to typical group I and group II kimberlites, characterised by deformed and anhedral olivine and phlogopite macrocrysts, with more subhedral to euhedral olivine and phlogopite phenocrysts and microphenocrysts, set in a groundmass of mostly serpentine, calcite and phlogopite (group I kimberlites), or calcite, serpentine, phlogopite and diopside (group II kimberlites). The transitional kimberlites tend to show intermediate characteristics, with the on- and off-craton transitional kimberlites showing more similarity to group I and group II kimberlites, respectively.

Bulk-rock geochemical analyses of hypabyssal kimberlite samples reveal some systematic differences between kimberlite varieties; MgO content and Mg-numbers between kimberlites tend to be comparable, although SiO_2 and K_2O contents are higher and TiO_2 concentrations lower in group II kimberlites, compared to group I kimberlites. SiO_2 and MgO concentrations of transitional kimberlites span the ranges for group I and group II kimberlites, but TiO_2 and K_2O contents tend to be intermediate. Off-craton group I kimberlites tend to lower SiO_2 and MgO but higher FeO*, TiO_2, CaO and CO_2 than their on-craton counterparts, although still broadly falling within the on-craton group I kimberlite field. These varied characteristics between on and off-craton group I kimberlites are argued to be controlled by the refractory nature of kimberlite source regions, as well as the depth/pressure of partial melting. No systematic geochemical differences have been identified between on- and off-craton group II kimberlites, whereas for the transitional kimberlite group on and off-craton transitional kimberlites have more in common with group I and group II kimberlites, respectively.

All kimberlite varieties are enriched in both the compatible (e.g. Ni, Cr) and incompatible trace elements (e.g. Th, Nb, REE), with the group II kimberlites tending to higher Rb, Ba and Pb, but having distinctively lower Nb and Ta than group I and transitional kimberlites. Chondrite normalised REE profiles are steep with very enriched light REE and only moderately enriched heavy REE contents. Light REE patterns of group II and transitional kimberlites also tend to be steeper (higher La/Sm) and heavy REE patterns flatter (lower Gd/Yb), than for group I kimberlites. Superimposed upon the relatively smooth, yet steep primitive mantle normalised patterns of kimberlites are distinct negative Rb, K, and Ti, and more subdued negative Sr and Hf, as well as Nb (group II kimberlites) anomalies,

that vary in magnitude between kimberlite groups and are argued to be unrelated to alteration or crystal fractionation processes.

The analysed group I kimberlites are characterised by radiogenic $^{143}Nd/^{144}Nd$ and unradiogenic $^{87}Sr/^{86}Sr$ ratios, whereas group II kimberlites have unradiogenic $^{143}Nd/^{144}Nd$, but radiogenic $^{87}Sr/^{86}Sr$. Transitional kimberlites are characterised by intermediate ratios and provide a continuum to the kimberlite isotope array, with the on-craton kimberlites showing more similarity to group I kimberlites, in contrast to their off-craton counterparts that are more similar to group II kimberlites. In addition to these intermediate isotopic characteristics, other major elements (e.g. K_2O, TiO_2) and trace element ratios (e.g. La/Nb, Ba/Nb, Th/Nb) suggest that the transitional kimberlites are derived from mixed group I and group II kimberlite source regions.

The bulk-rock geochemistry of the analysed kimberlites is highly variable and may be affected by alteration, crustal contamination, macrocryst entrainment and fractional crystallisation, but by careful evaluation the effects of these processes on kimberlite geochemistry can be recognised, and where necessary, corrected. Consequently, close-to-primary magma compositions have been constrained for virtually every kimberlite. Group I kimberlites have Mg-numbers = 0.82-0.87, ~22-27 wt% MgO , ~21-30 wt% SiO_2, ~10-17 wt% CaO, ~0.2-1.7 wt% K_2O and ~660-1190ppm Ni. Close-to-primary magmas of group II kimberlites have Mg-numbers = 0.86-0.89, ~23-29 wt% MgO, ~28-36 wt% SiO_2, ~0.9-1.4 wt% TiO_2, ~590-1410ppm Ni and ~1560-2290ppm Cr.

Compositions of source regions in equilibrium with close-to-primary group I and group II kimberlites have been calculated by using equations for non-modal batch melting and assuming low degrees of partial melting (F = 1%) of a metasomatised garnet lherzolite. Varying REE ratios indicate that the residual mineralogy differs between group I and group II kimberlites, with the sources of the latter being more highly metasomatised, having more residual clinopyroxene and less residual garnet than the former. Predicted source region compositions are more enriched in the light REE than the heavy REE relative to chondrite ($(La/Sm)_N$ = 2.3-7.0; $(La/Yb)_N$ = 1.9-28). Residual accessory phases (e.g. phlogopite) are argued to be absent during partial melting and therefore characteristic trace element anomalies on primitive mantle normalised patterns of close-to-primary kimberlites, appear to be intrinsic features inherited from their source regions.

High Mg-numbers and compatible trace element contents, as well as fractionated heavy REE patterns indicate kimberlites are derived from previously melt-depleted sources, postulated to be located within the subcontinental lithospheric mantle. Source regions are also characterised by subsequent metasomatic enrichment in the light REE and other highly incompatible elements, but the timing, nature and extent of enrichment are the key differences between group I and group II kimberlites. The similarity of isotope ratios ($^{87}Sr/^{86}Sr$, εNd) and diagnostic trace element ratios (Ce/Pb, Nb/U, La/Nb, Ba/Nb) of group I kimberlites to ocean island basalts, as well as Nd model ages indicative of recent enrichment (T_{Nd} = 0 - 700Ma), are consistent with the sources of group I kimberlites being enriched by

asthenospheric melts/fluids associated with the passage of a mantle plume/s beneath southern Africa during the Mesozoic. In contrast, diagnostic trace element ratios of both on- and off-craton group II kimberlites are unlike group I kimberlites or ocean island basalts, but show more similarity to calc-alkaline basalts, particularly in their Nb and Ta depletion. It is suggested that both the Archean and Proterozoic lithospheric sources of group II kimberlites have been metasomatised by melts/fluids associated with subduction, and that metasomatism of the source regions is unrelated to any mantle plume upwelling. However, the mantle plumes beneath southern Africa during the Mesozoic, may have contributed a heat source for partial melting and group II kimberlite production. Group II kimberlites are also characterised by time integrated Rb/Sr and Sm/Nd ratios indicative of more ancient enrichment (T_{Nd} = 600-1300Ma). Minimum Nd model ages indicate that the sources of group II kimberlites were likely enriched prior to Mesozoic Gondwana break-up and after the formation of the Proterozoic mantle beneath the Namaqua and Natal belts. It is therefore possible that the source regions of group II kimberlites may have been enriched by melts/fluids associated with multiple subduction and accretion events during the Kibaren Namaqua-Natal orogeny, that percolated upwards and metasomatised both Proterozoic and Archean kimberlite source regions.

DECLARATION

I hereby declare that all the work presented in this thesis is my own,
and where work has been obtained from others,
it has been appropriately cited in the text.

Megan Coetzee
November 2004

ACKNOWLEDGMENTS

First and foremost, I would like to thank my supervisor, Professor Anton le Roex, not only for the opportunity to embark on this thesis, but also for the encouragement, guidance and patience he has shown over the last two years. Thank you too, for always being willing to listen.

My thanks go to John Gurney for opening the door of kimberlites and mantle petrology to me and I am grateful for the opportunities this has brought. In addition, thank you for making samples from the UCT mantle room available for study. I am also appreciative to Jock Robey for time spent in the field and for arranging the chance for me to visit the Kimberley kimberlites.

At UCT, there are many people who have assisted me in preparing samples for analysis, collecting geochemical data and solving technical problems. Thank you to Dave Reid, Steve Richardson, Andreas Späth, Shireen Govender, Terry Davies, Fayrooza Rawoot, Ernest Stout, David Wilson, Robert Oliver, Ivan Wilson and Peter Meyer. I am appreciative to my fellow postgraduate students at UCT who have provided support and friendship. Thank you Nancy, for being around to discuss kimberlites with and Rochelle, for being willing to read a draft of my thesis.

I am indebted to the National Research Foundation and De Beers for providing funding for this thesis and also to De Beers for sending me some of their kimberlite samples. I am also grateful to the 7th International Kimberlite Conference Committee, for sponsoring my trip to attend the 8th International Kimberlite Conference in Canada. It was a wonderful opportunity and served to spark my enthusiasm for kimberlite research.

Thank you also to my friends and family, who have encouraged me and displayed a constant interest in my work. Lastly, to my husband Gavin, I am sincerely grateful not only for the sacrifices you have had to make, but also for the love and devotion you have shown.

TABLE OF CONTENTS

LIST OF TABLES AND FIGURES

List of figures

List of tables

CHAPTER I

INTRODUCTION

1.1 Definition and classification of kimberlite

Ever since the discovery over a century ago that kimberlite is the host rock to diamonds (Bonney, 1899), this volumetrically insignificant alkaline rock type has received an abundance of attention in unraveling the wealth of information that it carries. Valuable studies have been performed on the kimberlites themselves (e.g. le Roex *et al.*, 2003; Tainton & McKenzie, 1994; Fraser & Hawkesworth, 1992; Smith, 1983a; Clement, 1982; Allsopp & Barrett, 1975; Wagner, 1914), as well as on the suite of mantle peridotites, eclogites, megacrysts, diamonds and crustal xenoliths that they may entrain (e.g. Schmitz & Bowring, 2004; Hops *et al.*, 1992; Gurney, 1990; Richardson *et al.*, 1984; Hatton, 1978; Boyd, 1973), and have contributed to the understanding of the evolution of the underlying crust and mantle.

Wagner (1914) first recognised the existence of two petrographic types of kimberlite in southern Africa, namely basaltic and lamprophyric (micaceous) kimberlite, according to the relative abundance of mica phenocrysts present. Subsequently, Smith (1983a) demonstrated that these two broad distinctions of kimberlite could be classified according to their Sr, Nd and Pb isotopes. Group I kimberlites (basaltic) are slightly depleted relative to present day Bulk Earth, show similarity to ocean island basalts (OIB) and have been associated with a sublithospheric source (Smith, 1983a). Group II kimberlites (micaceous), are relatively enriched with radiogenic $^{87}Sr/^{86}Sr$ ratios and unradiogenic $^{143}Nd/^{144}Nd$ ratios, that require ancient enriched sources with high Rb/Sr and Nd/Sm, and have been associated with the subcontinental lithospheric mantle (Coe, 2004; Tainton, 1992; Fraser & Hawkesworth, 1992; Smith, 1983a). A third, minor transitional group of kimberlites has also been recognised, which has isotopic and petrographic characteristics intermediate to group I and group II kimberlites (Clark, 1994; Skinner *et al.*, 1992; Skinner, 1989).

Although the classification of kimberlite varieties into groups based on isotopic characteristics is relatively simple, the classification and definition of kimberlite groups according to petrographic characteristics is more debatable. Following the widely quoted definition of Clement *et al.* (1984), subsequent revisions have been made (e.g. Woolley *et al.*, 1996) and currently, two separate I.U.G.S. characterisations exist for group I and group II kimberlites (le Maitre, 2002). Some key aspects of the I.U.G.S. characterisation of group I kimberlites are (le Maitre, 2002):

i). Group I kimberlites are ultrabasic, potassic, volatile-rich (mostly CO_2) igneous rocks.

ii). Group I kimberlites are typically inequigranular in texture, due to the presence of macrocrysts set in a finer grained matrix.

iii). Serpentinisation and carbonatisation reactions may have affected the kimberlite.

iv). Kimberlites may entrain mantle xenoliths and xenocrysts as well as crustal xenoliths.

Many similarities exist between the characterisations of group I and group II kimberlites, but there are also a few crucial differences since group II kimberlites (also known as "orangeites"; Mitchell, 1995) show some features similar to lamproites (le Maitre, 2002; Tainton, 1992). Some of the essential differences recognised in group II kimberlites are (le Maitre, 2002):

i). Group II kimberlites are ultrapotassic, peralkaline volatile-rich (mostly H_2O) rocks.

ii). Group II kimberlites may also be evolved (characterised by groundmass sanidine and K-richterite).

Kimberlite intrusions occur as small pipes with allied dykes, dykes with associated blows, and less commonly, sill complexes (Dawson, 1980). Typical southern African kimberlite pipes are steep sided (80^0-85^0) with a "carrot-like" shape and consist of three zones; crater, diatreme and root zone (Clement & Skinner, 1985; Hawthorne, 1975). Due to the high volatile content of kimberlites, emplacement of the volcanic pipes is thought to have been rapid. One field of thought regarding the details of kimberlite emplacement, calls upon multiple intrusive events beneath a cap rock, followed by explosion triggered by the build up of degassing volatiles with subsequent fluidisation (Clement, 1982; Dawson, 1980). An alternate school of thought advocates kimberlite explosion triggered by the interaction of magmatic kimberlite with ground water (Lorenz *et al.*, 1999; Lorenz, 1975), although it is likely that both processes are operational during kimberlite emplacement (Field & Scott Smith, 1999). The majority of South African kimberlite pipes have been deeply eroded and only portions of the diatreme and root zones are still present (Hawthorne, 1975). The zones are classified by their respective type of pipe infill (Clement & Skinner, 1985), namely epiclastic or pyroclastic kimberlite (crater zone), tuffisitic kimberlite (diatreme zone) and hypabyssal kimberlite (root zone). Hypabyssal kimberlite can be further classified according to mineralogical criteria, based on the relative abundance of the five most common matrix minerals; serpentine, calcite, monticellite, phlogopite and diopside (Skinner & Clement, 1977). Mineralogical classification schemes of hypabyssal kimberlite ignore the presence of macrocrysts in the kimberlite, since the predominantly olivine and phlogopite macrocrysts are thought to represent disaggregated mantle peridotite (le Roex *et al.*, 2003; Shee, 1985; Clement *et al.*, 1984).

1.2 Distribution and emplacement of kimberlites in southern Africa

Kimberlites have been found both on stable Archean cratons and Proterozoic platforms, unlike other alkaline igneous rocks that may also occur on active tectonic margins (Dawson, 1980). Group I kimberlites have been recorded in most continents, but group II kimberlites appear to be confined to the vicinity of the Archean southern African Kaapvaal craton. The uniqueness of group II kimberlites would suggest that they are derived from source regions specific to southern Africa. South African transitional kimberlites occur dominantly in the Proterozoic mobile belt (Skinner *et al.*, 1992) and similarly, Venezuelan transitional kimberlites are intrusive through Proterozoic granitoids (Kaminsky *et*

al., 2004). However, transitional kimberlites have also been recognised on numerous other Archean cratons such as the Sáo Francisco craton (Brazil; Bizzi, 1995), Kola-Kuloi craton (Russia; Beard *et al.*, 2000), Sino-Korean craton (China; Tompkins *et al.*, 1999), Karelian craton (Finland; O'Brien & Tyni, 1999) and the Slave craton (Canada; Dowall *et al.*, 2003).

Abundant kimberlite fields exist on the Kaapvaal craton and many have been extensively studied and mined in the past due to the presence of diamond xenocrysts (Clifford, 1966). Several off-craton kimberlite fields, intrusive through the Proterozoic Namaqua-Natal mobile belt, have been recognised in southern Africa and most tend to host typical group I kimberlites (e.g. East Griqualand kimberlites; Nixon *et al.*, 1983 and Gibeon Kimberlites; Janse, 1975), except for the Central Cape Province or Prieska Province kimberlites that consist of group I, group II and transitional kimberlites (Clark, 1994; Skinner *et al.*, 1992; Robey, 1981).

Ages of group I kimberlites in southern Africa are variable from the 1600Ma Kuruman kimberlites (Bristow *et al.*, 1986) to the 72Ma Gibeon kimberlites (Davies *et al.*, 2001), with a peak in intrusive activity at 80-90Ma in the Cretaceous (e.g. Kimberley kimberlites). In contrast to group I kimberlites that show no obvious age distribution relationships, group II kimberlites have a sublinear age progression, younging from northeast to southwest. The oldest group II kimberlite, Dokolwayo (200Ma; Allsopp & Roddick, 1984) and youngest group II kimberlite, Eendekuil (110Ma; Allsopp, Unpubl. in Skinner, 1989), have emplacement ages that broadly coincide with the opening of the Indian and South Atlantic Oceans (180Ma and 130Ma; Storey, 1995), respectively, and suggest association with Gondwana breakup (Skinner, 1989).

1.3 Petrogenesis of kimberlites

In the past, studies of kimberlite geochemistry have generally been focused on characterising the major element geochemistry (Shee, 1985; Clement, 1982; Fesq *et al.*, 1975), trace element geochemistry (Smith *et al.*, 1985b; Wedepohl & Muramatsu, 1979) or isotope geochemistry (Fraser *et al.*, 1985/86; Smith, 1983a; Barrett & Berg, 1975). Only recently has an effort been made to maximise the use of trace element geochemistry, with a view to constraining petrogenetic processes and the evolution of kimberlite source regions (Chalapathi Rao *et al.*, 2004; Coe, 2004; Harris *et al.*, 2004; le Roex *et al.*, 2003; Beard *et al.*, 1998; Tainton, 1992; Fraser & Hawkesworth, 1992). These studies have shown that the SiO_2-poor and MgO-rich kimberlites are characteristically enriched in both compatible and incompatible trace elements and that their geochemistry is highly variable. Some of the observed variability is due to the influence of secondary processes; alteration, crustal contamination and peridotite entrainment, hence the common reference to kimberlites as hybrid rocks (Mitchell, 1986; Dawson 1980). However, it has been shown that with careful study these secondary effects can be accounted for and close-to-primary kimberlite magma compositions obtained (Coe, 2004; Harris *et al.*, 2004; le Roex *et al.*, 2003). Semi-quantitative genetic models argue for derivation

of kimberlite by very low degrees of partial melting of metasomatically enriched, previously melt-depleted, lithospheric garnet peridotite (le Roex *et al.*, 2003; Tainton & McKenzie, 1994).

The nature of kimberlite experimental studies has been to characterise the behaviour of natural or synthetic kimberlite and lamproite magmas at mantle pressures and temperatures. Aside from the procedural problems encountered during such experiments (e.g. systems are Fe-free and use a Co analogue for Fe; Ringwood *et al.*, 1992), these studies performed on group I and group II kimberlite and lamproite compositions have still contributed to the understanding of kimberlite melting relations. Proposed kimberlite source regions have varied from garnet peridotite (Ulmer & Sweeney, 2002; Dalton & Presnall 1998a), garnetite (Edgar & Charbonneau, 1993) to clinopyroxene and mica-rich veins (Foley, 1992a, b), since some authors have precluded the presence of olivine (Girnis *et al.*, 1995; Foley, 1992a) and orthopyroxene (Mitchell, 2004; Edgar & Charbonneau, 1993) in kimberlite source regions. Although Ringwood *et al.* (1992) precluded the existence of garnet in kimberlite source, this argument was later retracted by Kesson *et al.* (1994), who established the presence of garnet just below the kimberlite liquidus. However, Ulmer and Sweeney (2002), Dalton and Presnall (1998a) and Canil and Scarfe (1990) have shown that kimberlite-like magmas can be produced by low degree melting of carbonated garnet peridotite, and their experiments are of interest since they utilise the "solidus ledge" of Wyllie (1980). The invariant point and associated solidus ledge in the peridotite-CO_2-H_2O system cause the crystallisation of rising melts and the subsequent production of a CO_2-rich vapour, which is then free to percolate through the mantle and metasomatise possible kimberlite source regions (Wyllie, 1980).

Diamonds entrained by many on-craton kimberlites provide an estimate for the minimum pressure of kimberlite origin (> 4.5GPa; Kennedy & Kennedy, 1976). Similarly, geothermobarometry of mantle xenoliths entrained by kimberlites (e.g. Brey & Köhler, 1990) provide estimates of upper mantle conditions reflected in both on-craton (Finnerty & Boyd, 1987) and off-craton (Boyd *et al.*, 2004; Bell *et al.*, 2003) kimberlites that broadly coincide with estimates of heat flow in Archean terrains (41mWm^{-2}; Nyblade & Pollack, 1993). Sweeney and Winter (1999) have suggested segregation depths for kimberlite magmas between 6 and 14GPa using partial melting models based on kimberlite major element geochemistry. Experimental studies on group I and group II kimberlite compositions also suggest derivation of kimberlites from between 4 and 10GPa (Ulmer & Sweeney, 2002; Dalton & Presnall; 1998a; Yamashita *et al.*, 1995; Edgar & Charbonneau, 1993; Canil & Scarfe, 1990), although Ringwood and coworkers (Kesson *et al.*, 1994; Ringwood *et al.*, 1992) favour a deeper origin in the transition zone for group I kimberlites (400-650km; 10-16GPa), based on the presence of majoritic garnet inclusions in diamonds from the group I Monastery kimberlite (Moore & Gurney, 1985). Haggerty (1994) has argued for an even deeper source from the core-mantle boundary for proto-kimberlite magmas, although more recent research using the W isotope system challenges this possibility, since kimberlites show no evidence for a core contribution (Scherstén *et al.*, 2004).

However, these estimates provide few constraints on whether kimberlite source regions are located within the subcontinental lithospheric mantle or the sublithospheric mantle. The characteristic geochemical signature of group II kimberlites require derivation from a source that had experienced melt-depletion in the garnet stability field with subsequent ancient metasomatic enrichment (Coe, 2004; Tainton & McKenzie, 1994). It has been postulated that in order to maintain these geochemical heterogeneities, the source region must have been isolated from the convecting mantle and therefore a subcontinental lithospheric source has been proposed for group II kimberlites (Coe, 2004; Tainton & McKenzie, 1994; Fraser & Hawkesworth, 1992; Smith 1983a). le Roex *et al.* (2003) and Harris *et al.* (2004) have argued for a similar source region for group I kimberlites, except with a sublithospheric imprint from plume derived melts/fluids, which give rise to the OIB-like geochemical character of these kimberlites. However, Os isotopic characteristics of both group I and group II kimberlites show similarities to OIB (Pearson *et al.*, 2003; Pearson *et al.*, 1995), in contrast to the Hf isotopic signatures of kimberlites that require ancient source regions (Nowell *et al.*, 2004; Dowall *et al.*, 2003; Nowell *et al.*, 1999). The favoured model of Nowell *et al.* (2004) and Dowall *et al.* (2003) is that group I, group II and transitional kimberlites share a common sublithospheric source region with minimal contribution from the subcontinental lithosphere.

The correlation of kimberlite age distribution relationships has led various authors to suggest the influence of mantle plumes in kimberlite generation (Heaman *et al.*, 2004; Haggerty, 1994; le Roex, 1986; Crough *et al.*, 1980), with relevance in southern Africa since group II kimberlites correlate with the paleo-track of the South Atlantic Shona plume (le Roex, 1986). The roughly sublinear distribution of kimberlites in southern Africa has also led McCandless (1999) after Sharp (1974), to suggest that the presence of subducted oceanic lithosphere could be a trigger for kimberlite generation and that kimberlites are products of deep-seated melting of subducted oceanic lithosphere. More recently, Kaminsky *et al.* (2004) have proposed that the characteristic geochemistry of Venezuelan transitional kimberlites and the existence of a dominant eclogitic component in diamonds from the Guaniamo kimberlites, are evidence that the kimberlites likely formed from melting of subducted oceanic crust. Alternatively, kimberlites may form from partial melting of source regions metasomatised by volatiles released from the underlying subducted oceanic slab (Helmstaedt & Gurney, 1984).

Kimberlite, carbonatite and alkaline magmatism in Africa has been episodic and Bailey (1993) related this episodic activity to the effect of external forces acting upon the lithosphere. Kimberlite magmatism is then a result of stress release along zones of pre-existing lithospheric weaknesses (Bailey, 1993). Similarly, localised melting along a rift associated with Gondwana breakup has also been advocated as a possible explanation for group II kimberlite generation (Phillips *et al.*, 1998). The variety of hypotheses for kimberlite genesis and the location of kimberlite source regions, suggest that further research into kimberlite petrogenesis can only be of benefit.

1.4 Implications of kimberlite research and objectives of this study

Kimberlites are rocks with probably the deepest origin of all alkaline magmas and this has the power to provide understanding of deep mantle processes. Their unique ultramafic, potassic and volatile-rich character, with enrichment in compatible and incompatible trace elements suggests derivation from complex source regions. Kimberlite research is therefore aimed at understanding the evolution of these distinctive source regions with the following objectives in mind:

i). To characterise and compare the geochemistry of source region compositions for group I, group II and transitional kimberlites, with particular emphasis on trace elements.

ii). To evaluate the effect of different aged mantle terrains on the geochemistry of group I, group II and transitional kimberlites and determine whether the geochemical characteristics of kimberlites that have intruded through the Archean Kaapvaal craton (on-craton kimberlites) or through the Proterozoic Namaqua-Natal mobile belt (off-craton kimberlites) show any significant similarities or differences, that can be related to understanding of petrogenetic processes and timing of enrichment events.

iii). To evaluate the possible causes of kimberlite source region enrichment (metasomatism) with reference to the source of metasomatic melts/fluids.

In order to reach these objectives, close-to-primary magma compositions for individual kimberlites analysed in this study are determined, once the effect of various secondary processes and fractional crystallisation has been evaluated. Semi-quantitative modelling of kimberlite genesis and source geochemistry is then used to evaluate source region characteristics and evolutionary processes, before an integrated model describing the petrogenesis of selected group I, group II and transitional kimberlites is developed.

CHAPTER 2

GEOLOGICAL SETTING

2.1 Introduction

Given that kimberlites in this study have intruded through either Archean or Proterozoic basement, the geological history of southern Africa is briefly explored, since some of the major geological events that have occurred, may have played a key role in the evolution of kimberlite source regions and the subsequent petrogenesis of group I, group II and transitional kimberlite. The following is therefore a short description of the development of the 1.2 x 10^6 km^2 Archean Kaapvaal craton (de Wit *et al.*, 1992) and of the Proterozoic Namaqua-Natal belt that surrounds the southwestern and southeastern margins of the craton. In addition, the Phanerozoic geology of South Africa is summarised, since many of the on- and off-craton kimberlites in this study are emplaced within country rocks of this age.

The oldest rocks within South Africa are those found in the Barberton Greenstone belt (3.2-3.5Ga; Armstrong *et al.*, 1990) and the Ancient Gneiss Complex in Swaziland (3.2-3.6Ga; Kröner & Tegtmeyer, 1994). These rocks record the separation of the continental lithosphere from the mantle and its early stabilisation during the period ~3.7-3.1Ga (de Wit *et al.*, 1992). The second stage of the development of the Archean craton during the period 3.1-2.6Ga (de Wit *et al.*, 1992), is marked by extension and sedimentation as well as widespread granitoid emplacement (Tankard *et al.*, 1982). Volcanic rocks from the Dominion Group and Ventersdorp Supergroup were likely formed during periods of extension, whereas subtidal and fluvial sediments from the Witwatersrand Supergroup and the Pongola Supergroup, marked periods of deposition. Unconformably overlain on the Ventersdorp Supergroup are limestone, dolomite, chert and banded iron formations of the early Proterozoic Transvaal and Griqualand West Supergroups, which were likely formed in an epeiric environment. Extrusion of the Rooiberg volcanic rocks was shortly followed by intrusion of the Bushveld Igneous Complex (2.05-2.06Ma) and the formation of the Vredefort Dome, a ~70km wide up-domed structure of Archean basement exposed by a large meteorite impact (Reimold & Gibson, 1996). Prior to the intense orogenic activity that sutured the Namaqua and Natal belts to the Kaapvaal craton, was a period of deposition marked by alternating sediments and volcanic rocks from various tectonic settings around the Kaapvaal Craton and preserved in the Palaeoproterozoic Waterberg, Soutpansberg, Umkondo and Matsap Groups (Tankard *et al.*, 1982).

The Namaqua and Natal Mesoproterozoic metamorphic belts are exposed to the southwest and southeast of the Kaapvaal craton respectively, and the two mobile belts are believed to be connected at depth, south of the craton underneath a Karoo Supergroup cover (De Beer & Meyer, 1983). A variety of lithologies that vary from low grade meta-volcanic rocks and intercalated sediments (Richtersveld Subprovince) to intensely deformed, high grade gneisses, granitoids and granulites

(Bushmanland Subprovince) occur in surface exposures of the Namaqua-Natal belt (Hartnady *et al.*, 1985). The margin between the Namaqua-Natal belt and Kaapvaal craton is highly complex and reflects numerous structural events related to the deformation and metamorphism of the mobile belt (1.2-1.0Ga; Thomas *et al.*, 1994; Hartnady *et al.*, 1985). However, the precise location of the southwestern margin of the Kaapvaal craton is of interest, since some of the kimberlites in this study have been emplaced within its vicinity. Depending on whether the wedge shaped Marydale Terrain comprised of an Archean greenstone belt (2950Ma; Cornell *et al.*, 1986) as well as other rocks of not only varying lithologies with poorly constrained ages, but also of diverse nomenclature (e.g. Schmitz & Bowring, 2004; Thomas *et al.*, 1994; Cornell *et al.*, 1986; Tankard *et al.*, 1982), is interpreted as belonging to the Kaapvaal province or the Namaqua province, the margin can either be defined according to the location of the Brakbos or Dooringberg faults, respectively (Tankard *et al.*, 1982; Pretorius, 1974). Following Cornell *et al.* (1986) and Schmitz and Bowring (2004), the Marydale Terrain is correlated with the Kaapvaal craton and therefore the boundary between the Proterozoic Namaqua Province and Archean craton is defined by the location of the Brakbos fault.

The next major development in the geological history of southern Africa was the Pan-African formation of the Gondwana supercontinent. The period of Gondwana history was marked by the Ordovician to Carboniferous deposition of the Cape Supergroup and later Carboniferous to Jurassic sedimentation consisting of glaciogenic, offshore, deltaic and terrestrial deposits within the Karoo basin. It is these rocks of the Karoo Supergroup that form the country rock to many of the kimberlites analysed in this study. Prior to the Jurassic to Cretaceous emplacement of kimberlites, massive outpourings of Karoo continental flood basalts occurred at 180Ma (Marsh *et al.*, 1997) that later served as a barrier to kimberlite intrusion and resulted in violent kimberlite eruption (Clement, 1982). Associated with the eruption of the Karoo volcanic rocks, was the initiation of the breakup of Gondwana as well as the passage of more than one Mesozoic mantle plume beneath southern Africa (Hartnady & le Roex, 1985) that may have played a role in the petrogenesis of South African kimberlites (e.g. Harris *et al.*, 2004; Skinner, 1989; le Roex, 1986).

2.2 Location and geology of selected kimberlites

Kimberlites tend to intrude in fields and provinces (Mitchell, 1986), and so the following summary of the kimberlites, their relationship to the Kaapvaal craton (Figure 2.1), geographical coordinates (Table 2.1) and ages (Table 2.2), is described according to common characteristics of the kimberlites. More detailed descriptions of individual kimberlite localities are given in Appendix A.

2.2.1 The archetypal group I kimberlites

The archetypal group I kimberlites of South Africa that were associated with the first hard rock diamond mines (Wagner, 1914), were those kimberlites situated near the town of Kimberley in the Northern Cape Province. These on-craton kimberlites are generally small pipes eroded down to depths within the diatreme and subsequent mining operations have exposed the irregular root zones

(Clement, 1982). The main cluster of Kimberley kimberlites comprising the De Beers, Du Toitspan, Bultfontein, Wesselton and Kimberley kimberlites has been extensively described (e.g. Shee, 1985; Clement, 1982; Clement *et al.*, 1979) and are mentioned here, since they are integral in this study for comparison with the on-craton Koffiefontein kimberlite situated in the Free State Province (Table 2.1; Figure 2.1). Koffiefontein kimberlite is similarly a small pipe (11.1Ha; Naidoo *et al.*, 2004) of mica-poor character and has an intrusion age of 90Ma (Davis 1978; Table 2.2), roughly contemporaneous to the group I Kimberley kimberlites (84Ma; Clement *et al.*, 1979). The Kimberley kimberlites and Koffiefontein kimberlite have all intruded through Archean crystalline basement, overlain by rocks from the Karoo Supergroup and Karoo flood basalt province.

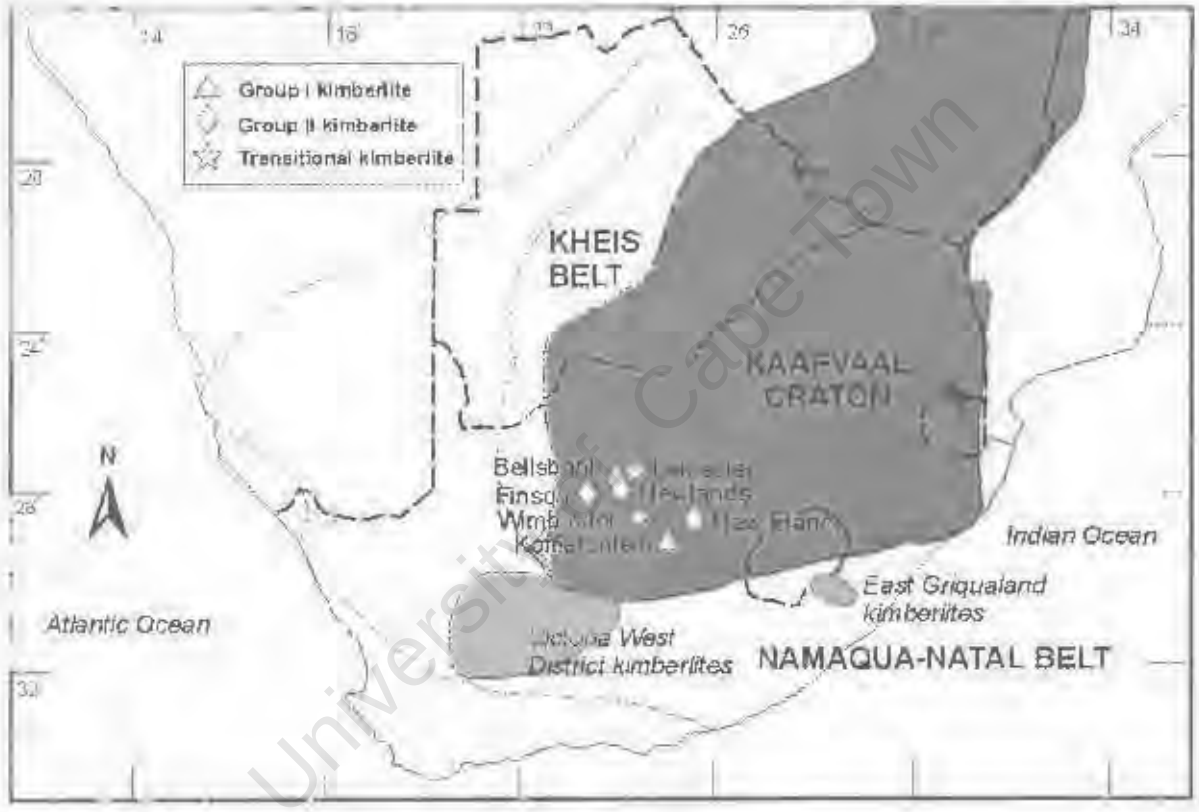

Figure 2.1. Location of the on-craton kimberlites analysed in this study. The off-craton East Griqualand and dominantly off-craton Victoria West District kimberlite provinces are illustrated as shaded fields. The position of the Kaapvaal craton within southern Africa is shown for reference. Figure adapted from Carlson *et al.* (2000).

2.2.2 East Griqualand kimberlites

The off-craton group I East Griqualand kimberlite province extends through the Kwazulu-Natal Province in South Africa and into Lesotho. Two kimberlite pipes from this province containing fifty dykes and twelve pipes (Nixon *et al.*, 1983) were selected for study, namely the Zeekoegat and Abbotsford East kimberlites (collectively shown as "East Griqualand", Figure 2.1). The two kimberlite pipes occur within the vicinity of five other dykes and may therefore be related (Nixon *et al.*, 1983). The Ramatseliso and Mzongwana kimberlites of the East Griqualand kimberlite province have been

Table 2.1. Location and intrusive style of kimberlites analysed in this study. The details of some of the kimberlites included for comparison in this study are also given.

Kimberlite	Location	Latitude (S)	Longitude (E)	Intrusive Style	Reference
Group I kimberlite: On-craton					
Goedehoop kimberlite	Hanover	30°50'	24°25'	pipe, dyke, blow	This study
Koffiefontein kimberlite	Koffiefontein	29°25'	25°00'	pipe, dyke	This study
Kimberlite kimberlites	Kimberley	-	-	pipe	le Roex *et al.* (2003)
Group I kimberlites: Off-craton					
Abbotsford East kimberlite	Cedarville	30°27'	28°50'	pipe	This study
Hebron kimberlite	Victoria West	31°17'	22°34'	pipe, dyke	This study
Klipgatsfontein kimberlite	Victoria West	31°19'	22°37'	pipe, dyke	This study
Uintjiesberg kimberlite	Carnarvon	30°50'	22°32'	pipe, dyke	Harris *et al.* (2004)
Zeekoegat kimberlite	Cedarville	30°27'	28°50'	pipe	This study
Group II kimberlites: On-craton					
Bellsbank kimberlite	Barkly West	28°05'	24°02'	dyke, blow	This study
New Elands kimberlite	Boshof	28°31'	25°29'	dyke, blow	This study
Newlands kimberlite	Barkly West	28°20'	24°02'	dyke, blow	This study
Finsch kimberlite	Postmasburg	28°21'	23°27'	pipe, dyke	Zwaan (2001)
Star kimberlite	Theunissen	-	-	dyke, blow	Coe (2004)
Swartruggens kimberlite	Rustenburg	-	-	dyke	Coe (2004)
Group II kimberlites: Off-craton					
Brandewynskuil kimberlite	Carnarvon	30°37'	22°41'	pipe	This study
Eendekuil kimberlite	Sutherland	32°15'	20°59'	dyke	This study
Markt kimberlite	Carnarvon	30°15'	22°21'	pipe, dyke	This study
Transitional kimberlites: On-craton					
Leicester kimberlite	Windsorton	27°22'	24°39'	pipe	This study
Wimbledon kimberlite	Kimberley	28°49'	24°43'	pipe	This study
Transitional kimberlites: Off-craton					
Droogfontein kimberlite	Fraserburg	31°39'	22°18'	dyke	This study
Melton Wold kimberlite	Victoria West	31°30'	22°45'	pipe, dyke	This study
Silvery Home kimberlite	Fraserburg	31°34'	22°16'	dyke, blow	This study

dated at 150Ma (Davis, 1977) and 152Ma (Smith *et al.*, 1985a), respectively. The East Griqualand kimberlites occur south of the inferred border of the Kaapvaal craton and have intruded through the Proterozoic Namaqua-Natal belt as well Karoo Supergroup shales, sandstones and mudstones and Stormberg basalts from the Karoo flood basalt province.

2.2.3 Victoria West District kimberlites

The Victoria West group of dominantly off-craton kimberlites comprises group I, group II and transitional kimberlite varieties and occurs just southwest of the Kaapvaal Craton (Figure 2.1). Some of these kimberlites were first described by Du Toit (1908) and more recently, Robey (1981) and Clark

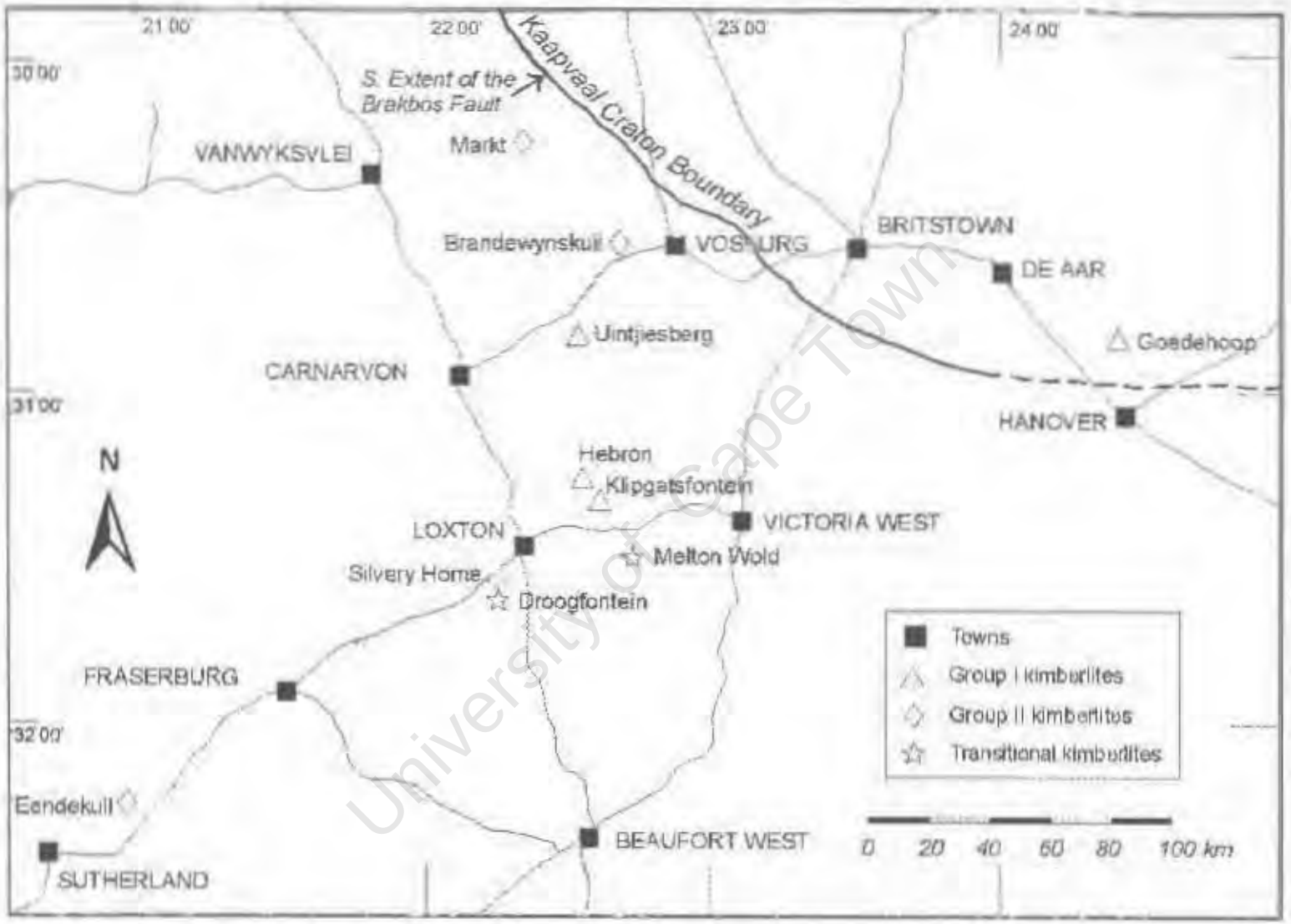

Figure 2.2. Location of group I, group II and transitional kimberlites within the Victoria West District. The inferred location of the southwestern craton margin (up to 24°E) following the magnetic lineament of the Brakbos Fault, from Schmitz and Bowring (2004) is shown. However, the location of the craton margin east of 24° is extrapolated. Figure adapted from Clark (1994).

Table 2.2. Published emplacement ages of some of the kimberlites analysed in this study and their respective dating methods.

Kimberlite	Age (Ma)	Dating Method	Ref.
Group I kimberlite: On-craton			
Koffiefontein kimberlite	90.4	U-Pb zircon	a
Group I kimberlite: Off-craton			
Uintjiesberg kimberlite	100.7 ± 1.4	Rb-Sr phlogopite & whole rock	b
Group II kimberlite: On-craton			
Bellsbank kimberlite	121.5 ±1.6	Rb-Sr phlogopite & whole rock	b
Finsch kimberlite	118.4 ±2.2	Rb-Sr phlogopite & whole rock	b
New Elands kimberlite	125.7 ±2.2	Rb-Sr phlogopite & whole rock	b
Newlands kimberlite	114.1 ±1.6	Rb-Sr phlogopite & whole rock	b
Group II kimberlite: Off-craton			
Eendekuil kimberlite	110	Rb-Sr phlogopite	c
Markt kimberlite	116.8 ±1.0	Rb-Sr phlogopite & whole rock	d
Transitional kimberlite: On-craton			
Leicester kimberlite	92.4	U-Pb zircon	a
Transitional kimberlite: Off-craton			
Droogfontein kimberlite	173.9 ±1.9	Rb-Sr phlogopite	d
Melton Wold kimberlite	143 ±14	U-Pb perovskite	d

References: (a) Davis (1978), (b) Smith *et al.* (1985a), (c) Allsopp (unpubl.) in Skinner (1989) and (d) Smith *et al.* (1994).

(1994) have studied various aspects of these kimberlites, but named them "Central Cape Province" and "Prieska Province" kimberlites, respectively. The kimberlites analysed in this study have been termed "Victoria West District" kimberlites since neither of the previous names are strictly applicable. The Victoria West District kimberlites are situated within approximately a 200km radius of the town of Victoria West, in the Northern Cape Province (Figure 2.2). Group I kimberlites selected for study include the Goedehoop, Hebron, Klipgatsfontein and Uintjiesberg kimberlites, group II kimberlites include the Markt, Brandewynskuil and Eendekuil kimberlites, and the Silvery Home, Melton Wold and Droogfontein kimberlites are the transitional kimberlites selected for this study.

The kimberlites generally form small pipes and/or dykes with occasional blows, that are poorly exposed unless there have been previous excavations. The largest kimberlite pipe within the Victoria West District is the group II Markt I kimberlite pipe that measures 300m in diameter (Robey, 1981). Although the kimberlites now consist mostly of weathered yellow ground (Figure 2.3a), fairly fresh hypabyssal kimberlite can still be found at some locations (Figure 2.3b).

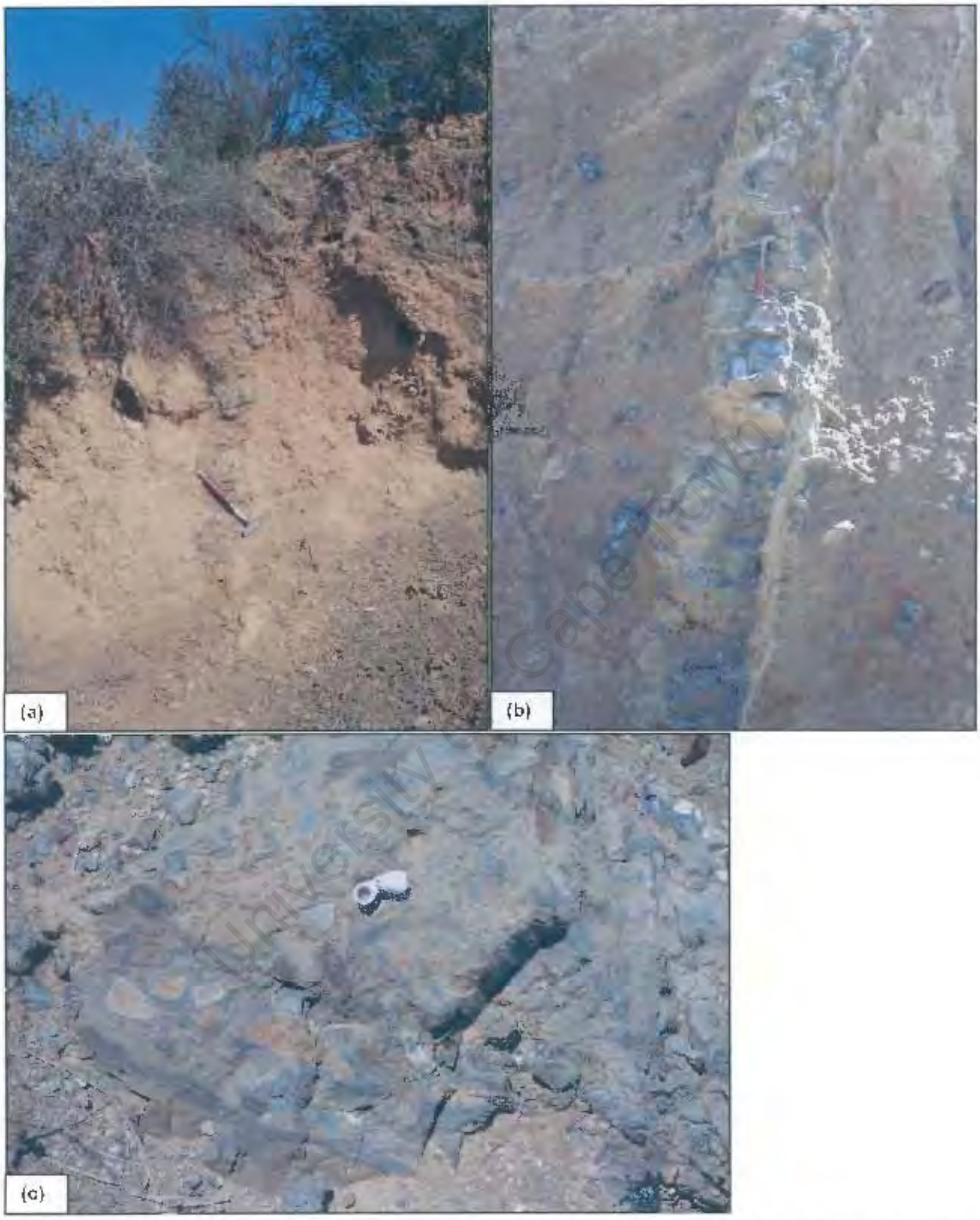

Figure 2.3: (a) Weathered yellow ground of the group II Lendekuil kimberlite dyke bisected by country rock. Geological hammer for scale. (b) Intrusion of a hypabyssal kimberlite dyke into weathered diatreme facies kimberlite from the transitional Melton Wold kimberlite. Geological hammer for scale. (c) Hydraulic fracturing between the transitional Silvery Home kimberlite and Beaufort Group country rock. Hand lens for scale.

The transitional kimberlites are the oldest kimberlites within the Victoria West District and have Jurassic emplacement ages (143-174Ma; Smith *et al.*, 1994). The group II Markt and Eendekuil kimberlite intrusion ages (117Ma and 110Ma, respectively; Smith *et al.*, 1994; Allsopp, 1989 in Skinner, 1989) are not too dissimilar in age to other Cretaceous on-craton group II kimberlites (Table 2.2). The group I Uintjiesberg kimberlite (101Ma; Smith *et al.*, 1985a) is, however, slightly older than the on-craton group I Koffiefontein and Kimberley kimberlites. A second pulse of group I kimberlite activity in the Victoria West District has also been recognised at ~75Ma for the Haartebeesfontein and Britstown kimberlites (Smith *et al.*, 1994). Given that the Haartebeesfontein kimberlite occurs on the same farm as the Hebron kimberlite, and the proximity of the Klipgatsfontein kimberlite to the Hebron kimberlite, a similar age is assumed for these two kimberlites.

The country rock into which most of the Victoria West District kimberlites have been emplaced and are subsequently exposed within, are shales and sandstones of the Beaufort Group (Figure 2.3c), whereas kimberlites situated in the northern part of the study area (Uintjiesberg, Markt and Brandewynskuil kimberlites), are surrounded by Ecca Group sedimentary rocks. Even though the Proterozoic Namaqua basement within this area is not exposed, most of the kimberlites are located to the west of the inferred location of the Brakbos fault and hence the Kaapvaal craton margin (Figure 2.2; the actual Brakbos fault is exposed to the north of the Victoria West District kimberlites, but its trace has been correlated by magnetic lineaments by Schmitz and Bowring (2004)). This is consistent with the suite of eclogite, granulite, amphibolite, and greenschist facies lower crustal xenoliths entrained by some of these kimberlites, that are Mesoproterozoic in age, and have geothermal gradients that most likely represent the Namaqua-Natal metamorphic event (Schmitz & Bowring, 2004; Huang *et al.*, 1995; Robey, 1981). However, the group I Goedehoop kimberlite is located further to east than the geological maps of Schmitz and Bowring (2004) and other authors (e.g. Skinner *et al.*, 1992) and therefore its location relative to the craton is speculative. If the trend of the position of the craton boundary of Schmitz and Bowring (2004) is continued, it appears as though the Goedehoop kimberlite has been emplaced through Archean basement of the Kaapvaal craton (Figure 2.2).

2.2.4. Barkly West and Boshof kimberlites

Two of the three on-craton group II kimberlites in this study are located near Barkly West (Newlands and Bellsbank kimberlites) in the Northern Cape Province, whereas the New Elands kimberlite occurs near Boshof in the Free State Province (Table 2.1). The Newlands and Bellsbank kimberlites both comprise *en echelon* dyke systems whereas the New Elands kimberlite consists of two intersecting dykes. The group II Finsch kimberlite pipe is a 17.9Ha pipe (Clement, 1982) with associated dykes situated near the town of Postmasburg in the Northern Cape Province and geochemical data from the Finsch kimberlite is also included in this study for comparison (Zwane, 2001; Fraser & Hawkesworth, 1992). Ages of intrusion for all four of the kimberlites are ~120Ma (Table 2.2), an age characteristic of group II kimberlites situated in the western half of the Kaapvaal craton. The kimberlites have intruded through Archean basement overlain by either the conglomerates, arenites, dolomites, and banded iron formations of the Griqualand West Supergroup (Finsch and Bellsbank kimberlites) or shales,

sandstones, mudstones of the Karoo Supergroup (Newlands, New Elands kimberlites). In addition, the Newlands kimberlite is covered with a veneer of Tertiary Kalahari Group calcrete.

2.2.5 Wimbledon and Leicester kimberlites

Both the Wimbledon and Leicester kimberlites are on-craton transitional kimberlites situated in the Northern Cape Province. The Wimbledon kimberlite pipe is situated close to the town of Kimberley and has an unusually mica-rich character in contrast to typical group I kimberlites. The Leicester kimberlite has a typical group I kimberlite age (92Ma; Davis, 1978) and is situated within a cluster of ~120Ma Barkly West group II kimberlite dykes. The Leicester kimberlite also carries the chrome-poor megacryst suite minerals like many group I kimberlites, but occurs in a district dominated by group II kimberlites that are known for their absence of megacrysts (Gurney & Menzies, 1998). The Wimbledon and Leicester kimberlites have intruded through Karoo shales and dolerites underlain by Archean basement.

2.3 Kimberlite sample selection

Kimberlites chosen for study were selected to represent the group I, group II and transitional kimberlite varieties distributed in both on- and off-craton tectonic environments. More specifically, hypabyssal kimberlite samples were chosen that showed the least degree of alteration, weathering and crustal contamination in hand specimen. Samples were selected to represent a variety of petrographic types such as macrocrystic and sparsely macrocrystic kimberlite, especially for cogenetic sample suites. The majority of the analysed kimberlite samples were obtained from a collection housed at the University of Cape Town. In addition, drill core samples from the Brandewynskuil, Droogfontein and Eendekuil kimberlites were obtained from the De Beers Geoscience Centre, some of which were geochemically analysed and dated by Clark (1994). The De Beers' Brandewynskuil, Droogfontein and Eendekuil kimberlite samples have the prefixes *173/26/K6/-*, *173/27/K19/-* and *173/18/K2/-* respectively, that have been dropped here for brevity. A few of the Victoria West district kimberlite samples were collected by the author during a field trip to observe field relationships shown at some of the kimberlite locations.

CHAPTER 3

PETROGRAPHY

3.1 Introduction

Wagner (1914) first recognised the existence of two distinct petrographic varieties of South African kimberlites, namely "basaltic" and "lamprophyric" (micaceous) kimberlites. However, given that kimberlites are not truly basaltic in texture or mineralogy (Skinner & Clement, 1977), a more appropriate mineralogical classification scheme was subsequently proposed by Skinner and Clement (1977) and then Clement and Skinner (1979). This later classification system has generally been accepted and is the basis on which the kimberlites in this study have been described and classified.

The samples analysed in this study are all hypabyssal facies kimberlite and can be divided according to texture, into macrocrystic or aphanitic kimberlite varieties (Clement *et al.*, 1984; Clement & Skinner, 1979). Macrocrysts have been designated as those anhedral crystals larger than 2mm in size and the non-genetic term refers to the predominantly olivine crystals that may have been derived from disaggregated mantle xenoliths (le Roex *et al.*, 2003; Clement *et al.*, 1984). Kimberlite samples with greater than 10 volume % macrocrysts have accordingly been classified as macrocrystic. A second population of euhedral to subhedral olivine phenocrysts as well as phlogopite and diopside phenocrysts have also been recognised. The term phenocryst has been used for those crystals with a euhedral habit that are greater than 1mm in size, although smaller microphenocrysts (< 1mm) may also be recognised. Fragments of macrocrysts may be smaller than 2mm in size, but can be distinguished from phenocrysts by their anhedral habit, deformation features and association with other minerals (Skinner, 1989). All crystals smaller than 0.5mm in size have been classified as either matrix phases or microphenocrysts. There are five minerals that commonly form the matrix of kimberlites, *viz.* phlogopite, calcite, serpentine, diopside and monticellite, and kimberlites are classified mineralogically according to the relative modal abundance of these minerals (Skinner & Clement, 1977). Ilmenite and spinel, collectively termed opaque oxides here, as well as perovskite and apatite are accessory minerals in the analysed kimberlites.

The petrographic variation shown by South African kimberlites is diverse and broad differences in texture and mineralogy occur even on the scale of petrographic thin sections. Bearing this in mind, the aim of this chapter is to give a general picture of the characteristics of the group I, group II and transitional kimberlites selected for analysis, as well as to highlight the differences and similarities between kimberlite varieties. This is essential in order to evaluate the degree to which the kimberlites have been affected by alteration, crustal contamination, macrocryst entrainment and fractional crystallisation (Section 8.2-8.5).

The classification of the kimberlite samples studied here and the relative modal proportion of their constituent mineral phases is presented in Table 3.1. Further petrographic descriptions and photomicrographs of individual kimberlite samples are given in Appendix B. Proportions of mineral phases have been deduced by visual estimation and not by point counting, given that the macrocrystic character of kimberlites may vary sharply over the distance of a few centimetres (e.g. le Roex *et al.*, 2003).

3.2 Group I kimberlites

Both on-craton (Goedehoop and Koffiefontein) and off-craton (Abbotsford East, Hebron, Klipgatsfontein and Zeekoegat) group I kimberlites are petrographically fairly similar and are mineralogically classified as serpentine calcite kimberlites or calcite kimberlites. The kimberlite samples have a typical macrocrystic texture comprising anhedral macrocrysts with smaller euhedral phenocrysts set in a fine-grained matrix. The macrocryst content of the kimberlite may vary from 10-33 volume % and kimberlites with less than 15 volume % macrocrysts have been classified as sparsely macrocrystic (Abbotsford East kimberlite). Olivine is the dominant macrocryst phase, with phlogopite and opaque oxide macrocrysts being less abundant. The olivine macrocrysts may constitute up to 20 volume % of the kimberlite (e.g. Koffiefontein kimberlite), be as large as 10mm and are generally subhedral to anhedral in character. Fresh olivine macrocryst cores occur in the Goedehoop, Klipgatsfontein and Zeekoegat kimberlites, but for the Koffiefontein, Abbotsford East and Hebron kimberlites, the serpentinisation reaction has been more pervasive and has proceeded beyond the alteration of just rims and fractures of macrocrysts. Some serpentinised olivine macrocrysts are yellow (Klipgatsfontein kimberlite), whereas others have turned slightly blue that may due to some additional chloritisation (Koffiefontein, Abbotsford East kimberlites). The blue colouration of olivine macrocrysts occurs in conjunction with opaque oxide rims around the macrocryst, inferred to be related to the exsolution of Fe during the serpentinisation reaction (Figure 3.1a; Clement, 1982).

Phlogopite macrocrysts are the next most abundant macrocryst phase and contribute ~10 volume % to the kimberlites. Even though the edges of the macrocrysts are typically corroded, their elongate habit is still well defined. Phlogopite macrocrysts in the Koffiefontein, Goedehoop, Hebron and Klipgatsfontein kimberlites all exhibit deformation features, e.g. kink banding and undulose extinction. The pale-coloured phlogopite macrocrysts are often wedged open along cleavage planes by calcite stringers. Equant opaque oxides may be concentrated along these calcite stringers or alternatively form rims surrounding the macrocrysts (Figure 3.1b; Goedehoop, Koffiefontein kimberlites). Phlogopite macrocrysts from Hebron kimberlite samples *HEB 1A* and *HEB 1B* are completely calcitised, but recognisable by their lath-shape and association with opaque oxide crystals. Euhedral to anhedral opaque oxide macrocrysts are present in the Hebron and Klipgatsfontein kimberlites (Figure 3.1c) and are correlated with numerous ilmenite macrocrysts identified in hand specimens (possibly belonging to the kimberlite "megacryst suite", Boyd & Nixon, 1975). In thin section, these ilmenite macrocrysts are typically characterised by groundmass perovskite aggregations along their rims.

Table 3.1 Summary table of macrocryst, phenocryst and microphenocryst, as well as matrix phases in group I, group II and transitional kimberlite samples. Volume percentages, defined by visual estimation are also given for reference.

		Macrocrysts					Phenos & Microphenos				Groundmass								
Kimberlite	Sample	Total %	Oliv.	Phlog.	Op-Ox.	Grt	Total %	Oliv.	Phlog.	Diop.	Total %	Calc.	Serp.	Phlog.	Diop.	Mont.	Op-Ox.	Per.	Ap.	Classification
Group I kimberlites: On-craton																				
Goedehoop	JAR 30012	20	10	10			30	30			50	28	15				5	2		Serp. calc. kimb.
Goedehoop	JJG 4282	15	10	5			30	30			55	29	20				4	2	Tr	Serp. calc. kimb.
Koffiefontein	KK 3	15	15				30	30			55	25	17	5			5	2	1	Serp. calc. kimb.
Koffiefontein	KK 5	20	17	3			30	30			50	20	17	5			5	2	1	Serp. calc. kimb.
Koffiefontein	KK 6	25	20	5			25	25			50	20	17	5			5	2	1	Serp. calc. kimb.
Group I kimberlites: Off-craton																				
Abbotsford East	JJG 3116	10	10				10	10			80	45	20	8			5	2		Calc. kimb.
Hebron	HEB 1A	25	7	13	5		15	15			60	30	24				4	2	Tr	Serp. calc. kimb.
Hebron	HEB 1B	25	7	13	5		15	15			60	31	24				4	2	Tr	Serp. calc. kimb.
Hebron	JJG 4295	33	17	8	8		22	17	5		45	20	15	3			6	1		Serp. calc. kimb.
Klipgatsfontein	JAR 31012	25	7	13	5		20	20			55	30	19				4	2		Serp. calc. kimb.
Klipgatsfontein	KGF 1	29	7	17	5		21	21			50	30	14				5	1		Serp. calc. kimb.
Klipgatsfontein	JJG 4323	27	5	17	5		23	23			50	25	19				5	1		Serp. calc. kimb.
Zeekoegat	JJG 1906	15	15				15	15			70	35	20	8			5	2		Calc. kimb.
Group II kimberlites: On-craton																				
Bellsbank	JJG 4076	30	25	5			10	10			60	15	10	30			2	1	2	Calc. phlog. kimb.
New Elands	NE K6	10	10				35	35			55	22		30			1	1		Calc. phlog. kimb.
New Elands	NE K10	10	10				35	35			55	22		30			1	1	1	Calc. phlog. kimb.
New Elands	NE K11	20	20				15	12	3		65		20	27	16		1	1		Serp. phlog. kimb.
Newlands	JJG 24	25	19	5	0.5	0.5	20	20			55	10	12	30			2	1	Tr	Phlog. kimb.
Newlands	JJG 6198	45	30	14	1		10	10			45	8	10	25			2	1	Tr	Phlog. kimb.
Newlands	KN 2	35	29	5		1	15	15			50	10	12	25			2	1	Tr	Phlog. kimb.
Newlands	KN 3	30	25	5			15	15			55	10	12	30			2	1	Tr	Phlog. kimb.
Group II kimberlites: Off-craton																				
Brandewynskuil	K6/8	25	15	10			25	20	5		50		15	25	9		1	Tr		Serp. phlog. kimb.
Brandewynskuil	K6/11	20	15	5			30	20	10		50		15	25	9		1	Tr		Serp. phlog. kimb.
Brandewynskuil	K6/12	30	20	10			15	15			55		19	15	20		1	Tr		Phlog serp. diop. kimb
Brandewynskuil	K6/14	30	20	10			15	15			55		19	15	20		1	Tr		Phlog serp. diop. kimb

Note: Oliv. = Olivine; Phlog. = Phlogopite; Grt = Garnet; Calc. = Calcite; Serp. = Serpentine; Diop. = Diopside; Mont. = Monticellite; Op-Ox. = Opaque Oxide; Per. = Perovskite; Ap. = Apatite; Tr. = Trace.

Table 3.1. *Continued.*

		Macrocrysts					Phenos & Microphenos					Groundmass								
Kimberlite	Sample	*Total %*	Oliv.	Phlog.	Op-Ox.	Grt	*Total %*	Oliv.	Phlog.	Diop.	*Total %*	Calc.	Serp.	Phlog.	Diop.	Mont.	Op-Ox.	Per.	Ap.	Classification
Eendekuil	EKL 1	25	5	20			30	5	20	5	45	20		22			2	1		Calc. phlog. kimb.
Eendekuil	K2/2	25	5	20			25	5	20		50	20		27			2	1		Phlog. calc. kimb.
Eendekuil	K2/3	30	10	20			15	5	10		55	24	6	20			2	1		Calc. phlog. kimb.
Eendekuil	K2/8	30	10	20			15	5	10		55	24	6	20			2	1		Calc. phlog. kimb.
Eendekuil	K2/9	30	10	20			15	5	10		55	24	6	20			2	1		Calc. phlog. kimb.
Eendekuil	K2/13	25	5	20			25	5	20		50	20		27			2	1		Phlog. calc. kimb.
Markt	JJG 2314	30	20	10			15	15			55	30	7.5	15			1	1	0.5	Phlog. calc. kimb.
Markt	JJG 2336	25	15	10			15	15			60	25	12.5	20			1	1	0.5	Phlog. calc. kimb.
Markt	MRK 1	30	20	10			15	15			55	25	7.5	20			1	1	0.5	Phlog. calc. kimb.
Markt	MRK 3	20	15	5			15	15			65	20	17	25			1	1	1	Calc. phlog. kimb.
Transitional kimberlites: On-craton																				
Leicester	JJG 4326	25	8	16.5	0.5		25	20	5		50	20	13	5		5	5	2		Serp. calc. kimb.
Leicester	JJG 4328	25	5	20			30	10	10		55	25	10	8		5	5	2		Serp. calc. kimb.
Leicester	JJG 6054	38	25	9.5	3	0.5	20	15	5		42	15	10	5		5	5	2		Serp. calc. kimb.
Wimbledon	WIMB 1	30	15	15			20	15	5		50	20	9	10			5	2	4	Phlog. calc. kimb.
Wimbledon	WIMB 2	30	20	10			15	15	5		55	20	10	14			5	2	4	Phlog. calc. kimb.
Transitional kimberlites: Off-craton																				
Droogfontein	K19/2	15	15				25	15	10		60		18	25	10		2	4		Serp. phlog. kimb.
Droogfontein	K19/3	15	15				25	15	10		60		18	25	10		2	4		Serp. phlog. kimb.
Droogfontein	K19/5	15	15				25	15	10		60		18	25	10		2	4		Serp. phlog. kimb.
Droogfontein	K19/10	15	15				25	15	10		60		19	25	10		2	4		Serp. phlog. kimb.
Melton Wold	MLW 1	20	20				30	30			50	25	7	15			2	1		Phlog. calc. kimb.
Melton Wold	MLW 3	15	15				25	25			60	25	12	20			2	1		Phlog. calc. kimb.
Melton Wold	MLW 4	20	20				30	20	10		50									Carbonated kimb.
Silvery Home	JAR 21022	15	15				20	20			65	18	19	25			2	1		Serp. phlog. kimb.
Silvery Home	SLH 1	20	20				30	30			50	13	16	18			2	1		Serp. phlog. kimb.
Silvery Home	SLH 3	10	10				25	25			65	13	15	16	16		2	4		Diop. phlog. kimb.
Silvery Home	SLH 7	15	15				30	18	12		55		14	20	15		2	4		Diop. phlog. kimb.
Silvery Home	SLH 9	15	15				30	18	12		55		5	23	21		2	4		Diop. phlog. kimb.
Silvery Home	SLH 10	15	15				35	25	10		50	13	19	15			2	1		Phlog. serp. kimb.
Silvery Home	SLH 11	15	15				30	25	5		55	10	23	19			2	1		Phlog. serp. kimb.

Note: Oliv. = Olivine; Phlog. = Phlogopite; Grt = Garnet; Calc. = Calcite; Serp = Serpentine; Diop. = Diopside; Mont. = Monticellite; Op-Ox. = Opaque Oxide; Per. = Perovskite; Ap. = Apatite; Tr. = Trace.

Euhedral to subhedral olivine phenocrysts and microphenocrysts are present in all of the samples, although the relative abundance may vary from 10 volume % (Abbotsford East kimberlite) up to 30 volume % (Koffiefontein, Goedehoop kimberlites). Serpentinisation of olivine phenocrysts has proceeded from just being confined to rims and fractures (Goedehoop, Klipgatsfontein kimberlites), to enveloping the entire phenocryst (Koffiefontein, Abbotsford East, Hebron, Zeekoegat kimberlites). Some calcitisation has also occurred along rims and fractures of olivine phenocrysts from the Goedehoop and Hebron kimberlites (Figure 3.1d). Phlogopite phenocrysts, which only occur in Hebron *kimberlite* sample *JJG 4295,* are euhedral to subhedral in character and show strong pleochroism.

Calcite and serpentine form the predominant groundmass phases of these serpentine calcite kimberlites and calcite kimberlites that are either uniform or segregationary in texture (Clement & Skinner, 1979). Kimberlites with uniform groundmass texture have regularly dispersed interstitial serpentine and calcite crystals (Abbotsford East, Goedehoop and Zeekoegat kimberlites), whereas the Koffiefontein, Klipgatsfontein and Hebron kimberlites, have groundmass serpentine and calcite crystals inter-grown with each other that have developed into lobate and irregular shaped segregations. The serpentine-calcite segregations are particularly well developed in the Klipgatsfontein kimberlite (Figure 3.1e, f), where the rhombohedral shaped calcite crystals may be as large as 500μm and the segregations themselves, up to a few millimetres in size.

Phlogopite also constitutes a groundmass phase in the Koffiefontein, Abbotsford East, and Zeekoegat kimberlites, as well as in Hebron kimberlite sample *JJG 4295*. The phlogopite crystals are fairly sparse (~5 volume % of the kimberlite), have a stubby character and vary in size between 100 and 300μm. Groundmass phlogopite crystals in the Koffiefontein kimberlite are orange-brown in colour, but colourless in Hebron kimberlite sample *JJG 4295*. Phlogopite crystals in the Abbotsford East and Zeekoegat kimberlites are very altered and rimmed by opaque oxide crystals.

Groundmass opaque oxide and lesser perovskite crystals may constitute up to 7 volume % of the kimberlite. The opaque oxide crystals are typically euhedral, equant and 100μm in size (Figure 3.1g). The subhedral perovskite crystals are of similar dimensions and may form aggregates 300-500μm in size. An atoll texture, comprising perovskite rims surrounding opaque oxide crystals occurs in the Hebron kimberlite (samples *HEB 1A* and *HEB 1B*). Euhedral needles of apatite, 100-300μm in size, that commonly occur within or surrounding serpentine-calcite segregations, have also been recognised in the analysed group I kimberlites samples.

Figure 3.1: Photomicrographs of selected features of group I kimberlite samples. Photomicrographs are shown in plane polarised light, unless otherwise indicated.

(a) Koffiefontein kimberlite *(KK 6):* Anhedral olivine macrocryst that is completely serpentinised. Opaque oxides form the rim of the macrocryst. Field of view is 3mm.

(b) Goedehoop kimberlite *(JAR 30012)*: A phlogopite macrocryst with an opaque oxide studded rim. Field of view is 1.2mm.

(c) Hebron kimberlite *(JJG 4295)*: Ilmenite macrocryst and a serpentinised olivine phenocryst. Field of view is 2.5mm.

(d) Goedehoop kimberlite *(JJG 4282):* Subhedral olivine phenocryst with serpentinisation and calcitisation along the phenocryst rim. Some fresh olivine still remains in the core of the phenocryst. Cross polarised light, field of view is 1.8mm.

(e) Klipgatsfontein kimberlite *(JAR 31012):* An irregular shaped serpentine-calcite segregation where individual calcite crystals are visible. Field of view is 1mm.

(f) Klipgatsfontein kimberlite *(JAR 31012):* Serpentine-calcite segregation comprising well developed euhedral calcite crystals, 0.5mm in size, is visible. Cross polarised light, field of view is 1mm.

(g) Koffiefontein kimberlite *(KK 3):* Euhedral to subhedral perovskite crystals with smaller opaque oxides. Serpentinised olivine phenocrysts also occur. Field of view is 0.8mm.

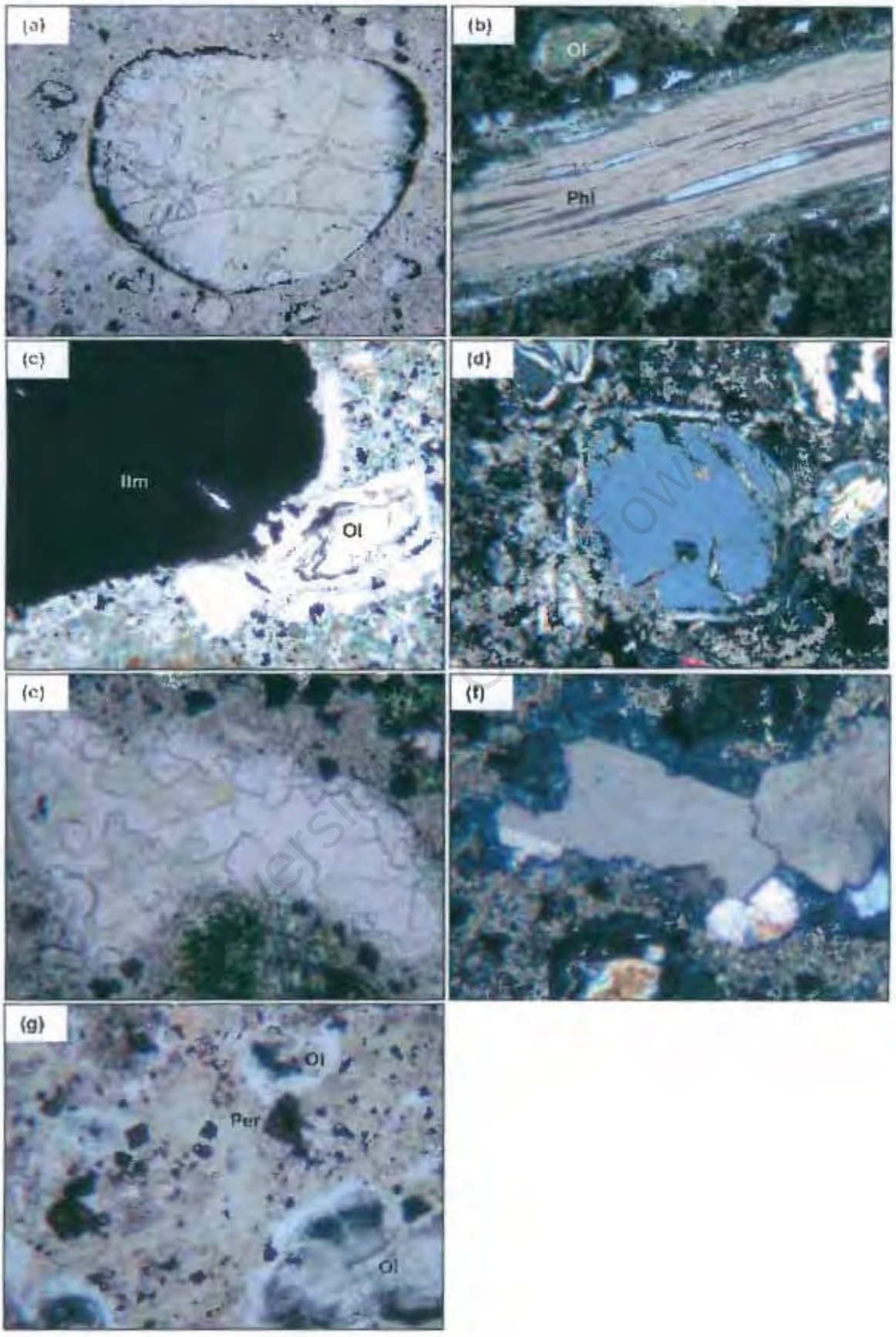
(a)
(b)
Ol
Phl
(c)
Ilm
Ol
(d)
(e)
(f)
(g)
Ol
Per
Ol

3.3 Group II kimberlites

Both on-craton group II kimberlites; Bellsbank, Newlands and New Elands kimberlites, as well as off-craton group II kimberlites; Brandewynskuil, Eendekuil and Markt kimberlites, are classified as phlogopite kimberlites or calcite phlogopite/phlogopite calcite kimberlites, according to the dominance of calcite and phlogopite as groundmass phases. The kimberlites are typically characterised by the presence of macrocrysts and phenocrysts set in a fine to very fine-grained matrix. All of the group II kimberlites are macrocrystic (up to 45 volume % macrocrysts), except for two sparsely macrocrystic New Elands kimberlite samples (*NE K6* and *NE K10*). Anhedral olivine macrocrysts are the most abundant macrocryst phase (10-30 volume % of the kimberlite), may be as large as 15mm (Eendekuil kimberlite sample *K2/6*) and are variably altered, either by serpentinisation along fractures (Bellsbank, Newlands and Markt kimberlites) or by calcitisation in patches (New Elands kimberlite). Olivine macrocrysts may also have chloritised rims (Markt kimberlite), or rims formed by phlogopite microphenocrysts (Brandewynskuil kimberlite). Fresh olivine macrocryst cores are however, still recognised in a few of the kimberlite samples (e.g. Eendekuil kimberlite; Figure 3.2a).

Phlogopite macrocrysts are typically strained (e.g. undulose extinction, kink banding) and variably altered by chloritisation. Phlogopite macrocrysts are notably absent in the New Elands kimberlite, in contrast to other group II kimberlites that host up to 20 volume % phlogopite macrocrysts. The macrocrysts tend to show strong pleochroism and are rimmed by tetraferriphlogopite or chlorite (e.g. Newlands kimberlite; Figure 3.2b). Phlogopite macrocrysts from the Eendekuil kimberlite have a slightly flow aligned texture and are always wedged open along cleavage planes by calcite stringers.

Garnet macrocrysts have been recognised in two of the Newlands kimberlite samples (*JJG 24* and *KN 2*). In sample *JJG 24,* two anhedral, heavily fractured, garnet macrocrysts of approximately 2mm in size occur, one of which is rimmed by kelyphite (Figure 3.2c), and the other, by chlorite. A 1mm anhedral orange garnet macrocryst also occurs in the hand specimen of Markt kimberlite sample *MRK 1*. Subhedral opaque oxide macrocrysts, 1mm in length are also present in some of the Newlands kimberlite samples (*JJG 24* and *JJG 6198*).

Olivine phenocrysts are ubiquitous in all of the analysed group II kimberlites and may constitute up to 35 volume % of the kimberlite. However, olivine microphenocrysts that may be as small as 200μm in size and characteristically occur in all kimberlite samples, are most notably absent from the Eendekuil kimberlite. The subhedral olivine phenocrysts are variably serpentinised in most kimberlites, although they are completely altered in the off-craton Brandewynskuil and Eendekuil kimberlite samples. Some calcitisation of the interior of olivine phenocrysts has also occurred in the New Elands kimberlite samples (*NE K6* and *NE K10)*. Similarly to the olivine macrocrysts, the olivine phenocrysts of the Brandewynskuil kimberlite are rimmed by aggregations of phlogopite microphenocrysts. Tabular phlogopite phenocrysts are characterised by tetraferriphlogopite rims and the phenocrysts themselves have only been recognised in a few of the kimberlite samples (New Elands kimberlite sample *NE K11*; Brandewynskuil kimberlite samples *K6/8* and *K6/11*), other than the Eendekuil kimberlite where they

are very common and characterised by the presence of calcite stringers (Figure 3.2d). Rare subhedral diopside phenocrysts are also present in Eendekuil kimberlite sample *EKL 1*.

Short stubby, interlocking phlogopite crystals, rimmed by tetraferriphlogopite form the dominant (15-40 volume %) groundmass phase in most of the analysed group II kimberlites (Figure 3.2e). Groundmass calcite crystals are the next most common matrix phase (up to 30 volume %). Consequently, the group II kimberlites are classified as phlogopite kimberlite (Newlands), calcite phlogopite kimberlite (Bellsbank, New Elands, Eendekuil) or phlogopite calcite kimberlite (Markt). Brandewynskuil kimberlite however, comprises both serpentine phlogopite kimberlite (*K6/8* and *K6/11*) and phlogopite serpentine diopside kimberlite varieties (*K6/12* and *K6/14*). The Bellsbank and Newlands kimberlites are characterised by very fine-grained groundmass phlogopite laths (50-100μm), in contrast to other group II kimberlites where the groundmass is not as fine-grained (100-500μm). The groundmass of the Bellsbank and Newlands kimberlites is also relatively green in colour due to the chloritisation of the matrix phlogopite.

Groundmass calcite tends to be interstitial although it occurs in segregations in the New Elands kimberlite samples *NE K6, NE K10,* Newlands kimberlite sample *JJG 24* and all of the Eendekuil kimberlite samples. Calcite segregations in the Eendekuil kimberlite may be as large as 4mm in size and the rhombohedral shape of calcite crystals is also evident (e.g. sample *EKL 1*). Groundmass calcite is generally colourless although in the Markt kimberlite, calcite crystals are distinctively brown. Many of the kimberlites have some interstitial groundmass serpentine (less than 12 volume %) but in New Elands kimberlite sample *NE K11* and in all of the Brandewynskuil kimberlites samples, serpentine occurs as the dominant groundmass phase (up to 20 volume % of the kimberlite), some of which is likely to be secondary in origin. Matrix serpentine in the Brandewynskuil kimberlite occurs in conjunction with acicular phlogopite laths as well as euhedral to subhedral diopside laths.

Accessory opaque oxides and perovskite crystals are very fine-grained (20-50μm) and relatively sparse (combined volume is ~3% of the kimberlite). Perovskite crystals may be poikolitically enclosed in phlogopite microphenocrysts (e.g. New Elands kimberlite; Figure 3.2f). Accessory apatite has also been recognised and varies in size from 50-100μm to 500μm, respectively, in the Markt (e.g. *MRK 1*) and New Elands kimberlite samples (*NE K6* and *NE K10*).

Figure 3.2: Photomicrographs of selected features of group II kimberlite samples. Photomicrographs are shown in plane polarised light, unless otherwise indicated.

(a) Eendekuil kimberlite *(EKL 1):* Fresh olivine macrocryst with some serpentinisation along rims and fractures. Field of view is 3mm.

(b) Newlands kimberlite *(JJG 24):* Green chlorite alteration rim that surrounds a tabular phlogopite macrocryst. Field of view is 1.2mm.

(c) Newlands kimberlite *(JJG 24):* Anhedral garnet macrocryst surrounded by a kelyphite rim. Field of view is 2.5mm.

(d) Eendekuil kimberlite *(EKL 1)*: Phlogopite microphenocrysts with stringers of calcite that have wedged open the phlogopite cleavage planes. Tetraferriphlogopite rims also occur on phenocrysts. Field of view is 1.2mm.

(e) Markt kimberlite *(MRK 1):* Tetraferriphlogopite and brown coloured calcite form the kimberlite matrix. Lesser amounts of small opaque oxide and perovskite crystals also occur in the groundmass. Field of view is 0.5mm.

(f) New Elands kimberlite *(NE K6):* Coarse-grained phlogopite microphenocrysts that have poikolitically enclosed opaque oxide and perovskite grains. Field of view is 0.4mm.

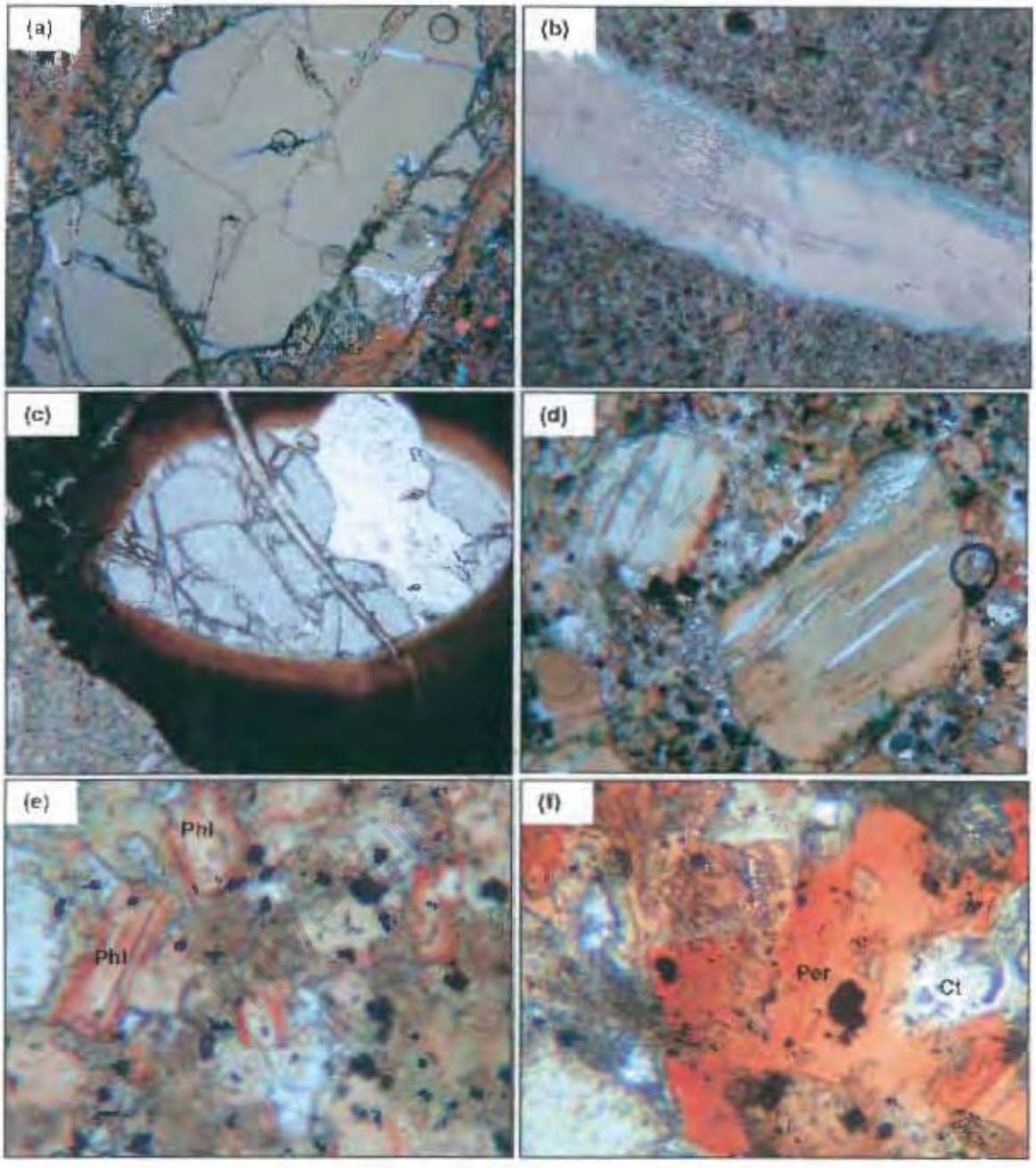
(a)
(b)
(c)
(d)
(e)
Phl
Phl
(f)
Per
Ct

3.4 Transitional kimberlites

On-craton transitional kimberlites (Wimbledon and Leicester) as well as off-craton transitional kimberlites (Droogfontein, Melton Wold and Silvery Home) show wide inter-kimberlite petrographic variation with serpentine, calcite, phlogopite or diopside occurring as dominant groundmass phases. All of the kimberlites are either macrocrystic (up to 33 volume % macrocrysts), or sparsely macrocrystic (e.g. Silvery Home kimberlite sample *SLH 3*). Olivine macrocrysts are ubiquitous and can be serpentinised along fractures (Melton Wold, Silvery Home kimberlites), pervasively serpentinised (Droogfontein kimberlite) or sometimes calcitised in the interiors of macrocrysts (Wimbledon kimberlite). Opaque oxides may occur as inclusions in the anhedral olivine macrocrysts and the association with serpentine, suggests a possible secondary origin of the opaque oxides (Leicester kimberlite sample *JJG 6054*). Opaque oxides may also form a fine dusting over the olivine macrocrysts (Melton Wold, Silvery Home kimberlites). Phlogopite macrocrysts identified in the Wimbledon and Leicester kimberlites are characterised by typical strain features, as well as calcite stringers that have wedged open cleavage planes (Figure 3.3a, b).

Subhedral olivine phenocrysts that constitute between 10 (Leicester kimberlite sample *JJG 4328*) and 30 volume % (Melton Wold kimberlite sample *MLW 1*) of the kimberlite are also variably altered, (Figure 3.3c), but fresh olivine cores do exist in some of the Silvery Home kimberlite samples (*SLH 7, SLH 9* and *SLH 11*). Phlogopite phenocrysts present in the Wimbledon and Leicester kimberlites tend to be green in colour due to the chloritisation of the rims and fractures (Figure 3.3d). In contrast, phlogopite phenocrysts from the Silvery Home and Droogfontein kimberlites are characterised by tetraferriphlogopite rims.

The types of groundmass phases present vary between individual kimberlites, with calcite being the predominant matrix phase for the phlogopite calcite Wimbledon kimberlite and serpentine calcite Leicester kimberlite. In contrast, phlogopite is the dominant matrix phase for samples from Droogfontein (serpentine phlogopite kimberlite), Silvery Home (serpentine phlogopite and diopside phlogopite kimberlite) and Melton Wold kimberlites (phlogopite calcite kimberlite). The groundmass of the Leicester kimberlite is characterised by interstitial and segregationary calcite and serpentine, with minor equant phlogopite laths and granular monticellite (10μm in size). Wimbledon kimberlite is characterised by interstitial and segregationary calcite, as well as stubby, green, chloritised groundmass phlogopite crystals. Two distinct facies of kimberlite have been recognised in the Silvery Home kimberlite, namely diopside phlogopite kimberlite and phlogopite serpentine kimberlite, the former phase showing similarity to the Droogfontein kimberlite. Groundmass diopside crystals in the Droogfontein and Silvery Home kimberlites (*SLH 3, SLH 7* and *SLH 9*) tend to be euhedral in character and fairly small (30-50μm). A second diopside kimberlite phase, characterised by pale green coloured, irregular shaped domains with a concentric ring structure has also been recognised in the Droogfontein kimberlite. These diopside kimberlite domains are similar to microxenoliths in the Dutoitspan kimberlite, described and interpreted by Clement (1982) to represent partially resorbed fragments of country rock. Melton Wold kimberlite sample *MLW 4* is classified as a carbonated

Figure 3.3: Photomicrographs of selected features of transitional kimberlite samples. Photomicrographs are shown in plane polarised light, unless otherwise indicated.

(a) Leicester kimberlite *(JJG 4326):* Phlogopite macrocryst where cleavage planes have been wedged open by calcite stringers. Abundant opaque oxide grains also occur along the calcite stringers. Field of view is 1.2mm.
(b) Leicester kimberlite *(JJG 4328):* Kink banded phlogopite macrocryst. Cross polarised light, field of view is 1.2mm.
(c) Wimbledon kimberlite *(WIMB 1):* Serpentinised and carbonatised olivine phenocryst with an opaque oxide rim. Cross polarised light, field of view is 1.8mm.
(d) Leicester kimberlite *(JJG 4328):* Phlogopite macrocryst and a phlogopite microphenocryst. Some chloritisation has occurred along the phenocryst rim. The neighbouring calcite segregation has a distinctive tabular habit and may be an alteration product of a previous phase. Field of view is 1.2mm.
(e) Droogfontein kimberlite *(K19/2):* A coarse-grained phlogopite microphenocryst that has poikolitically enclosed some opaque oxide and perovskite crystals. Field of view is 0.4mm.
(f) Droogfontein kimberlite *(K19/2):* Euhedral perovskite crystals that have been poikolitically enclosed by phlogopite. Green serpentine also occurs as a groundmass phase in the kimberlite. Field of view is 0.4mm.

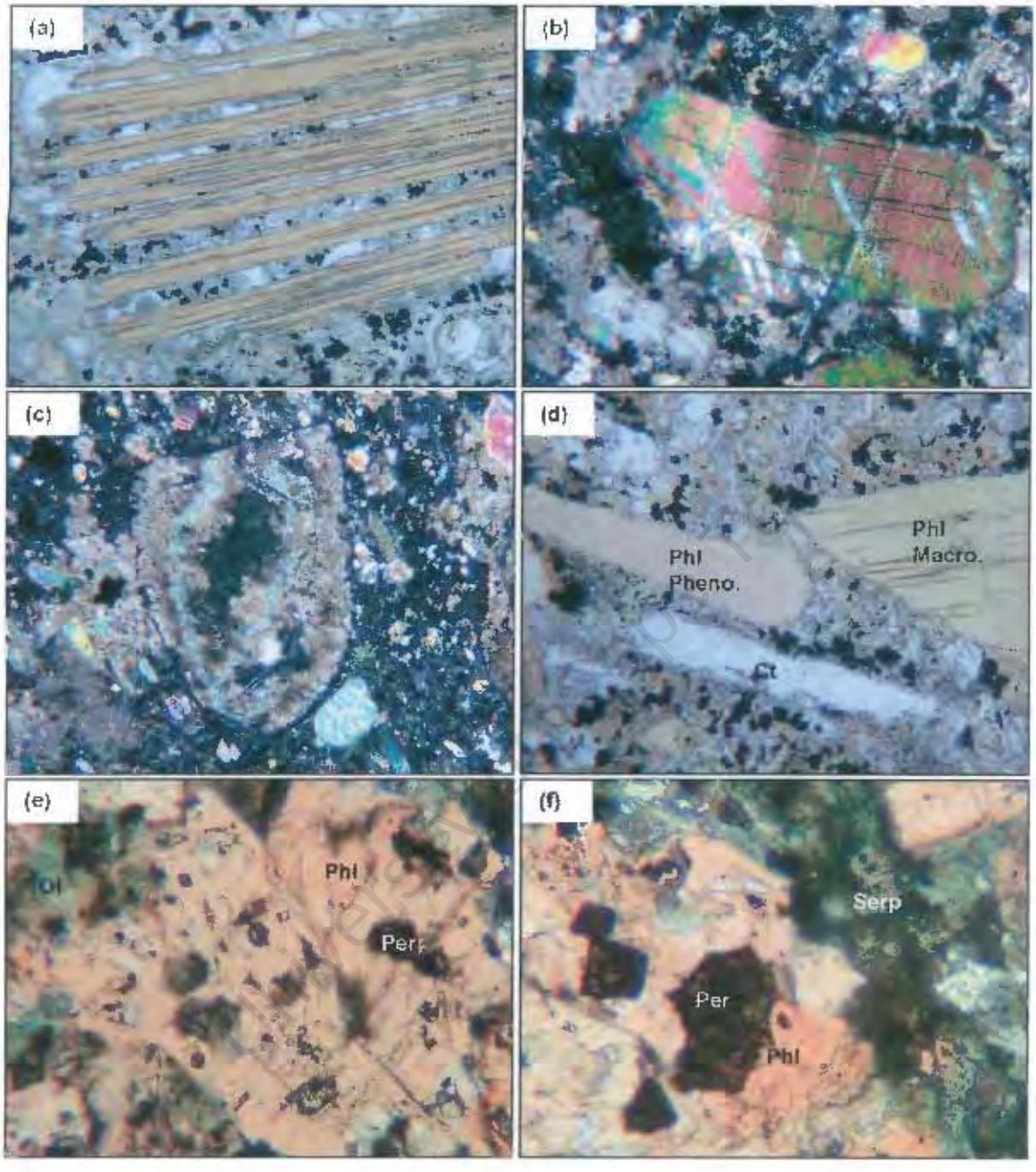
(a)
(b)
(c)
(d)
Phl
Pheno.
Phl
Macro.
Ct
(e)
Ol
Phl
Perr
(f)
Serp
Per
Phl

kimberlite since all macrocryst, phenocryst and matrix phases have been calcitised by very distinctive cross cutting calcite veins.

Equant opaque oxides (20-50μm) and euhedral perovskite crystals (50-100μm) together contribute 3-7 volume % to the kimberlite. Perovskite crystals may also be poikolitically enclosed in phlogopite crystals (Droogfontein, Silvery Home kimberlites; Figure 3.3e, f) and the perovskite crystals sometimes occur in small circular structures in the Droogfontein kimberlite. Apatite is particularly evident in the Wimbledon kimberlite (4 volume % of the kimberlite) and occurs as elongate laths or hexagonal basal sections up to 250μm in size.

3.5 Comparison of on- and off-craton kimberlites

Group I kimberlites analysed in this study are either serpentine-calcite kimberlites or calcite kimberlites and therefore show typical group I characteristics similar to the well-known on-craton Kimberley kimberlites (e.g. Clement, 1982). The only marked difference between the off-craton kimberlites and the Kimberley kimberlites is the lack of groundmass monticellite in the off-craton kimberlites, but since primary monticellite is prone to alteration by serpentine and calcite (Clement, 1982), its paucity may represent the more altered nature of the off-craton kimberlites. Off-craton kimberlites also tend to be relatively more sparsely macrocrystic in comparison to the Kimberley kimberlites (Shee, 1985; Clement, 1982) but the very macrocrystic nature of the off-craton Uintjiesberg kimberlite (Harris *et al.*, 2004), suggests that the difference is probably not significant.

Generally no systematic differences have been recognised between group II kimberlite occurrences. The relatively altered nature of some of the group II kimberlites (e.g. off-craton Brandewynskuil and Eendekuil kimberlites) also makes petrographic comparisons more ambiguous. Typically the on-craton New Elands and off-craton Brandewynskuil and Eendekuil kimberlites are similar to other on-craton kimberlite occurrences, such as the Finsch kimberlite (Clement, 1982) and Swartruggens and Star kimberlites (Coe, 2004) These kimberlites consist of fine-grained dominant groundmass phlogopite with or without diopside and typically are brown in thin section as well as hand specimen. Varying petrographic characteristics of the on-craton Newlands and Bellsbank kimberlite dykes (e.g. very fine-grained phlogopite with lesser groundmass calcite) in comparison to normal group II kimberlites are mostly just manifestations of differing crystallisation conditions. Other features of on-craton and off-craton group II kimberlites such as nature of macrocrysts and phenocrysts, abundance and size of groundmass opaque oxide and perovskite crystals are similar. Skinner *et al.* (1992) recognised the presence of groundmass sanidine and amphibole in some of the off-craton group II kimberlites from the Victoria West District, but these mineral phases have not been observed this study.

Significant differences in petrography are recognised between on- and off-craton transitional kimberlites, the first of which is the affinity of the on-craton transitional kimberlites to group I kimberlites, whereas off-craton transitional kimberlites are more petrographically similar to group II

kimberlites. On-craton transitional kimberlites are rich in groundmass calcite with lesser serpentine (Leicester kimberlite) or phlogopite (Wimbledon kimberlite). Off-craton transitional kimberlites are all rich in groundmass phlogopite, with or without minor groundmass diopside. Calcite segregations are common in the on-craton Wimbledon and Leicester kimberlites and also occur in the off-craton Melton Wold kimberlite. Groundmass monticellite is only recognised in the on-craton Leicester kimberlite. Matrix phlogopite crystals are also typically coarser grained in the off-craton kimberlites (300-500μm) than the on-craton kimberlites (~50μm).

3.6 Comparison of group I, group II and transitional kimberlites

Essential petrographic differences between the three kimberlite groups have been recognised in the nature of their groundmass and accessory minerals, both in this study and by previous authors (e.g. Mitchell, 1995; Skinner *et al.*, 1992; Skinner, 1989). Group I kimberlites are characterised by dominant groundmass calcite and serpentine (groundmass monticellite was not recognised in the kimberlites in this study), that may occur in a segregationary or interstitial groundmass texture, with accessory opaque oxides, perovskite and apatite. In contrast to group I kimberlites, group II kimberlites are dominated by groundmass phlogopite and diopside, although some very phlogopite-rich group I kimberlites have been recognised (Shee, 1985; Clement, 1982). Minor groundmass serpentine does occur in some group II kimberlites, but where it is more volumetrically abundant (e.g. Brandewynskuil kimberlite), it is probably secondary in origin. The matrix opaque oxides and perovskite crystals in group II kimberlites also tend to be smaller and sparser than in group I kimberlites. On-craton transitional kimberlites, Leicester and Wimbledon show no significant differences to group I kimberlites, whereas differences do occur between the off-craton transitional kimberlites and group II kimberlites. Both group II kimberlites and off-craton transitional kimberlites are characterised by dominant groundmass phlogopite, rimmed by tetraferriphlogopite but the matrix of the transitional kimberlites is generally not as fine-grained as group II kimberlites. In addition, perovskite and opaque oxide microphenocrysts in transitional kimberlites are slightly coarser and more abundant than in group II kimberlites. Olivine, phlogopite and opaque oxide macrocrysts are common to all kimberlite groups and although garnet macrocrysts were only observed in the group II kimberlites, this is likely just a feature of the sampling.

CHAPTER 4

MAJOR ELEMENT GEOCHEMISTRY

4.1 Introduction

Kimberlites are ultrabasic, potassic magmas that show diverse compositional variation influenced by various primary and secondary processes. Comparatively few bulk-rock major element geochemistry studies have been conducted on kimberlites (e.g. Shee, 1985; Clement, 1982), and this is perhaps due to the complex and hybrid nature of these magmas that are thought to represent the effects of a variety of petrogenetic processes (le Roex *et al.*, 2003; Dawson, 1980). Kimberlites show broad petrographic variation (Chapter 3) and the crystallisation of different phenocryst and groundmass mineral phases *viz*; serpentine, calcite, monticellite, phlogopite and diopside (Clement & Skinner, 1979), is a direct reflection of the natural variation in their bulk-rock geochemistry. Kimberlites are typically characterised by their ultramafic (atomic $Mg/(Mg+Fe^{2+}) > 0.80$-0.85), silica undersaturated ($SiO_2 < 35$-40 wt%) and potassic character ($Na_2O/K_2O < 0.5$), as well as high volatile content (up to 20 wt% CO_2 and 10 wt% H_2O^+; Coe, 2004; Harris *et al.*, 2004; le Roex *et al.*, 2003; Price *et al.*, 2000; Mitchell, 1995; Tainton, 1992; Fraser & Hawkesworth, 1992; Smith *et al.*, 1985b; Clement *et al.*, 1984).

Key studies of kimberlite bulk-rock geochemistry have shown that some of the broad variation in composition can be attributed to xenolith entrainment (Coe, 2004; Harris *et al.*, 2004; le Roex *et al.*, 2003, Fraser & Hawkesworth, 1992). Macrocrysts observed in kimberlites are thought to represent disaggregated xenolithic mantle peridotite entrained by the kimberlite (le Roex *et al.*, 2003; Clement *et al.*, 1984). Olivine and phlogopite are generally the most predominant macrocryst phases present in the kimberlites of this study, with minor diopside and garnet. Yet orthopyroxene, a constituent mineral of peridotite is not present as a macrocryst phase. Shee (1985) ascribed the absence of the silica-rich orthopyroxene to its assimilation by the silica-poor kimberlite magma. In the studies of the Uintjiesberg (Harris *et al.*, 2004) and Kimberley (le Roex *et al.*, 2003) kimberlites, up to 40% entrainment of mantle peridotite was inferred. Fraser and Hawkesworth (1992) similarly attributed the variation in the geochemistry of the Finsch kimberlite to be controlled by mixing of the primary kimberlite magma with entrained peridotite.

The major element geochemistry of kimberlite magmas can be used to characterise and understand the effect of fractional crystallisation on the primary kimberlite magma. Scott (1979) attributed the variation in the Holsteinborg kimberlites due to the fractionation of olivine and spinel, whereas Harris *et al.* (2004) recognised the effect of olivine and phlogopite fractionation in aphanitic Uintjiesberg kimberlite samples. le Roex *et al.* (2003) similarly argued for olivine plus possible calcite control on the generation of aphanitic kimberlite in the Kimberley kimberlites.

Many of the kimberlites studied here have intruded through the sedimentary sequence of the Karoo Supergroup. These shales, sandstones and mudstones have higher SiO_2, Al_2O_3, Na_2O and H_2O, as well as lower melting temperatures than the kimberlite magmas. The likelihood for melting and partial or complete assimilation of country rock material by the kimberlite magma, is therefore strong. One of the approaches that can be used to assess the degree of crustal contamination in the kimberlite is the contamination index (C.I.), defined by Clement (1982) as follows:

$$C.I. = (SiO_2 + Al_2O_3 + Na_2O)/ (MgO + 2K_2O)$$

Clement (1982) argued that a C.I. greater than unity (calculated using major element oxide weight %) indicates that the kimberlite has been contaminated. Since the numerator quantifies the proportion of clay minerals and the denominator the proportion of olivine and phlogopite, a large C.I. suggests assimilation of clay minerals (country rock). It has been recognised though, that some uncontaminated phlogopite and diopside-rich kimberlites may have a C.I. as large as 1.5 (Clement, 1982). The C.I. serves a dual purpose since it can also be used to evaluate the effect of secondary alteration, generally serpentinisation, to the kimberlite (Clement, 1982). The serpentinisation reaction is associated with a decrease in MgO and increase in volatiles in the kimberlite, caused by the difference in MgO and H_2O content between olivine and serpentine (Deer *et al.*, 1992; Mitchell, 1986). However, since kimberlites are charged with abundant volatiles (largely CO_2 and H_2O), primary alteration of the kimberlite is also likely to occur immediately following emplacement. One of the difficulties commonly faced in assessing the degree of alteration of the kimberlite is distinguishing between primary (autometasomatic) and secondary alteration (involving redistribution of mobile elements by ground water), since almost certainly some serpentinisation of olivine is associated with primary alteration (Barret & Berg, 1975). A detailed consideration of the effects of crustal contamination and alteration on major and trace element and isotope geochemistry will be presented in Chapter 8.

The primary aim of this chapter is to characterise the major element geochemistry of selected group I, group II and transitional kimberlites and then to explore some of the variation in bulk-rock geochemistry within individual kimberlite occurrences. Major element analyses of 54 on- and off-craton kimberlite samples were determined by X-ray fluorescence and are reported in Tables 4.1-4.3. Details of the sample preparation and analytical procedures are given in Appendix C and D, respectively. XRF major element analyses from Clark (1994) were used for Brandewynskuil kimberlite sample *K6/11*, Eendekuil kimberlite sample *K2/13* and Droogfontein kimberlite samples *K19/2* and *K19/5*. CO_2 concentration was determined with a karbonat bombe and analyses have not been corrected to a volatile free basis, since CO_2 and H_2O are important constituents of the kimberlite. Lack of sufficient fresh sample material precluded the measurement of CO_2 for some Droogfontein kimberlite (*K19/3*, *K19/5*, *K19/10*) and New Elands kimberlite samples (*NE K6*, *NE K10*).

Table 4.1: XRF major element analyses of on- and off-craton group I kimberlites given in weight %. All Fe is reported as Fe_2O_3, Mg-number (Mg #) is atomic Mg/(Mg + Fe^{2+}), calculated using an Fe_2O_3/FeO ratio of 0.15. H_2O^+ is defined as the difference between the loss on ignition (LOI) and CO_2 concentrations. The contamination index (CI) defined by Clement (1982) is also given for reference.

Group I kimberlites:	On-craton					Off-craton							
Kimberlite	**Goedehoop**		**Koffiefontein**			**Abbotsford E.**	**Hebron**			**Klipgatsfontein**			**Zeekoegat**
Sample	JAR 30012	JJG 4282	KK 3	KK 5	KK 6	JJG 3118	HEB 1A	HEB 1B	JJG 4295	JAR 31012	KGF1	JJG 4323	JJG 1906
% Macro.	20	15	15	20	25	10	25	25	33	25	29	27	15
SiO_2	25.64	26.10	32.10	33.29	31.35	23.45	26.35	24.66	26.25	23.58	25.07	24.96	24.80
TiO_2	2.95	3.25	2.30	1.32	1.33	2.63	3.32	3.43	2.21	2.79	2.87	2.95	2.54
Al_2O_3	2.53	2.54	3.07	1.87	1.83	3.19	2.78	2.83	2.27	2.62	3.42	3.11	3.43
Fe_2O_3	12.73	13.15	10.04	8.05	8.07	11.39	11.07	11.33	9.68	11.67	11.49	11.93	11.48
MnO	0.23	0.23	0.16	0.13	0.13	0.20	0.16	0.17	0.17	0.19	0.18	0.19	0.20
MgO	26.67	25.82	26.28	30.32	30.32	23.29	23.18	23.49	28.29	24.04	22.96	24.33	25.31
CaO	12.65	12.27	9.68	7.95	9.39	16.70	13.84	13.95	12.52	15.20	15.01	14.23	14.31
Na_2O	0.38	0.27	0.11	<0.06	n.d.	0.17	0.14	0.08	0.01	0.07	0.01	0.08	0.03
K_2O	0.22	0.23	1.43	0.73	0.56	0.20	0.50	0.47	0.89	0.20	0.60	0.39	0.26
P_2O_5	1.73	2.11	0.97	1.34	1.81	0.79	0.99	1.04	1.37	1.64	1.78	1.71	0.33
SO_3	0.08	0.10	0.47	0.12	0.15	0.41	n.d.	0.12	0.11	0.24	0.12	0.17	0.79
NiO	0.11	0.11	0.14	0.17	0.17	0.08	0.09	0.09	0.18	0.08	0.08	0.08	0.10
Cr_2O_3	0.15	0.17	0.22	0.24	0.26	0.13	0.13	0.13	0.23	0.15	0.11	0.12	0.15
H_2O^-	0.45	0.49	0.62	0.63	0.40	0.52	1.18	1.16	0.32	0.55	1.52	0.98	0.21
LOI	13.23	12.83	11.87	13.35	14.15	16.71	16.20	16.06	15.43	16.23	14.23	14.65	15.32
Total	99.75	99.67	99.46	99.52	99.90	99.84	99.93	99.00	99.91	99.23	99.43	99.88	99.24
H_2O+	6.35	6.53	6.92	9.15	8.65	6.51	6.11	5.97	4.24	5.04	2.51	3.85	4.82
CO_2	6.87	6.30	4.96	4.20	5.50	10.19	10.09	10.09	11.19	11.19	11.72	10.79	10.49
CI	1.1	1.1	1.2	1.1	1.1	1.1	1.2	1.1	0.9	1.1	1.2	1.1	1.1
100*Mg#	82.5	81.5	85.5	89.4	89.4	82.1	82.5	82.3	86.8	82.2	81.8	82.1	83.2

* *n.d. = not detected*

4.2 Group I kimberlites

The major element geochemistry of the analysed on- and off-craton group I kimberlites, reported in Table 4.1, is illustrated in Figure 4.1. Since the on-craton group I kimberlite dataset consists only of samples from the Goedehoop and Koffiefontein kimberlites, it is supplemented with analyses of the Kimberley kimberlites, recently published by le Roex *et al.* (2003). Analyses of the off-craton group I Uintjiesberg kimberlite (Harris *et al.*, 2004) have also been included for comparison, since Uintjiesberg kimberlite comprises one of the Victoria West District kimberlites.

SiO_2 and MgO concentrations of group I kimberlites show broad positive correlations (Figure 4.1a) with SiO_2 contents varying from 23.45 wt% (Abbotsford East kimberlite) to 33.29 wt% (Koffiefontein kimberlite), although samples do not extend to as low SiO_2 contents as some of the evolved aphanitic samples from the Kimberley and Uintjiesberg kimberlites (~19 wt% SiO_2; Harris *et al.*, 2004; le Roex *et al.*, 2003). Similarly, MgO contents of kimberlite samples (22.96-30.32 wt%) do not extend to as low MgO concentrations, in comparison to these reference kimberlite samples (Figure 4.1a). Most kimberlite samples in this study have 10-15 volume % olivine macrocrysts and tend to have very similar MgO concentrations and Mg-numbers (23-27 wt% MgO, 100*Mg# = 81.5-83.0; Figure 4.1a; Table 4.1). However, two of the Koffiefontein kimberlite samples are slightly more olivine macrocrystic than other kimberlite samples and have the highest MgO and lowest FeO* contents (~30.3 wt% MgO; ~7.3 wt% FeO*; Figure 4.1a, b). Nearly all of the kimberlite samples have higher FeO* contents (>10 wt%; Figure 4.1b) than the Kimberley and Uintjiesberg kimberlites, and particularly so for the Goedehoop kimberlite (~11.6 wt% FeO*).

TiO_2 and Al_2O_3 concentrations of the analysed group I kimberlites are fairly similar and both are negatively correlated with MgO, falling within the fields illustrated for the Kimberley and Uintjiesberg kimberlites (Figure 4.1c, d). The samples define narrow ranges in TiO_2 and Al_2O_3 contents from 1.32-3.43 wt% TiO_2 and 1.83-3.43 wt% Al_2O_3, with the Koffiefontein kimberlite having the lowest concentrations of these two oxides, but with the highest concentrations in the Hebron and Zeekoegat kimberlites, respectively (Table 4.1). Kimberlite samples tend to have low K_2O abundances, less than 0.89 wt% (Hebron kimberlite; Figure 4.1e), except for one of the Koffiefontein kimberlite samples that extends to 1.43 wt% K_2O (Table 4.1). Neither K_2O or P_2O_5 contents of samples show any correlation with MgO, nor do the absolute concentrations of these oxides extend to some of the higher values occurring in the aphanitic Uintjiesberg and Kimberley kimberlite samples (e.g. up to 2 wt% K_2O; 5 wt% P_2O_5; Figure 4.1e, f; Harris *et al.*, 2004; le Roex *et al.*, 2003). Na_2O contents of kimberlites are also very low and the highest analysed, is 0.38 wt% Na_2O (Goedehoop kimberlite; Table 4.1).

A well-defined negative correlation exists between CaO and SiO_2 abundances of kimberlites and similarly, a well-defined positive correlation occurs between CO_2 and CaO (Figure 4.2g, h). CaO and CO_2 concentrations tend to be the lowest in the Koffiefontein kimberlite (7.95 wt% CaO; 4.20 wt%

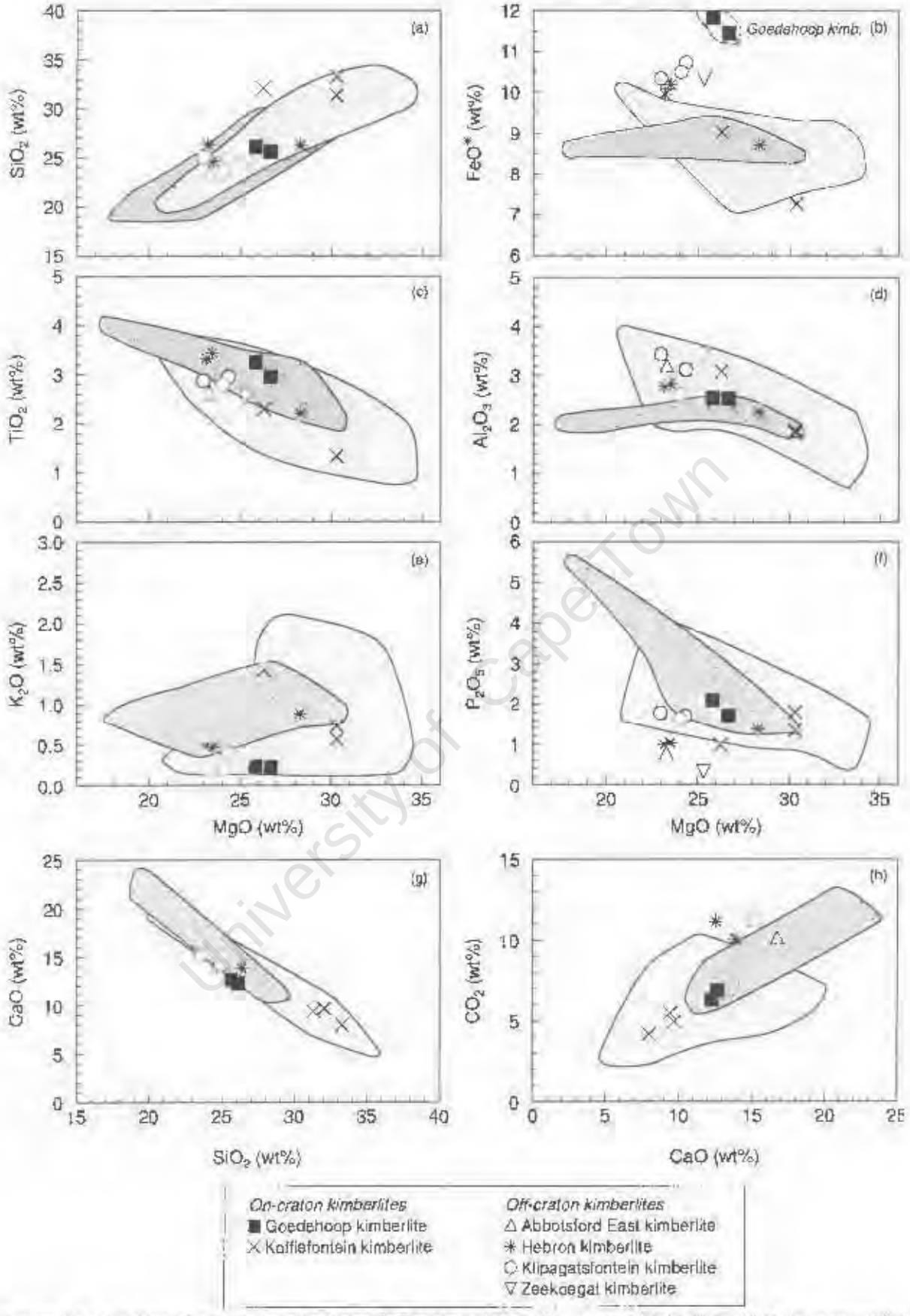

Figure 4.1: Variation of selected major elements for on- and off-craton group I kimberlites. All Fe is represented as Fe^{2+}, in the notation FeO*. Light grey shaded field represents the on-craton Kimberley group I kimberlites (le Roex *et al.*, 2003) and dark grey shaded field, the off-craton Uintjiesberg kimberlite (Harris *et al.*, 2004).

CO_2), whereas the highest CaO (16.70 wt%) and CO_2 (11.72 wt %) concentrations occur in the Abbotsford East and Klipgatsfontein kimberlites, respectively (Table 4.1). It is apparent that the off-craton kimberlites tend to higher CaO and CO_2 contents, although all of the on- and off-craton group I kimberlite samples still fall within the compositional fields defined for the Kimberley and Uintjiesberg kimberlites (Figure 4.1g, h).

4.2.1 On-craton group I kimberlites

Goedehoop kimberlite

The two on-craton Goedehoop kimberlite samples analysed are both macrocrystic (15-20 vol.% macrocrysts) and have SiO_2 and MgO concentrations that plot in the middle of the field defined for the group I Uintjiesberg and Kimberley kimberlites (Figure 4.2a). The FeO* content of both samples (11.45-11.83 wt%; Figure 4.1b) is greater than that of all other group I kimberlites and consequently the Mg-number (100*Mg# ~ 82.0) of the Goedehoop kimberlite, falls on the lower end of the range for other kimberlites (Table 4.1). TiO_2, (~3.1 wt%), Al_2O_3 (~2.5 wt%), K_2O (~0.2 wt%), CaO (~12.5 wt%) and CO_2 (~6.6 wt%) concentrations are similar for both samples (Figure 4.1c-h). The slightly higher Na_2O (0.27-0.38 wt%) and associated very low K_2O contents of the Goedehoop kimberlite results in a Na_2O/K_2O ratio greater than unity, in contrast to other group I kimberlites that have $Na_2O/K_2O < 1$.

Koffiefontein kimberlite

Three macrocrystic kimberlite samples have been analysed from the on-craton Koffiefontein kimberlite, although sample *KK 3* (15 vol.% macrocrysts) is less macrocrystic than samples *KK 5* and *KK 6* (20-25 vol.% macrocrysts). The latter two have very similar concentrations for most oxides and almost identical MgO contents (30.32 wt%; 100*Mg# = 89.4; Figure 4.1a-h), although all three samples have roughly equivalent SiO_2 concentrations (~32.2 wt%). Sample *KK 3* has comparatively lower MgO (26.28 wt%; 100*Mg# = 85.5; Table 4.1), but higher FeO* (9.03 wt%), TiO_2 (2.30 wt%), Al_2O_3 (3.07 wt%) and K_2O (1.43 wt%) contents than samples *KK 5* and *KK 6*. All three samples broadly fall within or very close to the compositional fields delineated for the on-craton Kimberley kimberlites (Figure 4.1).

4.2.2 Off-craton group I kimberlites

Abbotsford East and Zeekoegat kimberlites

The two samples analysed from the off-craton East Griqualand kimberlites are both sparsely macrocrystic containing 10 (Abbotsford East) to 15 (Zeekoegat) volume % macrocrysts. The higher Mg-number (100*Mg# = 83.2), MgO (25.31 wt%) and SiO_2 (24.80 wt%) content of the Zeekoegat kimberlite, in comparison to the Abbotsford East kimberlite (100*Mg# = 82.1; 23.29 wt% MgO; 23.45 wt% SiO_2; Table 4.1), reflects the greater abundance of olivine macrocrysts in the former (Figure 4.1a). Concentrations of FeO* (~10.3 wt%), TiO_2 (~2.6 wt%), Al_2O_3 (~3.3.wt%) and K_2O (~0.2 wt%) are generally similar (Figure 4.1b-e), whereas P_2O_5 is significantly lower in the Zeekoegat kimberlite (0.33 wt%) than in the Abbotsford East kimberlite. High CaO (16.70 wt%) and CO_2 (10.49 wt%) contents in both kimberlites, correlate with their calcite-rich nature (Section 3.2; Figure 4.1g, h).

Hebron kimberlite

Three samples from the off-craton Hebron kimberlite have been analysed, all of which are macrocrystic, although sample *JJG 4295* (33 vol.% macrocrysts) is slightly more macrocrystic, with a higher MgO concentration (28.29 wt%) and Mg-number (100*Mg# = 86.8) than samples *HEB 1A* and *HEB 1B* (25 vol.% macrocrysts; ~23.2 wt% MgO; 100*Mg# ~ 82.4; Figure 4.1a; Table 4.1). SiO_2 contents of all three kimberlite samples are fairly similar (24.66-26.35 wt%; Figure 4.1a), whereas sample *JJG 4295* has lower FeO* (8.71 wt%), TiO_2 (2.21 wt%) and Al_2O_3 concentrations (2.27 wt%; Figure 4.1d-e). CaO and CO_2 contents of all three samples tend to be comparable (~13.4 wt% CaO; ~10.5 wt% CO_2; Figure 4.1g, h). The Hebron kimberlite samples fall within or close to the compositional fields defined by the Kimberley and Uintjiesberg kimberlites (Figure 4.1).

Klipgatsfontein kimberlite

Three macrocrystic samples from the off-craton Klipgatsfontein kimberlite have been analysed, all of which tend to have similar geochemical compositions (Table 4.1). The samples have relatively low Mg-numbers (100*Mg# ~ 82.0); MgO (~23.8 wt%) and SiO_2 (~24.5 wt%) contents (Figure 4.1a; Table 4.1), that appear to be in contradiction to their macrocrystic character, but it is significant that the dominant macrocryst phase is phlogopite and not olivine (5-7 vol.% olivine macrocrysts). Klipgatsfontein kimberlite samples tend to plot within the field defined by the Kimberley and Uintjiesberg kimberlites but have notably high FeO* (~10.5 wt%) and slightly higher CO_2 (~11.2 wt%) contents (Figure 4.1).

4.3 Group II kimberlites

The variation in group II kimberlite major element geochemistry is illustrated in Figure 4.2, with individual analyses of samples reported in Table 4.2. Analyses of the on-craton group II Swartruggens and Star kimberlites (Coe, 2004) as well as the group I Kimberley kimberlites (le Roex *et al.*, 2003) are represented as fields on the graphs for comparison. The analysed group II kimberlites show broad variation in SiO_2 concentrations (Figure 4.2a) from 25.22 wt% (Eendekuil kimberlite) to 43.09 wt% (Brandewynskuil kimberlite). Variation in SiO_2 content is greater than that of the Swartruggens and Star kimberlites, but it is important to note that only unaltered and uncontaminated samples from these two kimberlites have been included (Coe, 2004). The MgO content of the kimberlites does not show a well-defined correlation with SiO_2, although intra-kimberlite correlations do exist (e.g. Markt kimberlite; Figure 4.2a). Inter-kimberlite variation in MgO concentrations and Mg-numbers is large from 10.13 wt% MgO, 100*Mg# = 70.2 (Eendekuil kimberlite) to 36.25 wt% MgO, 100*Mg# = 91.3 (Newlands kimberlite). Group II kimberlites with high MgO contents tend to be very olivine macrocrystic in character (Bellsbank, Newlands and Markt kimberlites; Table 4.2). All group II kimberlites other than the Eendekuil kimberlite (~9.6 wt% FeO*), have FeO* concentrations varying from 6.42 to 8.40 wt% (Figure 4.2b).

Table 4.2: XRF major element analyses of on- and off-craton group II kimberlites given in weight %. All Fe is reported as Fe_2O_3, Mg-number (Mg #) is atomic Mg/(Mg + Fe^{2+}), calculated using an Fe_2O_3/FeO ratio of 0.15. H_2O^+ is defined as the difference between the loss on ignition (LOI) and CO_2 concentrations. The contamination index (CI) defined by Clement (1982) is also given for reference.

Group II kimberlites: On-craton

Kimberlite	Bellsbank		New Elands			Newlands			
Sample	KBEL 2	JJG 4676	NE K6	NE K10	NE K11	JJG 24	JJG 6198	KN 2	KN 3
% Macro.	-	30	10	10	20	25	45	35	30
SiO_2	33.20	33.42	35.97	34.79	37.68	33.59	32.58	31.33	33.02
TiO_2	0.84	0.87	1.43	1.38	1.20	0.69	0.59	0.79	0.56
Al_2O_3	1.90	1.97	4.31	4.31	4.20	2.08	1.90	1.87	1.51
Fe_2O_3	7.65	7.80	9.02	9.19	9.34	7.85	7.18	7.77	7.15
MnO	0.16	0.15	0.23	0.20	0.19	0.13	0.14	0.16	0.13
MgO	30.77	31.76	23.86	23.34	28.38	32.74	32.39	36.25	32.30
CaO	7.64	8.07	8.08	8.82	3.22	6.35	7.96	6.88	7.61
Na_2O	0.04	0.12	0.23	0.23	0.14	<0.01	0.10	<0.03	<0.01
K_2O	1.88	1.89	4.56	5.03	4.07	1.26	1.12	1.12	0.53
P_2O_5	1.92	2.12	1.10	1.34	0.90	1.78	2.51	1.04	1.27
SO_3	0.20	0.10	0.03	0.04	0.13	0.24	0.26	0.08	0.55
NiO	0.17	0.17	0.12	0.11	0.15	0.20	0.18	0.19	0.20
Cr_2O_3	0.23	0.25	0.21	0.21	0.24	0.28	0.33	0.32	0.27
H_2O^-	0.77	0.44	1.57	1.94	1.75	0.43	0.24	0.21	0.54
LOI	11.92	10.26	9.21	8.97	7.90	11.45	12.35	11.06	13.74
Total	99.28	99.39	99.92	99.90	99.48	99.06	99.83	99.06	99.38
H_2O+	7.62	5.16	-	-	6.70	7.15	6.91	3.07	7.74
CO_2	4.30	5.10	-	-	1.20	4.30	5.44	7.99	6.00
CI	1.0	1.0	1.2	1.2	1.2	1.0	1.0	0.9	1.0
100*Mg#	90.0	90.2	85.6	85.1	87.2	90.4	91.0	91.3	91.0

Table 4.2 (cont.):

Group II kimberlites: Off-craton

Kimberlite	Brandewynskuil				Eendekuil					Markt			
Sample	K6/8	K6/11*	K6/12	K6/14	EKL 1	K2/2	K2/3	K2/9	K2/13*	JJG 2314	JJG 2336	MRK 1	MRK 3
% Macro.	25	20	30	30	25	25	30	30	25	30	25	30	20
SiO_2	43.09	41.01	38.99	42.58	38.17	31.81	25.22	29.33	30.17	34.40	30.28	33.54	31.53
TiO_2	0.98	1.24	1.42	1.20	2.96	2.55	2.56	3.11	2.71	0.69	0.91	0.72	0.86
Al_2O_3	8.36	6.43	6.52	8.61	4.47	5.42	5.53	7.57	5.95	3.42	2.84	3.40	2.74
Fe_2O_3	7.14	7.67	8.33	7.55	11.77	9.69	9.65	11.93	10.27	7.28	7.50	7.35	7.63
MnO	0.11	0.11	0.13	0.12	0.18	0.18	0.21	0.18	0.18	0.14	0.16	0.15	0.16
MgO	17.58	20.40	20.66	18.21	12.86	10.67	10.13	12.63	11.23	29.76	26.83	28.04	27.14
CaO	5.32	6.15	6.28	5.53	14.38	18.26	21.27	13.71	17.96	7.68	11.53	9.02	10.73
Na_2O	0.82	0.36	0.42	0.58	0.35	0.07	0.45	0.32	0.08	0.10	0.07	0.02	0.03
K_2O	3.38	3.17	3.05	3.98	4.08	4.15	3.61	4.88	4.33	2.64	2.28	2.85	2.32
P_2O_5	0.81	1.06	1.17	1.25	1.51	0.97	0.95	0.97	0.77	1.31	1.93	1.40	1.69
SO_3	0.02	-	0.01	0.01	0.08	0.61	0.29	0.09	-	0.05	0.01	0.07	0.02
NiO	0.07	-	0.12	0.09	0.03	0.04	0.04	0.05	-	0.15	0.10	0.14	0.11
Cr_2O_3	0.13	-	0.24	0.19	0.07	0.08	0.09	0.08	-	0.21	0.25	0.20	0.28
H_2O^-	6.12	3.97	6.89	5.09	0.36	0.56	1.13	1.68	0.78	0.79	0.41	0.63	0.32
LOI	5.85	8.42	5.36	4.83	8.63	14.41	18.14	12.50	15.50	10.95	14.04	11.69	13.55
Total	99.79	99.99	99.60	99.81	99.90	99.46	99.25	99.00	99.93	99.56	99.17	99.21	99.11
H_2O+	4.99	8.22	5.34	4.83	0.13	0.02	3.06	0.11	2.41	5.45	7.41	5.79	7.16
CO_2	0.86	0.20	0.02	n.d.	8.49	14.39	15.07	12.39	13.09	5.50	6.64	5.90	6.40
Cl	2.1	1.8	1.7	2.0	2.0	2.0	1.8	1.7	1.8	1.1	1.1	1.1	1.1
100*Mg#	84.7	85.7	84.8	84.4	71.1	71.2	70.2	70.4	71.1	90.2	88.9	89.6	88.9

* Brandewynskuil kimberlite sample *K6/11* and Eendekuil kimberlite sample *K2/13* have major element XRF analyses from Clark (1994). CO_2 analyses performed in this study.

** n.d. = not detected

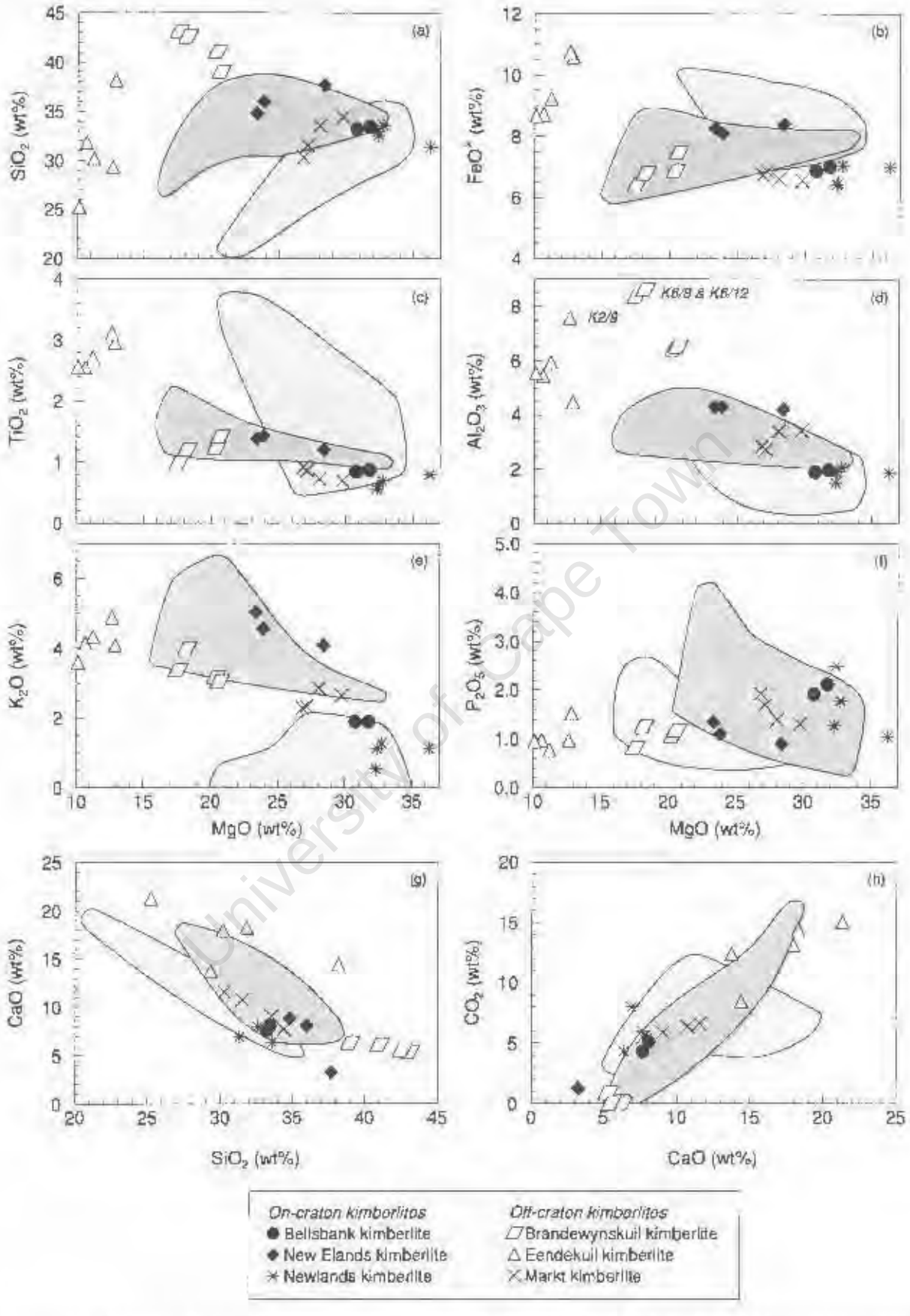

Figure 4.2: Variation of selected major elements for on- and off-craton group II kimberlites. All Fe is represented as Fe^{2+}, in the notation FeO*. Dark grey shaded field represents the on-craton Swartruggens and Star kimberlite dykes (Coe, 2004) and light grey shaded field, the on-craton group I Kimberley kimberlites (le Roex *et al.*, 2003).

TiO_2 and Al_2O_3 concentrations are negatively correlated with MgO (Figure 4.2c, d), and the analysed kimberlites, other than the Eendekuil and Brandewynskuil kimberlites, show similar concentrations of these oxides to the Swartruggens and Star kimberlites. The Eendekuil kimberlite has the highest TiO_2 concentration (3.11 wt%) and Brandewynskuil kimberlite, the highest Al_2O_3 concentration (8.61 wt%) compared to all other group II kimberlites, whereas the Newlands kimberlite has the lowest concentrations of these two oxides (0.56 wt% TiO_2, 1.51 wt% Al_2O_3; Table 4.2). K_2O contents of the Newlands and Bellsbank kimberlites are very low (0.53-1.89 wt%) and fall well outside of the range observed for other analysed kimberlites (2.28-5.03 wt%) as well as the Swartruggens and Star kimberlites (Figure 4.2e). A characteristic feature of the Swartruggens kimberlite is its K_2O enrichment (up to 6.5 wt%; Coe, 2004), but this feature is not shared by the analysed group II kimberlites of this study. The P_2O_5 concentration of the kimberlites varies from 0.77 wt% (Eendekuil kimberlite) to 2.51 wt% (Newlands kimberlite; Figure 4.2f).

Group II kimberlites show moderately large variation in CaO concentrations from 3.22 wt% (New Elands kimberlite; Figure 4.2g) up to 21.27 wt% (Eendekuil kimberlite) and the CaO content of the kimberlites correlates well with SiO_2, as well as with CO_2 (Figure 4.2g, h). CO_2 contents of some of the group II kimberlite samples approach zero (Brandewynskuil and New Elands kimberlites; Table 4.2) and are most likely below the detection limit of the karbonat bombe analytical technique (Appendix C). The highest CO_2 concentration of the group II kimberlites is 15.07 wt% (Eendekuil kimberlite) and is comparable to the highest CO_2 contents of the Swartruggens and Star kimberlites (Figure 4.2h).

4.3.1 On-craton group II kimberlites

Bellsbank kimberlite

One of the analysed on-craton Bellsbank kimberlite samples (*JJG 4676*) is macrocrystic (30 vol.% macrocrysts) and the geochemical similarity of sample *KBEL 2*, for which no thin section exists, is interpreted as evidence of the macrocrystic nature of that sample. Both samples have moderate SiO_2 contents (~33.3 wt%), with high MgO concentrations and Mg-numbers (~31.4 wt% MgO; 100*Mg# ~90.1; Figure 4.2a; Table 4.2). FeO*, TiO_2, Al_2O_3, CaO and CO_2 contents of both samples fall towards the lower limit of the compositional field defined for the on-craton Swartruggens and Star kimberlites (Figure 4.2b-h). The analysed samples also have particularly low K_2O contents (1.88 wt%, Figure 4.2e) for group II kimberlites and fall just within the field defined for the group I Kimberley kimberlites.

New Elands kimberlite

Three samples from the on-craton New Elands kimberlite were analysed, two of which are sparsely macrocrystic (*NE K6*, *NE K10*) and the third, macrocrystic (20 vol.% macrocrysts; *NE K11*). Sample *NE K11* is accordingly more SiO_2 (37.68 wt%) and MgO-rich (28.38 wt% MgO; 100*Mg# = 87.2) than the sparsely macrocrystic samples (Figure 4.2a; Table 4.2). Variation in most other oxide concentrations is however, limited (e.g. 1.20-1.43 wt% TiO_2; 4.20-4.31 wt% Al_2O_3; Figure 4.2c, d). New Elands kimberlite samples generally fall within the compositional fields of the on-craton group II Swartruggens and Star kimberlites (Figure 4.2 a-g).

Newlands kimberlite

Four samples from the on-craton Newlands kimberlite have been analysed, all of which are macrocrystic (25-45 vol.% macrocrysts), with high MgO concentrations (32.30-36.25 wt%; Figure 4.2a) and Mg-numbers (100*Mg# = 90.4-91.3; Table 4.2). Little intra-kimberlite variation exists within the Newlands kimberlite (e.g. 31.33-33.59 wt% SiO_2; 1.51-2.08 wt% Al_2O_3 and 6.35-7.96 wt% CaO; Table 4.2). The compositions rarely fall within the Swartruggens and Star group II kimberlite fields (e.g. Figure 4.2c), but tend to show more geochemical similarity to the Bellsbank kimberlite, particularly with respect in their unusually low K_2O concentration (0.56-1.26 wt%; Figure 4.2e).

4.3.2 Off-craton group II kimberlites

Brandewynskuil kimberlite

Samples from the off-craton Brandewynskuil kimberlite are all macrocrystic (20-30 vol.% macrocrysts), but are characterised by relatively low MgO (~19.2.5 wt%; Figure 4.2a) and FeO* concentrations (~6.9 wt%; Figure 4.2b), although still having moderate Mg-numbers (100*Mg# ~84.9; Table 4.2). In contrast, SiO_2 (~41.4 wt%) and Al_2O_3 contents are comparatively high (Figure 4.2a, d), with samples *K6/8* and *K6/14* having distinctly higher Al_2O_3 (~8.5 wt%) than samples *K6/11* and *K6/12* (~6.5 wt%). High SiO_2, Al_2O_3, C.I. (1.7-2.1) and H_2O^- (3.97-6.89 wt%) as well as negligible CO_2 (< 0.86 wt%, Figure 4.2h; Table 4.2) suggest extensive contamination/alteration of these two kimberlite samples (discussed in detail in Section 8.2 and 8.3). With the exception of having higher SiO_2 and Al_2O_3, as well as lower CaO, the Brandewynskuil kimberlite generally falls within the compositional field defined for the on-craton group II Swartruggens and Star kimberlites (Figure 4.2a-h).

Eendekuil kimberlite

Five macrocrystic samples from the off-craton Eendekuil kimberlite have been analysed and are characterised by unusually low MgO concentrations (10.13-12.86 wt%; Figure 4.2a) and moderately high FeO* contents (8.68-10.59 wt%; Figure 4.2b), resulting in low Mg-numbers (100*Mg# = 70.2-71.2; Table 4.2). Inter-sample variation with respect to SiO_2 (25.22-38.17 wt%), Al_2O_3 (4.47-7.57 wt%), CaO (13.71-21.27 wt%) and CO_2 (8.49-15.07 wt%) concentrations is substantial (Figure 4.2) and the Eendekuil kimberlite in general, has compositions clearly distinct from the on-craton group II Swartruggens and Star kimberlites with possible exception of K_2O, CO_2 and CaO (Figure 4.2e, g, h).

Markt kimberlite

Four samples from the off-craton Markt kimberlite have been analysed and all of the samples are macrocrystic (20-30 vol.% macrocrysts; Table 4.2). SiO_2 (30.28-34.40 wt%) and MgO (26.83-29.76 wt%) concentrations of samples show good positive correlations (Figure 4.2a), whereas FeO* (6.55-6.86 wt%) and TiO_2 (0.69-0.91 wt%) concentrations, correlate negatively with MgO (Figure 4.2b, c) and Mg-number (100*Mg# = 88.9-90.2; Table 4.2). Similarly, good correlations between SiO_2, CaO and CO_2 exist for the samples (Figure 4.2g, h). Markt kimberlite samples generally fall within the compositional range defined for the on-craton group II Swartruggens and Star kimberlites, although TiO_2 (Figure 4.2c) and K_2O (Figure 4.2e) contents of Markt kimberlite samples are slightly lower.

4.4 Transitional kimberlites

Major element analyses of the transitional kimberlites are reported in Table 4.3 and illustrated in Figure 4.3, with comparative fields for the group I Kimberley kimberlites (le Roex *et al.*, 2003) and group II Swartruggens and Star kimberlites (Coe, 2004). SiO_2 content varies from 26.80 wt% (Leicester kimberlite; Figure 4.3a) to 40.39 wt% (Silvery Home kimberlite), except for Melton Wold kimberlite sample *MLW 4* that has particularly low SiO_2 (19.80 wt%). Samples with high SiO_2 concentrations (Droogfontein and Silvery Home kimberlites) are associated with the presence of matrix diopside. MgO concentrations and Mg-numbers of samples correlate well with SiO_2 contents and vary from 21.39-32.70 wt% MgO and 100*Mg# = 83.1-90.0 (Figure 4.3a; Table 4.3), excluding Melton Wold kimberlite sample *MLW 4* that has unusually low MgO and FeO* (Figure 4.3a, b). FeO* contents of the transitional kimberlites tend to be less than 9.18 wt% (Figure 4.3b; Droogfontein kimberlite). The transitional kimberlites tend to broadly overlap the compositional fields of the group I Kimberley and group II Swartruggens and Star kimberlites (Figure 4.3a, b).

TiO_2 (0.79-3.20 wt%) and Al_2O_3 (1.76-4.28 wt%) concentrations show broad negative correlations with MgO and generally fall within the fields defined for the reference group I and group II kimberlites (Figures 4.3c, d). The Droogfontein kimberlite however, is an exception, since its Al_2O_3 concentration (6.31-6.85 wt%) is considerably higher than that of any other reference group I and group II kimberlites (Figure 4.3d). K_2O concentrations of kimberlites vary between 0.10 and 3.22 wt% (Melton Wold and Silvery Home kimberlites, respectively) and generally fall within the field defined for group I kimberlites (Figure 4.3e), although some of the samples with high SiO_2 (Droogfontein and Silvery Home kimberlites), are slightly more enriched in K_2O and show more similarity to the field defined for the group II Swartruggens and Star kimberlites (Figure 4.3e). P_2O_5 contents of the kimberlites are all less than 2.77 wt% (Figure 4.3f; Leicester kimberlite).

The analysed transitional kimberlite samples show a well-defined negative correlation between CaO and SiO_2 concentrations that vary between 4.23 wt% (Silvery Home kimberlite; Figure 4.3g) and 17.22 wt% CaO (Leicester kimberlite). The CaO (34.89 wt%) and CO_2 (27.67 wt%) contents of Melton Wold kimberlite sample *MLW 4* are however, the highest concentrations of all the transitional, group I and group II kimberlites (Figure 4.3g, h). CO_2 concentrations for other transitional kimberlites vary between negligible CO_2 (Droogfontein and Silvery Home kimberlite) and 13.39 wt% CO_2 (Leicester kimberlite). Samples tend to show a well-developed positive correlation between CaO and CO_2 contents and fall within the reference field defined for group I and group II kimberlites (Figure 4.3h).

4.4.1 On-craton transitional kimberlites

Leicester kimberlite

Three macrocrystic samples from the on-craton Leicester kimberlite have been analysed and their MgO concentrations (21.39-31.21 wt% MgO; 100*Mg# = 87.8-89.5; Figure 4.3a; Table 4.3) vary in accordance with the relative proportion of olivine macrocrysts (5-25 vol.% olivine macrocrysts). Although the variation in MgO and FeO* contents (5.53-7.43 wt%; Figure 4.3b) is significant, the

Table 4.3: XRF major element analyses of on- and off-craton transitional kimberlites given in weight %. All Fe is reported as Fe_2O_3, Mg-number (Mg #) is atomic Mg/(Mg + Fe^{2+}), calculated using an Fe_2O_3/FeO ratio of 0.15. H_2O^+ is defined as the difference between the loss on ignition (LOI) and CO_2 concentrations. The contamination index (CI) defined by Clement (1982) is also given for reference.

Transitional kimberlites:	On-craton					Off-craton			
Kimberlite	**Leicester**			**Wimbledon**		**Droogfontein**			
Sample	JJG 4326	JJG 4328	JJG 6054	WIMB 1	WIMB 2	K19/2*	K19/3	K19/5*	K19/10
% Macro.	25	25	38	30	30	15	15	15	15
SiO_2	27.04	26.80	28.77	29.21	30.13	36.07	36.33	35.98	36.91
TiO_2	1.97	1.58	1.49	0.92	0.95	3.20	3.10	3.17	3.02
Al_2O_3	2.85	4.14	1.76	1.88	2.18	6.70	6.85	6.48	6.31
Fe_2O_3	8.45	6.15	8.26	7.38	7.59	10.20	9.68	10.14	9.72
MnO	0.18	0.13	0.18	0.16	0.17	0.17	0.17	0.18	0.17
MgO	26.95	21.39	31.21	27.98	29.74	22.25	22.85	22.69	23.47
CaO	13.83	17.22	8.69	11.26	8.10	7.68	8.40	7.42	7.66
Na_2O	0.09	<0.06	0.05	0.03	0.27	0.05	0.11	0.04	0.12
K_2O	0.97	2.62	0.79	1.18	1.16	2.72	2.26	2.71	2.48
P_2O_5	2.77	2.68	1.23	2.18	2.13	2.03	1.69	2.00	1.52
SO_3	0.13	0.25	0.11	0.67	0.13	-	0.10	-	0.11
NiO	0.11	0.09	0.14	0.16	0.16	-	0.11	-	0.12
Cr_2O_3	0.29	0.23	0.21	0.25	0.28	-	0.19	-	0.17
H_2O^-	0.33	0.25	0.38	0.64	0.46	1.49	0.92	1.50	1.44
LOI	13.94	15.51	16.41	15.23	15.65	7.34	6.53	7.50	6.52
Total	99.91	99.03	99.68	99.13	99.09	99.90	99.29	99.81	99.76
H_2O+	4.15	2.12	6.02	6.44	5.66	7.14	-	-	-
CO_2	9.79	13.39	10.39	8.79	9.99	0.20	-	-	-
CI	1.0	1.2	0.9	1.0	1.0	1.5	1.6	1.5	1.5
100*Mg#	87.8	88.7	89.5	89.5	89.8	83.1	84.1	83.4	84.4

* Droogfontein kimberlite samples *K19/2* and *K19/5* have major element XRF analyses from Clark (1994). CO_2 analyses performed in this study.

Table 4.3 (cont.):

Transitional kimberlites: Off-craton

Kimberlite	Melton Wold			Silvery Home						
Sample	MLW 1	MLW 3	MLW 4	JAR 21022	SLH 1	SLH 3	SLH 7	SLH 9	SLH 10	SLH 11
% Macro.	20	15	20	15	20	10	15	15	15	15
SiO_2	32.85	33.64	19.80	34.69	35.23	40.39	39.26	39.97	35.05	34.30
TiO_2	0.79	1.02	1.23	1.69	1.43	1.62	1.96	2.61	1.64	1.61
Al_2O_3	1.86	2.40	2.43	2.32	3.19	4.11	4.28	3.95	3.71	3.47
Fe_2O_3	8.16	7.96	5.28	9.17	8.45	8.25	9.22	9.41	8.42	8.28
MnO	0.13	0.14	0.38	0.14	0.14	0.10	0.14	0.15	0.14	0.14
MgO	32.70	31.08	4.83	30.82	32.48	25.94	28.28	27.80	31.49	31.28
CaO	6.44	6.84	34.89	4.91	3.87	5.64	6.22	6.92	4.51	4.23
Na_2O	<0.02	<0.05	0.39	0.18	0.04	0.05	0.37	0.26	0.19	0.26
K_2O	1.16	1.82	0.10	2.24	1.59	3.22	2.41	3.00	1.40	1.56
P_2O_5	0.49	0.46	0.66	0.77	0.56	0.16	0.47	0.27	0.56	0.57
SO_3	0.09	0.25	0.11	0.31	0.25	0.34	0.03	0.04	0.06	0.08
NiO	0.20	0.18	0.14	0.18	0.18	0.18	0.15	0.14	0.17	0.17
Cr_2O_3	0.27	0.25	0.21	0.24	0.26	0.24	0.24	0.23	0.27	0.28
H_2O^-	0.55	0.18	0.23	0.25	0.40	1.21	0.91	0.31	0.62	0.69
LOI	13.28	12.93	28.82	11.65	11.16	8.22	5.38	4.69	11.74	12.19
Total	99.12	99.29	99.20	99.57	99.23	99.67	99.32	99.76	99.99	99.11
H_2O+	8.71	8.83	1.15	8.46	9.56	5.02	0.91	4.43	10.25	9.94
CO_2	4.57	4.10	27.67	3.20	1.60	3.20	n.d.	0.26	1.50	2.25
Cl	1.0	1.0	4.5	1.1	1.1	1.4	1.3	1.3	1.1	1.1
100*Mg#	90.0	89.8	67.3	88.3	89.6	87.6	87.3	86.9	89.4	89.5

** n.d. = not detected

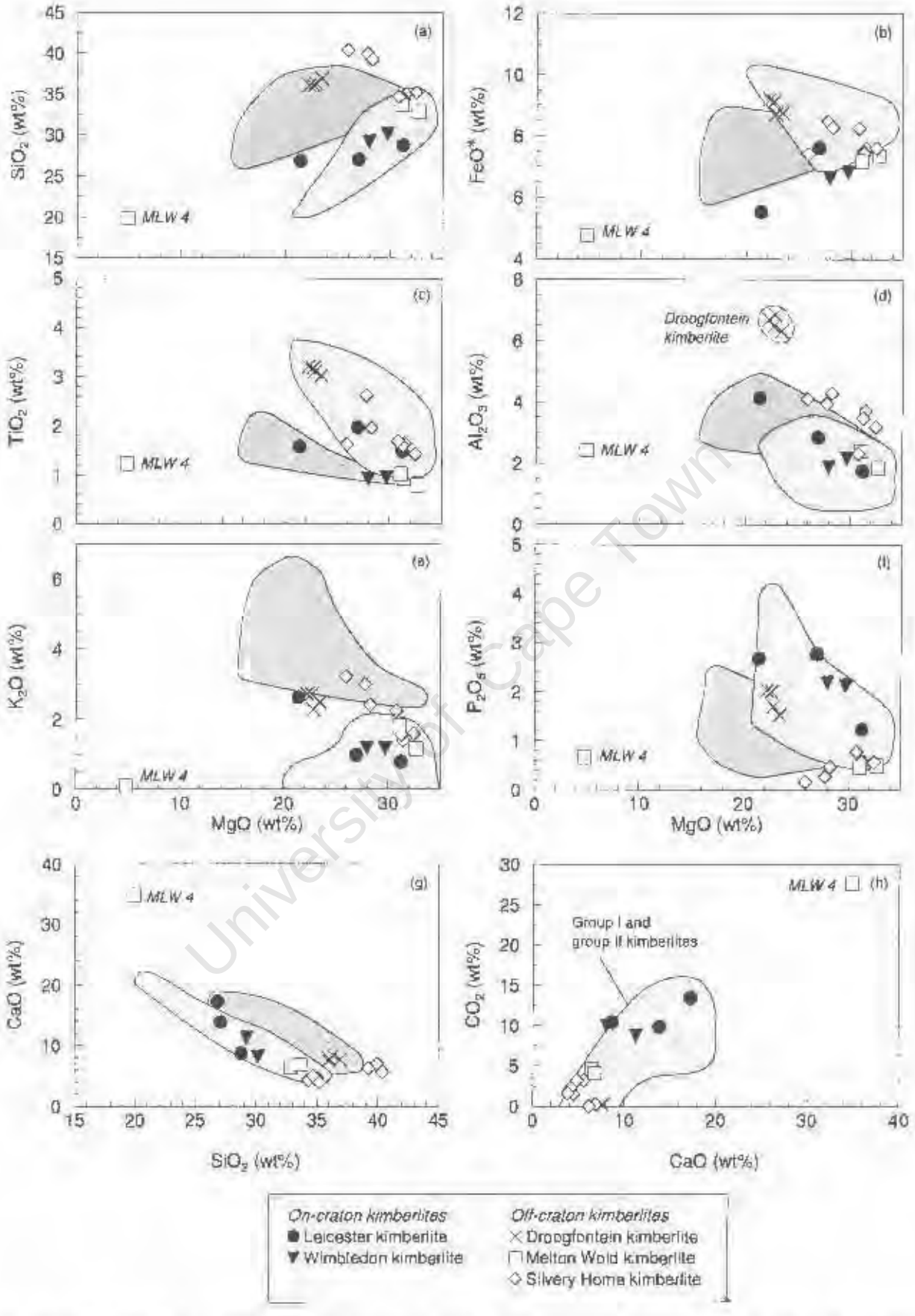

Figure 4.3: Variation of selected major elements for on- and off-craton transitional kimberlites. All Fe is represented as Fe^{2+}, in the notation FeO*. Light grey shaded field represents the group I Kimberley kimberlites (le Roex *et al.*, 2003) and dark grey shaded field, group II Swartruggens and Star kimberlites (Coe, 2004).

variation in SiO_2 concentration is particularly small (26.80-28.77 wt%; Figure 4.3a). Leicester kimberlite sample *JJG 4328* is characterised by FeO* (5.53 wt%), Al_2O_3 (4.14 wt%), K_2O (2.62 wt%), CaO (17.22 wt%) and CO_2 (13.39 wt%) concentrations that are different to samples *JJG 4326* and *JJG 6054* (Table 4.3) and consistent with petrographic evidence that suggests possible alteration and contamination of this sample. Samples *JJG 4326* and *JJG 6054* generally plot within the compositional fields defined for the group I Kimberley kimberlites (Figure 4.3).

Wimbledon kimberlite

Two macrocrystic samples from the on-craton Wimbledon kimberlite have been analysed and samples tend to have similar compositions. Both samples are MgO-rich (27.98-29.74 wt%; 100*Mg# ~89.7; Figure 4.3a; Table 4.3) with moderately low concentrations of FeO* (6.64-6.83 wt%), TiO_2 (0.92-0.95), Al_2O_3 (1.88-2.18 wt%) and K_2O (1.16-1.18 wt%; Figure 4.3b-e). The Wimbledon kimberlite samples show good overlap with the compositional field defined for the group I Kimberley kimberlites.

4.4.2 Off-craton transitional kimberlites

Droogfontein kimberlite

Samples from the off-craton Droogfontein kimberlite are all macrocrystic (15 vol.% macrocrysts) and have relatively low MgO contents and Mg-numbers (~22.5 wt% MgO; 100*Mg# ~83.8), as well as high SiO_2 (~36.0 wt%) and FeO* (~8.9 wt%) concentrations (Figure 4.3a, b; Table 4.3). The four analysed samples are similar in composition and are marked by high TiO_2 (~3.2 wt%) and Al_2O_3 (~6.6 wt%) concentrations. High SiO_2, Al_2O_3 and very low CO_2 contents of the kimberlite samples (0.2 wt% CO_2 for sample *K19/2;* Table 4.3), in addition to the petrographic identification of diopside-rich domains, suggests that the Droogfontein kimberlite is crustally contaminated (see Section 8.3). In composition, the Droogfontein kimberlite tends to variably overlap with both the fields defined for group I and group II kimberlites, depending on the element in question (e.g. Figure 4.3a or c).

Melton Wold kimberlite

Three samples from the off-craton Melton Wold kimberlite have been analysed, all of which are macrocrystic in character. Samples *MLW 1* and *MLW 3* are similar in geochemical character with high SiO_2 (~33.2 wt%), MgO (~31.9 wt%) and Mg-number (100*Mg# ~89.9), but low Al_2O_3 (~2.1 wt%), K_2O (~1.5 wt%), CaO (~6.6 wt%) and CO_2 (4.3 wt%) concentrations (Figure 4.3a-h). Sample *MLW 4* however, is characterised by very low MgO (4.83 wt%; Table 4.3), FeO* (4.76 wt%) and SiO_2 (19.80 wt%), but very high CaO (34.89 wt%) and CO_2 (27.67 wt%), which is consistent with petrographic evidence suggesting widespread calcitisation of the kimberlite sample. Melton Wold kimberlite samples *MLW 1* and *MLW 3* generally overlap the fields defined for group I and group II kimberlites although for K_2O, the samples are more similar to group I kimberlites (Figure 4.3a-h).

Silvery Home kimberlite

Seven samples from the off-craton Silvery Home kimberlite were analysed in order to ensure representation of both petrographic facies of kimberlite. The diopside kimberlite phase (samples *SLH 3, SLH 7, SLH 9*) is characterised by lower MgO (25.94-28.28 wt%; 100*Mg# = 86.9-87.8), but higher SiO_2 (39.26-40.39 wt%), Al_2O_3 (3.95-4.28 wt%) and K_2O (2.41-3.22 wt%) concentrations (Figure 4.3a, d, e) relative to samples dominated by groundmass serpentine and phlogopite (*JAR 21022, SLH 1, SLH 10, SLH 11*). However, FeO* (7.42-8.47 wt%) and TiO_2 (1.43-2.61 wt%) contents are similar for both facies of kimberlite (Figure 4.3b, c). Other than the high SiO_2, low CaO and CO_2 concentrations of the samples, the Silvery Home kimberlite is generally comparable in composition with the concentrations of reference group I and group II kimberlites (Figure 4.3a-h), showing similarities to group I kimberlites for some oxides (e.g. TiO_2; Figure 4.3c) and to group II kimberlites, for others (e.g. Al_2O_3; Figure 4.3d).

CHAPTER 5

TRACE ELEMENT GEOCHEMISTRY

5.1 Introduction

The trace element geochemistry of kimberlites is particularly interesting since these unique alkaline rocks are characterised by an unusual enrichment of both compatible (200-1900ppm Ni, 500-2500ppm Cr) and incompatible trace elements (60-400ppm La, 60-450ppm Nb, 150-670ppm Zr; Coe, 2004; Harris *et al.*, 2004; le Roex *et al.*, 2003; Tainton, 1992; Smith *et al.*, 1985b; Nixon *et al.*, 1983). Chondrite and primitive mantle normalised diagrams of kimberlites characteristically have steep patterns indicative of the incompatible element enrichment and relative heavy rare earth element depletion of kimberlite samples (le Roex *et al.*, 2003; Tainton & McKenzie, 1994). Historically, studies of the trace element geochemistry of kimberlites have either been used in a qualitative sense to characterise the kimberlite (e.g. Nixon *et al.*, 1983; Dawson, 1980; Wedepohl & Muramatsu, 1979; Fesq *et al.*, 1975), or as a means to discriminate between group I, group II and transitional kimberlites (e.g. Clark, 1994; Smith *et al.*, 1985b). More recently, there has been a tendency to use trace elements in a quantitative manner, to establish the geochemistry of primary kimberlite magmas and thereafter unravel the nature of melting processes, to characterise the source region geochemistry and to understand source region evolution (Chalapathi Rao *et al.*, 2004; Coe, 2004; Harris *et al.*, 2004; le Roex *et al.*, 2003; Beard *et al.*, 1998; Tainton & McKenzie, 1994; Fraser & Hawkesworth, 1992).

Trace elements are subdivided into various groups defined by their behaviour and the primary subdivision is into compatible and incompatible elements according to their calculated partition coefficient (D), defined as follows:

$$D = \frac{(\text{Concentration X})_{\text{Mineral}}}{(\text{Concentration X})_{\text{Liquid}}}$$

Compatible elements have D greater than unity and are preferentially partitioned into solid phases rather than the liquid phase, whereas incompatible elements (D < 1) are preferentially partitioned into the liquid phase. Elements such as V, Cr, Co, Ni, Cu and Zn are usually incorporated into olivine, spinel, clinopyroxene, phlogopite and ilmenite (Jang & Naslund, 2003; Duke, 1976), minerals that often occur as macrocrysts in kimberlite magmas and one would therefore expect the more macrocrystic kimberlites to be enriched in these compatible elements. In contrast, the incompatible element concentrations of kimberlites are enriched by fractional crystallisation and can be incorporated into groundmass phases such as calcite and accessory minerals; e.g. apatite and perovskite (Jones & Wyllie, 1984; Fesq *et al.*, 1975). Incompatible elements can be further divided into the large ion lithophile elements (LIL), high field strength elements (HFS) and rare earth elements (REE) according to various physical characteristics.

As mentioned in Chapter 4, kimberlites are prone to alteration that may disturb the concentrations of the mobile trace elements (e.g. Rb, U), as well as contamination that may either dilute or enrich concentrations of specific elements (e.g. Zr, Hf, Pb, heavy REE; Coe, 2004; le Roex *et al.*, 2003), and therefore disguise the composition of the primary magma. However, the chief aim of this chapter is to describe the trace element geochemistry of group I, group II and transitional kimberlite samples with further discussion of alteration and contamination in Chapter 8. The concentrations of over 30 trace elements in 54 kimberlite samples were determined by X-ray fluorescence (XRF) and inductively coupled plasma-mass spectrometry (ICP-MS) and the results are reported in Tables 5.1-5.3. Appendix C and D give further details of the sample preparation procedure and specifications of the analytical techniques used. Ni and Cr concentrations determined on fusion discs have preferentially been used instead of those determined on pressed powder briquettes or by ICP-MS (Appendix D). Zr and Nb analyses by XRF have also been preferentially used over ICP-MS determinations (Appendix C). XRF trace element analyses by Clark (1994) for Brandewynskuil kimberlite sample *K6/11*, Eendekuil kimberlite sample *K2/13* and Droogfontein kimberlite samples *K19/2* and *K19/5* have been incorporated into the kimberlite data set.

5.2 Group I kimberlites

The variation of selected ferromagnesian element concentrations with MgO for group I kimberlites is shown in Figure 5.1, with compositional fields of the on-craton group I Kimberley kimberlites (le Roex *et al.*, 2003) and the off-craton Uintjiesberg kimberlite (Harris *et al.*, 2004), illustrated for reference. Ni concentrations correlate positively with MgO (Figure 5.1a) and vary from 595ppm (Klipgatsfontein kimberlite) to 1377ppm (Hebron kimberlite) and broadly overlap both the Kimberley and Uintjiesberg kimberlite fields (Figure 5.1a). Cr contents show similar positive correlation with MgO (Figure 5.1b) and vary from 754ppm (Klipgatsfontein kimberlite) to 1795ppm (Koffiefontein kimberlite), whereas the Co concentration range is more limited (74.1-102ppm), showing a very shallow positive slope with MgO (Figure 5.1c). Sc however, shows a broad negative correlation with MgO and with samples generally overlapping the compositional fields of the Kimberley and Uintjiesberg kimberlites (Figure 5.1d).

LIL element concentrations of the analysed group I kimberlites generally overlap the compositional fields of the on-craton Kimberley and off-craton Uintjiesberg kimberlites (Figure 5.2), and tend to show a scattered distribution with the more immobile element La. Most samples have less than 50ppm Rb, except for one of the Koffiefontein kimberlite samples (Figure 5.2a). In contrast, samples are considerably more enriched in Sr and Ba (447-1470ppm Sr, 168-1572ppm Ba; Figure 5.2b, c). Pb contents tend to be very low, with the highest concentration occurring in the Koffiefontein kimberlite (12.9ppm; Figure 5.2d). Inter-element ratios are variable, possibly due to the more mobile behaviour of these elements (e.g. K/Rb = 79.0-240; Ce/Pb = 14.3-46.2; Table 5.1).

Table 5.1. XRF and ICP-MS trace element analyses (in ppm) of on- and off-craton group I kimberlites. Various inter-element ratios are given, as well as the chondrite normalised La/Sm and La/Yb ratios. Normalising values are from Sun and McDonough (1989).

Group I kimberlites:	On-craton					
Kimberlite:	**Goedehoop**		**Koffiefontein**			**Abbots.E.**
Sample	JAR 30012	JJG 4282	KK 3	KK 5	KK 6	JJG 3118
% Macro.	20	15	15	20	25	10
XRF						
Zr	404	453	-	-	-	353
Nb	273	297	157	191	185	128
Co	97.4	86.6	102	93.9	96.8	96.7
Cr	1222	1194	1289	1623	1547	1174
Ni	950	778	-	-	-	842
V	155	158	139	69.2	99.0	217
Cu	52.6	60.2	-	-	-	154
ICP-MS						
Sc	21.0	23.4	12.2	8.97	8.73	18.0
Ni	-	-	1008	1267	1221	-
Cu	-	-	86.7	40.7	46.6	-
Rb	16.6	16.9	82.3	36.4	29.6	10.2
Sr	1072	1164	816	898	1470	998
Y	30.3	35.5	13.8	12.4	13.5	17.5
Zr	371	436	247	212	245	341
Nb	279	316	166	194	193	138
Ba	1415	1572	707	1520	978	281
La	216	238	131	164	164	80.9
Ce	434	481	259	336	329	163
Pr	46.2	51.1	26.7	35.1	34.5	17.8
Nd	181	201	98.0	128	129	69.7
Sm	27.1	30.0	13.0	15.7	16.7	10.9
Eu	6.79	7.81	3.28	3.83	4.07	2.79
Gd	18.1	21.0	8.49	9.52	10.3	8.10
Tb	1.96	2.25	0.93	0.98	1.06	0.94
Dy	8.63	9.93	3.88	3.76	4.08	4.54
Ho	1.26	1.44	0.58	0.52	0.56	0.70
Er	2.79	3.21	1.27	1.06	1.14	1.65
Tm	0.29	0.34	0.15	0.11	0.12	0.19
Yb	1.52	1.75	0.79	0.59	0.60	1.07
Lu	0.18	0.21	0.10	0.07	0.07	0.13
Hf	7.23	8.30	5.12	3.85	4.57	7.24
Ta	12.5	14.1	8.55	8.89	9.66	8.20
Pb	9.39	11.8	9.00	7.65	12.9	4.83
Th	27.8	31.8	15.5	19.8	17.9	10.6
U	6.48	7.26	3.50	4.11	4.62	2.48
Nb/Ta	21.7	21.0	19.5	21.8	20.0	15.6
Zr/Hf	55.9	54.5	48.2	55.1	53.6	48.7
Zr/Nb	1.48	1.52	1.48	1.10	1.27	2.76
Ba/Nb	5.19	5.29	4.49	7.96	5.29	2.20
La/Nb	0.79	0.80	0.83	0.86	0.88	0.63
Nb/U	42.1	40.9	44.9	46.4	40.1	51.5
Ce/Pb	46.2	40.6	28.8	43.9	25.5	33.7
$(La/Sm)_N$	5.15	5.12	6.48	6.74	6.34	4.82
$(La/Yb)_N$	102	97.8	118	199	194	54.1

Table 5.1. Continued

Group I kimberlites:				Off-craton			
Kimberlite:	**Hebron**			**Klipgatsfontein**			**Zeekoeg.**
Sample	HEB 1A	HEB 1B	JJG 4295	JAR 31012	KGF1	JJG 4323	JJG 1906
% Macro.	25	25	33	25	29	27	15
XRF							
Zr	274	311	247	320	369	354	377
Nb	136	136	168	159	164	160	110
Co	95.9	81.9	93.9	96.0	74.1	85.9	90.0
Cr	1036	810	1485	892	754	859	1203
Ni	903	737	1553	887	576	878	883
V	220	190	140	177	182	169	150
Cu	87.4	72.7	72.6	106	66.3	87.2	137
ICP-MS							
Sc	14.9	15.3	16.8	13.6	18.1	18.3	16.8
Ni	-	-	-	-	-	-	-
Cu	-	-	-	-	-	-	-
Rb	49.1	49.1	44.7	12.2	41.7	28.2	8.93
Sr	733	852	1082	876	1345	1010	447
Y	14.7	15.7	14.5	19.3	19.9	19.3	16.9
Zr	260	294	234	309	343	341	369
Nb	142	142	174	165	171	167	117
Ba	920	940	1437	396	1188	721	168
La	80.4	85.4	131	115	129	121	66.7
Ce	158	167	255	227	250	238	143
Pr	17.0	18.5	26.7	24.3	26.9	25.8	16.0
Nd	68.8	73.9	103	96.4	106	102	63.6
Sm	10.9	12.0	15.0	14.8	16.6	15.9	10.0
Eu	3.00	3.19	3.81	3.84	4.26	4.08	2.53
Gd	8.02	8.50	9.62	10.3	11.5	11.2	7.54
Tb	0.89	0.95	1.00	1.12	1.27	1.22	0.88
Dy	4.02	4.24	4.08	5.32	5.60	5.39	4.357
Ho	0.60	0.65	0.60	0.78	0.85	0.81	0.69
Er	1.41	1.51	1.33	1.69	1.88	1.87	1.64
Tm	0.15	0.16	0.14	0.18	0.21	0.20	0.19
Yb	0.85	0.90	0.78	1.00	1.15	1.07	1.07
Lu	0.10	0.10	0.10	0.11	0.14	0.13	0.13
Hf	6.28	6.77	4.53	6.68	7.19	7.33	8.48
Ta	9.57	9.95	8.91	9.71	9.41	9.57	7.73
Pb	5.10	4.81	11.4	7.20	8.51	8.01	9.98
Th	10.1	12.7	16.8	16.4	17.7	16.7	9.03
U	2.54	2.87	4.51	3.94	3.86	3.86	2.06
Nb/Ta	14.2	13.7	18.8	16.4	17.4	16.7	14.3
Zr/Hf	43.5	46.0	54.6	47.9	51.4	48.3	44.5
Zr/Nb	2.01	2.29	1.47	2.01	2.25	2.22	3.42
Ba/Nb	6.76	6.92	8.57	2.49	7.25	4.51	1.52
La/Nb	0.59	0.63	0.78	0.72	0.79	0.76	0.60
Nb/U	53.6	47.4	37.2	40.5	42.5	41.3	53.6
Ce/Pb	30.9	34.8	22.3	31.5	29.4	29.7	14.3
$(La/Sm)_N$	4.75	4.59	5.64	5.00	5.03	4.91	4.29
$(La/Yb)_N$	67.7	68.1	120	82.3	80.9	81.0	44.7

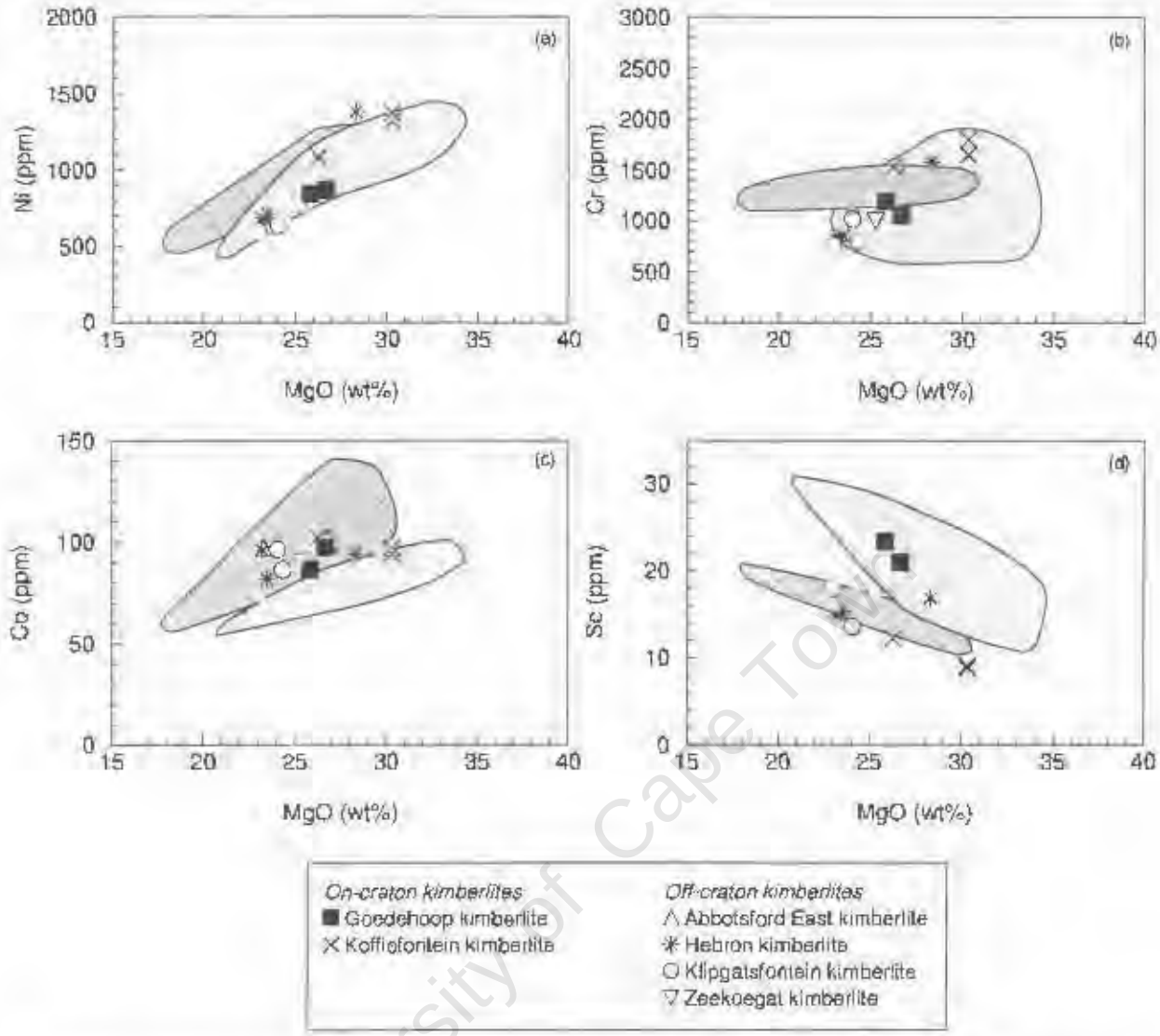

Figure 5.1: Variation of selected ferromagnesian elements versus MgO for on- and off-craton group I kimberlites. Light shaded field represents the on-craton Kimberley kimberlites (le Roex *et al.*, 2003) and dark shaded field, the off-craton Uintjiesberg kimberlite (Harris *et al.*, 2004).

The analysed group I kimberlites all show mutual positive correlations of Zr, Nb, Th and Y abundances with La (Figure 5.3) and have very similar HFS element concentrations to the group I Kimberley and Uintjiesberg kimberlites. Zr contents vary between 212ppm (Koffiefontein kimberlite; Figure 5.3a) and 453ppm (Goedehoop kimberlite). Similarly, Nb concentrations vary from 110ppm (Zeekoegat kimberlite; Figure 5.3b) to 297ppm (Goedehoop kimberlite). Inter-element ratios between Zr and Hf (Zr/Hf = 50±4.4; Figure 5.3c) as well as Nb and Ta (Nb/Ta = 17.7±2.8; Figure 5.3d) may show some scatter. Other ratios (Table 5.1), e.g. La/Nb = 0.7±0.1, Ba/Nb = 5.3±2.2 and Zr/Nb = 2.0±0.6, are similar to reference group I kimberlites. Although Th and Y show strong positive correlations with La (Figure 5.3e, f), the correlations appear to be governed by the higher Th and Y (~30ppm Th, ~33ppm Y) contents of the Goedehoop kimberlite.

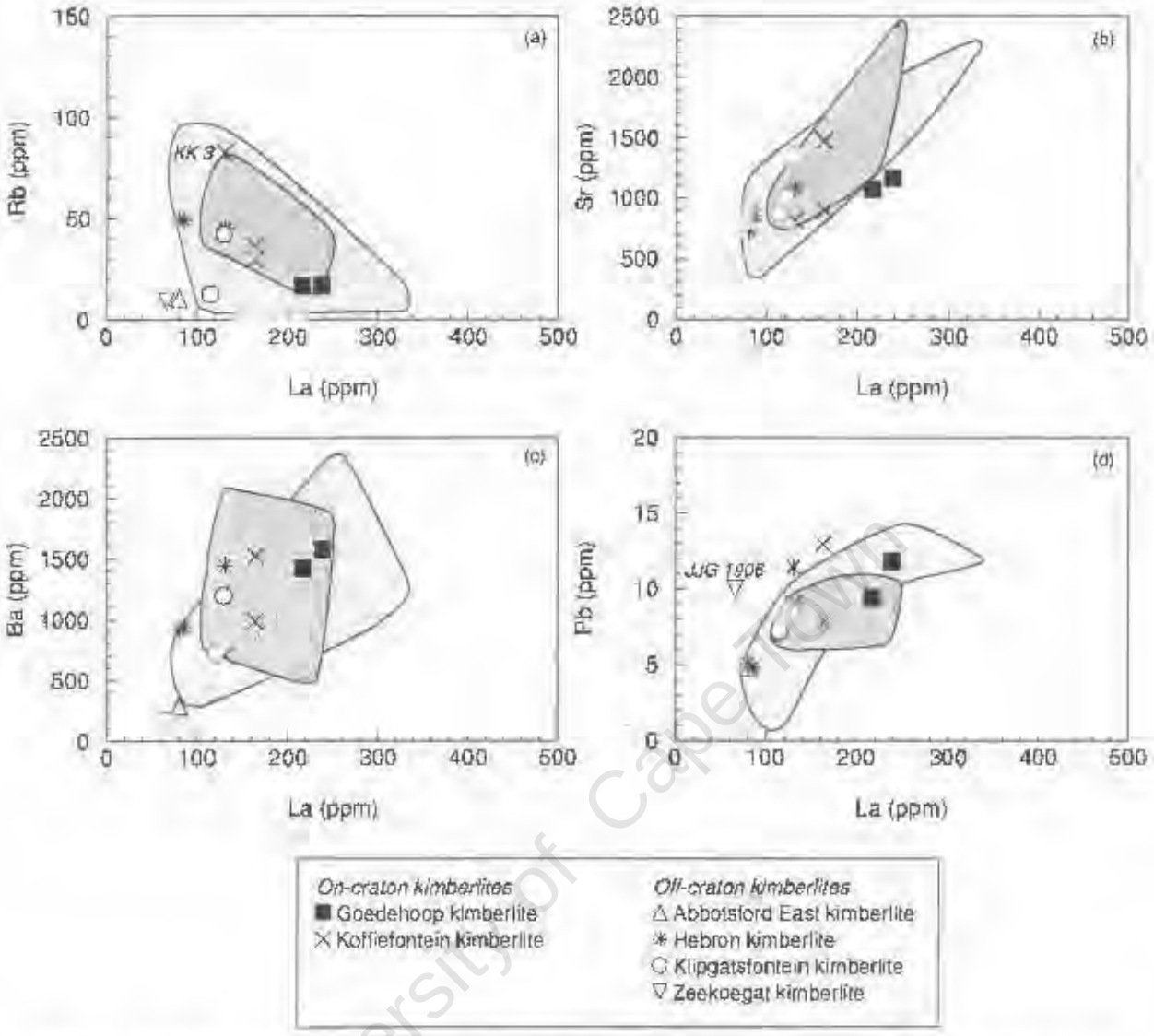

Figure 5.2: Variation of selected incompatible elements versus La for on- and off-craton group I kimberlites. Light shaded field represents the on-craton Kimberley kimberlites (le Roex *et al.*, 2003) and dark shaded field, the off-craton Uintjiesberg kimberlite (Harris *et al.*, 2004).

Chondrite normalised rare earth element (REE) abundances of group I kimberlites (Sun & McDonough, 1989) are illustrated in Figure 5.4, with compositional fields of the group I Kimberley and Uintjiesberg kimberlites for comparison. All of the analysed group I kimberlites have similar sub-parallel patterns (Figure 5.4) and show considerable enrichment of the light REE (La = 300-1000 times chondrite) and lesser enrichment of the heavy REE (Lu = 3-8 times chondrite), with the Goedehoop kimberlite being the most REE enriched. REE contents of the samples generally fall within or close to the field of the on-craton Kimberley or off-craton Uintjiesberg kimberlites (Figure 5.4), although REE contents of the Kimberley and Uintjiesberg kimberlites are fairly equivalent (Harris *et al.*, 2004). REE ratios of kimberlites are highly variable from $(La/Yb)_N$ = 44.7 to 199 and $(La/Sm)_N$ = 4.3 to 6.7 (Table 5.1).

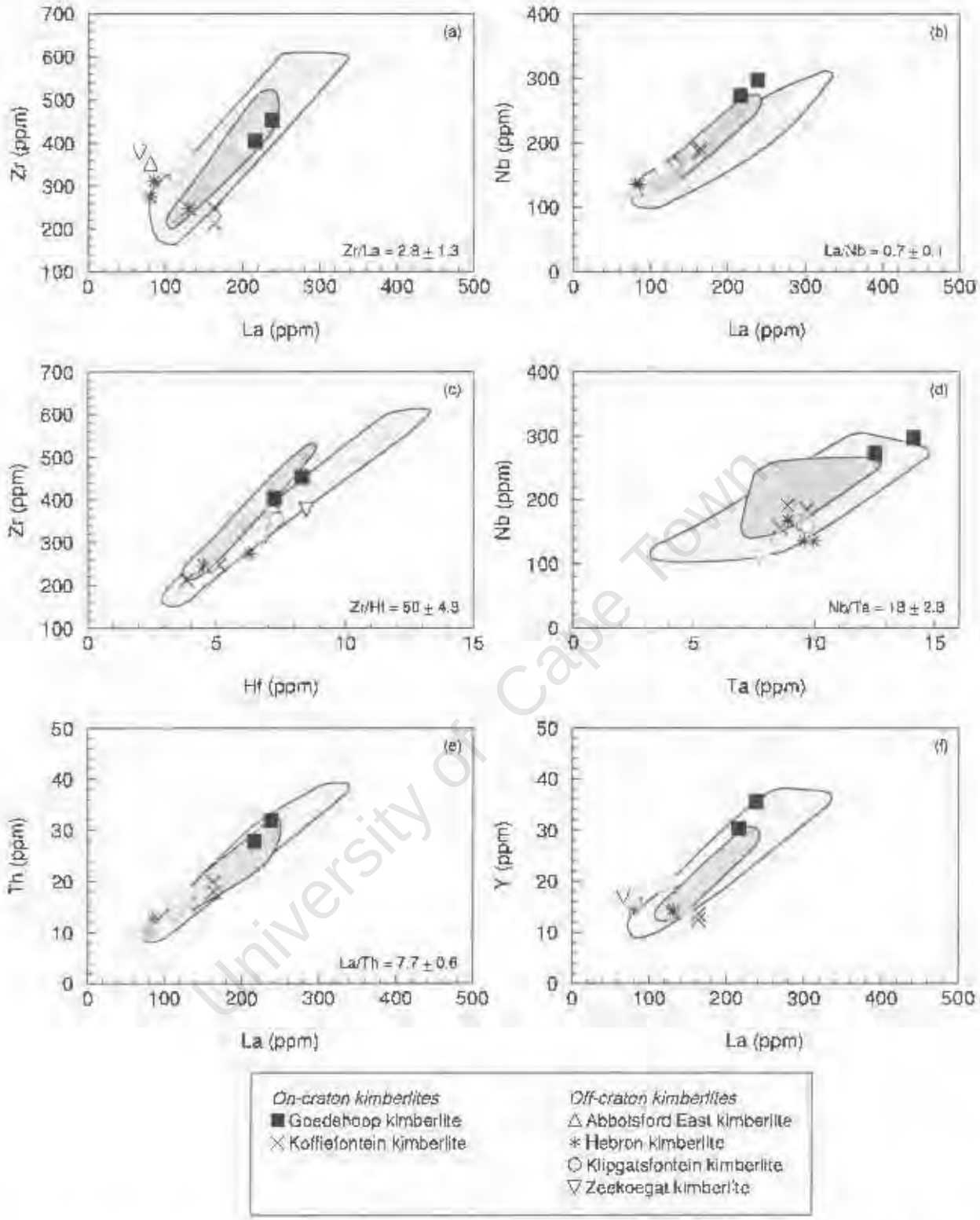

Figure 5.3: Variation of selected high field strength elements for on- and off-craton group I kimberlites. Light shaded field represents the on-craton Kimberley kimberlites (le Roex *et al.*, 2003) and dark shaded field, the off-craton Uintjiesberg kimberlite (Harris *et al.*, 2004).

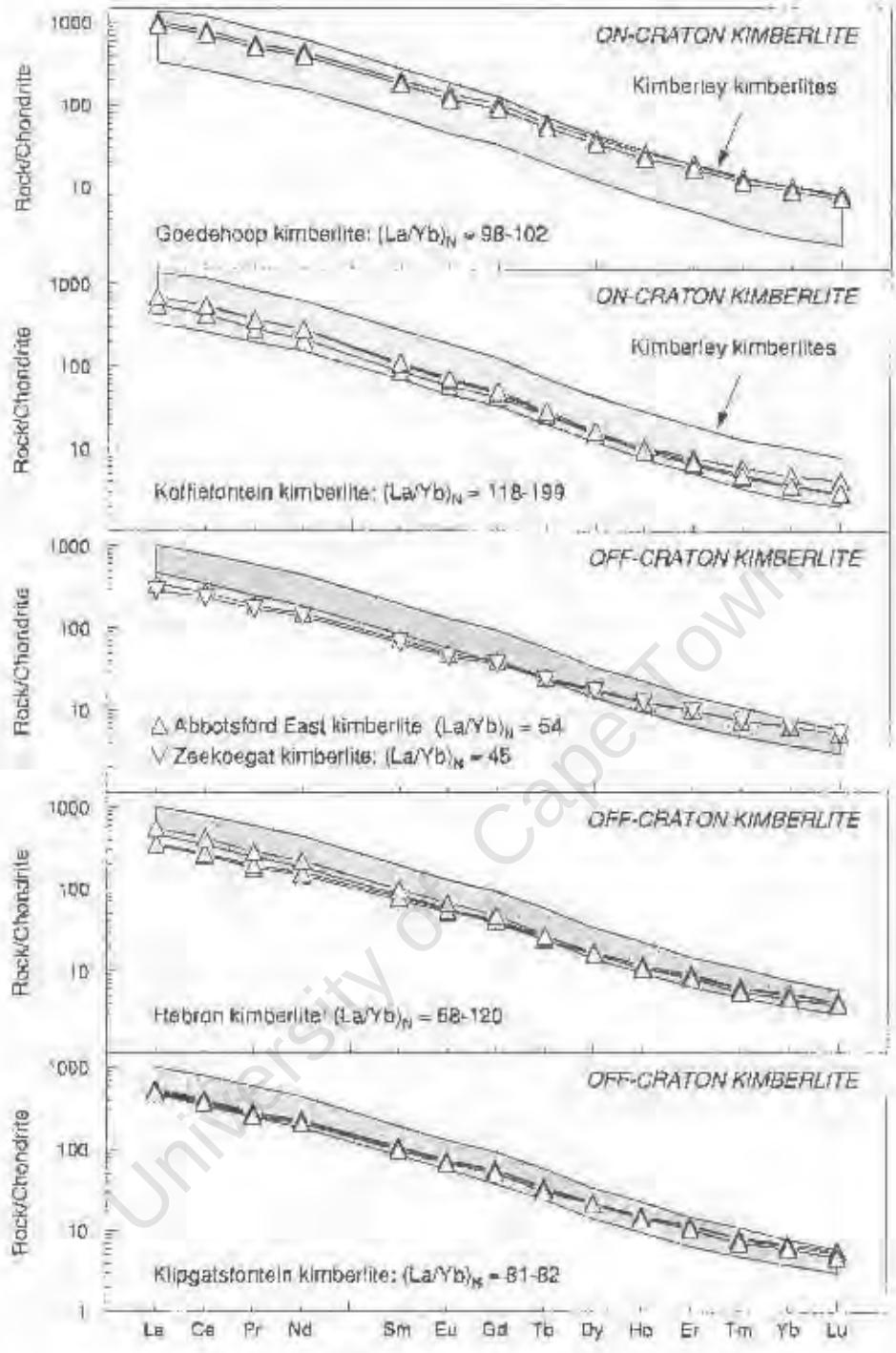

Figure 5.4: Chondrite normalised diagram of the rare earth elements for on- and off-craton group I kimberlites. Shaded field for the on-craton Goedehoop and Koffiefontein kimberlites, represents the on-craton Kimberley kimberlites (le Roex *et al.*, 2003), whereas the shaded field for analysed off-craton kimberlite samples is the off-craton Uintjiesberg kimberlite (Harris *et al.*, 2004). Chondrite normalising values are from Sun and McDonough (1989).

The primitive mantle normalised diagrams of the analysed kimberlites are fairly smooth and show the enrichment of the more incompatible elements (e.g. Nb = 155-416 and Ba = 24.0-225 times primitive mantle, Figure 5.5). Superimposed upon the trace element patterns, are systematic relative depletions of Rb, K, Sr, Hf and Ti (Figure 5.5). These negative anomalies appear to be characteristic features of group I kimberlite samples and have also been described for the Kimberley and Uintjiesberg kimberlites (Harris *et al.*, 2004; le Roex *et al.*, 2003). Magnitudes of the negative anomalies are either described by normalised trace element ratios (e.g. Ti/Eu) or else in the X/X* notation (X* is the interpolated value read from the primitive mantle normalised diagram, e.g. $Ti^* = [Eu^{1/2} \times Ta^{1/2}]$). Negative Rb and K anomalies tend to be larger (K/K* = 0.0-0.3; calculated using Th and La) than the Ti anomalies (Ti/Ti* = 0.3-1.0). In some instances, the magnitudes of these anomalies increase with the level of incompatible element enrichment (e.g. Goedehoop kimberlite; K/K* = 0.02 and La ~ 1000 times chondrite). Minor negative Sr anomalies as well as occasional Hf anomalies (e.g. Koffiefontein kimberlite) on primitive mantle normalised diagrams are also features of the analysed group I kimberlites.

5.2.1 On-craton group I kimberlites

Goedehoop kimberlite

Ferromagnesian and incompatible element concentrations of the on-craton Goedehoop kimberlite show good overlap with the compositional field defined for the on-craton Kimberley kimberlites (Figures 5.1-5.3). Sample *JAR 30012* is slightly more macrocrystic than sample *JJG 4282* and is more enriched in Ni, Cr and Co and less enriched in Sc (Table 5.1). Intra-kimberlite variation in Rb (16.6-16.9ppm), Ba (1415-1572ppm) and Sr (1072-1164ppm) contents tends to be limited (Figure 5.2). Goedehoop kimberlite is also enriched in HFS elements (~429ppm Zr, ~285 ppm Nb; Figure 5.3) with La/Nb = 0.8±0.01, Ba/Nb = 5.2±0.05 and Zr/Nb = 1.5±0.02 (Table 5.1). Similarly, light REE concentrations are high (La = 911-1004 times chondrite; Figure 5.4) with steep REE patterns ($(La/Yb)_N$ ~ 100). Primitive mantle normalised patterns of the two kimberlite samples are almost identical, with very pronounced negative Rb and K anomalies (K/K* = 0.02; Figure 5.5), and lesser Sr and Ti anomalies.

Koffiefontein kimberlite

Macrocrystic on-craton Koffiefontein kimberlite samples *KK 5* and *KK 6* are similar in geochemical character and have higher concentrations of Ni and Cr (~1340ppm Ni; ~1810ppm Cr; Figure 5.1a, b) than the less macrocrystic sample *KK 3* (1079ppm Ni; 1532ppm Cr). Rb, Sr, Ba and Pb contents are variable (Figure 5.2), whereas concentrations of HFS elements show less intra-kimberlite variation (212-247ppm Zr; 157-191ppm Nb; Figure 5.3). Inter-element ratios also tend to be fairly well constrained (e.g. Nb/Ta = 19.7±1.3; Zr/Nb = 1.3±0.2; La/Nb = 0.9±0.02; Table 5.1). Chondrite normalised REE patterns of samples *KK 5* and *KK 6* are almost identical (La = 690-693 and Lu = 2.79-2.89 times chondrite; Figure 5.4) and are typically steeper ($(La/Yb)_N$ ~ 197) than sample *KK 3* ($(La/Yb)_N$ = 118). Negative K and Ti anomalies on primitive mantle normalised diagrams tend to be

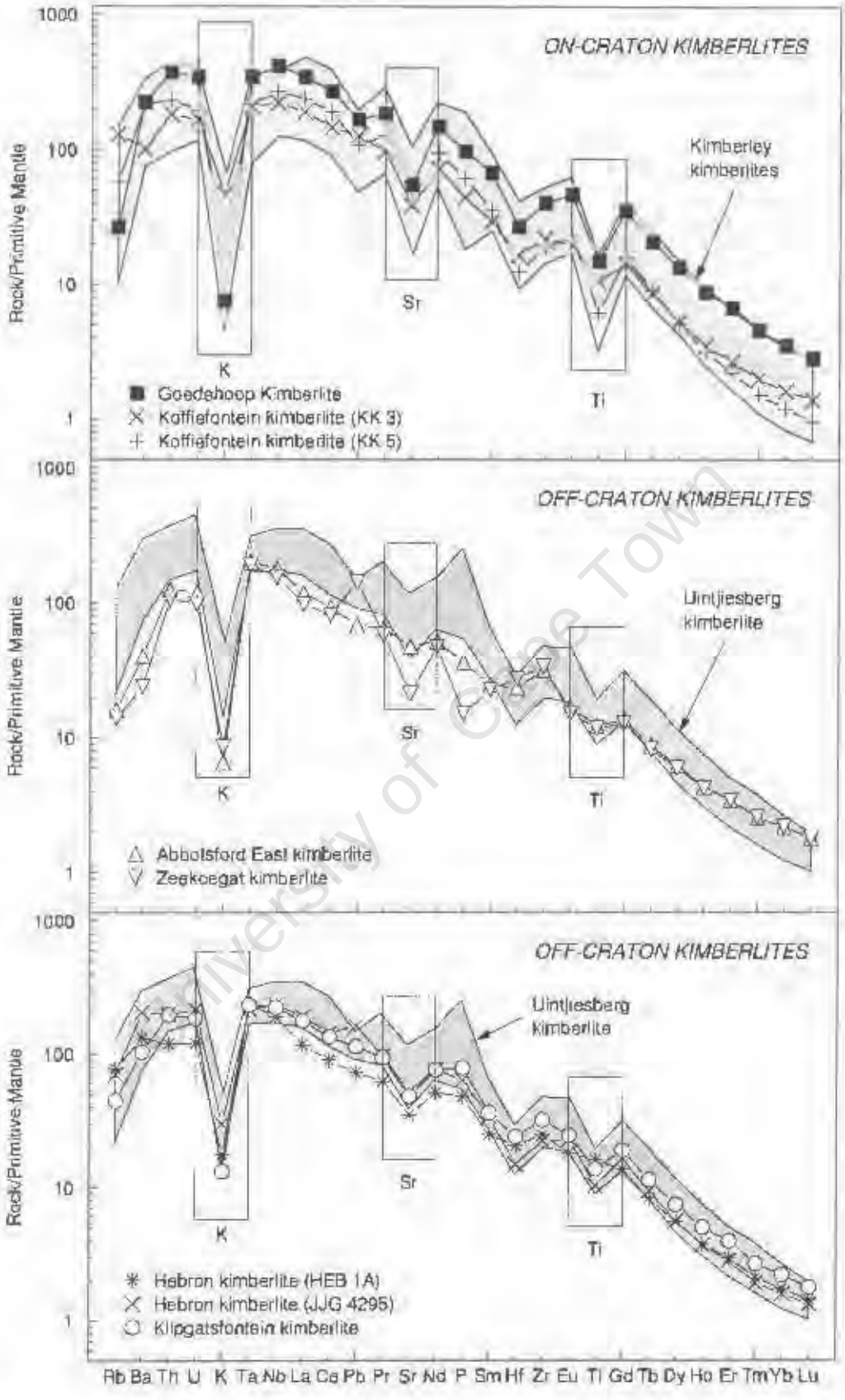

Figure 5.5: Primitive mantle normalised diagram of the incompatible trace elements for on- and off-craton group I kimberlites. Representative samples from each kimberlite are shown for simplicity. Shaded fields represent the on-craton group I Kimberley kimberlites (le Roex *et al.*, 2003) and off-craton Uintjiesberg kimberlite (Harris *et al.*, 2004). Primitive mantle normalising values are from Sun and McDonough (1989).

larger in magnitude for samples *KK 5* and *KK 6*, than sample *KK 3* (Figure 5.5). Sample *KK 3* also has a positive Rb anomaly on a primitive mantle normalised diagram (Figure 5.5).

5.2.2 Off-craton group I kimberlites

Abbotsford East and Zeekoegat kimberlites

Ferromagnesian element concentrations in the off-craton Abbotsford East and Zeekoegat kimberlites tend to be similar (~703ppm Ni; ~941 ppm Cr; Figure 5.1a, b), even though their MgO concentrations and macrocryst content differ. Concentrations of Rb, Ba and Sr are relatively low (168-281ppm Ba; 447-998ppm Sr; Figure 5.2) and samples tend to be slightly less enriched than the group I Kimberley and Uintjiesberg kimberlites. Zeekoegat kimberlite has a significantly higher Pb content (sample *JJG 1906*; Figure 5.2) and lower Ce/Pb ratio (9.98ppm Pb, Ce/Pb = 14.3) than Abbotsford East kimberlite (4.83ppm Pb, Ce/Pb = 33.7), and forms a positive Pb anomaly on a primitive mantle normalised diagram (Figure 5.5). Well-constrained inter-element ratios are consistent with the geochemical similarity of the two kimberlites (Zr/Hf = 46.6±2.1, Nb/Ta = 14.9±0.7, La/Nb = 0.6±0.01). Both kimberlites are slightly less light REE enriched (La ~ 311 times chondrite) than the Uintjiesberg kimberlite, although heavy REE contents still overlap the Uintjiesberg compositional field (Figure 5.4).

Hebron kimberlite

Macrocrystic off-craton Hebron kimberlite samples have higher Ni and Cr concentrations (1377ppm Ni; sample *JJG 4295*; Figure 5.1a, b) than the less macrocrystic samples (e.g. ~695ppm Ni; samples *HEB 1A, HEB 1B*). Although the variation in Rb (44.7-49.1 ppm), Sr (733-1082 ppm) and Pb (4.81-11.4ppm) contents is not very great (Figure 5.2), inter-element ratios for samples *HEB 1A* and *HEB 1B* (K/Rb ~ 82.5, Ce/Pb ~ 32.9; Table 5.1) are different to sample *JJG 4295* (K/Rb =166, Ce/Pb = 22.3). Other inter-element ratios (Zr/Nb, Ba/Nb, La/Nb; Table 5.1) and REE ratios also effectively discriminate between kimberlite samples (e.g. $(La/Yb)_N$ = 120 for *JJG 4295* and $(La/Yb)_N$ = 68 for *HEB 1A* and *HEB 1B*). Primitive mantle normalised patterns of Hebron kimberlite samples broadly overlap the group I Uintjiesberg compositional field and tend to show characteristic features of group I kimberlites (as described above; Figure 5.5), except that samples *HEB 1A* and *HEB 1B* show no depletion in Ti (Ti/Ti* ~ 1.0).

Klipgatsfontein kimberlite

Off-craton Klipgatsfontein kimberlite samples have low Ni (595-663 ppm), Cr (754-1012 ppm) and Co (74.1-96.0 ppm) concentrations, but still fall within the range defined for the group I Kimberley and Uintjiesberg kimberlites (Figure 5.1). REE and HFS element concentrations of samples show little intra-kimberlite variation (e.g. 115-129ppm La, 159-164 ppm Nb; Table 5.1), in contrast to Rb (12.2-41.7 ppm), Sr (876-1345 ppm) and Ba (396-1188 ppm) contents that vary independently to immobile element concentrations (Figure 5.2). HFS element and REE ratios are also well constrained with La/Nb = 0.8±0.03, Nb/Ta = 16.8±0.5, Zr/Nb = 2.2±0.1 and $(La/Yb)_N$ = 81.4±0.8, and with REE compositions showing good overlap with the compositional field of the off-craton Uintjiesberg kimberlite (Figure 5.4). Primitive mantle normalised patterns of the samples have characteristic group I kimberlite features, in addition to the presence of a slight positive P anomaly (Figure 5.5).

5.3 Group II kimberlites

The range of Ni and Cr concentrations of the analysed group II kimberlites is broad (Figure 5.6a, b) and varies from 200-300ppm Ni, 500-600ppm Cr for the off-craton Eendekuil kimberlite and up to ~1600ppm Ni, ~2000ppm Cr for the Newlands kimberlite. Ni and Cr concentrations correlate positively with MgO and tend to show just slightly more variation than the on-craton group II Swartruggens and Star kimberlites (Figure 5.6 a, b; Coe, 2004) and on-craton group I Kimberley kimberlites (le Roex *et al*., 2003). In contrast to Ni and Cr, the variation in Co content is limited, from 43ppm to 107ppm (Brandewynskuil and Markt kimberlites, respectively, Figure 5.6c). The co-variation of Sc and MgO concentrations is scattered, with most of the samples having Sc contents (9.40-29.5ppm; Figure 5.6d) similar to the Swartruggens and Star kimberlites.

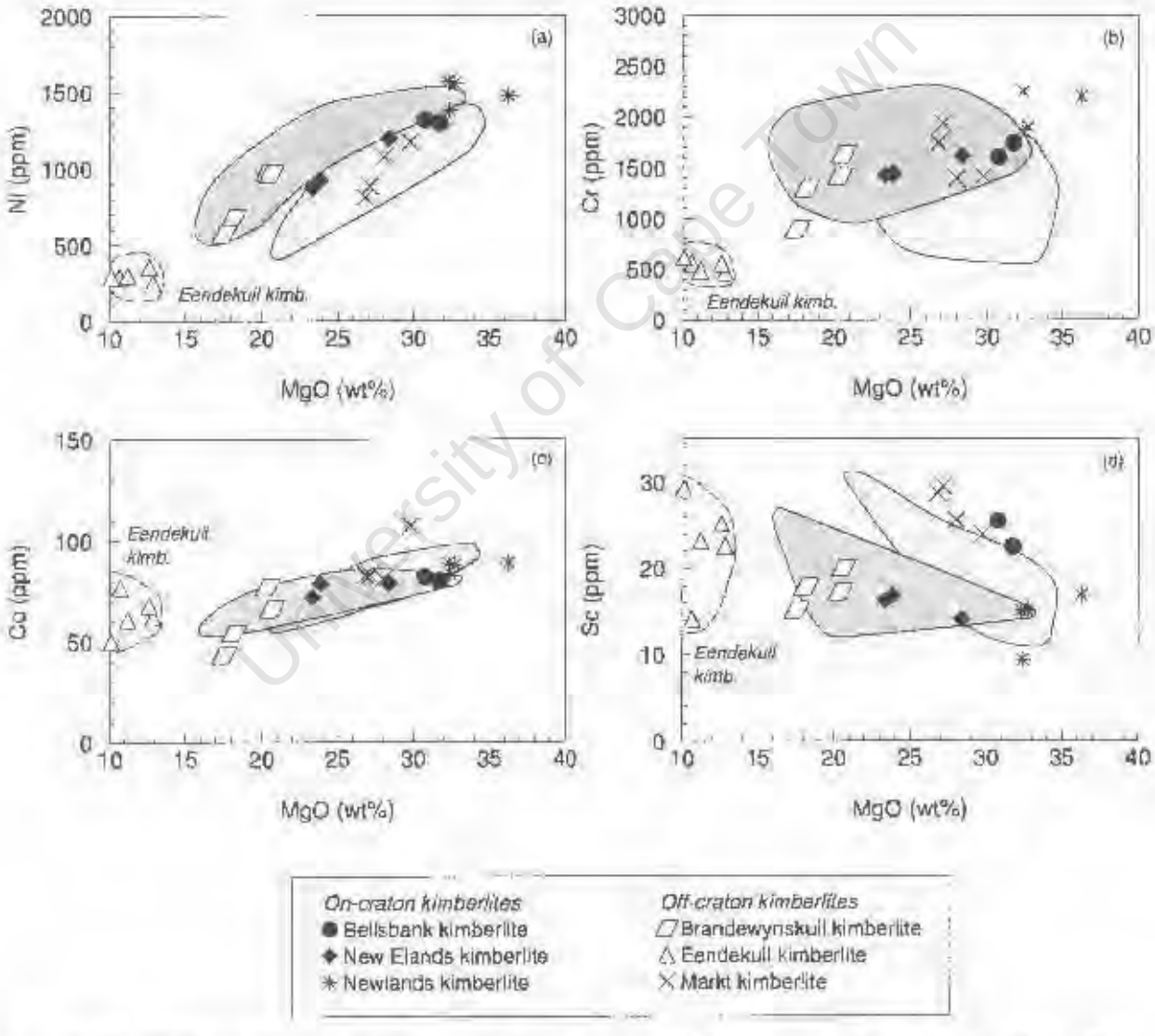

Figure 5.6: Variation of selected ferromagnesian elements versus MgO for on- and off-craton group II kimberlites. Dark shaded field represents the on-craton Swartruggens and Star kimberlites (Coe, 2004) and light shaded field, the on-craton group I Kimberley kimberlites (le Roex *et al*., 2003).

Table 5.2. XRF and ICP-MS trace element analyses (in ppm) of on- and off-craton group II kimberlites. Various inter-element ratios are given, as well as the chondrite normalised La/Sm and La/Yb ratios. Normalising values are from Sun and McDonough (1989).

			On-craton:						
Kimberlite:		Bellsbank	New Elands			Newlands			
Sample	KBEL 2	JJG 4676	NE K6	NE K10	NE K11	JJG 24	JJG 6196	KN 2	KN 3
% Macro.	-	30	10	10	20	25	45	35	30
XRF									
Zr	-	-	-	-	-	-	-	-	-
Nb	210	226	103	106	92.4	163	163	164	167
Co	81.9	80.5	79.2	72.0	78.6	83.9	88.3	88.7	89.0
Cr	1739	1938	1561	1530	1711	2163	1840	2206	1837
Ni	-	-	-	-	-	-	-	-	-
V	96.9	71.9	82.6	103	139	54.0	60.3	69.0	95.8
Cu	-	-	-	-	-	-	-	-	-
ICP-MS									
Sc	25.6	22.5	16.9	16.3	14.1	15.1	9.40	16.9	15.1
Ni	1274	1229	837	803	1109	1328	1466	1356	1520
Cu	16.6	24.0	48.2	45.7	15.8	38.7	52.1	39.0	18.4
Rb	127	120	163	165	140	72.9	64.7	60.4	30.7
Sr	1573	1947	1061	1358	1987	1000	2109	1364	1032
Y	16.2	15.2	17.6	19.8	17.9	9.69	7.74	10.8	11.1
Zr	376	276	432	317	392	199	159	202	154
Nb	204	222	99.0	102	87.8	158	155	158	168
Ba	4092	2617	1710	2414	3688	3883	4254	2449	7345
La	364	390	195	211	191	231	208	219	235
Ce	687	708	377	410	371	424	387	422	424
Pr	65.8	69.1	39.4	41.9	37.8	48.6	36.2	40.7	39.9
Nd	212	224	139	147	134	129	115	129	125
Sm	21.2	21.5	16.2	16.9	15.7	13.0	11.3	11.9	12.4
Eu	4.73	4.57	3.76	3.94	3.63	2.78	2.48	2.59	2.82
Gd	11.0	11.5	9.82	10.2	9.24	6.80	5.72	6.51	6.41
Tb	1.19	1.26	1.09	1.15	1.05	0.72	0.60	0.72	0.71
Dy	4.50	4.37	4.53	4.86	4.43	2.70	2.19	2.82	2.78
Ho	0.67	0.65	0.70	0.78	0.72	0.40	0.33	0.44	0.43
Er	1.52	1.45	1.57	1.77	1.62	0.92	0.75	1.05	1.13
Tm	0.18	0.17	0.20	0.21	0.20	0.11	0.09	0.14	0.15
Yb	1.00	0.93	1.12	1.18	1.17	0.60	0.46	0.86	0.87
Lu	0.13	0.12	0.14	0.15	0.15	0.08	0.06	0.12	0.13
Hf	8.58	7.21	9.62	8.71	8.69	4.25	3.34	4.57	3.15
Ta	11.1	11.6	4.57	4.58	4.01	7.40	6.50	8.28	6.88
Pb	34.6	35.0	21.8	35.7	57.3	26.6	64.3	23.8	43.5
Th	53.5	58.7	22.6	20.7	24.4	35.0	34.9	34.9	39.0
U	5.15	6.95	3.17	4.05	11.06	4.14	4.05	4.66	6.33
Nb/Ta	19.0	19.2	22.1	23.1	23.0	22.0	25.1	19.8	24.2
Zr/Hf	43.8	38.2	44.9	36.4	45.1	46.8	47.7	44.3	48.9
Zr/Nb	1.79	1.22	4.18	3.00	4.25	1.22	0.98	1.24	0.92
Ba/Nb	19.4	11.5	16.5	22.9	39.9	23.8	26.0	15.0	44.1
La/Nb	1.73	1.72	1.89	1.99	2.07	1.42	1.27	1.34	1.41
Nb/U	34.2	32.6	32.6	26.1	8.35	39.3	40.4	35.2	20.0
Ce/Pb	19.3	20.2	17.3	11.5	6.47	16.0	6.02	17.7	9.74
$(La/Sm)_N$	11.1	11.7	7.75	8.04	7.86	11.5	11.9	11.9	12.3
$(La/Yb)_N$	261	300	125	128	117	274	328	183	193

Table 5.2. Continued

Group II kimberlites:					Off-craton				
Kimberlite:	**Brandewynskuil**				**Eendekuil**				
Sample	K6/8	K6/11*	K6/12	K6/14	EKL 1	K2/2	K2/3	K2/9	K2/13*
% Macro.	25	20	30	30	25	25	30	30	25
XRF									
Zr	239	297	408	310	652	168	482	473	242
Nb	62.5	67.0	107	86.4	192	142	169	195	128
Co	43.0	77.0	65.9	54.3	61.6	77.2	49.9	67.9	61.0
Cr	824	1412	1507	1136	354	635	591	528	465
Ni	584	972	964	695	213	356	245	301	301
V	148	131	126	149	229	241	191	224	185
Cu	40.0	28.0	29.7	40.2	77.6	64.4	54.8	62.9	29.0
ICP-MS									
Sc	15.2	17.3	20.1	17.9	22.6	14.2	29.3	25.2	23.2
Ni	-	-	-	-	-	-	-	-	-
Cu	-	-	-	-	-	-	-	-	-
Rb	100	103	115	134	169	187	171	210	197
Sr	1003	1453	1434	1184	904	1438	1363	1099	1349
Y	17.2	16.5	18.4	19.6	21.7	18.6	22.9	28.0	23.7
Zr	199	299	362	272	601	147	439	431	244
Nb	53.4	72.4	93.3	73.6	164	133	149	166	142
Ba	1870	1786	1974	2287	780	1692	1978	1971	1484
La	90.4	135	153	121	202	177	153	193	183
Ce	181	273	316	245	406	342	287	366	326
Pr	19.1	28.6	32.8	25.6	40.1	34.4	28.7	36.0	33.5
Nd	70.6	105	121	94.6	143	126	104	130	123
Sm	9.22	12.6	14.8	12.1	17.1	15.5	13.6	16.6	15.9
Eu	2.24	2.76	3.52	2.90	4.26	3.56	3.47	4.48	3.79
Gd	6.37	7.31	9.19	7.99	11.6	9.28	9.71	12.2	10.3
Tb	0.76	0.79	1.03	0.93	1.31	1.00	1.14	1.43	1.20
Dy	3.80	3.83	4.57	4.40	5.57	4.72	5.23	6.72	5.95
Ho	0.67	0.62	0.73	0.76	0.89	0.71	0.87	1.11	0.94
Er	1.77	1.48	1.76	1.87	2.10	1.55	2.12	2.74	2.23
Tm	0.23	0.18	0.23	0.25	0.26	0.17	0.26	0.35	0.25
Yb	1.47	1.17	1.39	1.56	1.52	0.93	1.58	2.09	1.48
Lu	0.21	0.15	0.20	0.22	0.20	0.10	0.21	0.27	0.17
Hf	4.44	6.60	8.08	6.19	13.1	3.73	11.4	12.5	6.83
Ta	1.35	3.98	3.30	2.12	9.81	7.27	5.17	7.53	7.37
Pb	20.8	10.4	13.1	18.7	24.9	25.3	34.2	20.2	21.6
Th	13.1	16.4	20.4	17.1	37.9	25.3	34.8	31.2	24.9
U	3.09	2.26	3.06	3.95	3.62	2.27	6.86	2.48	2.01
Nb/Ta	46.3	16.9	28.3	40.8	19.6	19.5	32.7	25.8	17.4
Zr/Hf	53.9	45.0	50.5	50.8	49.8	45.1	42.2	37.9	35.4
Zr/Nb	3.83	4.43	3.81	3.59	3.39	1.19	2.85	2.43	1.89
Ba/Nb	25.9	26.7	18.4	26.5	4.06	11.9	11.7	10.1	11.7
La/Nb	1.45	2.01	1.43	1.40	1.05	1.25	0.91	0.99	1.28
Nb/U	20.2	29.7	35.0	21.9	53.1	62.5	25.4	78.5	63.5
Ce/Pb	8.71	26.2	24.1	13.1	16.3	13.5	8.39	18.1	15.2
$(La/Sm)_N$	6.33	6.90	6.66	6.45	7.64	7.38	7.25	7.49	6.64
$(La/Yb)_N$	44.0	82.8	78.6	55.7	95.5	137	69.7	66.2	79.1

*XRF analyses for Brandewynskuil and Eendekuil kimberlite samples. K6/11 and K2/13 are from Clark (1994).

Table 5.2. Continued

Group II kimberlites:			Off-craton	
Kimberlite		**Markt**		
Sample	JJG 2314	JJG 2336	MRK 1	MRK 3
% Macro.	30	25	30	20
XRF				
Zr	338	383	352	350
Nb	117	113	121	105
Ce	107	83.4	81.3	82.9
Cr	2036	2156	1682	2318
Ni	1854	1251	1244	1123
V	63.6	46.7	110	56.8
Cu	28.0	29.0	24.1	42.3
ICP-MS				
Sc	23.9	28.7	25.6	29.6
Ni	-	-	-	-
Cu	-	-	-	-
Rb	67.2	75.6	69.5	80.8
Sr	1651	1991	1741	1677
Y	16.5	16.8	16.3	15.6
Zr	305	372	320	343
Nb	118	114	125	107
Ba	2833	3604	3398	3569
La	187	203	209	189
Ce	389	413	432	391
Pr	41.2	43.4	45.0	41.9
Nd	153	163	168	157
Sm	18.5	20.3	20.4	19.3
Eu	4.31	4.75	4.78	4.57
Gd	10.3	11.3	11.3	10.8
Tb	1.08	1.17	1.20	1.11
Dy	4.33	4.65	4.74	4.35
Ho	0.67	0.68	0.70	0.63
Er	1.69	1.61	1.58	1.49
Tm	0.18	0.17	0.18	0.16
Yb	1.10	0.97	1.14	0.90
Lu	0.14	0.13	0.14	0.12
Hf	6.22	7.08	6.55	6.62
Ta	4.83	5.68	5.03	5.33
Pb	21.4	30.0	28.6	24.0
Th	22.6	24.4	23.9	22.7
U	4.49	17.3	4.21	5.76
Nb/Ta	24.2	19.9	24.1	19.7
Zr/Hf	54.0	54.1	53.8	53.6
Zr/Nb	2.88	3.38	2.90	3.33
Ba/Nb	24.3	31.8	28.0	34.0
La/Nb	1.60	1.79	1.72	1.80
Nb/U	26.0	6.55	28.8	18.2
Ce/Pb	18.2	13.8	15.1	16.3
$(La/Sm)_N$	6.51	6.48	6.61	6.31
$(La/Yb)_N$	122	151	132	151

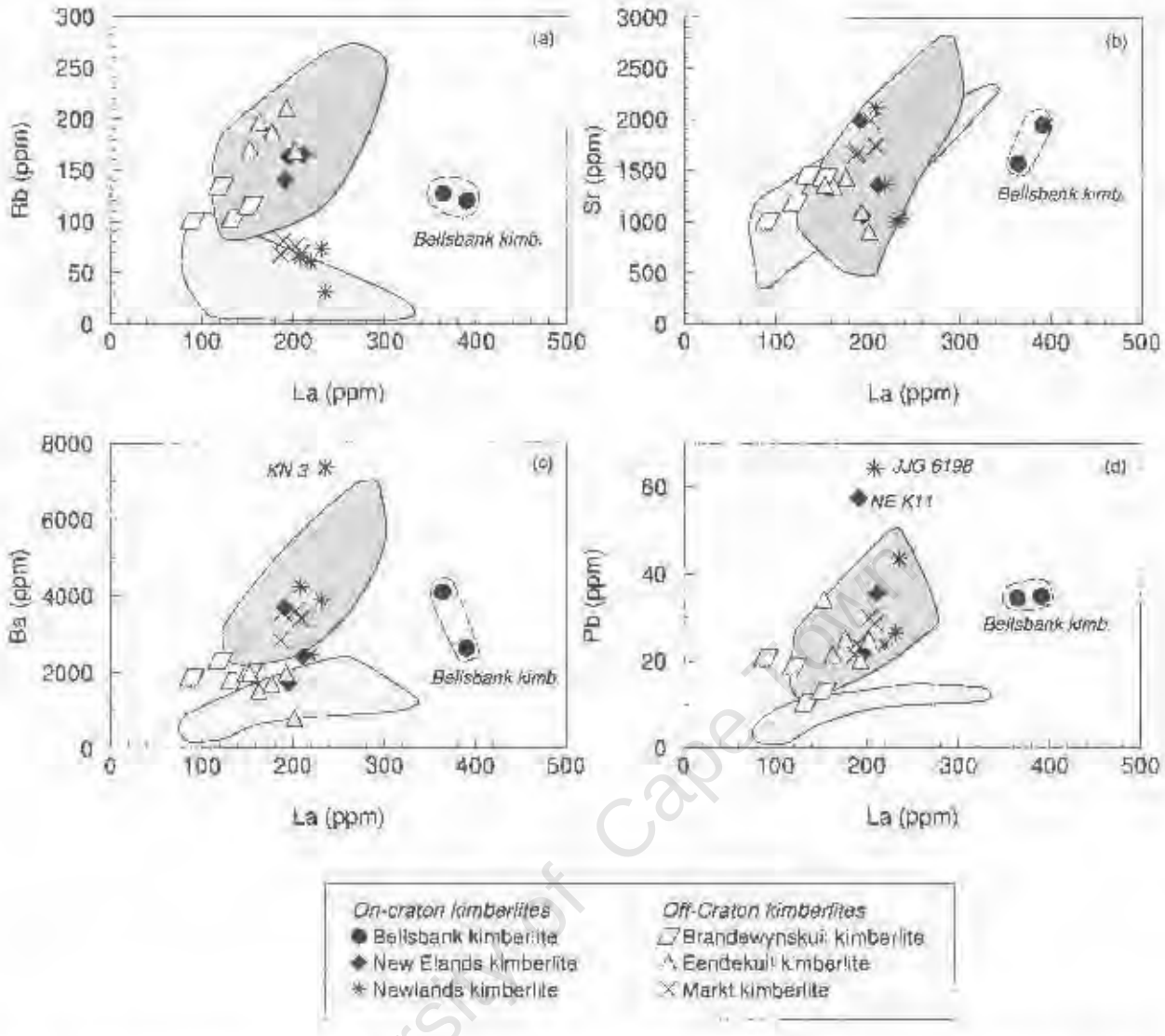

Figure 5.7: Variation of selected incompatible elements versus La for on- and off-craton group II kimberlites. Dark shaded field represents the on-craton Swartruggens and Star kimberlites (Coe, 2004) and light shaded field, the on-craton group I Kimberley kimberlites (le Roex *et al.*, 2003).

Rb concentrations of the analysed group II kimberlites are variable from 30.7ppm (Newlands kimberlite) to 210ppm (Eendekuil kimberlite) and show poor correlation with the immobile element La (Figure 5.7a). Samples overlap the compositional field of the Swartruggens and Star kimberlites for Rb, Sr and Pb (Figure 5.7), although the Brandewynskuil, Eendekuil and New Elands kimberlites have lower Ba contents (< 2400ppm) than the on-craton Swartruggens and Star kimberlites. Similarly to Rb, Pb concentrations also show a scattered distribution with La (also variable Ce/Pb = 6.0-26.2; Table 5.2) and varies between 10.4ppm (Brandewynskuil kimberlite) and 64.3ppm (Newlands kimberlite), although most samples tend to have less than 40ppm Pb (Figure 5.7d).

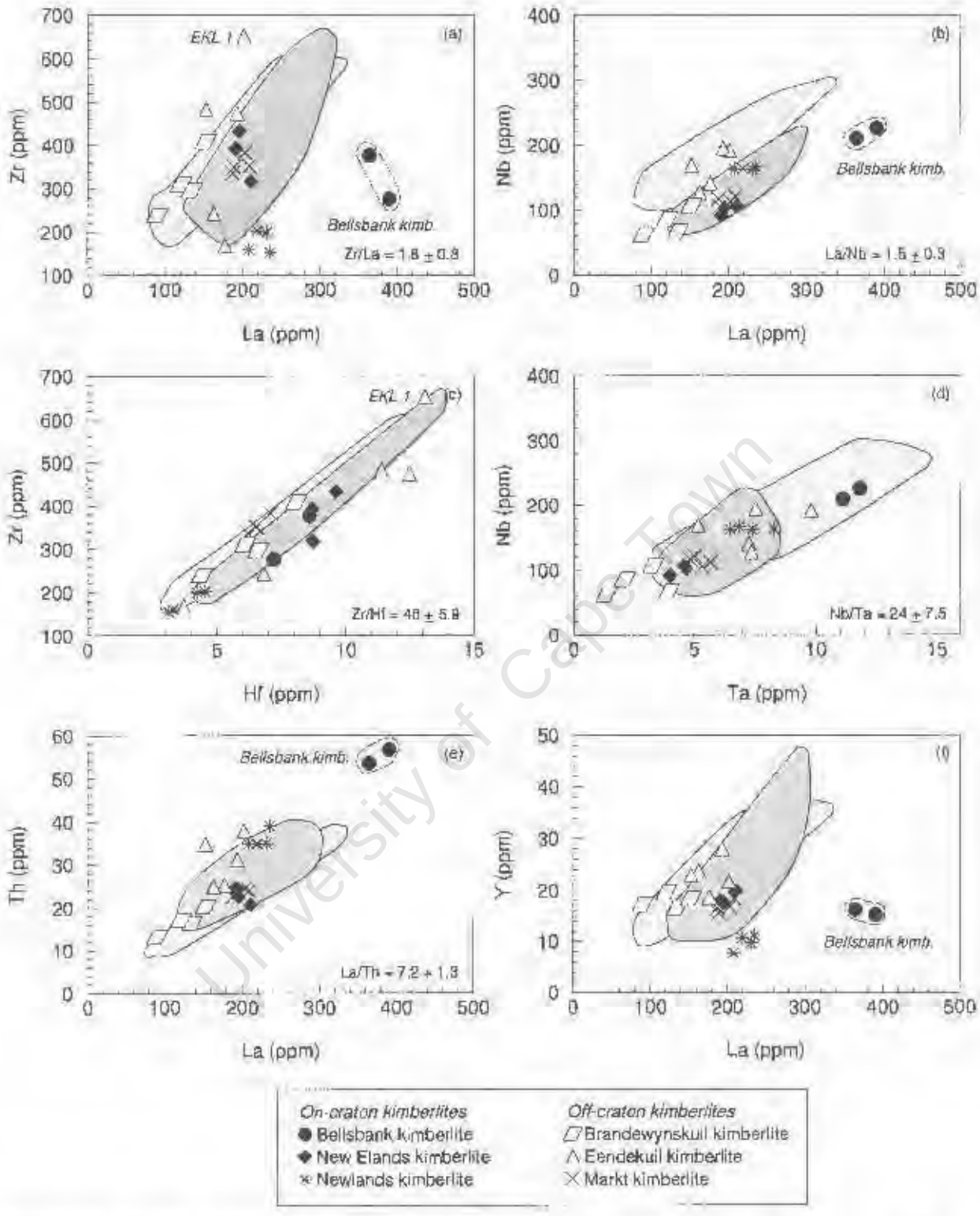

Figure 5.8: Variation of selected high field strength elements for on- and off-craton group II kimberlites. Dark shaded field represents the on-craton Swartruggens and Star kimberlites (Coe, 2004) and light shaded field, the on-craton group I Kimberley kimberlites (ie Roex *et al.*, 2003).

The range of measured Zr contents is high, variable and virtually encompassed by the intra-kimberlite variation of the Eendekuil kimberlite (168-652ppm; Figure 5.8a). In contrast to the scattered behaviour of Zr, a well-developed positive correlation exists between Nb and La (La/Nb = 1.5±0.3), with Nb concentrations varying between 62.5ppm and 226ppm (Brandewynskuil and Bellsbank kimberlites, respectively; Figure 5.8b). Zr and Hf concentration ranges are similar to Swartruggens and Star kimberlites, but Nb and Ta contents tend to show greater variation than the reference group II kimberlites (Figure 5.8c, d). Zr/Hf ratios vary between 35.4 and 54.1 whereas Nb/Ta ratios vary from 16.9 to 46.3 (Table 5.2). Similarly, other inter-element ratios; Nb/U varies from 6.6 to 78.5 and Ba/Nb varies between 4.1 and 39.9 (Table 5.2). Other HFS elements, e.g. Th and Y also show good correlation with La (Figure 5.8e, f), with most kimberlites having less than 39ppm Th and 28ppm Y, except for the Bellsbank kimberlite that is slightly more enriched in Th.

Sub-parallel chondrite normalised REE patterns of the analysed group II kimberlites are characterised by extreme light REE enrichment and lesser heavy REE enrichment. The light and heavy REE may show enrichment up to La ~ 1600 and Lu ~ 10 times chondrite (Bellsbank and Eendekuil kimberlites, respectively) with most samples overlapping the group II Swartruggens and Star kimberlites (Figure 5.9). On craton kimberlites (Bellsbank, Newlands, New Elands kimberlites) tend to more light REE enriched (La = 806-1647 times chondrite) in comparison to off-craton kimberlites (La = 381-882 times chondrite; Brandewynskuil, Eendekuil, Markt kimberlite). La/Yb and La/Sm ratios are generally high and illustrative of the steep light REE slope in chondrite normalised diagrams ($(La/Yb)_N$ = 44-326, $(La/Sm)_N$ = 6.3-12.3; Table 5.2). However, it is also noteworthy that the Bellsbank and Newlands kimberlites have distinctively greater La/Yb, La/Sm ratios than other kimberlite samples analysed in this study ($(La/Yb)_N$ < 150, $(La/Sm)_N$ < 8.0; Table 5.2).

Similar steep patterns occur on primitive mantle normalised diagrams, with the analysed samples showing distinct enrichment of incompatible elements (e.g. Ba = 112-609 and Th = 155-677 times primitive mantle; Figure 5.10). Superimposed upon smooth primitive mantle normalised patterns, the samples show distinct depletion in Rb, K, Ti with more subdued depletion in Ta-Nb and Sr, as well as a slight enrichment in Pb (Figure 5.10), features that are also common to the group II Swartruggens and Star kimberlites (Coe, 2004). However, some of the samples do not do not show a very distinct depletion of K relative to Nb, although K is still depleted relative to La ($K/K^* > 0.3$ and $K_2O > 2$ wt%). Consequently, group II kimberlites are subdivided into two groups, the first of which is hereafter notated as normal group II kimberlites, comprising the New Elands, Brandewynskuil, Markt and Eendekuil kimberlites and is characterised by a more subdued depletion in K. The second group (group IIb) consists of the Bellsbank and Newlands kimberlites, that are characterised by well-developed negative Rb and K anomalies as well as low K_2O concentrations (K/K^* = 0.0-0.1, < 1.9 wt% K_2O). Group IIb kimberlites also tend to have large negative Ti anomalies (Ti/Ti^* = 0.2-0.3) whereas Ti anomalies in normal group II kimberlites may be variable (Ti/Ti^* = 0.2-0.8). Most samples also show some minor depletion in Hf ($(Sm/Hf)_N$ < 2.7) that is only really noticeable as a well-developed negative Zr and Hf anomaly in the Eendekuil kimberlite ($(Sm/Hf)_N$ ~ 2.9; Figure 5.10). Depletion in Ta and Nb is a ubiquitous feature of the analysed group II kimberlites, as well as of the Swartruggens and Star

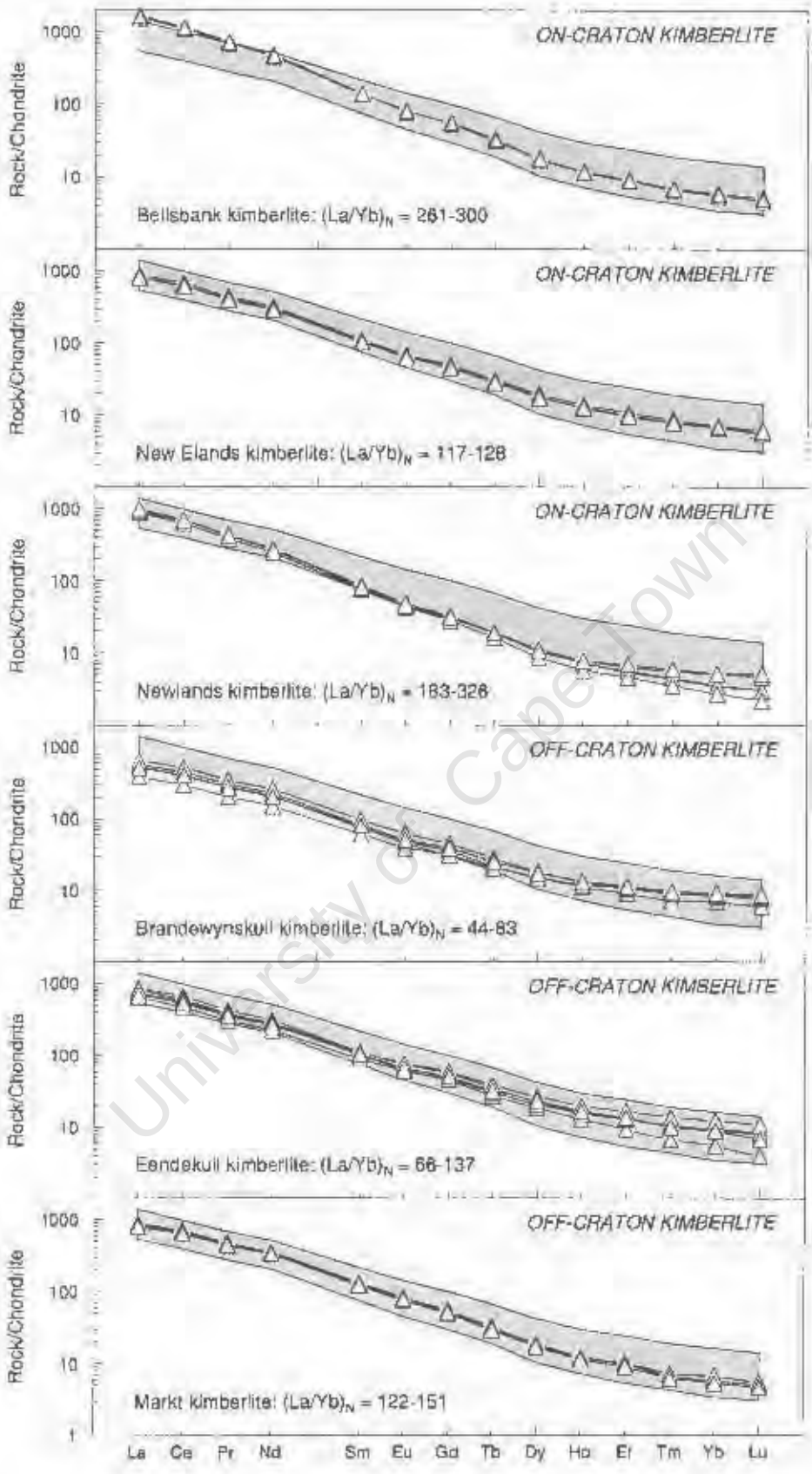

Figure 5.9: Chondrite normalised diagram of the rare earth elements for on- and off-craton group II kimberlites. Shaded field represents the on-craton Swartruggens and Star kimberlites (Coe, 2004). Chondrite normalising values are from Sun and McDonough (1989).

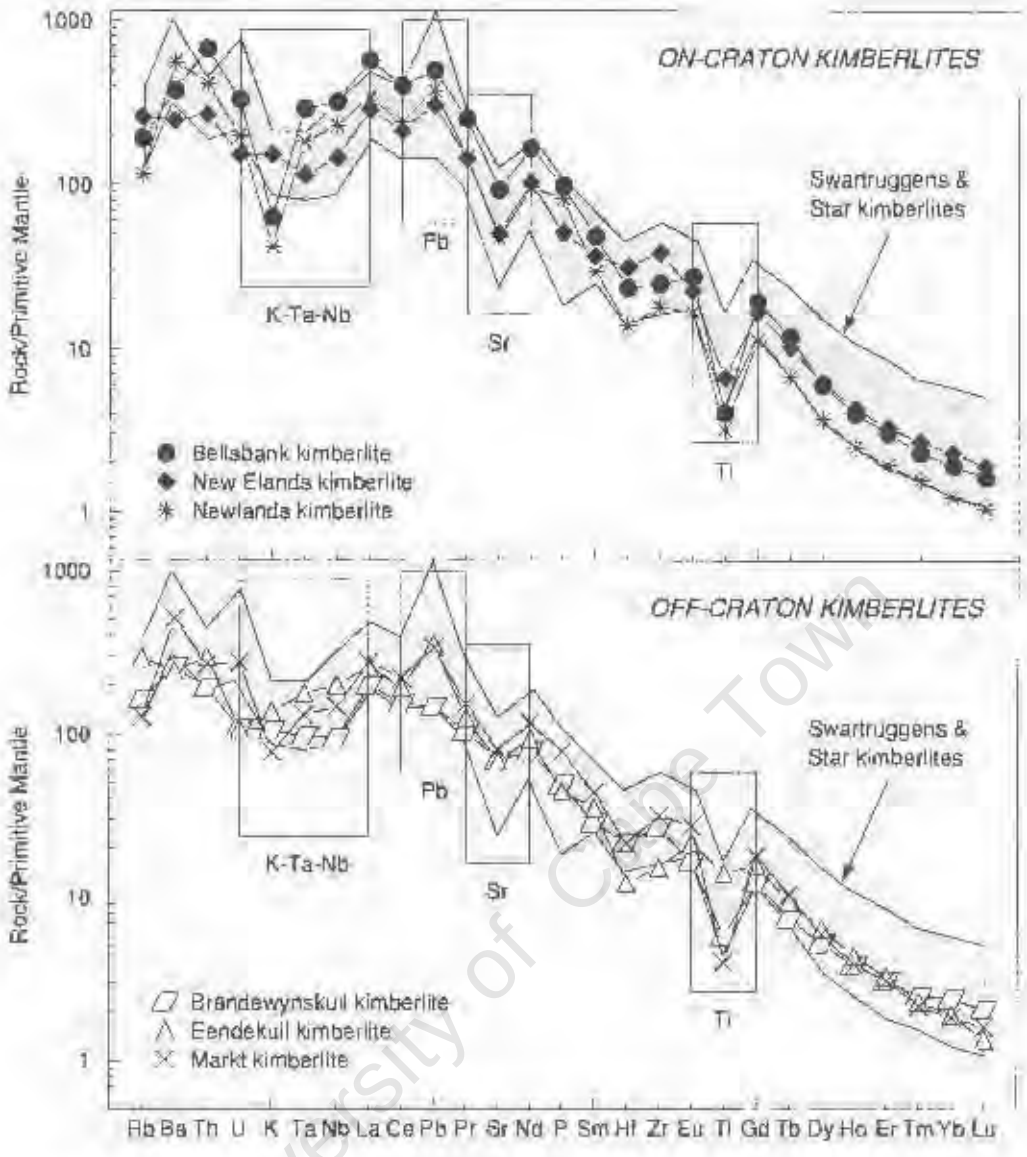

Figure 5.10: Primitive mantle normalised diagram of the incompatible trace elements for on- and off-craton group II kimberlites. Representative samples from each kimberlite are shown for simplicity. Shaded fields represent the on-craton group II Swartruggens and Star kimberlites (Coe, 2004). Primitive mantle normalising values are from Sun and McDonough (1989).

kimberlites (Coe, 2004) with $(La/Nb)_N$ ratios of the analysed samples generally being greater than 1.3. Positive Pb anomalies on primitive mantle normalised diagrams are also features of all of the analysed group II kimberlites ($(Ce/Pb)_N$ < 1; Figure 5.10), with some of the samples showing fairly large anomalies.

5.3.1 On-craton group II kimberlites

Bellsbank kimberlite

The macrocrystic on-craton Bellsbank kimberlite samples tend to be enriched in the ferromagnesian and LIL elements (e.g. 1297-1316ppm Ni, 1605-1740ppm Cr, 120-127ppm Rb, 1573-1947ppm Sr; Figure 5.6, 5.7) with LIL element contents that do not fall along the general group II kimberlite trend line defined by the correlation with La (Figure 5.7), a feature more caused by the very high La contents

of these samples (364-390ppm La). HFS element concentrations of the samples are generally equivalent (~218ppm Nb; La/Nb = 1.7±0.01; Nb/Ta = 19.1±0.2; Figure 5.8; Table 5.2) except for the contrasting Zr contents in the two samples (276 and 376ppm Zr). Samples are characterised by Zr/Nb = 1.2-1.8 and Ba/Nb = 11.6-19.4. Light REE concentrations of the samples (La ~ 1600 times chondrite; Figure 5.9) are more enriched than in the Swartruggens and Star kimberlites, whereas heavy REE concentrations (Lu ~ 4.9 times chondrite) are similar. Otherwise smooth primitive mantle normalised patterns, are characterised by large negative Rb, K and Ti anomalies (K/K* = 0.1; Ti/Ti* = 0.2), as well as more subdued depletions in Ta-Nb and Sr.

New Elands kimberlite

Sparsely macrocrystic and macrocrystic on-craton New Elands kimberlite samples tend to show good correlation of ferromagnesian element concentrations with MgO content (Figure 5.6), whereas variable Rb, Ba, Sr and Pb contents correlate poorly with La (Figure 5.7). Abundances of HFS elements (Figure 5.8) tend to be similar in individual samples (e.g. 92.4-106ppm Nb, 4.01-4.67ppm Ta; Table 5.2), although Zr concentrations are variable (317-432ppm). The New Elands kimberlite is characterised by La/Nb = 1.9-2.0, Ba/Nb = 16.5-39.9 and Th/Nb = 0.2-0.3. Light REE concentrations are generally equivalent between samples (La = 806-856 times chondrite; $(La/Yb)_N$ = 117-128; $(La/Sm)_N$ = 7.8-8.0; Figure 5.9). Primitive mantle normalised patterns of the samples are very similar to the Swartruggens and Star kimberlites, both in the absolute degree of enrichment and nature of the relative anomalies (Figure 5.10). Sample *NE K11* also has moderate positive Ba, U and large Pb anomalies (although not shown in Figure 5.10) superimposed upon its primitive mantle normalised pattern.

Newlands kimberlite

Concentrations of Ni, Cr and Co in macrocrystic on-craton Newlands kimberlite samples are high and show little inter-sample variation (~1495ppm Ni; ~2050ppm Cr; ~87ppm Co; Figure 5.6). Rb contents and K/Rb ratios (~66ppm Rb; K/Rb = 146; Figure 5.7a) are distinctively lower than the Swartruggens and Star kimberlites, whereas Sr, Ba, and Pb concentrations are more similar to the reference group II kimberlites (Figure 5.7). Sample *KN 3* however, has anomalously high Ba, Pb and low Rb contents (7345ppm Ba, 43.5ppm Pb, 30.7 ppm Rb; Table 5.2) that are reflected as relative positive and negative anomalies, respectively, on primitive mantle normalised diagrams. In contrast, inter-element ratios of the HFS elements do not show any significant differences between samples (e.g. Zr/Hf = 46.9 ±1.4; La/Nb = 1.4±0.07, Zr/Nb = 1.1±0.2; Table 5.2). Patterns on chondrite normalised graphs are characteristically steep ($(La/Yb)_N$ = 183-326; Figure 5.9) with comparatively flat heavy REE patterns for samples *KN 2* and *KN 3* ($(Gd/Lu)_N$ ~ 6.5). The Newlands kimberlite shows well-developed negative Rb, K (K/K* ~ 0.1) and Ti (Ti/Ti* ~0.2) anomalies on primitive mantle normalised diagrams, more similar to the Bellsbank kimberlite than the Swartruggens and Star kimberlites (Figure 5.10).

5.3.2 Off-craton group II kimberlites

Brandewynskuil kimberlite

Samples from the off-craton Brandewynskuil kimberlite are relatively macrocrystic and ferromagnesian element contents tend to be rather low and variable (e.g. 570-972ppm Ni, 888-1633 ppm Cr; Figure 5.6). Incompatible element concentrations generally fall within the field defined for the on-craton Swartruggens and Star group II kimberlites (Figure 5.7, 5.8) with inter-element ratios La/Nb and Zr/Nb, being more constrained than Ba/Nb (La/Nb = 1.6±0.3; Zr/Nb = 3.9±0.46; Ba/Nb = 25.4±4.9; Table 5.2). The samples tend to be less light REE enriched (La = 569-814 times chondrite; $(La/Yb)_N$ = 44-83) than the reference group II kimberlites (Figure 5.9), but heavy REE concentrations are equivalent due to the slight flattening out of heavy REE patterns (Lu = 5.94-8.94 times chondrite). Notable features of primitive mantle normalised patterns of the samples (Figure 5.10) are the small negative Rb, K (K/K* = 0.4-0.8), Sr, Ta-Nb anomalies and moderate negative Ti anomaly (Ti/Ti*~ 0.4).

Eendekuil kimberlite

Eendekuil kimberlite samples are characterised by particularly low ferromagnesian element concentrations (~296 ppm Ni, ~536ppm Cr; Figure 5.6) that correlate with the low MgO content of the predominantly phlogopite macrocrystic kimberlite samples. Variable LIL (171-210ppm Rb, 780-1978ppm Ba; Figure 5.7) and HFS (e.g. 128-195 ppm Nb; Figure 5.8) element concentrations of samples are generally similar to those of the Swartruggens and Star group II kimberlites. Most inter-element ratios of samples are fairly variable (e.g. Nb/Ta = 17.4-32.3, Ba/Nb = 4.1-11.9) and especially the Zr/Hf ratio (Zr/Hf = 35.4-49.8), since the variation of Zr is independent of La (Figure 5.8a). Consequently, primitive mantle normalised patterns are characterised by negative (sample *K2/2, K2/13*) as well as positive (samples *EKL 1, K2/3, K2/9*) Zr-Hf anomalies (only shown for sample *K2/2* in Figure 5.10). Other features of the primitive mantle normalised patterns of the moderately REE enriched kimberlite samples are the absence of a Rb anomaly and the presence of moderate negative K (K/K* = 0.3-0.5) and subdued Ta-Nb, Sr and Ti (Ti/Ti* = 0.6-0.8) anomalies as well as the flattening of the normalised heavy REE patterns ($(La/Yb)_N$ = 66.2-137; $(Gd/Lu)_N$ = 5.6-11.5; Table 5.2).

Markt kimberlite

Off-craton Markt kimberlite samples are all macrocrystic, with the more macrocrystic samples having higher Ni concentrations (1074-1171 ppm Ni, samples *JJG 2314, MRK 1*) than the less macrocrystic samples (812-885ppm Ni; samples *JJG 2336, MRK 3*). Other incompatible element concentrations are similar to those of the group II Swartruggens and Star kimberlites and are not correlated with the abundance of macrocrysts (Figure 5.7, 5.8). HFS element concentrations show little intra-kimberlite variation (e.g. 105-121ppm Nb, 336-383ppm Zr; Figure 5.8) with inter-element ratios La/Nb = 1.7±0.1, Zr/Nb = 3.1±0.3 and Th/Nb = 0.2±0.01, typical to other analysed group II kimberlites. Chondrite normalised REE patterns are relatively steep in character with La = 788-882 times chondrite and $(La/Yb)_N$ = 122-151 (Figure 5.9). Primitive mantle normalised trace element patterns of samples (Figure 5.10) show characteristic depletion in Rb, K, Ti and more minor depletion in Ta-Nb ($(La/Nb)_N$ = 1.7-1.9) and Sr, as well as slight enrichment in Pb $(Ce/Pb)_N$ = 0.6-0.7).

5.4 Transitional kimberlites

Ni concentrations in the analysed transitional kimberlite samples show a large range from 707ppm (Leicester kimberlite; Figure 5.11a) to 1609ppm (Melton Wold kimberlite), which overlaps the Ni contents of the on-craton group I Kimberley kimberlites (le Roex *et al.*, 2003) and group II Swartruggens and Star kimberlites (Coe, 2004). Cr concentrations show weak positive correlation with MgO (1193-1911ppm Cr; Figure 5.11b) and similarly overlap the fields for reference group I and group II kimberlites. Co and Sc contents are significantly lower than Ni and Cr, although equally variable (58.6-203ppm Co; 7.62-22.4ppm Sc; Figure 5.11c, d).

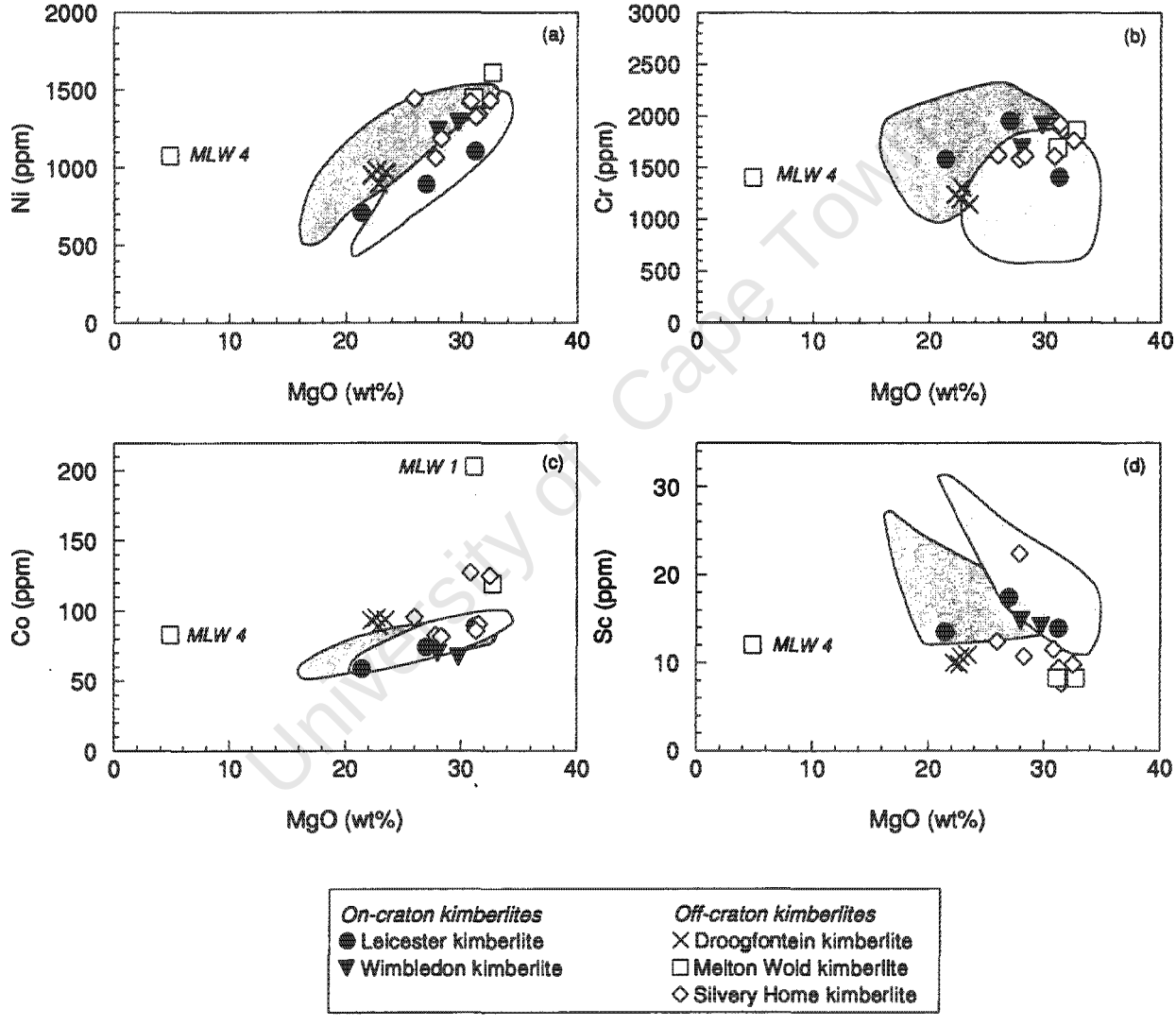

Figure 5.11: Variation of selected ferromagnesian elements versus MgO for on- and off-craton transitional kimberlites. Light shaded field represents the on-craton group I Kimberley kimberlites (le Roex *et al.*, 2003) and dark shaded field, the on-craton group II Swartruggens and Star kimberlites (Coe, 2004).

Table 5.3. XRF and ICP-MS trace element analyses (in ppm) of on- and off-craton transitional kimberlites. Various inter-element ratios are given, as well as the chondrite normalised La/Sm and La/Yb ratios. Normalising values are from Sun and McDonough (1989).

Transitional kimberlites:	On-craton					Off-craton			
Kimberlite:	**Leicester**			**Wimbledon**		**Droogfontein**			
Sample	JJG 4326	JJG 4328	JJG 6054	WIMB 1	WIMB 2	K19/2*	K19/3	K19/5*	K19/10
% Macro.	25	25	38	30	30	15	15	15	15
XRF									
Zr	-	-	-	371	382	369	-	382	-
Nb	299	231	208	478	523	223	-	220	-
Co	73.9	58.6	88.7	69.6	67.1	93.0	89.2	95.0	93.5
Cr	1659	1647	1333	1446	1630	1236	1255	1193	1297
Ni	-	-	-	1187	1152	951	1076	981	1131
V	112	103	60.6	99.0	97.8	148	95.0	174	167
Cu	-	-	-	35.0	31.2	84.0	77.8	91.0	59.3
ICP-MS									
Sc	17.4	13.5	13.9	14.8	14.1	10.0	10.7	9.85	10.9
Ni	860	659	1030	-	-	-	-	-	-
Cu	67.7	68.6	33.5	-	-	-	-	-	-
Rb	51.8	154	49.6	55.6	53.9	145	128	140	136
Sr	1256	1498	860	1744	1905	1578	1617	1556	1514
Y	24.4	16.3	11.0	28.3	28.7	23.2	20.7	22.8	20.0
Zr	475	358	273	-	341	371	389	407	416
Nb	300	231	197	452	476	251	266	254	246
Ba	2176	2130	1326	7722	7688	1631	1436	1470	1267
La	241	208	149	542	539	194	184	180	179
Ce	462	398	291	982	973	366	345	338	337
Pr	49.0	40.5	29.7	97.5	93.8	36.9	34.3	33.5	33.8
Nd	179	148	107	334	320	136	126	123	125
Sm	22.8	18.5	13.1	39.7	36.8	17.3	16.6	16.0	16.1
Eu	5.61	4.50	3.09	9.64	9.81	3.66	3.51	3.32	3.41
Gd	14.7	11.3	7.81	20.6	22.2	10.5	10.3	10.2	9.95
Tb	1.57	1.20	0.81	2.27	2.35	1.16	1.13	1.13	1.08
Dy	6.38	4.62	3.10	8.30	8.58	5.69	5.39	5.59	5.20
Ho	0.92	0.65	0.46	1.12	1.18	0.90	0.83	0.87	0.80
Er	1.94	1.36	1.02	2.13	2.40	2.10	1.96	2.10	1.84
Tm	0.21	0.15	0.12	0.24	0.25	0.25	0.22	0.25	0.21
Yb	1.03	0.81	0.68	1.17	1.29	1.51	1.34	1.50	1.29
Lu	0.13	0.10	0.09	0.13	0.15	0.18	0.16	0.17	0.16
Hf	9.14	6.87	5.50	5.99	5.62	8.76	9.03	9.38	9.58
Ta	9.26	11.2	9.97	15.2	13.7	13.6	13.2	12.9	13.1
Pb	14.7	24.4	12.9	48.7	46.8	22.0	26.0	22.7	25.7
Th	34.8	29.2	22.1	68.9	71.1	24.7	22.7	21.7	21.9
U	7.04	6.26	4.14	15.1	15.2	5.57	5.25	5.93	5.15
Nb/Ta	32.2	20.6	20.9	31.4	38.1	16.3	20.1	17.1	18.8
Zr/Hf	51.9	52.1	49.7	61.9	68.0	42.1	43.1	40.7	43.4
Zr/Nb	1.59	1.55	1.31	0.77	0.73	1.65	1.46	1.74	1.69
Ba/Nb	7.29	9.21	6.37	16.1	14.7	7.32	5.40	6.68	5.14
La/Nb	0.81	0.90	0.72	1.13	1.03	0.87	0.69	0.82	0.73
Nb/U	42.4	36.9	50.2	31.8	34.4	40.1	50.6	37.1	47.8
Ce/Pb	31.5	16.3	22.5	20.2	20.8	16.7	13.3	14.8	13.1
$(La/Sm)_N$	6.82	7.27	7.35	8.81	9.46	7.27	7.17	7.25	7.18
$(La/Yb)_N$	167	183	156	334	299	92.5	98.6	85.9	100

**XRF* analyses for Droogfontein kimbertite samples, *K19/2* and K19/5 are from Clark (1994).

Table 5.3. Continued

Transitional kimberlites:				Off-craton						
Kimberlite:	**Melton Wold**			**Silvery Home**						
Sample	MLW 1	MLW 3	MLW 4	JAR 21022	SLH 1	SLH 3	SLH 7	SLH 9	SLH 10	SLH 11
% Macro.	20	15	20	15	20	10	15	15	15	15
XRF										
Zr	79.0	83.8	128	283	154	177	362	445	211	179
Nb	97.6	115	178	177	115	91.7	169	195	154	152
Co	119	203	82.6	127	125	95.3	81.4	82.2	90.0	85.6
Cr	2193	3370	1271	2047	2085	1671	1404	1413	1545	1616
Ni	2191	2911	1178	2142	2534	1508	1109	1009	1410	1385
V	61.3	121	90.1	134	82.9	51.6	83.2	60.9	32.4	70.2
Cu	41.3	58.4	45.3	157	63.4	8.77	38.4	19.9	35.3	36.6
ICP-MS										
Sc	8.24	8.26	12.0	11.5	9.80	12.4	10.7	22.4	7.62	9.40
Ni	-	-	-	-	-	-	-	-	-	-
Cu	-	-	-	-	-	-	-	-	-	-
Rb	61.2	96.6	4.89	102	86.6	140	152	147	83.1	92.8
Sr	742	1074	514	561	531	467	765	492	746	595
Y	7.52	8.96	16.4	6.70	8.16	5.26	11.4	9.51	9.51	9.11
Zr	-	-	-	238	137	175	298	428	197	169
Nb	94.2	114	179	168	115	90.3	148	179	140	135
Ba	1930	2508	612	978	2423	3640	3663	3072	3094	3500
La	92.0	124	147	92.6	112	76.8	121	173	147	145
Ce	166	207	254	171	205	145	225	368	272	271
Pr	17.5	21.2	26.7	17.2	20.5	14.4	22.2	36.9	26.4	26.4
Nd	58.6	71.4	92.0	61.5	73.5	52.1	80.8	135	95.3	95.1
Sm	7.30	9.27	12.6	7.71	9.46	6.82	10.5	16.1	12.1	11.8
Eu	1.87	2.38	3.22	1.89	2.36	1.57	2.83	3.97	3.14	3.12
Gd	4.10	5.27	7.93	4.49	5.36	3.723	6.76	9.08	7.35	6.96
Tb	0.47	0.61	0.90	0.48	0.56	0.39	0.76	0.94	0.77	0.76
Dy	1.87	2.36	3.70	2.15	2.32	1.57	3.12	3.38	2.89	2.76
Ho	0.30	0.36	0.59	0.31	0.35	0.24	0.48	0.46	0.40	0.40
Er	0.63	0.76	1.25	0.65	0.81	0.56	1.09	0.95	0.88	0.82
Tm	0.08	0.09	0.15	0.08	0.09	0.06	0.13	0.10	0.10	0.09
Yb	0.41	0.46	0.76	0.47	0.50	0.42	0.80	0.62	0.53	0.51
Lu	0.06	0.06	0.10	0.06	0.06	0.06	0.11	0.08	0.07	0.07
Hf	1.41	1.45	2.79	4.73	3.37	5.52	7.37	12.42	4.59	3.96
Ta	6.47	7.20	9.31	6.47	7.31	5.83	6.95	13.57	7.85	7.92
Pb	8.50	16.3	16.3	9.96	12.4	13.5	12.9	7.32	11.7	12.0
Th	16.3	15.9	20.0	11.2	13.1	9.78	15.2	34.5	17.0	16.9
U	5.09	2.74	3.93	2.98	2.23	1.74	2.98	3.08	2.65	2.58
Nb/Ta	15.1	16.0	19.1	27.3	15.8	15.7	24.3	14.3	19.6	19.1
Zr/Hf	56.1	57.7	45.8	59.8	45.6	32.2	49.2	35.8	46.0	45.1
Zr/Nb	0.81	0.73	0.72	1.60	1.33	1.93	2.14	2.29	1.37	1.18
Ba/Nb	19.8	21.7	3.43	5.54	21.0	39.7	21.6	15.8	20.2	23.1
La/Nb	0.94	1.07	0.83	0.52	0.97	0.84	0.71	0.89	0.95	0.96
Nb/U	19.2	42.2	45.3	59.4	51.7	52.9	56.7	63.2	57.9	58.7
Ce/Pb	19.5	12.7	15.6	17.2	16.5	10.7	17.5	50.3	23.2	22.5
$(La/Sm)_N$	8.14	8.61	7.56	7.75	7.65	7.27	7.45	6.92	7.82	7.93
$(La/Yb)_N$	161	193	138	140	162	132	108	199	197	204

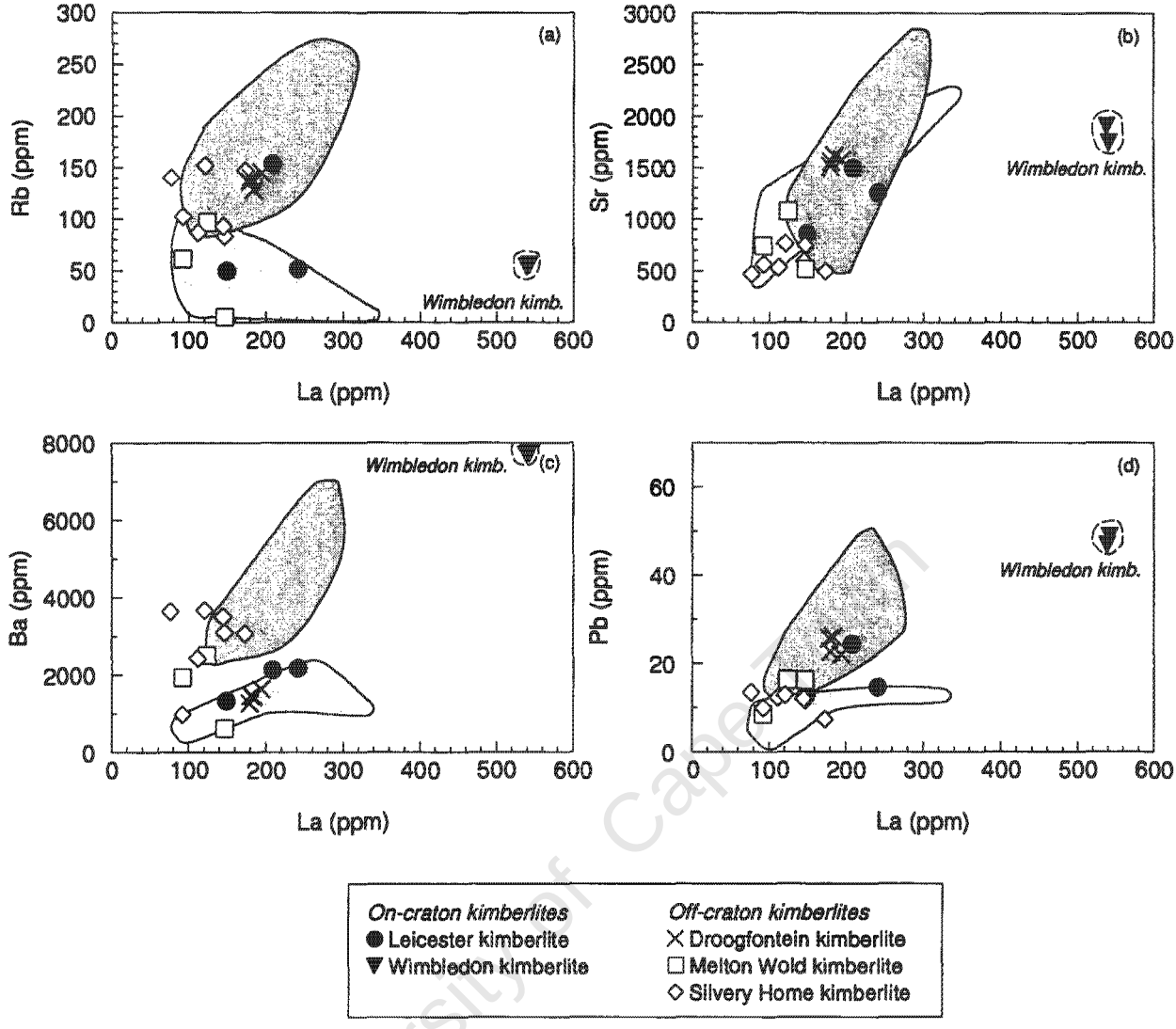

Figure 5.12: Variation of selected incompatible elements versus La for on- and off-craton transitional kimberlites. Light shaded field represents the on-craton group I Kimberley kimberlites (le Roex *et al.*, 2003) and dark shaded field, the on-craton group II Swartruggens and Star kimberlites (Coe, 2004).

Rb shows a scattered variation against the more immobile element La in the analysed transitional kimberlites (Figure 5.12a) and varies in abundance between 4.89ppm and 152ppm (Melton Wold and Silvery Home kimberlites, respectively). Sr and Ba concentrations show a slightly better correlation with La, and all kimberlite samples fall in the compositional fields defined for reference group I and group II kimberlites, except for the Wimbledon kimberlite, which has a much higher La content (Figure 5.12b, c). The samples tend to have less than 3700ppm Ba (Silvery Home kimberlite; Figure 5.12c), except for the Wimbledon kimberlite that is very enriched in Ba (~7800ppm). Most samples also have low Pb concentrations (< 26ppm; Droogfontein kimberlite; Figure 5.12d) with Ce/Pb ratios varying between 12.7 and 50.3 (Table 5.3).

HFS element concentrations of the transitional kimberlites tend to show good positive correlations with La (Figure 5.13a, b). Zr and Nb contents show good overlap with the compositional field of the on-craton group I Kimberley kimberlites, except for the Melton Wold kimberlite that extends to lower Zr (79ppm; Figure 5.13a) and the Wimbledon kimberlite which is very enriched in Nb (up to 523ppm; Figure 5.13b; Table 5.3). Correlations between the concentrations of Zr and Hf as well as Nb and Ta are generally good (Zr/Hf = 49±8.8; Nb/Ta = 19±3.5; Figure 5.13c,d), except for the Wimbledon kimberlite that has a considerably higher Nb/Ta ratio (Nb/Ta = 31-38). Some inter-element ratios (e.g. La/Nb = 0.5-1.1; Th/Nb = 0.06-0.1; Ba/Nb = 3.4-39.7; Table 5.3) tend to be more similar to the group I Kimberley kimberlites than the group II Swartruggens and Star kimberlites. Th and Y contents are low for most samples (11.2-34.8ppm Th; 7.52-28.7ppm Y; Figure 5.13e, f) and plot within the compositional field of reference group I and group II kimberlites.

The analysed transitional kimberlites show wide variation in REE concentrations and chondrite normalised patterns do not always fall within the compositional field defined for the on-craton group I Kimberley kimberlites (e.g. Wimbledon kimberlite; Figure 5.14). On-craton kimberlites are typically more enriched in the light REE than off-craton kimberlites (La = 629-2288 and La = 324-820 times chondrite, respectively) although heavy REE concentrations, La/Yb and La/Sm ratios tend to be more similar between samples (Lu = 2.20-6.99 times chondrite; $(La/Yb)_N$ = 100-334 and $(La/Sm)_N$ = 6.8-9.5).

Characteristic features on smooth primitive mantle normalised diagrams of the transitional kimberlites (Figure 5.15) are the superimposition of distinct negative Rb, K, Ti anomalies and small Sr anomalies relative to neighbouring elements (K/K* = 0.0-0.6, Ti/Ti* = 0.1-1.0). The on-craton kimberlites have the largest negative K anomalies, similar to the Kimberley kimberlites, whereas K anomalies in off-craton kimberlites tend not to be as pronounced. Of particular note is that the Melton Wold and Wimbledon kimberlites show distinct depletion in Zr and Hf ($(Sm/Hf)_N$ = 3.1-4.6; Figure 5.15), that can be correlated with larger negative Ti anomalies (Ti/Ti* <0.4) relative to other transitional kimberlites. Most of the kimberlites also show slight positive Pb anomalies on primitive mantle normalised diagrams ($(Ce/Pb)_N$ < 0.9). Only the Wimbledon kimberlite and one of the Melton Wold kimberlite samples show any depletion in Nb relative to La ($(La/Nb)_N$ > 1.1). Transitional kimberlites have incompatible element contents that generally fall within the compositional field defined for the group I Kimberley kimberlites, with the exception of the very enriched Wimbledon kimberlite (Figure 5.15).

5.4.1 On-craton transitional kimberlites

Leicester kimberlite

Trace element concentrations of the on-craton Leicester kimberlite samples are variable, but generally fall within the compositional range of the on-craton group I Kimberley kimberlite samples (Figure 5.11-5.15). Mutual positive correlations tend to exist between Ni (707-1104ppm), Co (58.6-88.7ppm) and MgO (Figure 5.11), that broadly correspond with olivine macrocryst content. Although concentrations of Rb, Sr, Ba and Pb are variable (Figure 5.12), sample *JJG 4328* tends to be the most enriched in these elements (154ppm Rb, 1498ppm Sr, 24.4ppm Pb) even though it is not the most enriched in the

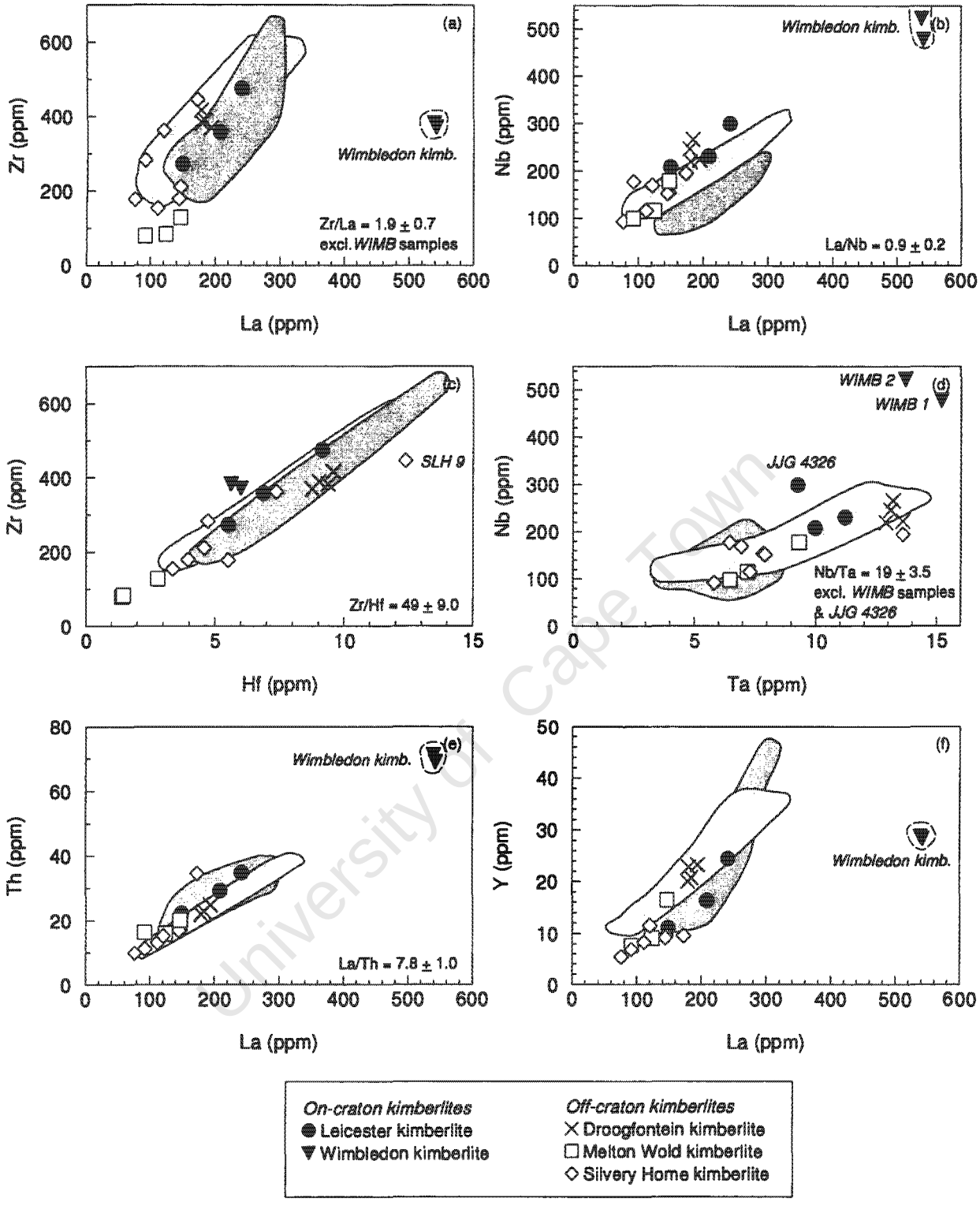

Figure 5.13: Variation of selected high field strength elements for on- and off-craton transitional kimberlites. Light shaded field represents the on-craton group I Kimberley kimberlites (le Roex *et al.*, 2003) and dark shaded field, the on-craton group II Swartruggens and Star kimberlites (Coe, 2004).

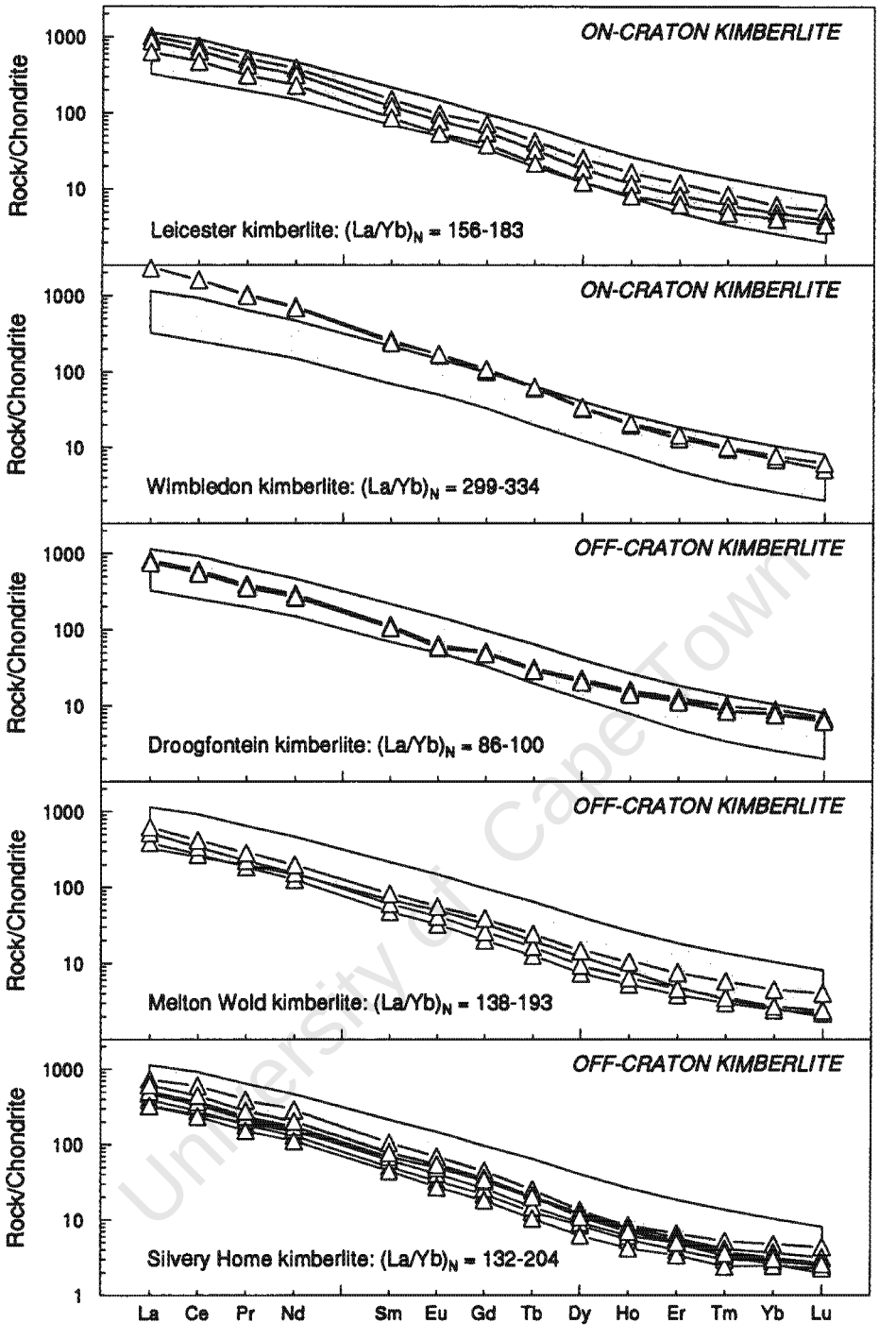

Figure 5.14: Chondrite normalised diagram of the rare earth elements for on- and off-craton transitional kimberlites. Light shaded field represents the on-craton group I Kimberley kimberlites (le Roex *et al.*, 2003). Chondrite normalising values are from Sun and McDonough (1989).

immobile element La. Consequently, the primitive mantle normalised diagram of this sample has a larger positive Pb and smaller negative Rb anomalies than samples *JJG 4326* and *JJG 6054*. Correlations of the HFS elements with La and with each other are generally good (e.g. La/Nb = 0.8±0.0.9; Ba/Nb = 7.6±1.5; Zr/Hf = 51.2±1.4), although Nb/Ta ratios are rather variable (Nb/Ta = 20.6-32.2), likely caused by the low Ta content of sample *JJG 4326* (9.26ppm Ta; Figure 5.13d).

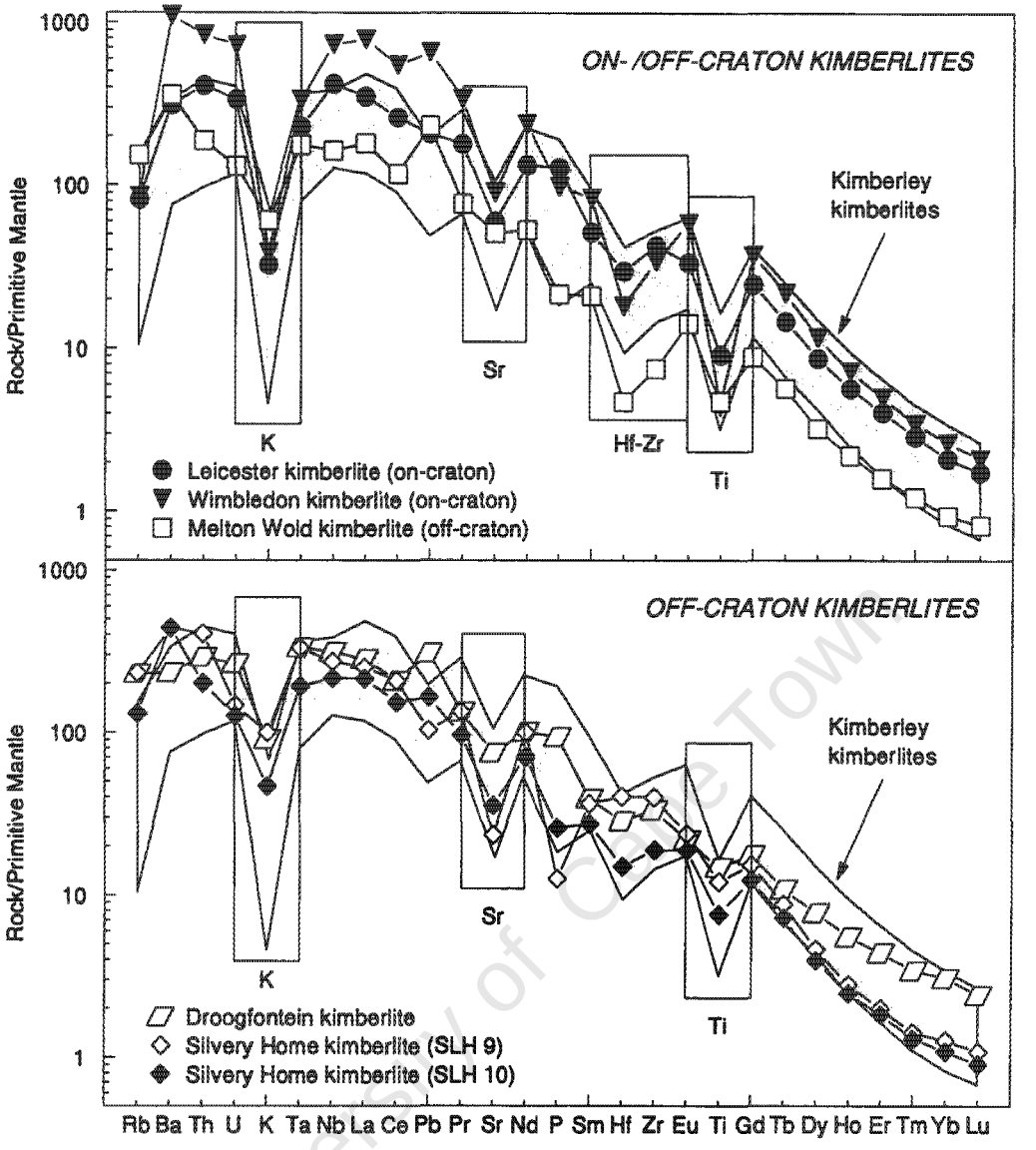

Figure 5.15: Primitive mantle normalised diagram of the incompatible trace elements for on- and off-craton transitional kimberlites. Representative samples from each kimberlite are shown for simplicity. Shaded fields represent the on-craton group I Kimberley kimberlites (le Roex *et al.*, 2003). Primitive mantle normalising values are from Sun and McDonough (1989).

Features of the primitive mantle normalised pattern of the Leicester kimberlite are the large negative Rb and K anomalies, a moderate negative Ti anomaly and subdued Sr anomalies, similar to patterns for the group I Kimberley kimberlites (Figure 5.15).

Wimbledon kimberlite

On-craton Wimbledon kimberlite samples are macrocrystic and similar in geochemical character having moderate abundances of Ni, Cr, Co and Sc (~1264ppm Ni, ~1800ppm Cr, ~68.4ppm Co, ~14.5ppm Sc) that are comparable to those of the group I Kimberley kimberlites (Figure 5.11). Incompatible element concentrations are generally high (e.g. ~7700ppm Ba, ~1825ppm Sr; Table 5.3), although Rb, Zr and Hf show relative depletion in comparison to other kimberlites (~55ppm Rb; ~377ppm Zr; ~5.8ppm Hf; Figure 5.12, 5.13). Samples are extremely light REE enriched, with very

steep REE patterns (La ~ 2280 and Lu ~ 5.59 times chondrite, $(La/Yb)_N$ ~ 282; $(La/Sm)_N$ ~ 9.1; Figure 5.14). Similarly, primitive mantle normalised patterns are steep with large negative Rb and K (K/K* ~ 0.05), Ti (Ti/Ti* ~ 0.09) and small negative Sr anomalies comparable to group I kimberlites. However, the distinctive depletion in Zr-Hf and minor depletion in Nb and Ta, are features of this kimberlite ($(Sm/Hf)_N$ ~4.6; $(La/Nb)_N$ ~ 1.2; Figure 5.15) that are only shared with the Melton Wold kimberlite.

5.4.2 Off-craton transitional kimberlites

Droogfontein kimberlite

Macrocrystic kimberlite samples from the off-craton Droogfontein kimberlite show little geochemical variation. Although incompatible element concentrations broadly overlap the field of both reference group I and group II kimberlites, for certain elements, samples overlap with the compositional field of the Swartruggens and Star kimberlites (e.g. 128-145ppm Rb; 22.0-26.0ppm Pb; Figure 5.12), whereas they overlap more with the Kimberley kimberlites for others (e.g. 369-416ppm Zr, 220-266ppm Nb; Figure 5.13). Trace element ratios Nb/U = 37.1-50.6, La/Nb = 0.7-0.9, Ba/Nb = 5.1-7.3 are similar to reference group I kimberlites, whereas Ce/Pb = 13.1-16.7, is more similar to reference group II kimberlites. REE patterns of kimberlite samples are not very steep and show flattening of the heavy REE (La ~778 times chondrite; $(La/Yb)_N$ ~ 94.1; $(Gd/Lu)_N$ ~ 16.5; Figure 5.14). Features of primitive mantle normalised trace element patterns, are the moderate depletion in K (K/K* ~ 0.3) but lack of Rb depletion and presence of subdued negative Sr, Ti and positive Pb anomalies (Figure 5.15).

Melton Wold kimberlite

Macrocrystic kimberlite samples from the off-craton Melton Wold kimberlite show wide inter-sample variability and have ferromagnesian element contents that vary from 1073-1609ppm Ni, 1403-1860ppm Cr and 82.6-203ppm Co (Figure 5.11). LIL element concentrations of sample *MLW 4* (e.g. 4.89ppm Rb, 612ppm Ba; Figure 5.12) always tend to be markedly lower than for samples *MLW 1* and *MLW 3* (61.2-96.6ppm Rb, 1930-2508ppm Ba; Table 5.3). HFS element contents are similar to those of the Kimberley kimberlites (Figure 5.13) except for Zr and Hf concentrations that are relatively depleted (79.0-128ppm Zr, 1.41-2.79ppm Hf). However, the Zr/Hf ratio (Zr/Hf = 45.8-57.7) is not significantly different to that of other analysed kimberlites. Sample *MLW 4* is comparatively more REE enriched than the other two samples (La = 620 and 388-521 times chondrite, respectively). Moderate negative Rb and K (K/K* = 0.0-0.3), Ti and strong Zr-Hf anomalies as well as small positive Pb anomalies (e.g. sample *MLW 3*) are features of the Melton Wold kimberlite on primitive mantle normalised diagrams (Figure 5.15). Sample *MLW 3* also shows subdued depletion in Nb and Ta on primitive mantle normalised diagrams ($(La/Nb)_N$ = 1.1).

Silvery Home kimberlite

Ferromagnesian element concentrations (e.g. 1062-1444ppm Ni) in the sparsely macrocrystic to macrocrystic off-craton Silvery Home kimberlite samples tend to correlate with MgO content (Figure 5.11), with both compatible and incompatible element concentrations broadly overlapping the compositional fields of the group I Kimberley and group II Swartruggens and Star kimberlites (Figure

5.11-5.15). Diopside phlogopite kimberlite samples (*SLH 3, SLH 7, SLH 9*) are richer in incompatible elements Rb and Ba (~146ppm Rb, ~3458ppm Ba; Table 5.3) than non-diopside bearing samples (*JAR 20122, SLH 1, SLH 10, SLH 11*). However, HFS element (154-445ppm Zr, 91.7-195ppm Nb; Figure 5.13) and REE (La = 324-509 and Lu = 2.25-4.34 times chondrite; Figure 5.14) concentrations are independent of this petrographic difference and are in fact, rather variable. Primitive mantle normalised patterns of all samples (Figure 5.15) show depletion in Rb, K and Sr with minor negative Ti ($Ti/Ti^* > 0.6$) anomalies. However, the diopside-bearing samples have comparatively smaller negative K anomalies as well as negative P and positive Zr-Hf anomalies on primitive mantle normalised diagrams (Figure 5.15).

CHAPTER 6

ISOTOPE GEOCHEMISTRY

6.1 Introduction

Studies of the radiogenic isotope geochemistry of kimberlites are marked by the pioneering work of Smith (1983a) who recognised the existence of two isotopic groups of southern African kimberlites. The first group (group I kimberlites) is characterised by having initial $^{87}Sr/^{86}Sr$ ratios between 0.7033 and 0.7049, and with initial $^{143}Nd/^{144}Nd$ ratios varying from 0.51271 to 0.51277 (Smith, 1983a), corresponding to the "basaltic" kimberlite of Wagner (1914). The second group (group II kimberlites) is characterised by significantly more radiogenic $^{87}Sr/^{86}Sr$ (0.7074-0.7109) and relatively unradiogenic $^{143}Nd/^{144}Nd$ (0.51208-0.51228) ratios and corresponds to the "micaceous" kimberlite variety of Wagner (1914). The source of group I kimberlites is inferred to be depleted relative to present day Bulk Earth, and similar to enriched mid-ocean ridge basalt (MORB) and ocean island basalt (OIB; Smith, 1983a). In contrast, group II kimberlites are inferred to derive from ancient enriched sources characterised by high Rb/Sr and low Sm/Nd ratios and postulated to be located within the subcontinental lithospheric mantle (Coe, 2004; Tainton, 1992; Fraser & Hawkesworth, 1992; Smith, 1983a). Skinner (1989) noted the existence of some petrographically intermediate kimberlites and subsequent isotope analyses showed that these kimberlites have isotopic signatures transitional to group I and group II kimberlites. This largely off-craton group of transitional kimberlites have $^{87}Sr/^{86}Sr_{(i)}$ ratios varying from 0.7055 to 0.7070 and $^{143}Nd/^{144}Nd_{(i)}$ ratios between 0.51215 and 0.51235 (Skinner *et al.*, 1992).

The early investigations by Mitchell and Crocket (1971) and Berg and Allsopp (1972) on the Sr isotope geochemistry of kimberlites, led to conflicting results that were later shown to be caused by the analysis of altered kimberlite samples (Barret & Berg, 1975). This highlights the fact that Sr isotope ratios of kimberlites are susceptible to post emplacement alteration, particularly since the rocks are permeable and often brecciated (Berg & Allsopp, 1972). Ground waters percolating through the kimberlite are likely to affect Rb concentrations (given its mobile nature) and to increase the $^{87}Sr/^{86}Sr$ ratio of the kimberlite since the $^{87}Sr/^{86}Sr$ ratios of meteoric waters are generally greater than 0.7120 (Barrett & Berg, 1975). The Nd isotope system on the other hand is far more robust due to the relative immobility of Nd and Sm, in contrast to Rb and Sr (Richardson, 1984).

Crustal contamination may affect isotope ratios of kimberlites since crustal rocks are generally characterised by high Sr and low Nd concentrations (325ppm Sr, 20ppm Nd; Rudnick & Fountain, 1995), as well as radiogenic $^{87}Sr/^{86}Sr$ and unradiogenic $^{143}Nd/^{144}Nd$ ratios ($^{87}Sr/^{86}Sr$ = 0.750-0.800, $^{143}Nd/^{144}Nd$ = 0.5115; Smith, 1983b). Assimilation of country rock may cause intra-kimberlite variation with increased $^{87}Sr/^{86}Sr$ and decreased $^{143}Nd/^{144}Nd$ ratios. However, an unrealistically large portion of xenolith assimilation would be necessary to leave a marked imprint on the kimberlite bulk-rock

geochemistry (Smith, 1983b). The group II Bellsbank kimberlite has intruded through Proterozoic Campbell Rand dolomite and the possibility that the kimberlite may have assimilated radiogenic Sr cannot be ignored (Kirkley, 1987).

Kimberlites are commonly macrocrystic in character due to contamination by entrained mantle material (le Roex *et al.*, 2003; Clement *et al.*, 1984). Peridotite xenoliths hosted by kimberlites illustrate the heterogeneous nature of the lithospheric mantle (εNd = -40 to +20; $^{87}Sr/^{86}Sr$ = 0.700-0.710; Pearson & Nowell, 2002; McDonough, 1990) reflecting the prior metasomatic history of the mantle (e.g. Hawkesworth *et al.*, 1990). Fraser and Hawkesworth (1992) have argued that the εNd variation in the group II Finsch kimberlite samples is due to the effect of the entrainment of 50-60% mantle peridotite by the kimberlite. Similarly, it would be reasonable to expect that some of the variation in general kimberlite isotope geochemistry, can be attributed to peridotite entrainment.

Sr and Nd isotope ratios of kimberlites were measured by thermal ionisation mass spectrometry (TIMS), with the aim of characterising the isotope geochemistry of each kimberlite forming part of this study and ascertaining characteristic features of the source region of every kimberlite. The objective of this chapter is therefore to characterise and compare the isotope geochemistry of samples, with further discussion into the influence of secondary processes (e.g. alteration) in Chapter 8. Twenty-five kimberlite samples were analysed, consisting of generally one representative sample per kimberlite, but where no previous isotope analyses existed for a particular kimberlite (e.g. Leicester and Wimbledon kimberlites), a second sample was analysed. Details of the sample preparation procedure and instrument running conditions, as well as a brief description of some of the analytical problems experienced are given in Appendix C and D, respectively. Measured Sr and Nd isotope ratios of the analysed kimberlite samples are reported in Tables 6.1 and 6.2, respectively, and initial $^{87}Sr/^{86}Sr$ and $^{143}Nd/^{144}Nd$ isotope ratios have been calculated according to the published (Table 2.2) or assumed age of kimberlite emplacement. Parent/daughter element concentrations and two-sigma errors are also given in Tables 6.1 and 6.2. In addition, initial Nd isotope ratios are reported in the epsilon (ε) notation, calculated as follows:

$$\varepsilon Nd_{(i)} = \left[\frac{^{143}Nd/^{144}Nd \text{ sample at T}}{^{143}Nd/^{144}Nd \text{ CHUR at T}} - 1 \right] \times 10^4$$

The parameter εNd describes the deviation of the sample from the chondritic uniform reservoir (CHUR, O'Nions *et al.*, 1979; De Paolo & Wasserberg, 1976) at time T, which is conventionally the age of magma formation/kimberlite emplacement. Rocks with positive or near zero εNd values (e.g. MORB and group I kimberlites) have source regions with time averaged depletion in Nd relative to Sm, compared to Bulk Earth. Rocks with negative εNd values (e.g. continental crust, group II kimberlites, lamproites) have time integrated light REE enriched source regions, characterised by low Sm/Nd ratios.

Table 6.1. Measured Sr isotope ratios and calculated parent/daughter ratios for on- and off-craton group I, group II and transitional kimberlites. Rb and Sr concentrations of kimberlite samples are from ICP-MS analyses (Tables 5.1-5.3), and from Harris *et al.* (2004) for the Uintjiesberg kimberlite. Initial isotope (i) ratios were calculated using kimberlite emplacement ages (Table 2.2) unless otherwise indicated (*), for which ages have been assumed. Newlands kimberlite sample *JJG 24D* is a duplicate analysis of sample *JJG 24*.

Kimberlite	Sample	Rb (ppm)	Sr (ppm)	$^{87}Rb/^{86}Sr$	$^{87}Sr/^{86}Sr_{(M)}$	2-sigma	Age (Ma)	$^{87}Sr/^{86}Sr_{(I)}$
Group I kimberlites: On-craton								
Goedehoop kimberlite	JAR 30012	16.6	1072	0.0448	0.703633	18	74*	0.703586
Goedehoop kimberlite	JJG 4282	16.9	1164	0.0420	0.703731	15	74*	0.703687
Koffiefontein kimberlite	KK 3	82.3	816	0.2919	0.704587	16	90	0.704212
Koffiefontein kimberlite	KK 6	29.6	1470	0.0583	0.704850	17	90	0.704775
Group I kimberlites: Off-craton								
Abbotsford East kimberlite	JJG 3118	10.2	998	0.0296	0.704046	15	150*	0.703983
Hebron kimberlite	HEB 1A	49.1	733	0.1938	0.703887	14	74*	0.703684
Klipgatsfontein kimberlite	JAR 31012	12.1	876	0.0400	0.703906	15	74*	0.703864
Klipgatsfontein kimberlite	JJG 4323	28.2	1010	0.0808	0.703917	15	74*	0.703832
Uintjiesberg kimberlite	UB 1	46.4	1232	0.1090	0.704704	17	101	0.704548
Uintjiesberg kimberlite	UB 6	38.9	1465	0.0768	0.704669	17	101	0.704559
Zeekoegat kimberlite	JJG 1906	8.93	447	0.0578	0.704285	15	150*	0.704161
Group II kimberlites: On-craton								
Bellsbank kimberlite	JJG 4676	120	1947	0.1784	0.708296	17	122	0.707988
New Elands kimberlite	NE K6	163	1061	0.4448	0.708189	17	126	0.707394
Newlands kimberlite	JJG 24	72.9	1000	0.2110	0.708161	18	114	0.707819
Newlands kimberlite	JJG 24D	72.9	1000	0.2110	0.708155	14	114	0.707813
Group II kimberlites: Off-craton								
Brandewynskuil kimberlite	K6/11	103	1453	0.2052	0.708712	17	117*	0.708371
Eendekuil kimberlite	K2/2	187	1438	0.3765	0.707862	17	110	0.707273
Markt kimberlite	MRK 3	80.8	1677	0.1395	0.708606	16	117	0.708374
Transitional kimberlites: On-craton								
Leicester kimberlite	JJG 4326	51.8	1256	0.1194	0.706456	17	92	0.706300
Leicester kimberlite	JJG 6054	49.6	860	0.1670	0.707696	14	92	0.707477
Wimbledon kimberlite	WIMB 1	55.6	1744	0.0923	0.706118	17	90*	0.706000
Wimbledon kimberlite	WIMB 2	53.9	1905	0.0819	0.705748	18	90*	0.705643
Transitional kimberlites: Off-craton								
Droogfontein kimberlite	K19/2	145	1578	0.2660	0.707025	18	174	0.706368
Melton Wold kimberlite	MLW 3	96.6	1074	0.2603	0.706674	16	143	0.706145
Silvery Home kimberlite	SLH 9	147	492	0.8650	0.708726	17	170*	0.706636
Silvery Home kimberlite	SLH 10	83.1	746	0.3225	0.707386	16	170*	0.706607

Note: Decay constant for Rb-Sr isotope system = $1.42 \times 10^{-11} a^{-1}$ and measured isotope ratios are normalised to $^{86}Sr/^{88}Sr = 0.1194$.

Table 6.2. Measured Nd isotope ratios and calculated parent/daughter ratios for on- and off-craton group I, group II and transitional kimberlites. Sm and Nd concentrations of kimberlite samples are from ICP-MS analyses (Tables 5.1-5.3), and from Harris *et al.* (2004) for the Uintjiesberg kimberlite. Initial isotope (i) ratios were calculated using kimberlite emplacement ages (Table 2.2) unless otherwise indicated (*), for which ages have been assumed.

Kimberlite	Sample	Sm (ppm)	Nd (ppm)	$^{147}Sm/^{144}Nd$	$^{143}Nd/^{144}Nd_{(M)}$	2-sigma	Age (Ma)	$^{143}Nd/^{144}Nd_{(i)}$	$\varepsilon Nd_{(i)}$
Group I kimberlites: On-craton									
Goedehoop kimberlite	JAR 30012	27.1	181	0.0905	0.512732	8	74*	0.512688	2.83
Goedehoop kimberlite	JJG 4282	30.0	201	0.0902	0.512738	9	74*	0.512695	2.96
Koffiefontein kimb.	KK 3	13.0	98.0	0.0802	0.512607	17	90	0.512560	0.74
Koffiefontein kimb.	KK 6	16.7	129	0.0783	0.512607	16	90	0.512561	0.76
Group I kimberlites: Off-craton									
Abbotsford East kimb.	JJG 3118	10.9	69.7	0.0945	0.512593	11	150*	0.512500	1.07
Hebron kimberlite	HEB 1A	10.9	68.8	0.0958	0.512752	9	74*	0.512705	3.17
Klipgatsfontein kimb.	JAR 31012	14.8	96.4	0.0928	0.512720	9	74*	0.512675	2.59
Klipgatsfontein kimb.	JJG 4323	15.9	102	0.0942	0.512723	10	74*	0.512678	2.63
Uintjiesberg kimberlite	UB 1	24.8	171	0.0877	0.512602	10	101	0.512544	0.69
Uintjiesberg kimberlite	UB 6	19.1	131	0.0881	0.512582	8	101	0.512524	0.31
Zeekoegat kimberlite	JJG 1906	10.0	63.6	0.0950	0.512579	9	150*	0.512485	0.78
Group II kimberlites: On-craton									
Bellsbank kimberlite	JJG 4676	21.5	224	0.0580	0.512051	9	122	0.512005	-9.30
New Elands kimb.	NE K6	16.2	139	0.0704	0.511972	8	126	0.511914	-10.97
Newlands kimberlite	JJG 24	13.0	129	0.0609	0.512004	8	114	0.511958	-10.40
Group II kimberlites: Off-craton									
Brandewynskuil kimb.	K6/11	12.6	105	0.0637	0.511989	10	117*	0.511934	-10.81
Eendekuil kimberlite	K2/2	15.5	126	0.0744	0.512098	8	110	0.512045	-8.82
Markt kimberlite	MRK 3	19.3	157	0.0743	0.512010	10	117*	0.511953	-10.43
Transitional kimberlites: On-craton									
Leicester kimberlite	JJG 4326	22.8	179	0.0770	0.512538	9	92	0.512491	-0.54
Leicester kimberlite	JJG 6054	13.1	107	0.0740	0.512529	9	92	0.512484	-0.69
Wimbledon kimberlite	WIMB 1	39.7	334	0.0719	0.512480	8	90*	0.512438	-1.65
Wimbledon kimberlite	WIMB 2	36.8	320	0.0695	0.512465	10	90*	0.512424	-1.91
Transitional kimberlites: Off-craton									
Droogfontein kimb.	K19/2	17.3	136	0.0769	0.512239	9	174	0.512152	-5.13
Melton Wold kimb.	MLW 3	7.30	58.6	0.0753	0.512351	11	143	0.512281	-3.38
Silvery Home kimb.	SLH 9	16.1	135	0.0633	0.512217	8	170*	0.512137	-5.51
Silvery Home kimb.	SLH 10	12.1	95.3	0.0767	0.512163	8	170*	0.512078	-6.67

Note: Decay constant for Sm-Nd isotope system = 6.54 x 10^{-12} a^{-1} and measured isotope ratios are normalised to $^{146}Nd/^{144}Nd$ = 0.7219. $^{143}Nd/^{144}Nd$ = 0.512638, $^{147}Sm/^{144}Nd$ = 0.1966 for CHUR.

6.2 Group I kimberlites

Calculated initial $^{87}Sr/^{86}Sr$ ratios and $^{143}Nd/^{144}Nd$ values of the analysed group I kimberlites are illustrated in Figure 6.1, with the compositional field of southern African group I kimberlites shown for comparison (Nowell *et al.*, 2004; Nowell *et al.*, 1999; Smith, 1983a). Additional samples *UB 1* and *UB 6* from the off-craton Uintjiesberg kimberlite were also analysed (Figure 6.1), since Harris *et al.* (2004) only report major and trace element analyses. Initial $^{87}Sr/^{86}Sr$ ratios of group I kimberlites vary from 0.70359±2 (Goedehoop kimberlite sample *JAR 30012;* Figure 6.1) to 0.70478±2 (Koffiefontein kimberlite sample *KK 6*). Initial $^{87}Sr/^{86}Sr$ ratios of the more olivine macrocrystic samples (10-20 vol.% olivine macrocrysts; Koffiefontein, Abbotsford East and Zeekoegat kimberlites) tend to be higher than the less olivine macrocrystic samples (Hebron, Goedehoop and Klipgatsfontein kimberlites), but the equivalence of $^{87}Sr/^{86}Sr$ ratios for macrocrystic and aphanitic Uintjiesberg kimberlite samples ($^{87}Sr/^{86}Sr_{(i)}$ = 0.70456 for macrocrystic sample *UB 6* and 0.70455 for aphanitic sample *UB 1;* Table 6.1) suggests that this apparent trend is likely fortuitous. Intra-kimberlite variation of $^{87}Sr/^{86}Sr$ ratios is limited for samples from the Goedehoop, Klipgatsfontein and Uintjiesberg kimberlites (Figure 6.1), although ratios of the on-craton Koffiefontein kimberlite ($^{87}Sr/^{86}Sr_{(i)}$ = 0.70421 and 0.70478) are slightly more variable, possibly due to contamination or alteration (see Chapter 8).

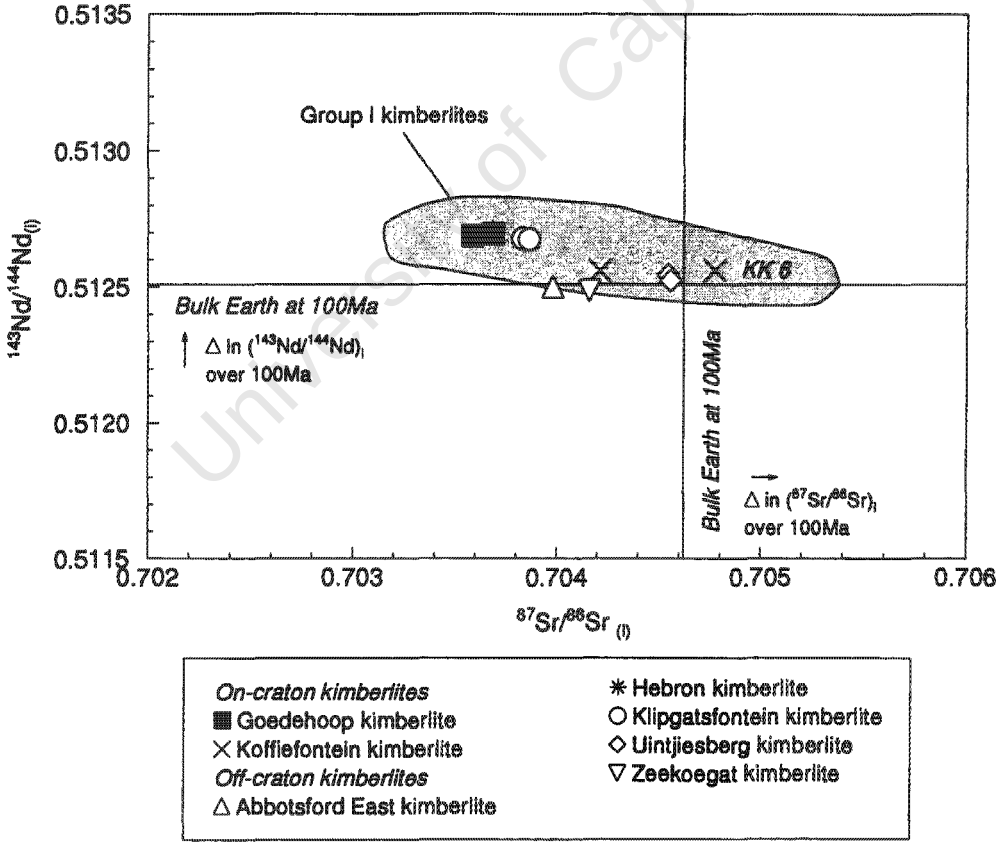

Figure 6.1: Initial $^{143}Nd/^{144}Nd$ and $^{87}Sr/^{86}Sr$ isotope correlation diagram for group I on- and off-craton kimberlites. Initial isotope ratios are calculated according to the age of kimberlite emplacement and two-sigma errors of isotope ratios are less than the symbol size. Shaded field represents southern African group I kimberlites (Nowell *et al.*, 2004; Nowell *et al.*, 1999; Smith, 1983a). Bulk Earth at 100Ma calculated from present day $^{87}Sr/^{86}Sr$ = 0.70475 and $^{87}Rb/^{86}Sr$ = 0.0863, $^{143}Nd/^{144}Nd$ = 0.512638 and $^{147}Sm/^{144}Nd$ = 0.1966.

Initial $^{143}Nd/^{144}Nd$ ratios of the analysed group I kimberlites vary between 0.51249±1 (Zeekoegat kimberlite sample *JJG 1906*; Figure 6.1) and 0.51271±1 (Hebron kimberlite sample *HEB 1A*). Isotope ratios of analysed kimberlites show negative correlation between $^{143}Nd/^{144}Nd$ and $^{87}Sr/^{86}Sr$ (Figure 6.1), with $^{143}Nd/^{144}Nd$ values describing two clusters of kimberlites, one with $^{143}Nd/^{144}Nd$ greater than 0.51260 (Goedehoop, Klipgatsfontein and Hebron kimberlites), and the other with $^{143}Nd/^{144}Nd$ between 0.51249 and 0.51256 (Koffiefontein, Uintjiesberg, Abbotsford East and Zeekoegat kimberlites). Intra-kimberlite variation in $^{143}Nd/^{144}Nd$ ratios for most kimberlite localities tends to be less than two-sigma, except for the Uintjiesberg kimberlite ($^{143}Nd/^{144}Nd$ = 0.51254 and 0.51252±1; Table 6.2). No on- and off-craton kimberlite variations are evident in the samples. Since most of the analysed group I kimberlites have $^{143}Nd/^{144}Nd$ and $^{87}Sr/^{86}Sr$ ratios greater and less than Bulk Earth at 100Ma, respectively (Figure 6.1), samples fall within the "depleted quadrant" of the isotope correlation diagram (although the initial $^{143}Nd/^{144}Nd$ ratios of the East Griqualand kimberlites are less than Bulk Earth at 100Ma, $^{143}Nd/^{144}Nd$ ratios are greater than Bulk Earth at 150Ma, the inferred age of kimberlite emplacement). Kimberlite samples analysed in this study broadly fall within the compositional field defined for southern African group I kimberlites, but do not extend to some of the higher $^{143}Nd/^{144}Nd$ ratios of the reference kimberlites (Figure 6.1; Nowell *et al.*, 2004; Nowell *et al.*, 1999; Smith, 1983a).

6.3 Group II kimberlites

Initial $^{87}Sr/^{86}Sr$ ratios of the analysed group II kimberlites in this study vary from 0.70728±2 (Eendekuil kimberlite sample *K2/2*; Figure 6.2; Table 6.1) to 0.70837±2 (Markt kimberlite sample *MRK 3* and Brandewynskuil kimberlite sample *K6/11*). Off-craton kimberlites show a broader range in $^{87}Sr/^{86}Sr$ ratios than on-craton kimberlites ($^{87}Sr/^{86}Sr_{(i)}$ = 0.70739 for New Elands kimberlite sample *NE K6* and 0.70799 for Bellsbank kimberlite sample *JJG 4676;* Figure 6.2). The initial $^{87}Sr/^{86}Sr$ ratio of New Elands kimberlite sample *NE K6* is comparable with that of sample *NE K10* (Figure 6.2), analysed by Smith (1983a). $^{87}Sr/^{87}Sr$ and $^{87}Rb/^{86}Sr$ ratios of kimberlite samples correlate negatively (although not shown) with the correlation being governed by some of the higher $^{87}Rb/^{86}Sr$ ratios measured in New Elands and Eendekuil kimberlites ($^{87}Rb/^{86}Sr$ = 0.38-0.44; Table 6.1). Initial $^{87}Sr/^{86}Sr$ ratios of the analysed kimberlites are comparable to those reported for South African group II kimberlites (Figure 6.2), but do not extend to some of the higher $^{87}Sr/^{86}Sr$ ratios measured for the Swartruggens and Finsch kimberlites (Coe, 2004; Nowell *et al.*, 2004; Nowell *et al.*, 1999; Fraser & Hawkesworth, 1992; Tainton, 1992; Smith, 1983a).

Initial $^{143}Nd/^{144}Nd$ ratios of group II kimberlite samples are characteristically unradiogenic and vary from 0.51191±1 (New Elands kimberlite sample *NE K6*; Figure 6.2) to 0.51205±1 (Eendekuil kimberlite sample *K2/2*). Inter-kimberlite variation of $^{143}Nd/^{144}Nd$ ratios is moderate (Table 6.2), with no apparent trends in $^{143}Nd/^{144}Nd$ ratios between sparsely macrocrystic and macrocrystic kimberlites or on- and off-craton kimberlites. The co-variation of initial $^{143}Nd/^{144}Nd$ and $^{87}Sr/^{86}Sr$ ratios tends to show a scattered distribution (Figure 6.2), although all kimberlite samples have compositions that lie within the field defined for South African group II kimberlites and within the "enriched quadrant" of an isotope

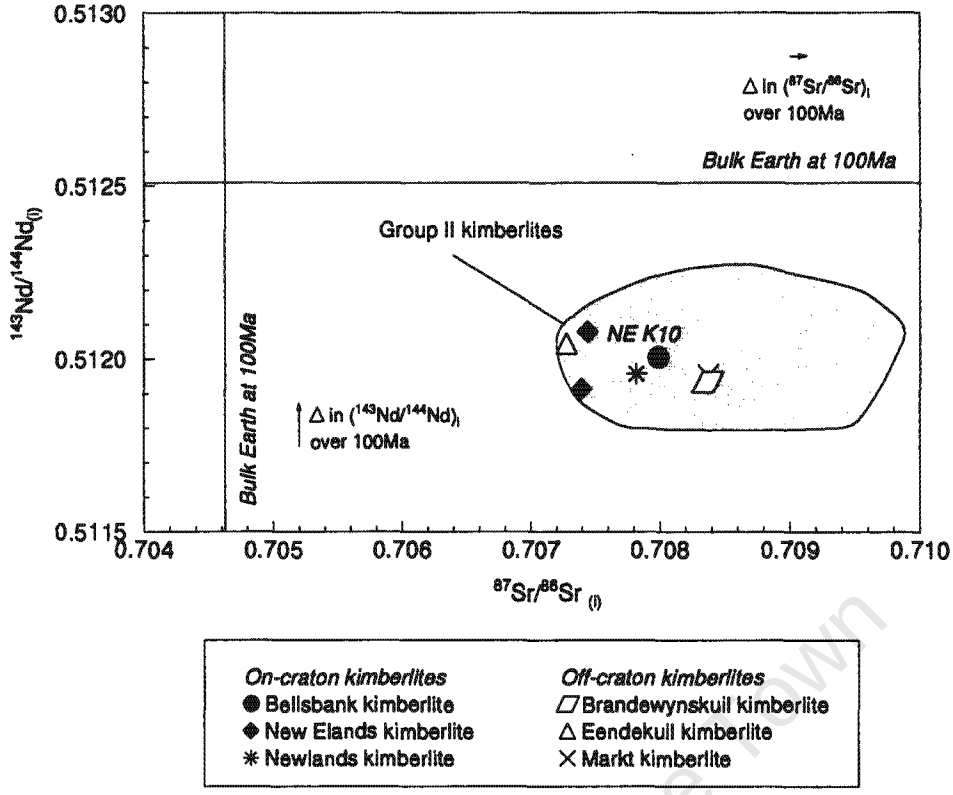

Figure 6.2: Initial $^{143}Nd/^{144}Nd$ and $^{87}Sr/^{86}Sr$ isotope correlation diagram for group II on- and off-craton kimberlites. Initial isotope ratios are calculated according to the age of kimberlite emplacement and two-sigma errors of isotope ratios are less than the symbol size. Isotope ratios of New Elands kimberlite sample *NE K10* are from Smith (1983a). Shaded field represents South African group II kimberlites (Coe, 2004; Nowell *et al.*, 2004; Nowell *et al.*, 1999; Fraser & Hawkesworth, 1992; Tainton, 1992; Smith, 1983a). Bulk Earth at 100Ma calculated from present day $^{87}Sr/^{86}Sr = 0.70475$ and $^{87}Rb/^{86}Sr = 0.0863$, $^{143}Nd/^{144}Nd = 0.512638$ and $^{147}Sm/^{144}Nd = 0.1966$.

correlation diagram (Coe, 2004; Nowell *et al.*, 2004; Nowell *et al.*, 1999; Fraser & Hawkesworth, 1992; Tainton, 1992; Smith, 1983a).

6.4 Transitional kimberlites

The analysed transitional kimberlites have initial $^{87}Sr/^{86}Sr$ ratios intermediate between group I and group II kimberlites and range from 0.70564±2 (Wimbledon kimberlite sample *WIMB 2;* Figure 6.3) to 0.70748±1 (Leicester kimberlite sample *JJG 6054*). The latter $^{87}Sr/^{86}Sr$ ratio may have been modified to a higher value by ground water alteration (also increased $^{87}Rb/^{86}Sr$; Table 6.1; Chapter 8) and therefore the $^{87}Sr/^{86}Sr$ ratio of sample *JJG 4326*, is considered more representative of the Leicester kimberlite ($^{87}Sr/^{86}Sr_{(i)} = 0.70630±2$). The $^{87}Sr/^{86}Sr$ ratios of the analysed off-craton kimberlite samples are more radiogenic than the on-craton kimberlite samples and vary from 0.70615±2 (Melton Wold kimberlite sample *MLW 3;* Figure 6.3) to 0.70664±2 (Silvery Home kimberlite sample *SLH 9*). Intra-kimberlite variation of $^{87}Sr/^{86}Sr$ ratios in the on-craton Wimbledon kimberlite samples is moderate ($^{87}Sr/^{86}Sr_{(i)} = 0.70564$ and 0.70600), in contrast to the off-craton Silvery Home kimberlite samples where the ratios fall just beyond the two-sigma error of each other ($^{87}Sr/^{86}Sr_{(i)} = 0.70661$ and 0.70664 where $2\sigma = 2$; Table 6.1). All of the initial $^{87}Sr/^{86}Sr$ ratios of the analysed transitional kimberlites

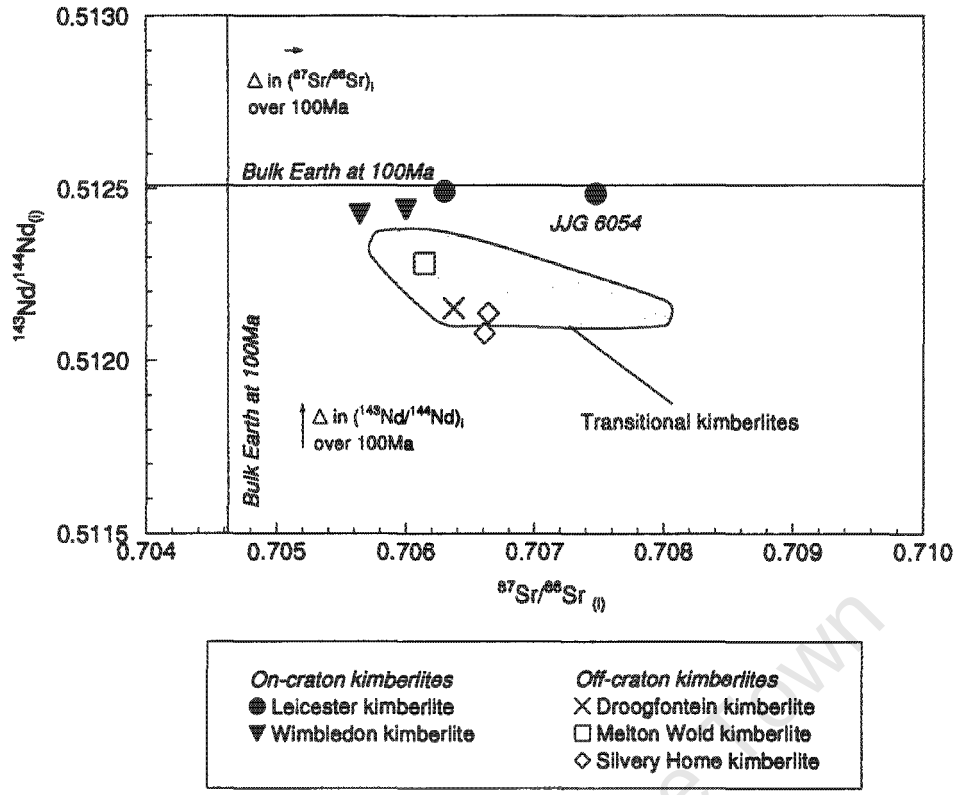

Figure 6.3: Initial $^{143}Nd/^{144}Nd$ and $^{87}Sr/^{86}Sr$ isotope correlation diagram for transitional on- and off-craton kimberlites. Initial isotope ratios are calculated according to the age of kimberlite emplacement and two-sigma errors of isotope ratios are less than the symbol size. Shaded field represents South African transitional kimberlites (Nowell *et al.*, 2004; Clark, 1994). Bulk Earth at 100Ma calculated from present day $^{87}Sr/^{86}Sr$ = 0.70475 and $^{87}Rb/^{86}Sr$ = 0.0863, $^{143}Nd/^{144}Nd$ = 0.512638 and $^{147}Sm/^{144}Nd$ = 0.1966.

broadly fall within the range defined for South African transitional kimberlites (Figure 6.3; Nowell *et al.*, 2004; Clark, 1994).

Initial $^{143}Nd/^{144}Nd$ ratios of transitional kimberlites are relatively unradiogenic and vary between 0.51214±1 (Silvery Home kimberlite sample *SLH 9*; Figure 6.3) and 0.51249±1 (Leicester kimberlite sample *JJG 4326*). One of the most prominent characteristics observed is that the on-craton kimberlites have $^{143}Nd/^{144}Nd$ ratios (0.51242-0.51249) greater than those of the off-craton kimberlites ($^{143}Nd/^{144}Nd$ = 0.51208-0.51229; Figure 6.3), although it is recognised that this may a feature of low sample numbers. Intra-kimberlite variation of $^{143}Nd/^{144}Nd$ ratios tends to be small for Wimbledon and Leicester kimberlite samples and the similarity of $^{143}Nd/^{144}Nd$ ratios for Leicester kimberlite samples ($^{143}Nd/^{144}Nd$ = 0.51248 for sample *JJG 6054* and 0.51249 for *JJG 4326*), suggests that the variation in $^{87}Sr/^{86}Sr$ ratios is caused by alteration. In contrast to the equivalent $^{87}Sr/^{86}Sr$ ratios of the diopside phlogopite (sample *SLH 9*) and phlogopite serpentine (sample *SLH 10*) facies kimberlite recorded at Silvery Home, $^{143}Nd/^{144}Nd$ ratios of samples are different ($^{143}Nd/^{144}Nd$ = 0.51214±1 for sample *SLH 9* and 0.51208±1 for *SLH 10*; Figure 6.3).

Transitional kimberlites analysed in this study all have $^{143}Nd/^{144}Nd_{(i)}$ and $^{87}Sr/^{86}Sr_{(i)}$ ratios less and greater than Bulk Earth at 100Ma, respectively (Figure 6.3) and therefore plot in the "enriched

quadrant" of the isotope correlation diagram. Comparison of $^{143}Nd/^{144}Nd$ and $^{87}Sr/^{86}Sr$ ratios of the kimberlites with published data on South African transitional kimberlites (Nowell *et al.*, 2004; Clark, 1994), shows that off-craton transitional kimberlites analysed in this study plot generally within the reference field (Figure 6.3). However, the on-craton Wimbledon and Leicester kimberlites have slightly different compositions to reference South African transitional kimberlites since although the $^{87}Sr/^{86}Sr$ ratios are similar, the kimberlites tend towards higher initial $^{143}Nd/^{144}Nd$ ratios and therefore extend the range of published isotopic compositions for South African transitional kimberlites (Figure 6.3).

CHAPTER 7

COMPARISON OF GROUP I, GROUP II AND TRANSITIONAL, ON- AND OFF-CRATON KIMBERLITES

7.1 Introduction

The comparison of the geochemistry of group I, group II and transitional on- and off-craton kimberlites is potentially a powerful tool, in which to identify significant similarities or differences that can be related to the understanding of the evolution of kimberlite source regions. Past studies of this nature have tended to characterise the differences in major and trace element geochemistry between kimberlite varieties (Mitchell, 1995; Clark, 1994; Taylor *et al.*, 1994; Skinner *et al.*, 1992; Smith *et al.*, 1985b) and only a few of them have actively compared the geochemistry of on- and off-craton kimberlites. Radiogenic isotope geochemistry has also previously been used to compare the nature of group I and group II kimberlite source regions (Nowell *et al.*, 2004; Clark, 1994; Smith, 1983a). Similarly, Janney *et al.* (2002) have examined the isotopic signatures of a suite of olivine melilitites in South Africa, intrusive through continental lithosphere of varying age and thickness, in order to compare source region characteristics and similarities to group I kimberlites.

In order to compare the kimberlite groups in this study, it is important to note that kimberlite varieties are classified into groups according to their initial $^{87}Sr/^{86}Sr$ and $^{143}Nd/^{144}Nd$ isotope ratios (Smith, 1983a), although first order classifications have previously been made using differences in petrography (basaltic or micaceous; Wagner, 1914) or major and trace element geochemistry (e.g. Smith *et al.*, 1985b). Some of the kimberlites in this study have previously been inferred to be group I in isotopic character (e.g. East Griqualand kimberlites; Nixon *et al.*, 1983) and this has now been confirmed by the $^{87}Sr/^{86}Sr$ and $^{143}Nd/^{144}Nd$ isotope analyses. Similarly, the on-craton Wimbledon and Leicester kimberlites have been shown to be transitional in isotopic character and are additions to the transitional kimberlite group, consisting of the on-craton Frank Smith kimberlite (Smith, 1983a) and the on-/off-craton Prieska Province kimberlites (e.g. Sweetput-Soutput and Melton Wold kimberlites, Skinner *et al.*, 1992). However, it must be acknowledged that the unusual character of the Leicester kimberlite has previously been noted (e.g. Gurney & Menzies, 1998).

The aim of this comparative exercise is to qualitatively show where real differences and similarities exist, although this is not done using statistical methods, but rather through inspection. Comparisons for kimberlites are made using bulk-rock geochemical analyses that have not been corrected for alteration, crust or mantle contamination or fractional crystallisation. It is recognised that these processes are almost certain to alter the kimberlite geochemistry, but all kimberlites are likely to be affected in a similar manner. In order not to diminish the natural variability within kimberlite

compositions and since only a few transitional kimberlite samples exist, comparisons are made with raw analyses and the effect of the processes mentioned above, will be noted at all times when considering significant differences or similarities. However, Melton Wold carbonated kimberlite sample *MLW 4* has been omitted from the discussion due to its extreme alteration both petrographically and geochemically.

7.2 Comparison of on- and off-craton kimberlites

Differences in the bulk-rock geochemistry of on- and off-craton group I, group II and transitional kimberlites are illustrated in Figure 7.1, with additional analyses from the off-craton group I Uintjiesberg kimberlite (Harris *et al.*, 2004) and the on-craton group II Finsch kimberlite (Zwane, 2001) included in the dataset. Compositional fields of the on-craton group I Kimberley kimberlites (le Roex *et al.*, 2003) and the on-craton group II Swartruggens and Star kimberlites (Coe, 2004) are also shown for comparison (Figure 7.1). Significant differences of on- and off-craton kimberlites are qualitatively identified mainly using major elements and the REE as discriminating parameters (Figure 7.1). It is apparent that off-craton group I kimberlites tend to lower SiO_2, MgO and higher FeO* than on-craton kimberlites (Figure 7.1a, b). However, it is important to note that these oxides may be directly influenced by fractional crystallisation and that the compositions of the off-craton kimberlites broadly fall within the on-craton Kimberley kimberlites field. In addition, the on-craton group I Goedehoop kimberlite has considerably higher FeO* in comparison to other on- and off-craton group I kimberlites (Figure 7.1b). Recognising these processes however, If does appear significant that the majority of the off-craton group I kimberlites do not have some of the higher SiO_2, MgO and lower FeO* concentrations apparent for the on-craton kimberlites. Off-craton group II kimberlites tend to have lower MgO and FeO* contents than their on-craton equivalents (Figure 7.1a, b), but this observation is only based on the compositions of two kimberlites and therefore is speculative. Although, the MgO content of on- and off-craton transitional kimberlites is equivalent, SiO_2 and FeO* concentrations of the off-craton kimberlites are higher than their on-craton counterparts (Figure 7.1a, b).

Group I kimberlites are the only kimberlite variety to have differing TiO_2 concentrations; with off-craton kimberlites not tending towards low TiO_2 like some of the on-craton group I kimberlites (Figure 7.1c). Although some of the off-craton group II (Eendekuil and Brandewynskuil kimberlites) and transitional kimberlites (Droogfontein kimberlite) have higher Al_2O_3 concentrations and contamination indices (5.0 - 8.5 wt% Al_2O_3, C.I. > 1.5; Figure 7.1c; Table 4.2, 4.3) than the on-craton kimberlites, they are considered to be crustally contaminated (Clement, 1982). Off-craton transitional kimberlites are more K_2O-rich than the on-craton kimberlites. CaO and CO_2 concentrations of on- and off-craton group I and transitional kimberlites are also variable (Figure 7.1d), with the off-craton transitional kimberlites tending to lower CaO and CO_2 than their on-craton counterparts. Although CaO and CO_2 may be enriched by crystal fractionation, it is apparent that the off-craton group I kimberlites have CaO and CO_2 contents that fall towards the upper end of the concentration range for on-craton group I kimberlites (Figure 7.1d).

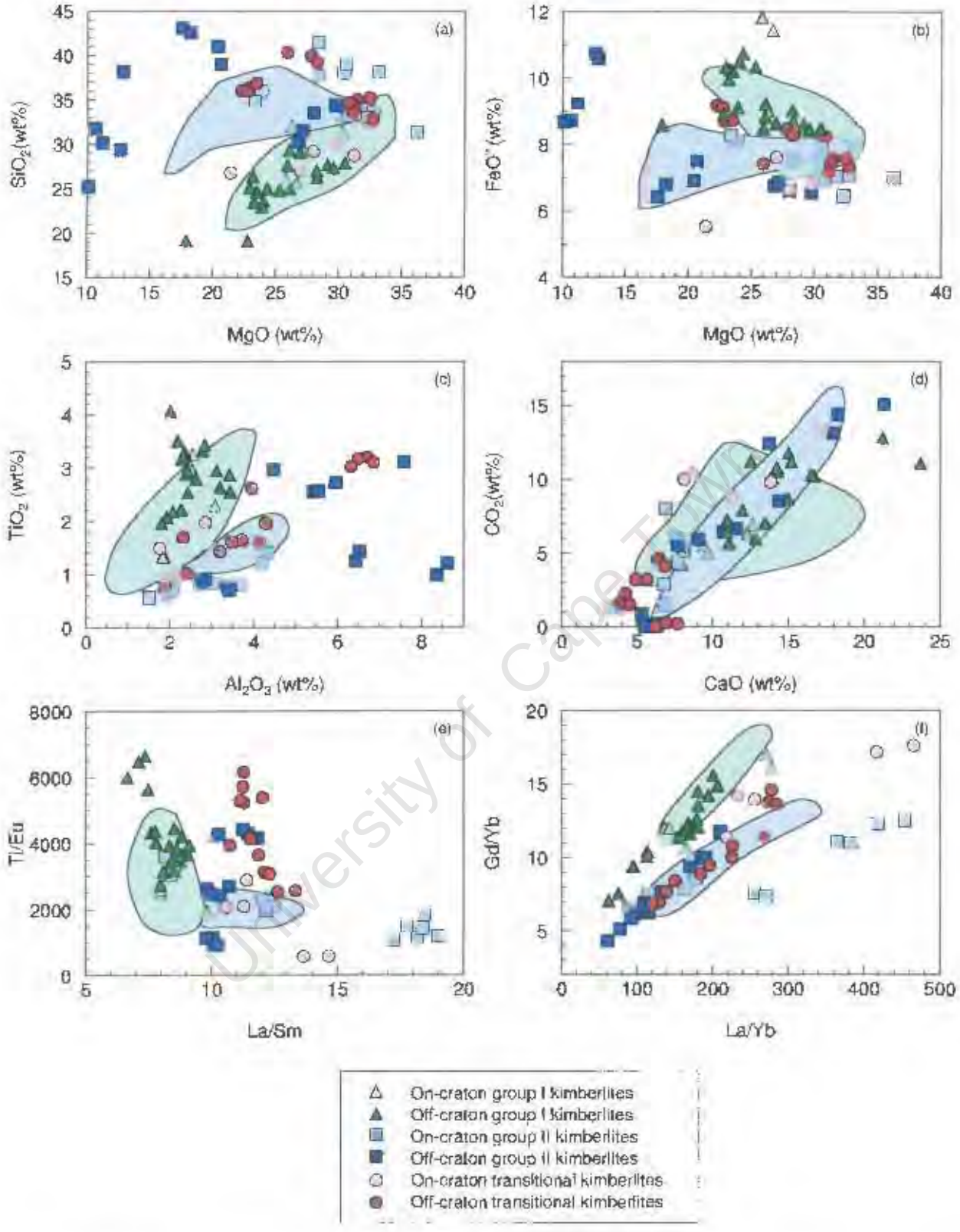

Figure 7.1: Variation of selected major elements and trace element ratios for on- and off-craton group I, group II and transitional kimberlites. Symbols for off-craton group I kimberlites include analyses from the Uintjiesberg kimberlite (Harris *et al.*, 2004) and similarly, symbols for on-craton group II kimberlites include analyses from the Finsch kimberlite (Zwane, 2001). Green shaded field represents the on-craton group I Kimberley kimberlites (le Roex *et al.*, 2003) and blue shaded field represents the on-craton group II Swartruggens and Star kimberlites (Coe, 2004).

The majority of compatible and incompatible trace element concentrations show no systematic differences between on- and off-craton kimberlites, although it is recognised that potential variations might exist within the transitional kimberlite group. For example, the on-craton Leicester kimberlite tends to have lower LIL element abundances (e.g. Rb, Ba and K) than the off-craton transitional kimberlites, but this cannot be confirmed due to the very enriched nature of the on-craton Wimbledon kimberlite and because of the low number of on-craton kimberlite samples in this study. In terms of the Ti/Eu ratio, both off-craton group I and transitional kimberlites tends towards higher Ti/Eu ratios (Figure 7.1e) and therefore smaller negative Ti anomalies on primitive mantle normalised diagrams, than on-craton kimberlites. Similarly, REE ratios also provide discrimination between on- and off-craton kimberlites, both on-craton group I and transitional kimberlites tend towards higher La/Yb and Gd/Yb than the off-craton kimberlites (Figure 7.1f). Only the transitional group of kimberlites shows any differences in isotopic composition that can be related to tectonic setting, since on-craton kimberlites have lower initial $^{87}Sr/^{86}Sr$ ratios and higher $^{143}Nd/^{144}Nd$ ratios (Section 6.4, Figure 6.3), although this may due to fortuitous sampling.

The comparison of kimberlite geochemistry by Smith *et al.* (1985b), found mostly similar systematic differences between on- and off-craton group I kimberlites (group IA and group IB kimberlites; Smith *et al.*, 1985b), although differences in P_2O_5, Nb, Zr and Y concentrations are not apparent for the current kimberlite dataset. Differences between on-/off-craton group II and transitional kimberlites were not considered in the study of Smith *et al.* (1985b).

7.3. Comparison of group I, group II and transitional kimberlites

7.3.1 Major element geochemistry

Group I kimberlites tend to have lower SiO_2 concentrations (< 33 wt%, Figure 7.2a) than group II kimberlites (> 30 wt%) at comparable Mg-numbers (Mg-numbers = 0.80-0.90), although the group II Eendekuil kimberlite is significantly less Mg-rich (Mg-number ~ 0.71). SiO_2 contents and Mg-numbers of transitional kimberlites largely span the range shown by group I and group II kimberlites (Figure 7.2a). Kimberlite groups show overlapping FeO* concentrations, with group I kimberlites perhaps tending to slightly higher FeO* (7-12 wt% FeO*; Figure 7.2b) than group II (6-11 wt% FeO*) and transitional kimberlites (6.5-9.0 wt% FeO*). The majority of the analysed kimberlite samples have similar Al_2O_3 contents (< 4.5 wt%; Figure 7.2b), with uncontaminated group II kimberlites and the Swartruggens and Star kimberlites (Coe, 2004) showing subtly higher Al_2O_3 concentrations than group I kimberlites.

The differences in TiO_2 and K_2O contents between group I and group II kimberlites are commonly used as discriminators of kimberlite varieties (e.g. Chalapathi Rao *et al.*, 2004; Taylor *et al.*, 1994; Smith *et al.*, 1985b), since group I kimberlites have higher TiO_2 (up to ~4 wt% TiO_2 for the Uintjiesberg kimberlite; Harris *et al.*, 2004; Figure 7.2c) and lower K_2O concentrations (< 1.75 wt% K_2O for the

CHAPTER 8

PETROGENESIS

8.1 Introduction

Experimental studies on kimberlite petrogenesis have shown that both group I and group II kimberlite-like magmas can be produced by small degrees of partial melting of a carbonated garnet peridotite at typical mantle conditions (Ulmer & Sweeney, 2002; Dalton & Presnall, 1998a; Canil & Scarfe, 1990; Eggler & Wendlant, 1979). Although some experimentalists have argued for non-peridotitic kimberlite sources based on the absence of olivine or orthopyroxene on the kimberlite liquidus (Mitchell, 2004; Girnis *et al.*, 1995; Edgar & Charbonneau, 1993; Foley, 1992a), to date there have been no trace element studies on kimberlite petrogenesis that support this hypothesis. Rather, semi-quantitative modelling of kimberlite source regions by Coe (2004), Chalapathi Rao *et al.* (2004), Harris *et al.* (2004), le Roex *et al.* (2003) and Tainton and McKenzie (1994) are consistent with the derivation of kimberlites by low degrees of melting from garnet lherzolite source regions. These studies have also suggested that the source regions of kimberlites are enriched in incompatible elements, due to metasomatism upon previously melt-depleted mantle source regions.

Both Tainton and McKenzie (1994) and le Roex *et al.* (2003) have argued that group I and group II kimberlite sources are located within the subcontinental lithosphere. These interpretations were based on the depleted heavy REE character of kimberlite source regions, formed by previous melting events. The conclusion of Tainton and McKenzie (1994) is consistent with the enriched radiogenic isotopic character of group II kimberlites, characterised by time integrated Rb/Sr and Sm/Nd ratios that suggest their sources were isolated from the convecting asthenosphere and are therefore likely located within the subcontinental lithospheric mantle (Coe, 2004; Fraser & Hawkesworth, 1992; Tainton, 1992; Smith, 1983a). However, group I kimberlites are characterised by isotopic signatures depleted relative to present day Bulk Earth and similar to ocean island basalts that are inferred to be derived from source regions located within the asthenosphere (Smith, 1983a), in apparent contradiction to the model of le Roex *et al.* (2003). le Roex *et al.* (2003) and Harris *et al.* (2004) resolved this conflict by arguing that the asthenospheric signature carried by group I kimberlites, was due to metasomatism of the lithospheric source by plume related melts/fluids. Harris *et al.* (2004) have explicitly suggested that the enrichment of the group I Uintjiesberg kimberlite source region, may be related to metasomatism by melts/fluids associated with the passage of southern Africa over the Shona mantle plume.

Since the aims of this study are to characterise and compare source region compositions and genetic processes giving rise to group I, group II and transitional, on- and off-craton kimberlites, it is first necessary to investigate the nature of processes that have affected kimberlites subsequent to the

segregation of the primary magmas from their sources. Since the early studies of kimberlite bulk-rock geochemistry, it has been recognised that kimberlites are highly contaminated and altered (Clement, 1982; Dawson, 1980; Fesq *et al.*, 1975) and that understanding of petrogenetic processes can be disguised by these effects. Firstly, the degree of alteration may be hard to constrain given that kimberlites are volatile-rich magmas and have the ability to auto-metasomatise (le Roex *et al.*, 2003; Barrett & Berg, 1975). Therefore one needs to distinguish between primary metasomatism and secondary alteration by ground water circulation (Barrett & Berg, 1975). Secondly, kimberlites are also efficient samplers of the crust and mantle, which they traverse *en route* from source to surface and although this can provide valuable information for crust and mantle studies (e.g. Schmitz & Bowring, 2004; Shirey *et al.*, 2002; Carlson *et al.*, 2000) it does, however, sometimes cause significant contamination to kimberlite geochemistry (Dawson, 1980). Numerous schemes have been developed in the past to quantify the degree of crustal contamination and alteration (e.g. Taylor *et al.*, 1994; Clement, 1982) and use of these schemes, in addition to the general evaluation of the behaviour of trace elements (Coe, 2004; le Roex *et al.*, 2003; Mahotkin *et al.*, 2000), allow one to identify kimberlite samples that have been the least affected by the above-mentioned processes. In addition to these processes, the effect of macrocryst entrainment (thought to represent disaggregated mantle peridotite; le Roex *et al.*, 2003; Shee, 1985) and late stage crystal fractionation have also been shown to be important, but quantifiable processes affecting the primary kimberlite magma compositions (Coe, 2004; Harris *et al.*, 2004; le Roex *et al.*, 2003).

Once the effects of alteration, crustal contamination, macrocryst entrainment and fractional crystallisation have been evaluated and corrected for where necessary, an attempt is made to obtain one or more close-to-primary kimberlite magma compositions for each kimberlite in this study. Thereafter, semi-quantitative modelling of partial melting processes will be undertaken in order to evaluate source region compositions of kimberlite varieties and ascertain the effects of degree of melting, choice of source region mineralogy and role of residual accessory phases on the primary kimberlite compositions. Further aspects of kimberlite petrogenesis are then explored with a view to constraining the nature of depletion and enrichment events, location of kimberlite source regions and the geodynamical significance of similarities or differences between group I, group II and transitional kimberlites as well as on- and off-craton kimberlites. Finally, an attempt is undertaken to place some of the observations made regarding petrogenetic processes affecting kimberlite varieties into perspective.

8.2 Alteration of kimberlites

The brecciated and permeable nature of kimberlites makes them prone to alteration (Berg & Allsopp, 1972), particularly since primary kimberlite magmas are volatile-rich. Abundant volatiles typically form amoeboid or lobate pools of serpentine and calcite, and the movement of these phases during late stage crystallisation of the kimberlite may cause autometasomatism (le Roex *et al.*, 2003; Clement & Skinner, 1985). Alteration of the kimberlite can be both a primary (movement of crystallising fluids) and

a secondary (movement of meteoric waters) process, neither of which is strictly a closed system process, given that kimberlites are thought to suffer volatile loss during emplacement (Price *et al.*, 2000; Dawson, 1980). Characteristics of oxygen isotope signatures in kimberlites are also consistent with alteration reactions being primary (e.g. Jericho kimberlite; Price *et al.*, 2000), as well as secondary (e.g. Finsch kimberlite; Kirkley, 1987). These alteration reactions are typically complex with calcite and serpentine being the favoured reaction products, although formation of clay minerals (e.g. chlorite, talc, brucite) have also been recognised (Clement, 1982).

Serpentinisation is a common secondary alteration reaction of olivine and other minerals (e.g. phlogopite, monticellite) and is typically associated with a relative decrease in MgO and corresponding increase in the volatile content of the kimberlite (Deer *et al.*, 1992; Clement, 1982). Kimberlites in this study show various petrographic features characteristic of alteration:

i). Serpentinisation of rims and fractures to pervasive serpentinisation of olivine phenocrysts and macrocrysts, although the initial serpentinisation is likely due to primary alteration (Barret & Berg, 1975).

ii). Development of Fe-oxides in the vicinity of olivine macrocrysts as a by-product of the serpentinisation reaction (Koffiefontein and Hebron kimberlites; Clement, 1982).

iii). Calcitisation of rims or interiors of olivine or phlogopite phenocrysts and/or macrocrysts, in selected samples from the Koffiefontein, Goedehoop and Wimbledon kimberlites, or pervasive carbonatisation of the kimberlite (Melton Wold kimberlite sample *MLW 4*).

iv). Development of calcite stringers in deformed phlogopite macrocrysts (Klipgatsfontein, Markt, Wimbledon, Leicester and Eendekuil kimberlites) that likely involves some secondary redistribution of groundmass calcite.

v). Chloritisation of rims of macrocrysts and/or phenocrysts (Wimbledon, Newlands and Markt kimberlites).

Some of the variation of bulk-rock major element geochemistry is also consistent with petrographic evidence suggesting alteration of a few of the samples in this study. In particular, the very low MgO but high $CaCO_3$ content of Melton Wold kimberlite sample *MLW 4* is probably due to open system secondary alteration. Similarly, the low MgO and high $CaCO_3$ content of Eendekuil kimberlite samples, manifested in the presence of abundant calcite stringers in both phlogopite phenocrysts and macrocrysts, suggests the effects of alteration. However, trace element characteristics suggest there are other petrogenetic processes that are more responsible for the depletion in MgO and enrichment in $CaCO_3$ of the Eendekuil kimberlite (Section 8.5, 8.8). Both Brandewynskuil and Droogfontein kimberlites have negligible CO_2 concentrations, in contrast to high H_2O^- contents. The H_2O^+ cation is typically structurally bound in mineral lattices, whereas the H_2O^- anion is free to circulate and high concentrations of the latter, may also indicate alteration (Smith *et al.*, 1985b).

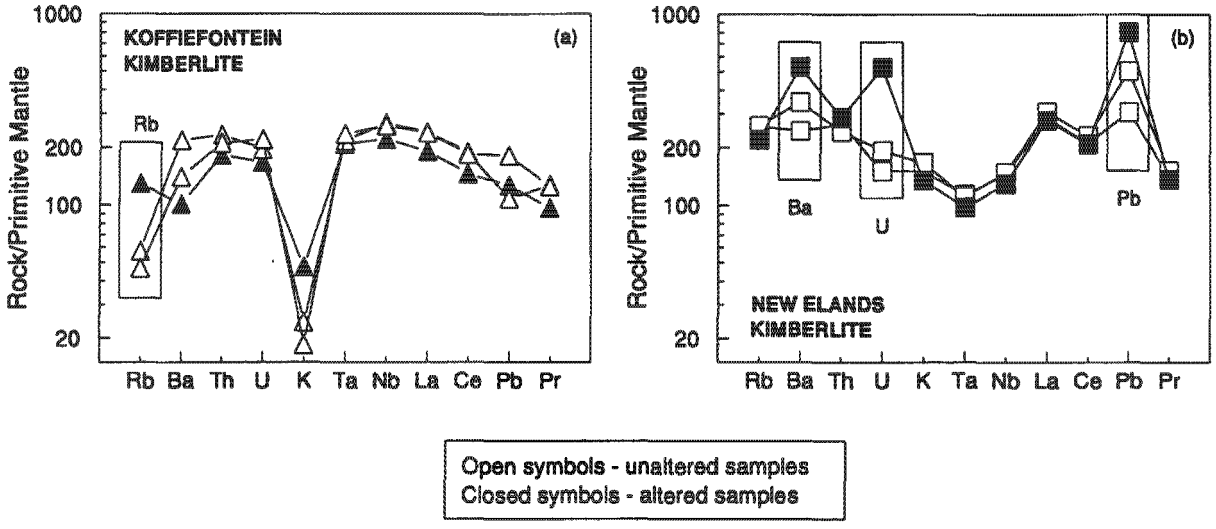

Figure 8.1: Illustration of the effect of alteration on the concentrations of the fluid mobile elements for (a) the group I Koffiefontein kimberlite and (b) group II New Elands kimberlite, shown as a portion of a primitive mantle normalised diagram. Elements of interest are highlighted in the insets. Normalising values are from Sun and McDonough (1989).

Both primary and secondary alteration processes have the potential to disturb and redistribute the fluid mobile elements (e.g. Rb, Ba, U, K and Pb; Fesq *et al.*, 1975), in contrast to the more immobile REE and HFS elements. Consequently, correlations between these elements in kimberlite samples (Figure 5.2, 5.7, 5.12) are generally poor if alteration has occurred. Given that multiple samples from a single kimberlite should ideally show subparallel patterns on primitive mantle normalised diagrams, any individual samples that show positive or negative anomalies of these mobile elements in comparison to other samples from the same locality, are likely to be altered. The positive Rb anomaly (Figure 8.1a) and positive Ba, U and Pb anomalies (Figure 8.1b), present in Koffiefontein kimberlite sample *KK 3* and New Elands kimberlite sample *NE K11*, respectively, are examples of how alteration may affect kimberlite geochemistry. The mobile behaviour of Rb also means that $^{87}Sr/^{86}Sr$ isotope ratios are susceptible to alteration with circulation of meteoric water through the kimberlites being likely to increase the measured $^{87}Sr/^{86}Sr$ ratio (Barrett & Berg, 1975).

The above narrative is a brief description of some of the characteristics of alteration in kimberlites as documented by various authors, with illustrations from selected samples in this study. Accordingly, the degree of alteration of all kimberlites in this study has been assessed and samples thought to be severely altered, are subsequently discarded from the dataset (e.g. Melton Wold kimberlite sample *MLW 4*), whereas others that show some anomalous behaviour of the fluid mobile elements or volatiles will hereafter be treated with caution (e.g. U in Markt kimberlite sample *JJG 2338*).

8.3 Crustal contamination of kimberlites

Kimberlites may entrain numerous crustal xenoliths varying in size from large rafts to microxenoliths, most of which are concentrated in diatreme facies kimberlite (Clement & Skinner, 1985; Hawthorne, 1975). Although hypabyssal facies kimberlite generally does not carry a visibly significant amount of xenoliths, the degree of assimilation of country rock by kimberlite samples in this study and its affect on bulk-rock geochemistry, still needs to be addressed. Crustal contamination typically increases SiO_2, Al_2O_3 and Na_2O and decreases MgO concentrations of kimberlites and is quantified here by the contamination index of Clement (1982; Section 4.1). Kimberlites in this study with C.I. greater than 1.5 are diopside- and phlogopite-rich (Eendekuil, Brandewynskuil and Droogfontein kimberlites), and in these cases the validity of the C.I. in indicating the degree of contamination is questionable, since uncontaminated diopside and phlogopite-rich kimberlites may have a C.I. up to 1.5 (Clement, 1982). However, there are various lines of evidence other than high C.I., SiO_2 and Al_2O_3 contents (Table 4.2, 4.3), that suggest crustal contamination of some of these kimberlites, first of which is the presence of diopside kimberlite domains in the Droogfontein kimberlite and also very fine-grained circular structures in some of the Brandewynskuil kimberlite samples, both of which are interpreted to represent microxenoliths (Clement, 1982).

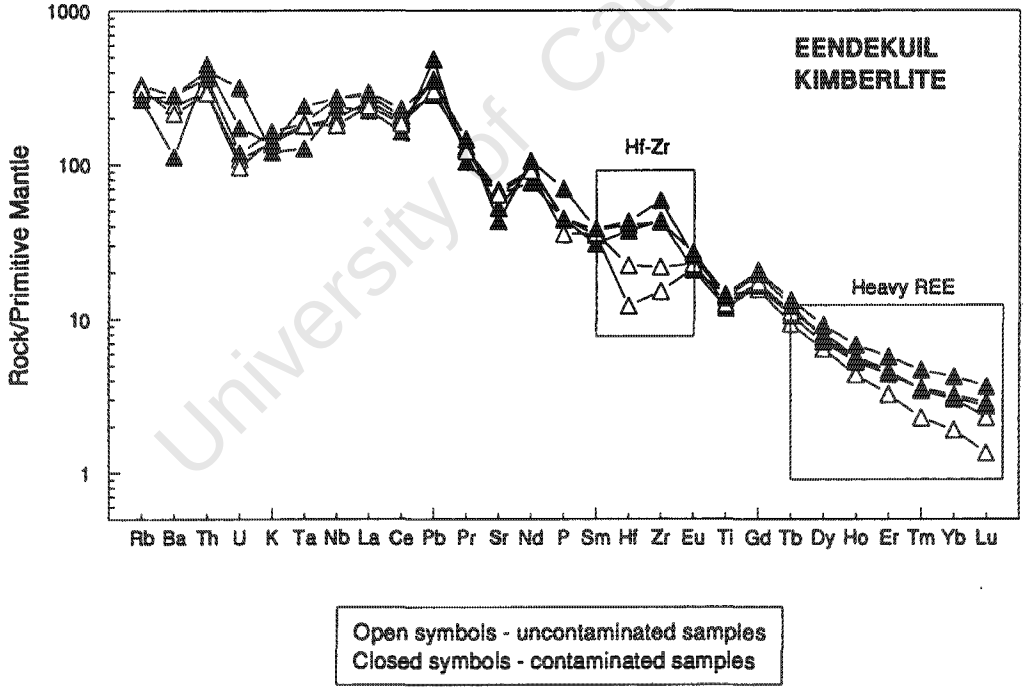

Figure 8.2: Primitive mantle normalised diagram illustrating the effect of crustal contamination on samples from the group II Eendekuil kimberlite. Elements of interest are highlighted in the insets. Normalising values are from Sun and McDonough (1989).

Although kimberlites are enriched in the compatible and incompatible elements, depending on the element in question, the concentration of trace elements may either be concentrated or diluted by crustal contamination. In the study of le Roex *et al.* (2003), it was shown that positive Pb anomalies in association with flattened heavy REE patterns (low Gd/Lu) on primitive mantle normalised diagrams of group I kimberlites were indicative of the assimilation of crustal material. Similarly, flattened heavy REE patterns as well as positive Zr and Hf anomalies on primitive mantle normalised diagrams of group II kimberlites suggest crustal contamination (e.g. Eendekuil kimberlite; Figure 8.2; Coe, 2004).

Smith (1983b) examined the effect of crustal contamination on kimberlites and concluded that an unrealistically large degree of crustal contamination was necessary to substantially alter the Sr isotopic geochemistry of kimberlites. However, the Bellsbank kimberlite has intruded through the Campbell Rand dolomite, which has highly radiogenic $^{87}Sr/^{86}Sr$ (Kirkley, 1987). Tainton (1992) concluded that the Bellsbank kimberlite samples in his study did not show any influence of crustal contamination, although the samples analysed in that study were more radiogenic than sample *JJG 4676* analysed here.

Owing to the regional nature of this study, few of the kimberlites have been sampled in sufficient detail to study the intra-kimberlite geochemical variation and relation to crustal contamination processes. However, using the above mentioned characteristics, selected samples from the group II Eendekuil (*EKL 1, K2/3, K2/9*), Brandewynskuil (*K6/8, K6/14*) and Newlands kimberlites (*KN 2, KN 3*), are classified as crustally contaminated. Various transitional kimberlite samples are also classified as crustally contaminated (all Droogfontein kimberlite samples and Silvery Home kimberlite samples *SLH 3, SLH 7, SLH 9*). In addition, Silvery Home kimberlite samples *SLH 3, SLH 7* and *SLH 9* show negative P anomalies in conjunction with positive Zr and Hf anomalies on primitive mantle normalised diagrams. The above-mentioned kimberlite samples are subsequently discarded from the kimberlite datasets, except for the phlogopite diopside Silvery Home kimberlite samples (*SLH 3, SLH 7, SLH 9*), which will hereafter be treated with caution.

8.4 Effect of macrocryst entrainment on kimberlites

Macrocrysts entrained by kimberlites typically are anhedral with strained physical characteristics that suggest they are xenocrysts incorporated into the host kimberlite. The origin of these xenocrysts is commonly believed to be disaggregated mantle peridotite xenoliths, sampled by the kimberlite as it travels through the mantle (Shee, 1985; Clement *et al.*, 1984) and subsequently, macrocrystic kimberlites are in fact partial cumulates of mantle minerals as opposed to pure liquid compositions (le Roex *et al.*, 2003). The previous studies of Coe (2004), Harris *et al.* (2004), le Roex *et al.* (2003) Beard *et al.* (2000) and Fraser and Hawkesworth (1992) have demonstrated that some of the variation in both group I and group II kimberlite bulk-rock geochemistry can be attributed to the entrainment of mantle peridotite. The group II Markt kimberlite samples are good examples of how variably

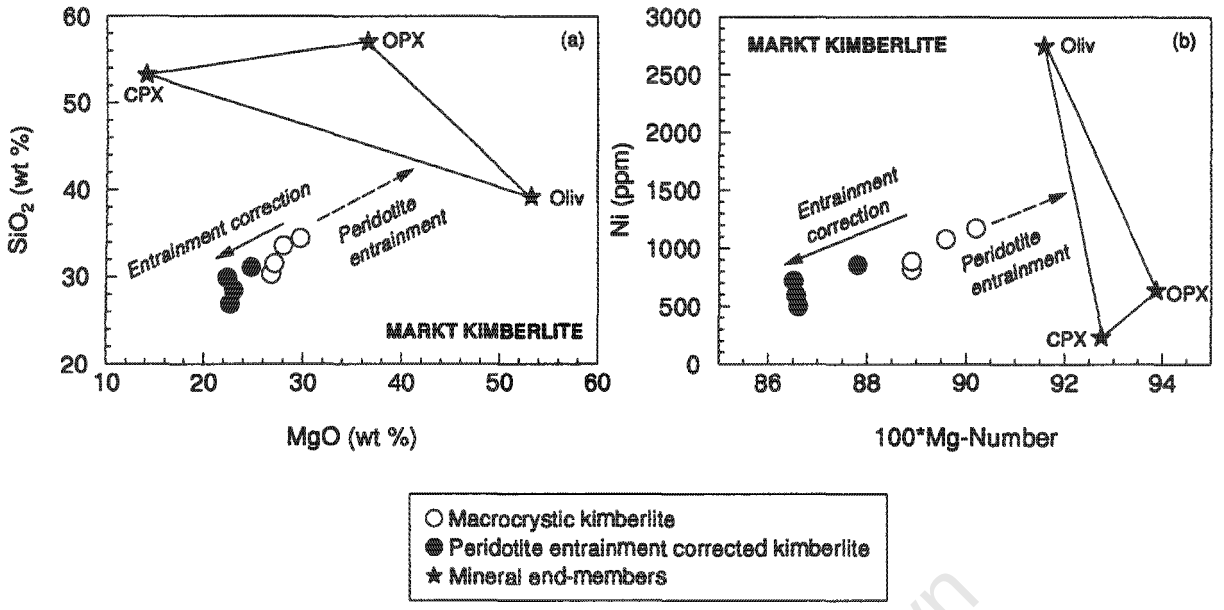

Figure 8.3: Variation in the composition of group II Markt kimberlite samples caused by peridotite entrainment and the corresponding effect of the macrocryst correction procedure used in this study (see text for explanation). Mineral end-member compositions are also shown for reference (Gregoire *et al.*, 2003; Robey, 1981).

macrocrystic kimberlite may show compositional trends for major and trace elements that reflect the effect of peridotite entrainment (Figure 8.3).

In the attempt to obtain a close-to-primary magma composition for each kimberlite locality in this study, the effect of macrocryst entrainment has to be recognised and removed. Ideally, a cogenetic data set consisting of aphanitic to macrocrystic kimberlite is needed to recognise the effect of peridotite entrainment on kimberlite geochemistry (e.g. Harris *et al.*, 2004). However, the regional nature of this study has resulted in few of the kimberlites being sampled in sufficient detail to evaluate evolutionary trends and the effect of peridotite entrainment, as has been done in other kimberlite studies (e.g. le Roex *et al.*, 2003). Consequently, a correction to remove the effects of macrocryst entrainment on kimberlite geochemistry for all macrocrystic samples in this study needs to be implemented. In order to correct kimberlite compositions for mantle entrainment, knowledge of the modal mineralogy and composition of the entrained peridotite is required. In reality, this can vary widely and can include in addition to peridotite, both eclogite and megacryst phases. Since the sampling nature of this study prohibits this level of detail to be inferred, a simplified correction procedure is all that can be reasonably undertaken.

Recognising the inherent uncertainties associated with such a correction procedure, the application of the correction procedure has been limited to only kimberlite samples with greater than 10 volume % olivine macrocrysts and to use as a peridotite proxy, an average garnet lherzolite composition (Gregoire *et al.*, 2003), and to assume that all olivine macrocrysts in a single sample derive from the peridotite. The geochemical composition of a Kaapvaal garnet lherzolite (68% olivine, 26%

orthopyroxene, 1% clinopyroxene and 5% garnet, Gregoire *et al.*, 2003) has been proportionally subtracted from the kimberlite according to the modal percentage of macrocrystic olivine. Therefore, if the Markt kimberlite samples contain between 20 and 30% olivine macrocrysts, the Markt kimberlite must have entrained ~29-44% peridotite. The effect of the macrocryst correction procedure has been to decrease SiO_2, MgO and Ni contents (Figure 8.3) and increase TiO_2, Al_2O_3, FeO* and CaO concentrations in kimberlite samples.

The effect of mantle entrainment is to dilute the REE and other incompatible element concentrations in the kimberlites. Although the degree of dilution depends on the relative concentration of incompatible elements in the constituent minerals, the low modal abundance of clinopyroxene and garnet (D_{La} for Cpx > 0.01 and D_{Lu} for Gnt >> 0; Adam & Green, 1994; Sweeney *et al.*, 1992), in contrast to the dominance of olivine and orthopyroxene (D_{REE} for Oliv, Opx < 0.1; Kelemen *et al.*, 1993) results in near uniform dilution across the spectrum of the incompatible trace elements. On a REE diagram the effect of peridotite entrainment, is to cause subparallel downwards displacement of the pattern (Coe, 2004; Harris *et al.*, 2004; le Roex *et al.*, 2003) and therefore the correction procedure should do the opposite. A detailed correction procedure should take into account the relative incompatibility of every trace element, however, on the scale of the diagrams used here (Figure 8.4) there is no significant difference in the concentrations of corrected data calculated assuming the bulk partition coefficient is zero for every incompatible element. Subsequent application of the correction procedure, assuming D = 0, for the Markt kimberlite causes a relatively uniform increase in REE concentrations of the kimberlite samples (Figure 8.4).

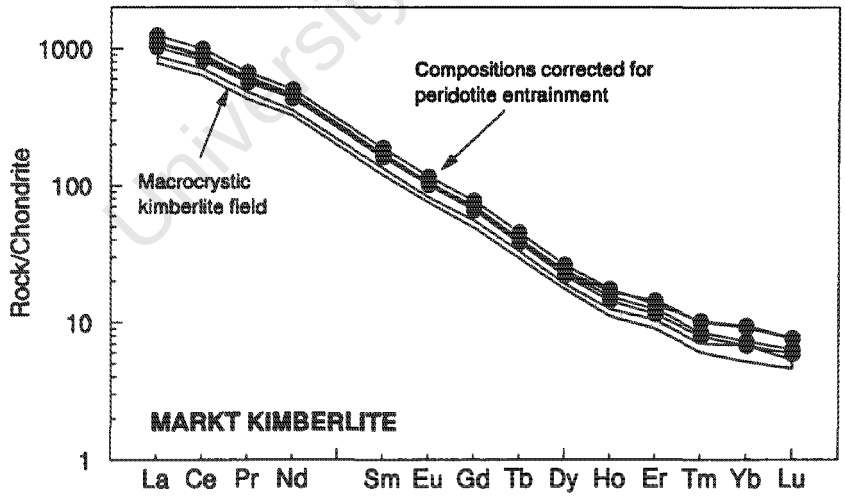

Figure 8.4 Effect of the macrocryst correction procedure on the chondrite normalised rare earth element patterns of macrocrystic group II Markt kimberlite samples. Normalising values are from Sun and McDonough (1989).

Using the above described procedure, macrocrystic kimberlite with greater than 10 volume % olivine macrocrysts has accordingly been corrected for the effect of peridotite entrainment on bulk-rock major and trace element geochemistry. However, the effect of peridotite entrainment on the isotope geochemistry of kimberlites is more difficult to quantify, given that mantle xenoliths entrained by South African kimberlites have a broad range in $^{87}Sr/^{86}Sr$ and $^{143}Nd/^{144}Nd$ isotope ratios (e.g. Pearson & Nowell, 2002; Walker *et al.*, 1989; Erlank *et al.*, 1987; Menzies *et al.*, 1987). The range of isotope ratios of mantle xenoliths spans the fields encompassed by group I, group II and transitional kimberlite varieties and the isotopic heterogeneity of Kaapvaal mantle xenoliths, would make the choice of a representative peridotite composition for the entrainment correction difficult. In reality, the effect on $^{87}Sr/^{86}Sr$ and $^{143}Nd/^{144}Nd$ ratios of kimberlites is relatively small for the entrainment of peridotite (Δ in $^{87}Sr/^{86}Sr$ ~ 0.0001, Δ in $^{143}Nd/^{144}Nd$ ~ 0.00001 for 50% peridotite entrainment by a group I kimberlite), and even more so given the low Nd concentrations in mantle peridotites (< 5ppm Nd; Pearson & Nowell, 2002; Walker *et al.*, 1989). Therefore, the isotopic compositions of kimberlites have been left unchanged.

8.5 Effect of fractional crystallisation on kimberlites

Crystal fractionation *en route* to the surface or during shallow emplacement and cooling of kimberlites can affect the composition of primary kimberlite magmas. Some of the best-known examples of fractionated kimberlites are sills in the Kimberley area (e.g. Benfontein sill) and are characterised by evolved compositions (le Roex *et al.*, 2003; Shee, 1985). Olivine and phlogopite are phenocryst phases that have been recorded to have fractionated from kimberlite magmas (Coe, 2004; Harris *et al.*, 2004; le Roex *et al.*, 2003; Beard *et al.*, 2000). Even though none of kimberlites in this study are aphanitic in texture, the role of fractional crystallisation in modifying primary kimberlite compositions still needs to be evaluated, with respect to whether any of the samples that show anomalous major element geochemistry or characteristic anomalies on primitive mantle normalised diagrams, can be considered primary kimberlites.

When inter-kimberlite variation within the respective kimberlite groups is compared, most kimberlite samples in this study have compositions that do not appear to be outliers, except for two kimberlites, the group II Eendekuil and transitional Wimbledon kimberlites. Wimbledon kimberlite is extremely enriched with the highest light REE concentrations (La ~ 2280 times chondrite) of all the kimberlites analysed in this study and therefore may have evolved through crystal fractionation. However, the major element geochemistry of the Wimbledon kimberlite is not atypical to other group I, group II and transitional kimberlites, which suggests that its characteristic enriched composition was not produced through crystal fractionation but more likely through partial melting processes.

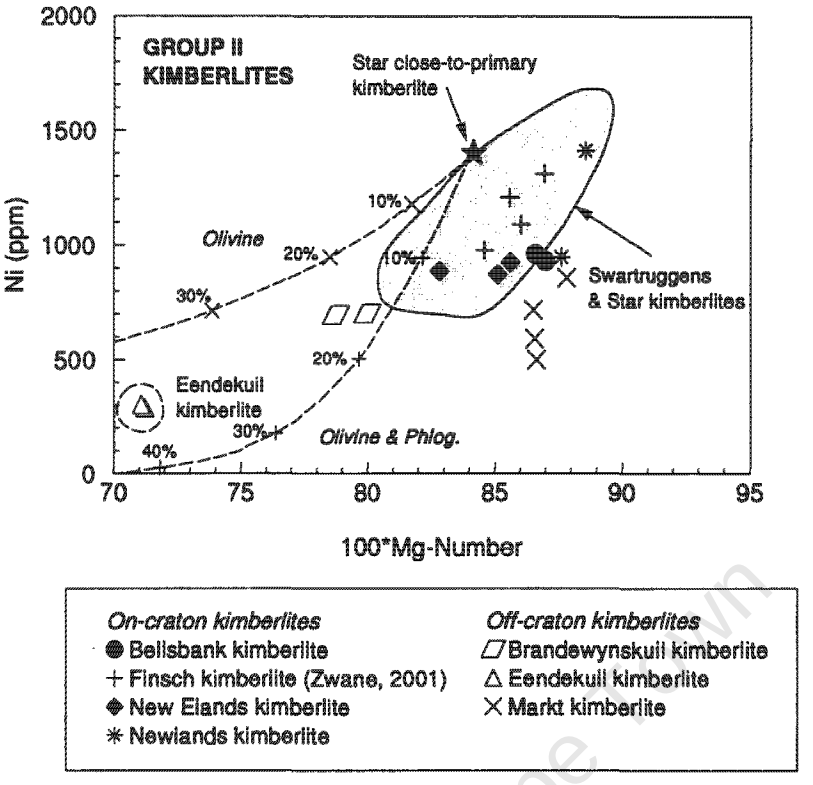

Figure 8.5: Crystallisation trajectories for the fractionation of olivine, as well as olivine and phlogopite (70% olivine and 30% phlogopite) from the Star close-to-primary kimberlite magma composition (Coe, 2004). Numbers illustrated represent the percentage of fractional crystallisation. Shaded field represents the group II Swartruggens and Star kimberlites (Coe, 2004). Ni partition coefficients are from Gregoire *et al.* (2003) and Hart and Davis (1978) and $K_D^{Fe\text{-}Mg}$ = 0.30-0.34 is from Herzberg and O'Hara (2002).

In contrast, uncontaminated samples from the off-craton Eendekuil kimberlite (*K2/2* and *K2/13*) are characterised by lower MgO, Mg-number and SiO_2 (~11.0 wt% MgO; Mg-number ~0.71; ~30.1 wt% SiO_2) and compatible trace element concentrations (~290ppm Ni), but with higher FeO*, TiO_2, Al_2O_3, CaO and CO_2 concentrations in comparison to most other group II kimberlites (Figure 4.2, 5.6). It could be argued that CaO and CO_2 have been introduced into the kimberlite by carbonated ground water that also leached MgO, but the distinctive trace element signature of the Eendekuil kimberlite suggests otherwise. The primitive mantle normalised diagram of the Eendekuil kimberlite is characterised by moderate negative Ti, Hf and Zr anomalies, in addition to negative Rb, K and Sr anomalies (Figure 5.10), that show an affinity to a carbonatite signature (Nelson *et al.*, 1988), and are more likely features inherited from the mantle source region than from percolating meteoric waters. Since the anomalous composition of the Eendekuil kimberlite is unlikely to be from alteration, crustal contamination or macrocryst entrainment, the possibility that the kimberlite may have evolved by fractionation needs to be assessed. Using the Star kimberlite as a hypothetical group II primary kimberlite magma composition (Coe, 2004), the effect of olivine fractionation as well as the combined fractionation of olivine and phlogopite, are illustrated in Figure 8.5. Fractionation of approximately 30-40% olivine and phlogopite is able to account for the concentrations of major and compatible trace elements in the Eendekuil kimberlite (Figure 8.5), but not for the REE since they are not as enriched as other group II kimberlites. However, this approach is subjective since the parental kimberlite

composition is unknown and all that can be reasonably concluded is that the Eendekuil kimberlite is probably not representative of a primary kimberlite, but more likely has been modified through crystal fractionation processes.

8.5.1 Role of crystal fractionation on trace element anomalies

A characteristic feature of the kimberlites in this study and of previously described group I and group II kimberlites (Coe, 2004; Harris *et al.*, 2004; le Roex *et al.*, 2003; Tainton, 1992) is the presence of negative Rb, K, Ti and Sr anomalies on primitive mantle normalised diagrams. Coe (2004), Harris *et al.* (2004) and le Roex *et al.* (2003) have all argued that the origin of these anomalies are not related to alteration or crystal fractionation processes, but rather, are features of the primary magmas of the Kimberley, Uintjiesberg, Swartruggens and Star kimberlites. These anomalies are not limited to the above-mentioned kimberlites, but are moderately to well-developed in all on- and off-craton kimberlites analysed in this study and the ubiquity of these characteristics in group I, group II and transitional kimberlites, suggests that they are not alteration or contamination features.

The magnitude of the negative K and Rb anomalies in group I kimberlites shows some correlation with the relative degree of enrichment, suggesting that crystal fractionation is important. The only crystallising phase in a kimberlite capable of removing Rb and K is phlogopite and therefore the behaviour of this mineral has been explored in detail, by Harris *et al.* (2004) and le Roex *et al.* (2003). These authors demonstrated that an unrealistically large proportion of phlogopite-only fractionation would be needed to produce a negative K and by inference, Rb anomaly, equivalent to that observed in group I kimberlites. Similarly, greater than 40% phlogopite-only fractionation would be required to generate the same relative K depletion in group I kimberlites of this study (Figure 8.6a) and therefore it is likely that the relative depletion in Rb and K is an intrinsic feature of group I primary kimberlite magmas.

Group II kimberlites in this study also show relative depletion of Rb and K on primitive mantle normalised diagrams, although of differing degrees, and with negative anomalies being generally smaller than in group I kimberlites. Normal group II kimberlites do not always appear to show a negative K anomaly on primitive mantle normalised diagrams (e.g. Brandewynskuil kimberlite; Figure 5.10), but this is an artefact due to the depletion of neighbouring elements, Nb and Ta. In these circumstances, however, K is still depleted relative to La on primitive mantle normalised diagrams ($K/K^* = 0.3$-0.6). In contrast, a subset referred to as the group IIb kimberlites (Bellsbank and Newlands), show well-developed negative K anomalies ($K/K^* = 0.1$), more similar to that of the group I kimberlites. Following a similar argument as for the group I kimberlites, fractionation of phlogopite with K as a stoichiometric constituent from a parental magma is unable to account for the large negative K anomaly in the group IIb kimberlites (Figure 8.6b), despite phlogopite being an important constituent phase. In addition, if phlogopite-only fractionation was the mechanism in which the large negative K anomaly was produced in the group IIb kimberlites, then the calculated K_2O content of the parental

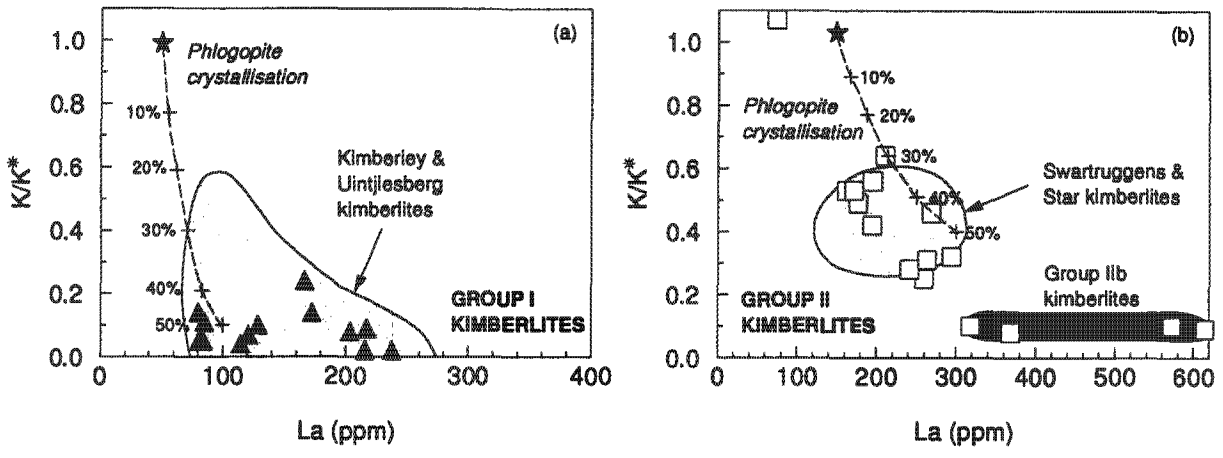

Figure 8.6: Variation of K/K* for (a) group I and (b) group II kimberlites. Superimposed is the crystallisation trajectory for the fractionation of phlogopite from a hypothetical parental kimberlite magma with no negative K anomaly (K/K* = 1) and where K is removed from the melt as a stoichiometric constituent of phlogopite. The group II kimberlite dataset is supplemented with analyses from the Finsch kimberlite (Zwane, 2001). Shaded fields represent the group I Kimberley and Uintjiesberg kimberlites (Harris *et al.*, 2004; le Roex *et al.*, 2003) and group II Swartruggens and Star kimberlites (Coe, 2004). Partition coefficients used are from Späth *et al.* (2001).

magma with no initial K anomaly (K/K* = 1) would have been as great as 20 wt% K_2O (e.g. Bellsbank kimberlite), a value even higher than that of lamproites (Jaques *et al.*, 1983).

Fractionation of phlogopite from a group II kimberlite would deplete K_2O at a slower rate relative to group I kimberlites, due to the higher absolute K_2O content of the magma and therefore the calculated fractionation curve is shallower than for group I kimberlites (Figure 8.6a, b). Consequently, a parental group II kimberlite would not need as much phlogopite fractionation (30-50%; Figure 8.6b), in order to produce a relative K depletion similar to that in normal group II kimberlites. Given that a negative K anomaly is thought to be an inherent feature of group I, group IIb and the Swartruggens and Star primary kimberlite magmas (Coe, 2004), it appears likely that this is a trend and therefore it is considered that negative K anomalies are characteristics of group II primary kimberlite magmas. By inference of the similar behaviour of Rb and K, negative Rb anomalies are also features of group II primary kimberlite magmas. However, it is recognised that minor amounts of phlogopite crystallisation and redistribution, as well as K mobility may have a slight influence on the magnitudes of the relative anomalies in all kimberlite samples.

Negative Ti anomalies on primitive mantle normalised diagrams are present in both group I and group II kimberlites, increasing in size from Ti/Ti* = 1.0 to 0.2, with the group IIb kimberlites showing the largest relative depletion in Ti. Consistent with arguments for the negative K anomaly being a primary feature of group I kimberlites, Harris *et al.* (2004) and le Roex *et al.* (2003) have also suggested that the negative Ti anomaly is not due to phlogopite fractionation. Most group I kimberlites in this study would require greater than 30% phlogopite-only fractionation from a parental magma in order to produce the observed negative Ti anomaly (Figure 8.7a), but this is considered unlikely since

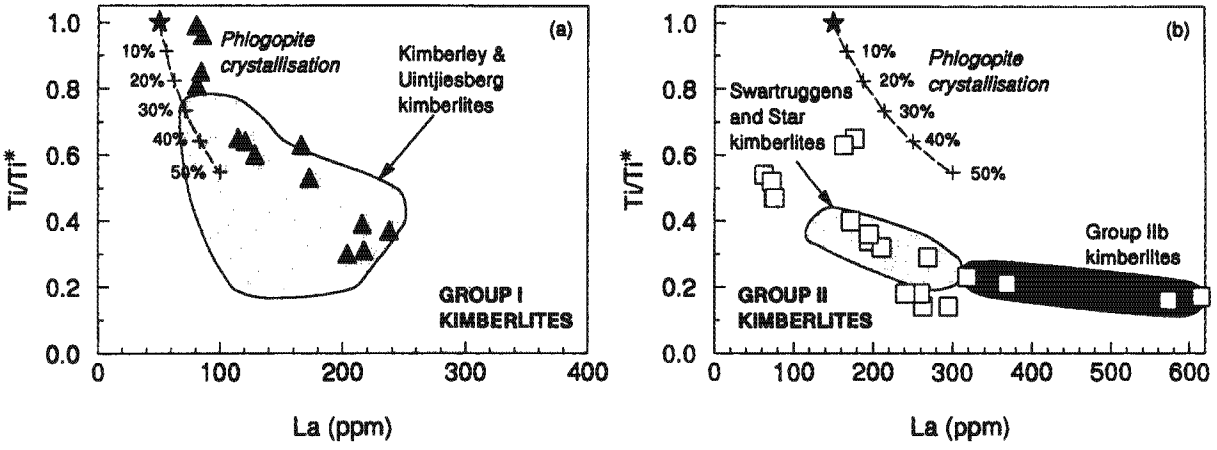

Figure 8.7: Variation of Ti/Ti* for (a) group I and (b) group II kimberlites. Superimposed is the crystallisation trajectory for the fractionation of phlogopite from a hypothetical parental kimberlite magma with no negative Ti anomaly (Ti/Ti* = 1). The group II kimberlite dataset is supplemented with analyses from the Finsch kimberlite (Zwane, 2001). Shaded fields represent the group I Kimberley and Uintjiesberg kimberlites (Harris *et al.*, 2004; le Roex *et al.*, 2003) and group II Swartruggens and Star kimberlites (Coe, 2004). Partition coefficients used are from Späth *et al.* (2001).

phlogopite is usually absent in group I kimberlites. Although phlogopite fractionation might be able to account for the presence of small negative Ti anomalies (Ti/Ti* > 0.8) in some of the group I kimberlite samples (Figure 8.7a), it is inconsistent with petrographic evidence and may well reflect assimilation of ilmenite macrocrysts identified in hand specimens of these particular samples. Groundmass phases in group I kimberlites capable of fractionating Ti are ilmenite and perovskite but the lack of an associated negative Nb and Ta anomaly on primitive mantle normalised diagrams, suggests that ilmenite or perovskite fractionation is not the cause of the Ti anomaly.

Theoretical curves for the fractionation of phlogopite from a parental group II kimberlite with no initial relative depletion in Ti, suggest that this is not a suitable mechanism to produce the observed negative Ti anomaly in group II and group IIb kimberlites, as more than 50% phlogopite-only fractionation would be required (Figure 8.7b). Consequently, the relative depletion of Rb, K and Ti in group II kimberlites, is believed not to be due to the fractionation of phlogopite. However, group II kimberlites do show characteristic depletion in Nb and Ta that could in theory be linked to the fractionation of ilmenite or perovskite, but considering that a petrographic characteristic of group II kimberlites is their paucity of groundmass ilmenite and perovskite (e.g. Skinner, 1989), this seems unlikely.

Small negative Sr anomalies in group I and group II kimberlites as well as the presence of negative Zr and Hf anomalies in the group II Eendekuil kimberlite, show no correlation with the degree of differentiation and therefore are not likely to be caused by fractional crystallisation. It is therefore argued that negative Rb, K, Ti and Sr anomalies on primitive mantle normalised diagrams are primary features of on- and off-craton group I and group II kimberlites in this study, and is similar to the conclusions of other kimberlite studies (Coe, 2004; Harris *et al.*, 2004; le Roex *et al.*, 2003). The transitional kimberlites show a combination of group I and group II kimberlite characteristics and

therefore the same arguments are applicable to this group, in that their relative depletion of Rb, K, Ti and Sr, as well as Zr and Hf (Wimbledon and Melton Wold kimberlites), are unrelated to crystal fractionation processes.

8.6 Composition of close-to-primary kimberlite magmas

Primary magmas have been defined as liquids produced by partial melting that have been unmodified by any differentiation process since the segregation from their sources (BVSP, 1981). It was suggested by Turner and Verhoogen (1960) that primary magmas can be identified by their tendency to appear throughout geologic time and that two broad subdivisions of primary magmas existed, granitic and basaltic. However, O'Hara (1965) later argued that most basalts are not truly primary, but rather have undergone fractional crystallisation at depth. Based on the Fe-Mg equilibrium that exists between olivine and liquid (Roeder & Emslie, 1970), primary magmas are generally accepted as having a Mg-number ($Mg/(Mg+Fe^{2+})$) greater than 0.68, since a liquid of this composition is likely to be in equilibrium with undepleted mantle olivine ($\sim Fo_{88-92}$). Similarly, high Ni in olivine can suggest equilibrium with the upper mantle (Sato, 1977), although high Ni and MgO may also be a characteristic of partial cumulates (Nisbet *et al.*, 1993; Hart & Davis, 1978).

Constraining the composition of primary magmas is important since it provides a window into the mantle and allows understanding of petrogenetic processes. Primary magmas have been used to investigate the nature and degree of melting (e.g. Kinzler & Grove, 1992a; Hanson & Langmuir, 1978), temperature of the melts (e.g. Herzberg & O'Hara, 2002; Larson & Pederson, 2000; Hanson & Langmuir, 1978) and effects of pressure, temperature and variable bulk composition on the composition of primary magmas (e.g. Kinzler & Grove, 1992b). Methods for constraining the compositions of primary magmas generally involve olivine compositions and Fe-Mg exchange coefficients, or using projections of magma compositions on phase diagrams (e.g. Herzberg & O'Hara, 2002; Larson & Pederson, 2000). However, due to the hybrid nature of kimberlites and that no examples of quenched kimberlite exist (Mitchell, 2004), aphanitic kimberlite has been considered a proxy for a primary magma and has been used in conjunction with experimental data to model melting of the kimberlite source (Price *et al.*, 2000), and as the basis for experimental studies investigating phase relationships of kimberlite magmas (e.g. Yamashita *et al.*, 1995; Edgar & Charbonneau, 1993). More recently, Coe (2004), Harris *et al.* (2004) and le Roex *et al.* (2003) have constrained the compositions of primary kimberlite magmas by using the trajectories between macrocrystic and aphanitic kimberlite on variation diagrams.

In order to allow meaningful and regional inter-group comparison of the geochemistry of on- and off-craton group I, group II and transitional kimberlites, it is important to identify a representative composition for each kimberlite that is close-to-primary in character. It is also important that modelling of source regions is based on close-to-primary kimberlite compositions, otherwise source region characteristics may just be reflections of secondary processes. Owing to the regional nature of this

Table 8.1: List of kimberlite samples representing the best estimates of close-to-primary kimberlite magma compositions. Samples labelled with an asterisk (*) have been corrected for the effects of macrocryst entrainment.

Kimberlite	Sample	Kimberlite	Sample
Group I kimberlites: *On-Craton*		*Off-craton*	
Goedehoop kimberlite	JJG 4282	East Griqualand kimberlites	JJG 3118
Koffiefontein kimberlite	KK 3, KK 5*	Hebron kimberlite	HEB 1A, JJG 4295*
		Klipgatsfontein kimberlite	JJG 4323
Group II kimberlites: *On-craton*		*Off-craton*	
Bellsbank kimberlite	JJG 4676*	Markt kimberlite	MRK 3*
New Elands kimberlite	NE K6		
Newlands kimberlite	JJG 24*		
Transitional kimberlites: *On-craton*		*Off-craton*	
Leicester kimberlite	JJG 4326	Melton Wold kimberlite	MLW 3*
Wimbledon kimberlite	WIMB 2*	Silvery Home kimberlite	SLH 9*, SLH 10*

study, primary kimberlite magmas compositions cannot be constrained using similar methods to Coe (2004), Harris *et al.* (2004) and le Roex *et al.* (2003) but rather, are constrained by selecting representative compositions from each kimberlite that are thought to be the least affected by alteration, crustal contamination, fractional crystallisation and corrected for macrocryst entrainment where necessary (Section 8.4). Samples thought to represent close-to-primary kimberlite magmas are listed in Table 8.1 and it is noteworthy that not every kimberlite represents a primary magma (e.g. Eendekuil kimberlite), whereas others may have more than one close-to-primary magma composition (e.g. Hebron kimberlite).

Inferred close-to-primary magma compositions of group I kimberlites analysed in this study have ~22-27 wt% MgO, ~21-30 wt% SiO_2, ~10-17 wt% CaO, ~5.0-14 wt% CO_2, ~0.2-1.7 wt% K_2O and 660-1190ppm Ni, with Mg-numbers varying between 0.82 and 0.87 (Table 8.2) and are broadly similar to primary group I kimberlite compositions proposed by other studies (Harris *et al.*, 2004; le Roex *et al.*, 2003; Price *et al.*, 2000). Group II kimberlites in this study have close-to-primary kimberlite compositions with ~28-36 wt% SiO_2, ~23-29 wt% MgO, ~2.6-4.3 wt% Al_2O_3, ~1.6-4.6 wt% K_2O and 590-1410ppm Ni, with Mg-numbers between 0.86 and 0.89 (Table 8.2). Close-to-primary compositions of the analysed group II kimberlites are generally similar to those of the group II Swartruggens and Star kimberlites (Coe, 2004), although samples (especially the group IIb kimberlites) tend be slightly more Mg-rich than reference group II kimberlites (~21.6 wt% MgO, Mg-number ~0.85) and not as K_2O-rich as the Swartruggens close-to-primary kimberlite magma (6.6 wt% K_2O; Coe, 2004). Close-to-primary compositions of the transitional kimberlites tend to be intermediate to group I and group II kimberlites, but may also be slightly more SiO_2 -rich (27-39 wt%) and CO_2-poor (1.7-12 wt%; Table 8.2).

Table 8.2: Ranges of selected major element oxides (wt%) and ferromagnesian trace elements (ppm) of group I, group II and transitional kimberlites, representing the best estimates of close-to-primary kimberlite magma compositions. Mg-number (Mg#) is atomic $Mg/(Mg + Fe^{2+})$, calculated using a Fe_2O_3/FeO ratio of 0.15 and FeO* represents all iron as Fe^{2+}.

	Group I kimberlites	Group II kimberlites	Transitional kimberlites
SiO_2	21-30	28-36	27-39
TiO_2	1.3-3.3	0.9-1.4	1.3-3.3
Al_2O_3	2.2-3.7	2.6-4.3	2.5-4.8
MgO	22-27	23-29	24-29
FeO*	7.8-12	7.2-8.1	7.1-9.3
CaO	10-17	8.1-14	5.6-14
K_2O	0.2-1.7	1.6-4.6	1.0-3.7
CO_2	5.0-14	2.1-7.4	1.7-12
Mg #	0.82-0.87	0.86-0.89	0.84-0.88
Ni	660-1190	590-1410	820-1300
Cr	860-1940	1560-2290	1660-2200
Co	83-104	74-87	61-130
Sc	10-23	17-35	9.4-27

Close-to-primary group I kimberlite magma compositions are broadly consistent with experimental kimberlite compositions (20-36 wt% SiO_2, 1.8-3.2 wt% Al_2O_3, 26-30 wt% MgO, 15-31 wt% CaO), obtained from low degrees of melting of a carbonated lherzolite by Dalton and Presnall (1998a), except that the CaO content from their study is higher than that of the samples in this study (10-17 wt% CaO; Table 8.2). MgO and SiO_2 contents of close-to-primary group II and transitional kimberlites also show some overlap with experimental compositions produced by less than 1% partial melting of a carbonated lherzolite at 6GPa (Dalton & Presnall, 1998a), suggesting that all the samples in this study could be considered very low degree partial melts.

8.7 Source region characteristics

8.7.1 The transitional kimberlites

Comparison of the major element, trace element and isotope geochemistry of the transitional kimberlites with group I and group II kimberlites (Section 7.3), has shown that they may either span the entire range in element concentrations occurring for group I and group II kimberlites (e.g. SiO_2, MgO), or else have an intermediate geochemical character (e.g. TiO_2, K_2O, La/Nb, Ba/Nb, $^{87}Sr/^{86}Sr_{(i)}$, $\varepsilon Nd_{(i)}$). These intermediate geochemical and petrographic characteristics suggest that the transitional kimberlites are genetically related to group I and group II kimberlites, and since kimberlite age and spatial distribution relationships preclude that they are mixtures of group I and II kimberlite magmas, it is more likely that the transitional kimberlites are derived from mixed source regions. Mixing of source regions has also previously been invoked as the mechanism responsible for the development of isotope arrays in other igneous rock types (e.g. Hart, 1988).

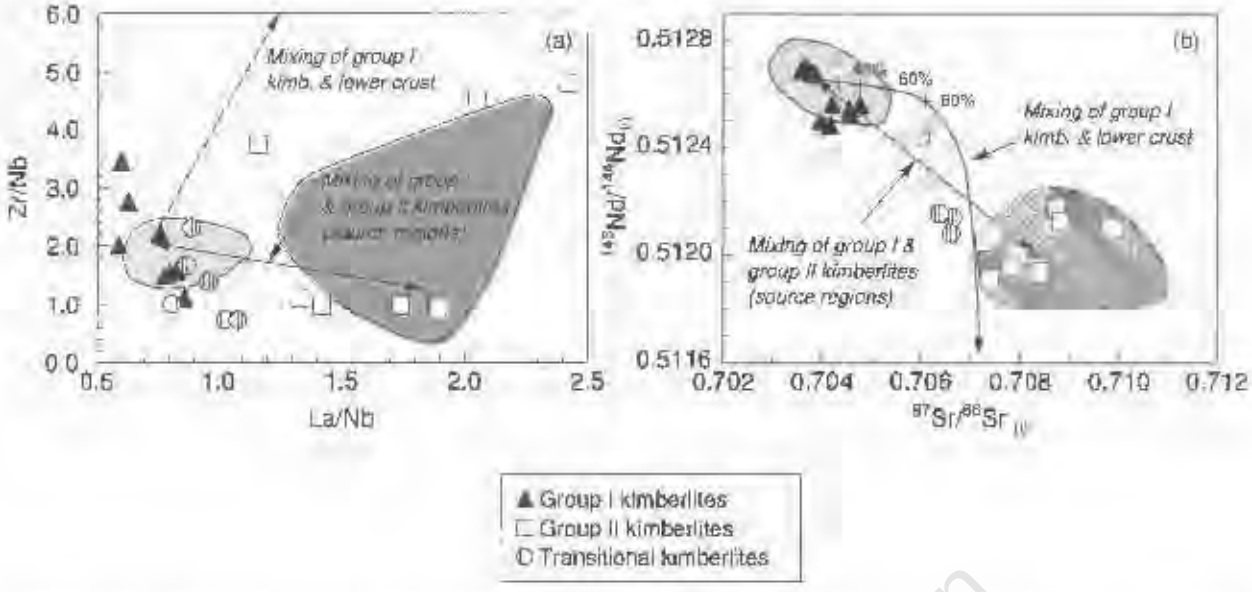

Figure 8.8: Variation of (a) selected incompatible trace element ratios and (b) isotope ratios for group I, group II and transitional kimberlites. Illustrated trajectories represent mixing (Langmuir *et al.*, 1978) of group I and group II kimberlite sources, as well as mixing of group I kimberlite magmas with lower continental crust. Parameters for lower crust (8ppm La; 5ppm Nb, 68ppm Zr, 399ppm Sr, 1.8ppm Nd, $^{87}Sr/^{86}Sr$ = 0.70721 and $^{143}Nd/^{144}Nd$ = 0.51163,) are from Rudnick and Fountain (1995) and Huang *et al.* (1995). Light shaded field represents group I kimberlites and dark shaded field, group II kimberlites (Coe, 2004; Harris *et al.*, 2004; Nowell *et al.*, 2004; le Roex *et al.*, 2003; Nowell *et al.*, 1999; Fraser & Hawkesworth, 1992; Tainton, 1992; Smith, 1983a).

Calculated mixing curves between group I and group II kimberlites correspond well with the variation of incompatible element ratios and isotope ratios shown by the transitional kimberlites (Figure 8.8), with mixing curves constructed using parameters of typical group I and group II kimberlite source compositions (see Section 8.7.3). Mixing of sources can account for the range of La/Nb ratios between kimberlite varieties, whereas minor differences in Zr/Nb are more likely a melting effect (Figure 8.8a), since the Zr/Nb ratio may be fractionated by low degrees of partial melting. Calculated mixing curves that represent the assimilation of lower continental crust (Huang *et al.*, 1995; Rudnick & Fountain, 1995) by a group I kimberlite magma, are also shown in Figure 8.8 for comparison. Just as Smith (1983b) showed that group II kimberlites are not formed by the crustal contamination of group I kimberlite magmas, it is apparent that transitional kimberlites are unlikely to represent crustally contaminated group I kimberlites. For instance, a group I kimberlite with a $^{143}Nd/^{144}Nd$ ratio of 0.51265, would need up to 60% contamination by lower crust to dilute the isotope ratio to 0.51262 (Figure 8.8b).

Given that transitional kimberlites are interpreted to have been derived from mixed group I and group II kimberlite source regions, for simplicity hereafter, the transitional kimberlite group is omitted from further semi-quantitative modelling of source compositions. The transitional kimberlite group will however, be reintroduced when the evolution of kimberlite source region characteristics is further evaluated (Section 8.8).

8.7.2 Approach to semi-quantitative modelling of kimberlite source regions

Experimental studies on group I kimberlites have shown that kimberlite-like magmas can be produced by low degrees of partial melting of a carbonated garnet peridotite at ~3-8GPa (Dalton & Presnall, 1998a; Canil & Scarfe, 1990; Eggler & Wendlandt, 1979) and that a continuum exists between carbonatitic and kimberlitic melts, with the transition between magma types taking place between 0 and 1% melting (Dalton & Presnall, 1998a). Ulmer and Sweeney (2002) have also shown that group II kimberlites may have formed by partial melting of a carbonated garnet harzburgite or lherzolite. Semi-quantitative trace element modelling of group I and group II kimberlite source regions are consistent with the derivation of these kimberlite varieties through low degrees of partial melting of a garnet lherzolite (Chalapathi Rao *et al.*, 2004; Coe, 2004; Harris *et al.*, 2004; le Roex *et al.*, 2003; Tainton & McKenzie, 1994). Semi-quantitative modelling of kimberlite petrogenesis is used in this study to explore the features of source regions, specifically for comparison of:

(i) Differing characteristics between the sources of group I and group II kimberlites.

(ii) Differing characteristics between the sources of on- and off-craton kimberlites.

However, before any modelling can be attempted, it is necessary to establish the residual mineralogy of the source and the degree of partial melting, and to understand how these parameters may affect the composition of the calculated sources.

The high degree of incompatible element enrichment and fractionated REE patterns of kimberlites, suggests that they have been derived by very low degrees of partial melting, not of normal depleted mantle, but rather of metasomatically enriched sources (e.g. Wass & Rogers, 1980; Kable *et al.*, 1975). Metasomatised lherzolite xenoliths from the Kaapvaal craton typically contain clinopyroxenes that have been enriched in the light REE (Gregoire *et al.*, 2003; van Achterberg *et al.*, 2001) and therefore, clinopyroxene is likely to be the major mineral host of these elements during partial melting. The low heavy REE abundances and fractionated heavy REE patterns in both on- and off-craton kimberlites relative to typical MORB, also indicates that partial melting took place in the presence of residual garnet (le Roex *et al.*, 2003; Rogers *et al.*, 1992; Tainton & McKenzie, 1992). Semi-quantitative modelling is therefore based on the following two assumptions:

(i) Kimberlites are formed by very low degrees of partial melting ($F < 2\%$).

(ii) The residual mineralogy of the kimberlite source is a metasomatised garnet lherzolite.

Some authors have argued that because of the absence of olivine and orthopyroxene as liquidus phases during the experimental melting of kimberlites and lamproites, the source of these alkaline magmas is not a lherzolite (Mitchell, 2004; Girnis *et al.*, 1995; Edgar & Charbonneau, 1993; Foley, 1992a), but rather some more exotic mineral assemblage (e.g. clinopyroxene-phlogopite veins; Foley, 1992b). Once kimberlite petrogenesis involving garnet lherzolite sources has been explored, the question of whether more exotic source regions are necessary will be addressed.

Table 8.3: Partition coefficients used for semi-quantitative modelling. Partition coefficients are from compilations in le Roex *et al.* (2003), Späth *et al.* (2001) and inferred from Gregoire *et al.* (2003).

	Rb	Ba	Th	U	K	Ta	Nb	La	Ce	Pb	Pr	Sr	Nd	P
Oliv	0.001	0.001	0.001	0.001	0.001	0.001	0.001	0.001	0.001	0.001	0.001	0.001	0.001	0.001
Opx	0.001	0.001	0.001	0.001	0.001	0.001	0.001	0.001	0.001	0.001	0.001	0.001	0.001	0.001
Cpx	0.001	0.001	0.001	0.001	0.01	0.01	0.01	0.05	0.08	0.08	0.1	0.12	0.14	0.1
Gnt	0.001	0.001	0.001	0.001	0.001	0.001	0.001	0.01	0.021	0.021	0.054	0.001	0.087	0.05

	Sm	Hf	Zr	Eu	Ti	Gd	Tb	Dy	Ho	Er	Tm	Yb	Lu
Oliv	0.001	0.001	0.001	0.001	0.001	0.001	0.001	0.001	0.001	0.001	0.001	0.001	0.001
Opx	0.001	0.01	0.01	0.01	0.1	0.016	0.019	0.022	0.022	0.03	0.03	0.1	0.1
Cpx	0.14	0.2	0.2	0.15	0.17	0.2	0.25	0.3	0.3	0.28	0.29	0.3	0.3
Gnt	0.13	0.1	0.1	0.2	0.1	0.3	0.6	0.9	1.4	2	3	4	6

** Note: Oliv = olivine, Opx = orthopyoxene, Cpx = clinopyroxene and Gnt = garnet*

Using the composition of the close-to-primary Markt kimberlite as an example, the kimberlite source region composition can be calculated, by applying the equations for non-modal batch melting (Shaw, 1970) and partition coefficients in Table 8.3, and with the residual source modal mineralogy and degree of melting as assumed parameters. By varying these assumed parameters, it can subsequently be shown that the lower the degree of partial melting, the less enriched the source needs to be (Figure 8.9). Varying the degree of melting between F = 0.5% and 2%, results in a calculated source with the light REE enriched between 10 and 25 times chondrite, respectively, but with no significant change in the heavy REE concentrations (~1.3 times chondrite) because of the relative compatibility of the heavy REE in the residual garnet. Increasing the proportion of residual clinopyroxene in the source from 3% to 7%, results in calculated source regions being more enriched in the light REE (13 to 15 times chondrite, respectively; Figure 8.9) and similarly, increasing the proportion of residual garnet results in sources being more enriched in the heavy REE (1.3 to 2.6 times chondrite, respectively). It is also apparent that changing the modal proportion of residual garnet in the source has a greater effect on the calculated REE concentrations, than changing the proportion of clinopyroxene (Figure 8.9).

Although it has been assumed that kimberlites in this study are derived from metasomatised garnet lherzolites, it is necessary to establish whether the xenolith load entrained by on- and off-craton, as well as group I and group II kimberlites show any differences that could possibly be significant when selecting the best estimates of the residual modal mineralogy of their source regions. Modal analyses of peridotite xenoliths entrained by kimberlites, illustrate that the proportion of clinopyroxene typically varies between 2% and 7%, whereas garnet varies between 3% and 9% (Table 8.4). Garnet proportions tend to be similar for both on- and off-craton xenoliths, but on-craton xenoliths appear to have slightly less modal clinopyroxene (< 4%). Since it has been illustrated that small variations in the proportion of residual clinopyroxene do not have a very marked effect on the composition of the

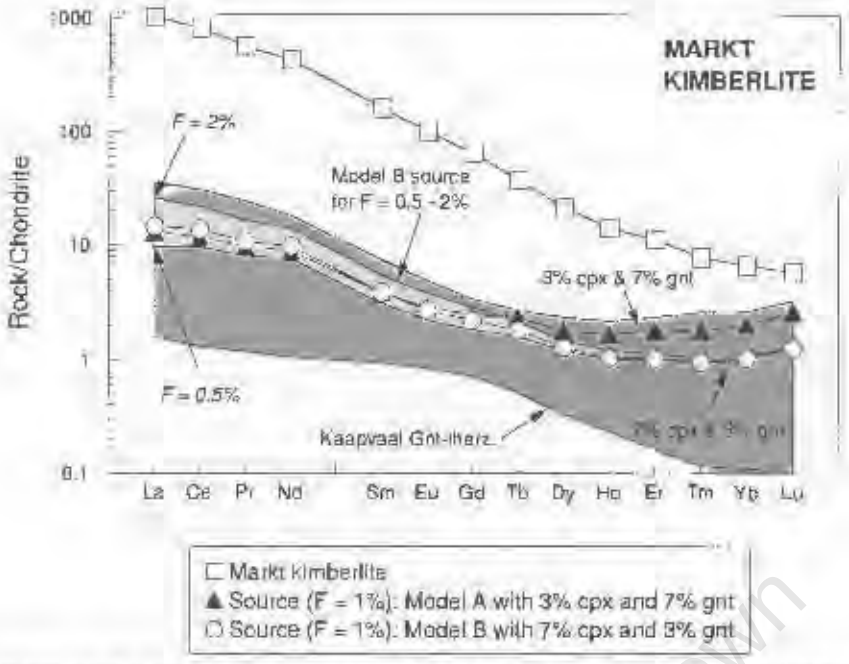

Figure 8.9: Chondrite normalised REE composition of a kimberlite source region in equilibrium with the group II Markt close-to-primary kimberlite magma, calculated by semi-quantitative forward modelling and with partition coefficients from Table 8.3. The effect of varying the degree of melting (F = 0.5-2%, shown as the light shaded field) and residual source region mineralogy is illustrated for the predicted kimberlite source region composition. Dark shaded field represents the composition of Kaapvaal craton xenoliths (Gregoire *et al.*, 2003). Chondrite normalising values from Sun and McDonough (1989). See text for further discussion.

Table 8.4: Average modal mineralogy of garnet lherzolite xenoliths entrained by various southern African on- and off-craton kimberlites.

Location	Oliv (%)	Opx (%)	Cpx (%)	Gnt (%)	Reference
Off-craton kimberlites					
Louwrensia kimberlites	69	24	4	3	Boyd *et al.* (2004)
Gibeon kimberlite	68	16	7	9	Franz *et al.* (1996)
Melton Wold kimberlite	65	24	5	6	This study
On-craton kimberlites					
Compilation	62	31	2	5	Boyd & Mertzman (1987)
Compilation	71	21	3	5	Gregoire *et al.* (2003)
Compilation	62	30	2	6	Maaloe & Aoki (1977)
Compilation	64	27	3	7	Mathias *et al.* (1970)

** Oliv = olivine, Opx = orthopyroxene, Cpx = clinopyroxene and Grt = garnet*

*** The modal mineralogy of Melton Wold kimberlite xenoliths was point counted in this study on some of the samples described by Robey (1981). However, due to the altered nature of the xenoliths, the ratio of olivine and opx has been assumed.*

calculated kimberlite source (Figure 8.9), this is not thought to be significant. Although there appear to be more descriptions of metasomatised xenoliths entrained by group I rather than group II kimberlites (e.g. Gregoire *et al.*, 2003; Simon *et al.*, 2003b; van Achterberg *et al.*, 2001), this does not necessarily imply any major differences between the sources of kimberlite varieties, since the xenolith load of any particular kimberlite likely reflects random sampling of the mantle (Harte, 1983).

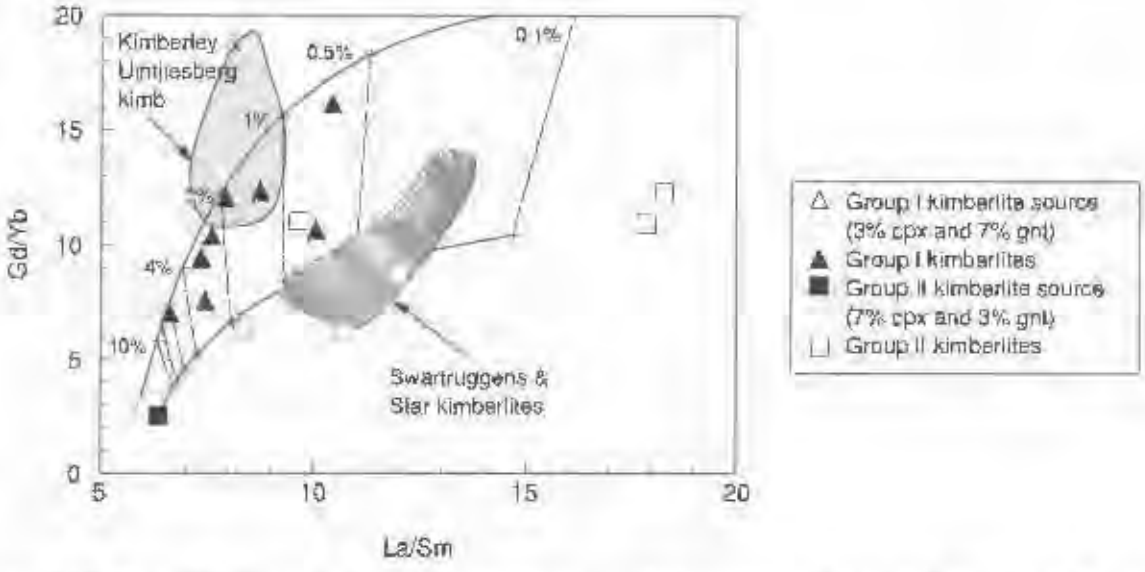

Figure 8.10: Rare earth element ratios of group I and group II close-to-primary kimberlite magmas. Illustrated curves represent melting trajectories of group I (La/Sm = 6.0; Gd/Yb = 3.0) and group II kimberlite source regions (La/Sm = 5.4; Gd/Yb = 2.5). Numbers shown represent the degree of melting. Shaded fields represent the group I Kimberley and Uintjiesberg kimberlites (Harris *et al.*, 2004; le Roex *et al.*, 2003) and group II Swartruggens and Star kimberlites (Coe, 2004).

However, the observation that group II kimberlites have steeper light REE (higher La/Sm), but flatter heavy REE slopes (lower Gd/Yb) than group I kimberlites (Section 7.3), can potentially relate to differences in source mineralogy. Calculated melting trajectories in Figure 8.10 illustrate that although increasing the degree of partial melting decreases the La/Sm and Gd/Yb ratios, these changes cannot account for the varying ratios between group I and group II kimberlites. Rather, it appears that group II kimberlites are derived from sources with higher La/Sm but lower Gd/Yb than group I kimberlites. The lower Gd/Yb ratios of group II kimberlites are consistent with less residual garnet in the source holding back the heavy REE during partial melting (e.g. 3% garnet; Figure 8.10), whereas higher Gd/Yb in group I kimberlites suggests a stronger role of residual garnet and hence more garnet in the source region (e.g. 7% garnet). In contrast, the higher La/Sm and La/Yb of group II kimberlites can be argued to be the result of a greater proportion of residual clinopyroxene (eg. 7% cpx instead of 3% cpx, Figure 8.10) retaining Sm during partial melting ($D_{Sm} > D_{La}$ in cpx; Table 8.3). La/Sm and Gd/Yb ratios used as hypothetical kimberlite sources for modelling in Figure 8.10 are similar to those of Kaapvaal garnet lherzolites and although whole rock La/Sm and Gd/Yb ratios of lherzolites are variable, showing little correlation with the proportion of modal garnet or clinopyroxene (Gregoire *et al.*, 2003; Simon *et al.*, 2003b; van Achterberg *et al.*, 2001), the arguments for varying proportions of residual clinopyroxene and garnet between kimberlite source regions are based on the behaviour of the REE during melting.

Having assessed the effect of varying residual modal mineralogy and degree of partial melting on kimberlite source regions, these parameters will now be fixed so that differences in source characteristics between kimberlite varieties can be evaluated. All kimberlites source regions are therefore calculated for 1% partial melting. The residual mineralogy of a group I kimberlite source is selected to have 65% olivine, 25% orthopyroxene, 3% clinopyroxene and 7% garnet (Model A; Figure

8.9), whereas the source of group II kimberlites has been chosen to have more clinopyroxene but less garnet (7% clinopyroxene, 3% garnet, Model B). Both the selected proportions of the residual mineralogy are broadly coincident with those of Kaapvaal garnet lherzolites (Table 8.4).

8.7.3 Geochemistry of kimberlite source regions

Geochemistry of group I kimberlite source regions

Calculated source regions in equilibrium with close-to-primary group I kimberlites are all enriched in the light REE and only slightly enriched in the heavy REE relative to chondrite (Figure 8.11a). Predicted source compositions generally show good overlap with that of the group I Kimberley kimberlites (ie Roex *et al.*, 2003), Uintjiesberg kimberlite (calculated in this study using the primary magma of Harris *et al.*, 2004) and with garnet lherzolites from the Kaapvaal craton (Figure 8.11a; Gregoire *et al.*, 2003). However, the source of the Kimberley kimberlites is not as enriched in the heavy REE compared to the group I kimberlites in this study (Figure 8.11a), since le Roex *et al.* (2003) assumed only 2% residual garnet rather than the 7% garnet used here. Light REE concentrations of calculated sources are enriched by a factor between 4 and 12 times chondrite (East Griqualand and Koffiefontein kimberlites, respectively) and are more enriched than the heavy REE contents, that vary between 1.8 and 3.6 times chondrite (Koffiefontein and Goedehoop kimberlites, respectively). REE ratios, such as $(La/Sm)_N$ vary between 2.3 and 3.5, whereas $(La/Yb)_N$ varies from 1.9 to 8.6. Predicted source compositions show the same degree of enrichment relative to each other as do the close-to-primary kimberlite magmas. For example, the off-craton Abbotsford East kimberlite is the least light REE enriched of the group I kimberlites and consequently, so is the source composition.

Modelling of source regions in equilibrium with close-to-primary group I kimberlite magmas can be extended to show geochemical characteristics of the full incompatible trace element suite (Figure 8.11b). Calculated sources are enriched in the more incompatible elements and depleted in the less incompatible elements relative to primitive mantle (e.g. Th = 1-4 and Zr = 0.6-1 times primitive mantle, respectively). Characteristic features on primitive mantle normalised patterns of close-to-primary kimberlite magmas are transferred to the predicted source regions (Figure 8.11b), due to the absence of any residual accessory phases (e.g. phlogopite) capable of fractionating these elements. Consequently, calculated sources show negative Rb, K and Ti anomalies ($K/K^* \sim 0.1$; $Ti/Ti^* = 0.2$-0.7) as well as more subdued negative Sr and Hf anomalies on primitive mantle normalised diagrams. Calculated source compositions overlap the field of garnet lherzolites from the Kaapvaal craton for virtually all trace elements other than K, which is significantly more depleted in the predicted kimberlite sources than in peridotites (Figure 8.11b; Gregoire *et al.*, 2003). However, many of the samples from the study of Gregoire *et al.* (2003) contain modal phlogopite and consequently, the peridotites are likely to have elevated K concentrations.

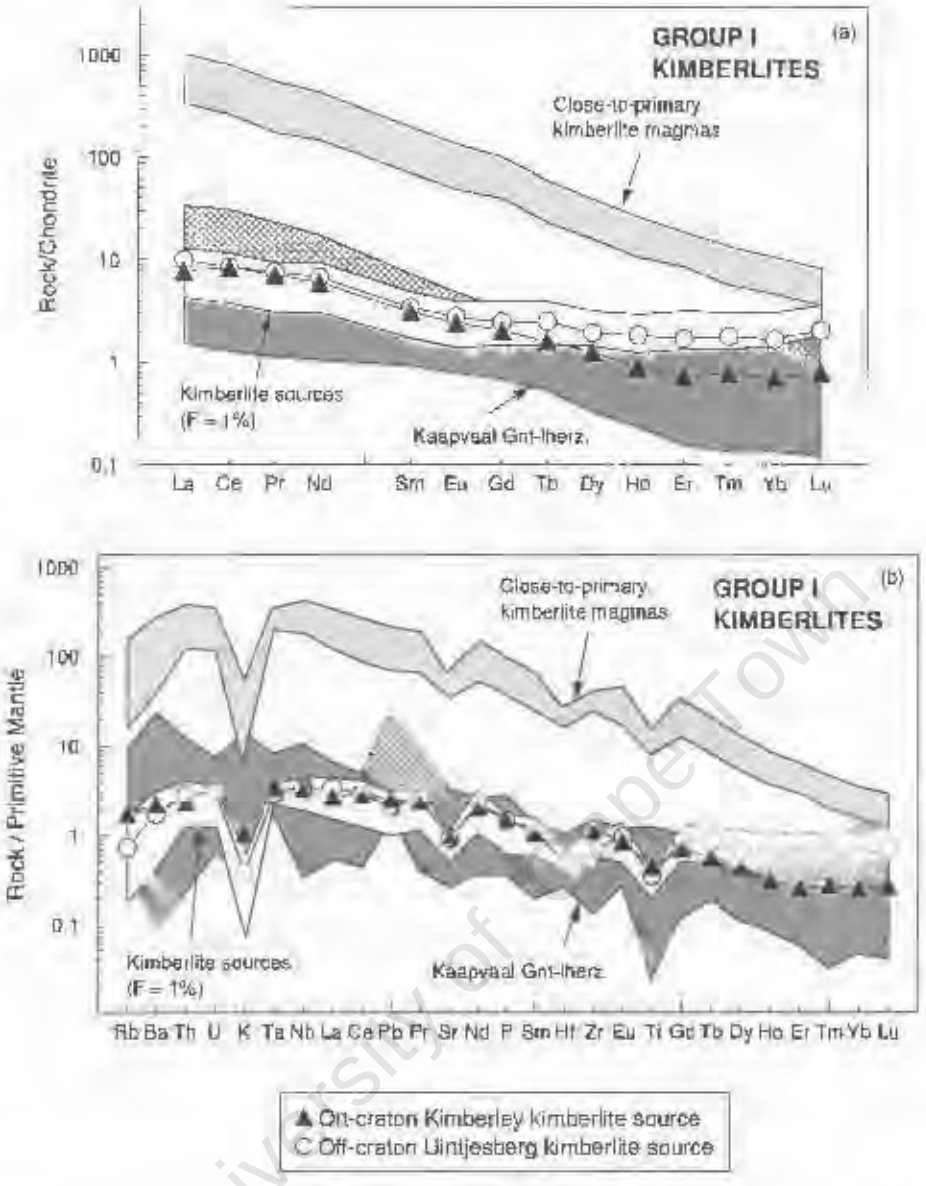

Figure 8.11: Predicted (a) chondrite normalised and (b) primitive mantle normalised patterns of the source compositions of group I kimberlites, calculated by semi-quantitative forward modelling from close-to-primary kimberlite magmas with F = 1% and residual source region mineralogy corresponding to a garnet lherzolite (65% oliv, 25% opx, 3% cpx, 7% gnt). Source regions for the group I Kimberley kimberlites (le Roex *et al.*, 2003) and Uintjesberg kimberlite (calculated from the primary kimberlite magma of Harris *et al.*, 2004) are shown. Dark shaded field represents garnet lherzolites from the Kaapvaal craton (Gregoire *et al.*, 2003). Normalising values are from Sun and McDonough (1989).

Since the compositions of group I kimberlite source regions have all been calculated using the same parameters, any differences in the close-to-primary magmas between on- and off-craton kimberlites (Section 7.2), will be transferred to the calculated sources. Therefore, predicted sources of off-craton kimberlites appear to have lower La/Sm, La/Yb and Gd/Yb than on-craton kimberlites. However, it can be argued that were the sources of on- and off-craton group I kimberlites to have identical initial REE ratios, then the lower La/Yb and Gd/Yb (also La/Sm) of off-craton kimberlites is due to slightly higher degrees of partial melting, since all group I kimberlites roughly fall on the same melting trajectory (Figure 8.12).

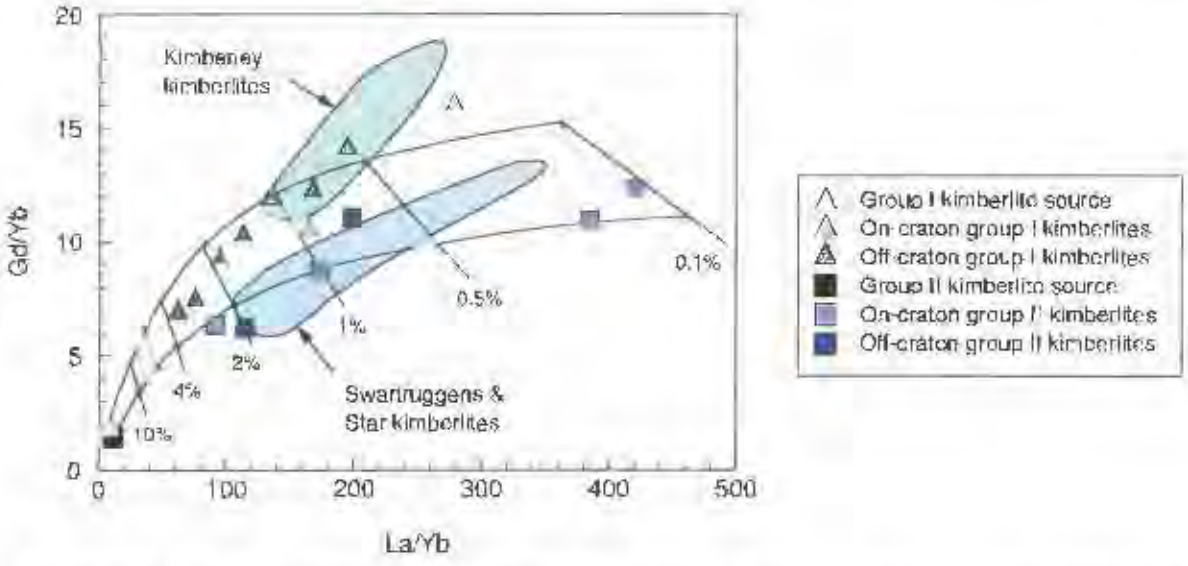

Figure 8.12: Rare earth element ratios of group I and group II, on- and off-craton close-to-primary kimberlite magmas. Illustrated curves represent melting trajectories of group I (Gd/Yb = 2.0; La/Yb = 8.4) and group II kimberlite source regions (Gd/Yb = 1.4; La/Yb = 10.7). Numbers shown represent the degree of melting. The composition of the close-to-primary off-craton group I Uintjiesberg kimberlite is included in the group I kimberlite dataset (Harris *et al.*, 2004). The green shaded field represents the on-craton group I Kimberley kimberlites (le Roex *et al.*, 2003) and blue field the on-craton group II Swartruggens and Star kimberlite (Coe, 2004).

Geochemistry of group II kimberlite source regions

Predicted source regions in equilibrium with close-to-primary group II kimberlite magmas are also all enriched relative to chondrite, although the light REE are considerably more enriched than the heavy REE (Figure 8.13a). Source compositions have also been determined for the Finsch close-to-primary kimberlite magma calculated from the analyses of Zwane (2001), as well as for Eendekuil kimberlite (although not strictly speaking a close-to-primary kimberlite composition, but has been included because of its striking negative Zr and Hf anomaly). Light REE concentrations of sources are enriched between 5 and 36 times chondrite (Finsch and Bellsbank kimberlites, respectively) whereas heavy REE concentrations tend to be similar to chondrite (0.9 - 1.6 times chondrite; Eendekuil and Brandewynskuil kimberlites, respectively). Sources of the group IIb kimberlites tend to be more enriched in the incompatible elements with higher La/Sm and La/Yb ratios ($(La/Sm)_N$ ~ 6.9) than those of normal group II kimberlites ($(La/Sm)_N$ = 3.2-4.6), possibly suggesting that they are lower degree partial melts than some of the other group II kimberlites in this study. Calculated source compositions generally show good overlap with those of the group II Swartruggens and Star kimberlites (Figure 8.13a; Coe, 2004), except that the Swartruggens kimberlite source is more enriched in the heavy REE. All predicted source regions of group II kimberlites overlap the compositional field defined for Kaapvaal garnet lherzolite xenoliths (Gregoire *et al.*, 2003).

Calculated source compositions of group II kimberlites in equilibrium with close-to-primary magmas are enriched in the incompatible elements and depleted in the less incompatible elements (Figure 8.13b), relative to primitive mantle (e.g. Th = 1-11 and Zr = 0.4-1 times primitive mantle, respectively). Source compositions also show negative anomalies on primitive mantle normalised diagrams, similarly

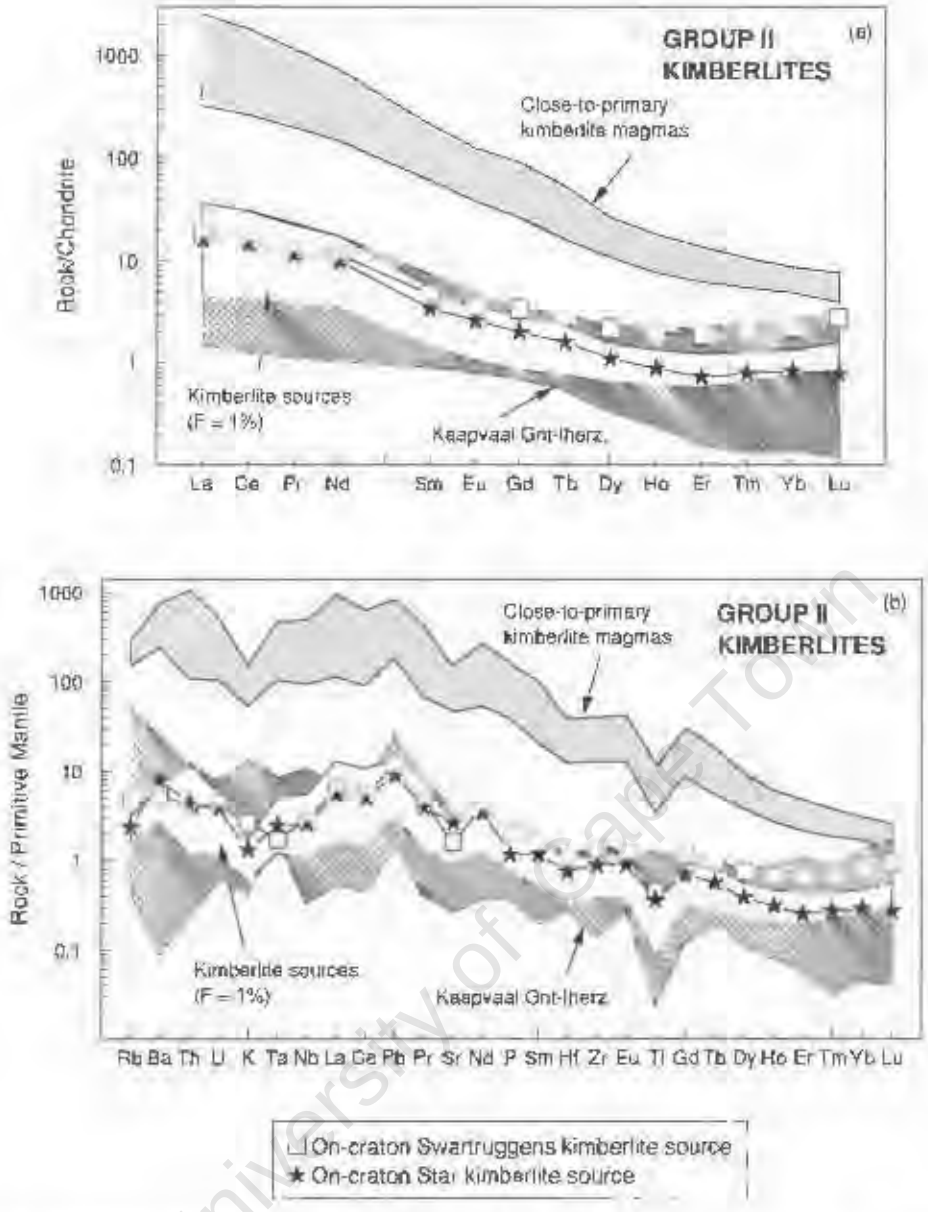

Figure 8.13: Predicted (a) chondrite normalised and (b) primitive mantle normalised patterns of the source compositions of group II kimberlites, calculated by semi-quantitative forward modelling from close-to-primary kimberlite magmas with F= 1% and residual source region mineralogy corresponding to a garnet lherzolite (65% oliv, 25% opx, 7% cpx, 3% grt). Source regions for the group II Swartruggens and Star kimberlites (Coe, 2004) are shown. Dark shaded field represents garnet lherzolites from the Kaapvaal craton (Gregoire *et al.*, 2003). Normalising values are from Sun and McDonough (1989).

to close-to-primary group II kimberlite magmas, with negative Rb, K and Ti anomalies being larger in magnitude for group IIb kimberlites ($K/K^* \sim 0.1$, $Ti/Ti^* \sim 0.2$), than normal group II kimberlites ($K/K^* = 0.3\text{-}1.0$, $Ti/Ti^* = 0.2\text{-}0.6$). All group II kimberlite source regions show subdued depletion in Sr and Nb ($(La/Nb)_N = 1.5\text{-}2.7$) as well as slight enrichment in Pb ($(Ce/Pb)_N = 0.2\text{-}1.0$). Although all of the sources may be slightly depleted in Hf, only the Eendekuil kimberlite source shows pronounced depletion in Hf and Zr ($Hf/Hf^* \sim 0.4$). Calculated source compositions correspond with the field of garnet lherzolite xenoliths from Gregoire *et al.* (2003), especially since the peridotite xenoliths are also characterised by

depletion in Ti as well as Nb, Ta, Zr and Hf (Gregoire *et al.*, 2003). No significant differences are identified between calculated source compositions of on- and off-craton group II kimberlites.

8.7.4 Residual accessory mineral phases

Since forward modelling was based upon a residual garnet lherzolite source with no accessory phases present, bulk partition coefficients for Rb, K, Ti, Sr and Nb during partial melting are all less than unity. Hence, any anomalies in the close-to-primary group I and group II kimberlite magmas, are automatically transferred to their source regions since there is no phase present to fractionate these elements (Figure 8.11b, 8.13b). It therefore needs to be determined whether these anomalies in the close-to-primary kimberlite magmas are inherent features of the sources, or are the result of the presence of residual accessory phases during partial melting, not considered in the previous calculations. The presence of residual phlogopite (Williams *et al.*, 2004; Yang *et al.*, 2003; Rogers *et al.*, 1992) and amphibole (Späth *et al.*, 2001) during partial melting has previously been suggested to be the cause of negative K anomalies in some other alkaline magmas. Many peridotite xenoliths entrained by kimberlites in southern Africa are metasomatised and bear modal phlogopite or K-richterite (Gregoire *et al.*, 2003; Waters & Erlank, 1988; Erlank *et al.*, 1987) and therefore it is important to evaluate the role of these minerals as possible residual phases. Similarly, titanate minerals such as rutile, armalcolite and lindsleyite also occur in metasomatised peridotite xenoliths (Haggerty, 1987) and may have played a role in the development of negative Ti, Nb and Ta anomalies in kimberlite magmas.

Since K is a major element in phlogopite, its concentration in a melt in equilibrium with a residual K-phase is not governed by its partition coefficient in the residual phase, rather the concentration of K in the liquid is only dependent upon the proportion and melt mode of the residual phase in the source (Späth *et al.*, 2001; Greenough, 1988). Consequently, K_2O concentrations of liquids in equilibrium with residual phlogopite will be buffered over a range of degrees of melting, as long as there is still residual phlogopite present (Rogers *et al.*, 1992). Following the approach of Späth *et al.* (2001), the K content of a liquid in equilibrium with a residual K- phase can be calculated and compared with the true composition of the melt (Figure 8.14a). Group I close-to-primary kimberlite magmas have a maximum of 14000ppm K and are unlikely to be in equilibrium with residual phlogopite or K-richterite (>22000ppm K; Figure 8.14a). On the basis of the arguments presented by le Roex *et al.* (2003) and Harris *et al.* (2004), it is similarly interpreted that the negative K and Rb anomalies in group I kimberlites are not a result of residual phlogopite or K-richterite, but rather a feature of metasomatism.

Group II kimberlite magmas have between 13000 and 38000ppm K and are more likely to be in equilibrium with residual phlogopite than amphibole (Figure 8.14a). The possibility of residual K-richterite however, is unlikely, since it is not stable in the presence of garnet (Erlank *et al.*, 1987), which has already been argued to be a residual phase (Section 8.7.2). The magnitude of the negative K anomaly of a melt in equilibrium with residual phlogopite can also be calculated, providing that the melt mode of the residual K-phase is known (Späth *et al.*, 2001). Assuming mantle phlogopite contains

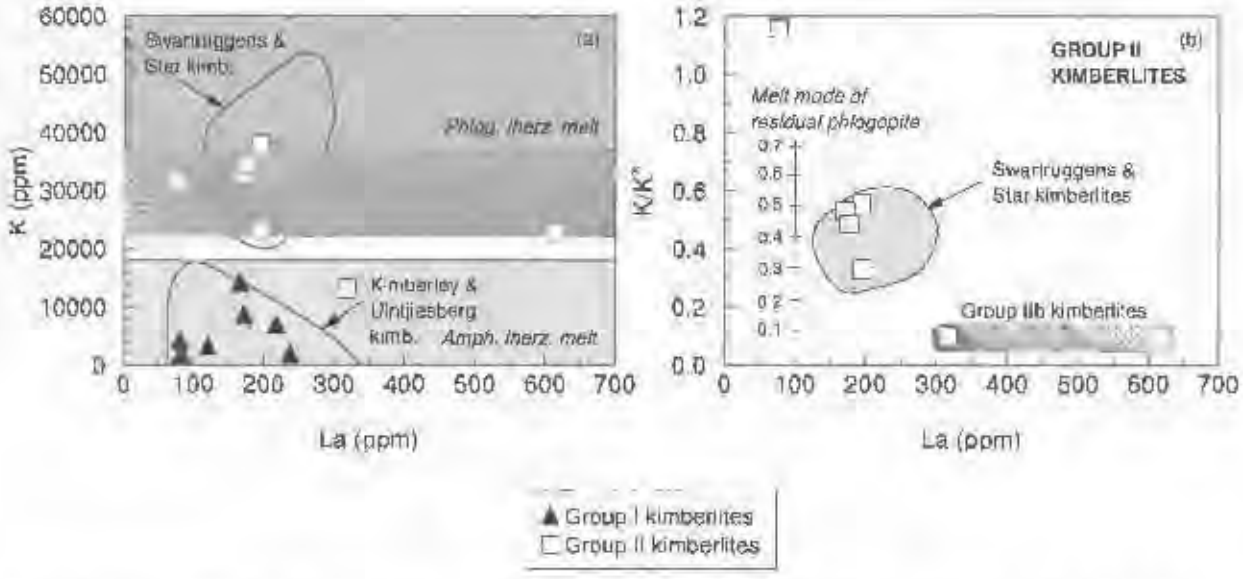

Figure 8.14: (a) The K content of close-to-primary group I and group II kimberlite magmas is illustrated with the corresponding fields of reference kimberlites. Rectangular fields illustrate the range of K concentrations expected for primary magmas in equilibrium with residual amphibole lherzolite, K-richterite lherzolite or phlogopite lherzolite (from Späth *et al.*, 2001). (b) Magnitude of the negative K anomaly (K/K*) in normal group II kimberlites and group IIb kimberlites. The bar with numbers represents the melt mode of residual phlogopite, with individual marks representing the calculated magnitude of a negative K-anomaly in a hypothetical melt in equilibrium with residual phlogopite (see text for explanation). The compositional fields of reference group I and group II kimberlites are also shown for comparison (Coe, 2004; Harris *et al.*, 2004; le Roex *et al.*, 2003). Partition coefficients are from Späth *et al.* (2001).

~9 wt% K_2O (Gregoire *et al.*, 2003), then in order to produce a negative K-anomaly similar to that observed in the group II kimberlites, the melt mode of the residual phlogopite would have to be 0.1 for group IIb kimberlites, and between 0.3 and 0.5 for normal group II kimberlites (Figure 8.14b). The above calculations suggest that the melt mode of phlogopite would need to be considerably lower than inferred estimates of 0.5 to 0.7 (Greenough, 1988; Wass & Rogers, 1980), in order to derive a melt with a K-anomaly similar to that in the group II kimberlites.

Experimental studies have shown that both phlogopite and K-richterite are stable at upper mantle conditions, especially if fluorine is present to stabilise the phase (Harlow & Davies, 2004; Trønnes, 2002; Sato *et al.*, 1997). However, according to the experimental study of Ulmer and Sweeney (2002) based on the average group II kimberlite composition of Smith *et al.* (1985b), phlogopite is not stable on the kimberlite liquidus during melting in the presence of a carbonate at pressures greater than 4GPa, but rather breaks down to form garnet, orthopyroxene and a K-rich liquid. Yamashita *et al.* (1995) similarly argued that phlogopite is not stable during melting of a group II kimberlite above 6.5GPa. This additional evidence affirms the unlikelihood of phlogopite as a residual phase during partial melting and group II kimberlite production. Based on similar grounds, Coe (2004) argued for the absence of residual phlogopite during partial melting to produce the group II Swartruggens and Star kimberlites. However, it is recognised that a K and Rb-rich phase is necessary in the mantle sources to impart the K_2O-rich and radiogenic $^{87}Sr/^{86}Sr$ character to the group II kimberlites (Schmidt *et al.*, 1999), but that this phase is likely entirely consumed during melting.

Calculated source regions of both group I and group II kimberlites are depleted in Ti and since it has been argued that phlogopite is unlikely to occur as a residual phase during kimberlite production, it cannot have influenced the development of the negative Ti anomaly in the close-to-primary kimberlite magmas. The role of a residual titanate phase also needs to be assessed and can be evaluated using Nb and Ta, whose partition coefficients are high in titanates (e.g. D_{Nb} in rutile = 28-540; Foley *et al.*, 2000; Green & Pearson, 1987). Since, group I kimberlites have no corresponding negative Nb and Ta anomaly, the presence of a residual titanate phase can be precluded. However, the partition coefficient of Ti in clinopyroxene is dependent upon numerous parameters (e.g. presence of CO_2; summarised in Harris *et al.*, 2004 and le Roex *et al.*, 2003) and a change in D_{Ti} for clinopyroxene from 0.17 (Table 8.4) to 0.73, a value more suitable for carbonatites (Bizimis *et al.*, 2003), is sufficient enough to negate the presence of a negative Ti anomaly in the predicted sources.

The magnitude of the negative Ti anomaly in the sources of group II kimberlites tend to be larger than for group I kimberlites and calculations show that it cannot be removed by a simple change in the Ti partition coefficient. However, since group II kimberlites are characterised by negative Ti as well as negative Nb and Ta anomalies on primitive mantle normalised diagrams (Figure 5.10), the effect of a residual titanate needs to be explored. Although small degrees of partial melting with residual rutile can account for the relative depletion of Nb and Ta in group II kimberlites (Figure 8.15; Coe, 2004), simple calculations involving the Ti budget and melt mode suggest that the presence of residual rutile is unlikely. If the calculated group II kimberlite source regions were to have no Ti anomaly ($Ti/Ti^* = 1$) then the Ti content would need to be approximately 1000ppm Ti. Assuming all the Ti was hosted in rutile (94% TiO_2 or 563 530ppm Ti; Gregoire *et al.*, 2003), the proportion of rutile in the source would be 0.18%. Since rutile is typically a metasomatic phase (Haggerty, 1987), it is likely to be preferentially melted and therefore, will not have a very small melt mode. Assuming a melt mode of 50% (similar to phlogopite), then after 0.36% partial melting there would be no rutile remaining. Other titanate minerals have lower TiO_2 concentrations than rutile and would require even lower degrees of melting to remain as residual phases. Negative Nb, Ta and Ti anomalies are however, interpreted to be features of the group II kimberlite source regions because of the following three observations:

(i). Other group II kimberlites show depletion in Nb, Ta and Ti (Coe, 2004; Clark, 1994; Tainton, 1992).

(ii). Negative Nb and Ta anomalies occur in the Karoo flood basalts (Figure 8.15; Marsh *et al.*, 1997), that are higher degree melts than kimberlites and even more unlikely to have equilibrated against a residual titanate phase. Hawkesworth *et al.* (1984) have suggested that depletion of Nb and Ta may also be a feature of the Karoo mantle source.

(iii). Negative Nb and Ta anomalies occur in Kaapvaal craton xenoliths as well as in some of their constituent minerals (Gregoire *et al.*, 2003; van Achterberg *et al.*, 2001).

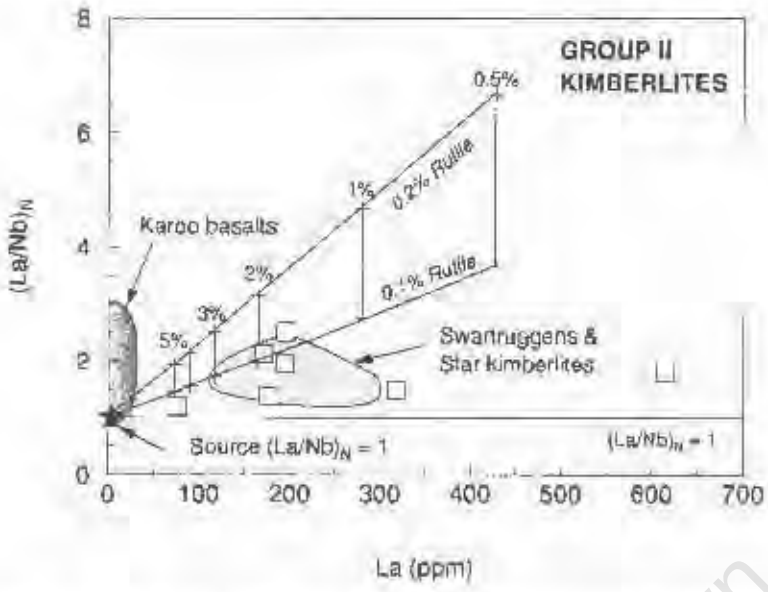

Figure 8.15: Variation of $(La/Nb)_N$ with La for close-to-primary group II kimberlite magmas and where kimberlites with $(La/Nb)_N > 1$ are characterised by relative depletion of Nb on primitive mantle normalised diagrams. Illustrated trajectories correspond to melting of a group II kimberlite source region with either 0.1 or 0.2% residual rutile and with numbers shown, representing the degree of partial melting. Melting was calculated assuming the kimberlite source had no initial Nb depletion [$(La/Nb)_N = 1$] and that the melt mode of rutile is 0.5. Partition coefficients are from Foley *et al.* (2000) and Green and Pearson (1987). Shaded fields represent the group II Swartruggens and Star kimberlites (Coe, 2004) and Karoo basalts (Marsh *et al.*, 1997).

The calculated source region of the group II Eendekuil kimberlite also shows a well-developed negative Zr and Hf anomaly. Yang *et al.* (2003) have shown that negative Zr and Hf anomalies in Hawaiian alkalic lavas can be accounted for by the presence of residual clinopyroxene and since Hf is also a HFS element, its partition coefficient in clinopyroxene will be affected by the same parameters as D_{Ti}. However, increasing D_{Hf} in clinopyroxene from 0.2 (Table 8.3) to a partition coefficient of 0.46, that is more appropriate for a carbonate system (Bizimis *et al.*, 2003), does not remove the negative Hf anomaly in the calculated source of the Eendekuil kimberlite. Close-to-primary magmas of the transitional Melton Wold and Wimbledon kimberlites also show large negative Zr and Hf anomalies that are correlated with depletion in Ti (Figure 5.15), features that are similarly transferred to the predicted source compositions of these kimberlites. Although the presence of a residual Zr-bearing phase (e.g. zircon, zirconalite; Haggerty, 1987) during partial melting cannot be precluded, the characteristic depletion of HFS elements in the Eendekuil, Wimbledon and Melton Wold kimberlites is interpreted as suggesting a possible source region relationship to carbonatites, magmas that are also typically characterised by depletion in the HFS elements (Nelson *et al.*, 1988).

Close-to-primary group I and group II kimberlite magmas are therefore argued to have been unaffected by residual phlogopite or any titanate phases. Similarly, residual apatite is unlikely to account for the subdued negative Sr anomalies present in the kimberlites, given that no corresponding negative P anomaly has been observed. Following the preferred model of Coe (2004), Harris *et al.* (2004) and le Roex *et al.* (2003), the depletion of group I and group II close-to-primary kimberlite magmas in Rb, K, Ti and lesser depletion in Sr, Hf and Nb-Ta (group II kimberlites) are characteristics

directly inherited from their sources, although the magnitudes of some of these anomalies may have been slightly modified by alteration and fractional crystallisation.

8.8 Source region evolution

It has previously been debated whether kimberlites can be derived from ordinary mantle (Kramers *et al.*, 1981), but is now generally recognised that source enrichment in incompatible elements is a prerequisite for alkaline magma generation (e.g. Wass & Rogers, 1980). The key study by Tainton and McKenzie (1994) not only showed that the source regions of the group II Bellsbank and Newlands kimberlites must have been enriched in incompatible trace elements, but also that a melt-depletion event occurred prior to enrichment. Tainton and McKenzie (1994) demonstrated using REE inversion modelling that the sources of these group II kimberlites were depleted by approximately 20% melting in the garnet stability field with subsequent enrichment by a metasomatic melt, considered to have been produced by 0.5% melting of a MORB source. More recently, Chalapathi Rao *et al.* (2004), Coe (2004), Harris *et al.* (2004), le Roex *et al.* (2003), Beard *et al.* (2000) and Beard *et al.* (1998), have all shown that the source regions of kimberlites have a two stage evolutionary history comprising initial melt-depletion with subsequent metasomatic enrichment.

Metasomatism is typically postulated to take place by the percolation of melts or aqueous fluids enriched in incompatible elements (Eggler, 1987). Varying styles of metasomatism between cryptic and modal metasomatism have been recognised within the Kaapvaal craton (Erlank *et al.*, 1987; Harte, 1983; Dawson, 1980). Metasomatising melts and fluids may vary in character from alkali- and silica-rich to carbonate-rich, depending on the CO_2/H_2O ratio and may therefore carry different elements, depending on their relative solubility (Eggler, 1987). Evidence of recent (Konzett *et al.*, 1998; Hawkesworth *et al.*, 1990), as well as ancient metasomatic events (Simon *et al.*, 2003a; Richardson *et al.*, 1984) have been identified within various mantle studies of the Kaapvaal craton. Similarly, isotopic signatures of group I kimberlites are consistent with recent metasomatic enrichment of their sources, whereas the isotopic signatures of group II kimberlites suggest ancient enrichment (Coe, 2004; Tainton, 1992; Fraser *et al.*, 1985/86; Smith 1983a).

8.8.1 Depletion of the source region

Close-to-primary magmas of group I, group II and transitional kimberlites all have high Mg-numbers (Mg # = 0.80-0.89) and compatible trace element concentrations (e.g. 650-1400 ppm Ni) that suggest equilibration with residual olivine of Fo_{92-96}, having greater than 2000ppm Ni (Figure 8.16; with K_D^{Fe-Mg} = 0.34-0.36 from Hertzberg & O'Hara, 2002; D_{Ni} from Beattie *et al.*, 1991). Calculated compositions of residual olivine in equilibrium with close-to-primary kimberlites are more similar to diamond inclusion olivines than to olivine from Kaapvaal peridotite xenoliths (Figure 8.16). All kimberlite varieties have low Al_2O_3 and Sc concentrations as well as relative depletion in the heavy REE and fractionated heavy REE patterns, indicative of the role of residual garnet and suggest derivation from previously depleted mantle source regions (Tainton & McKenzie, 1994).

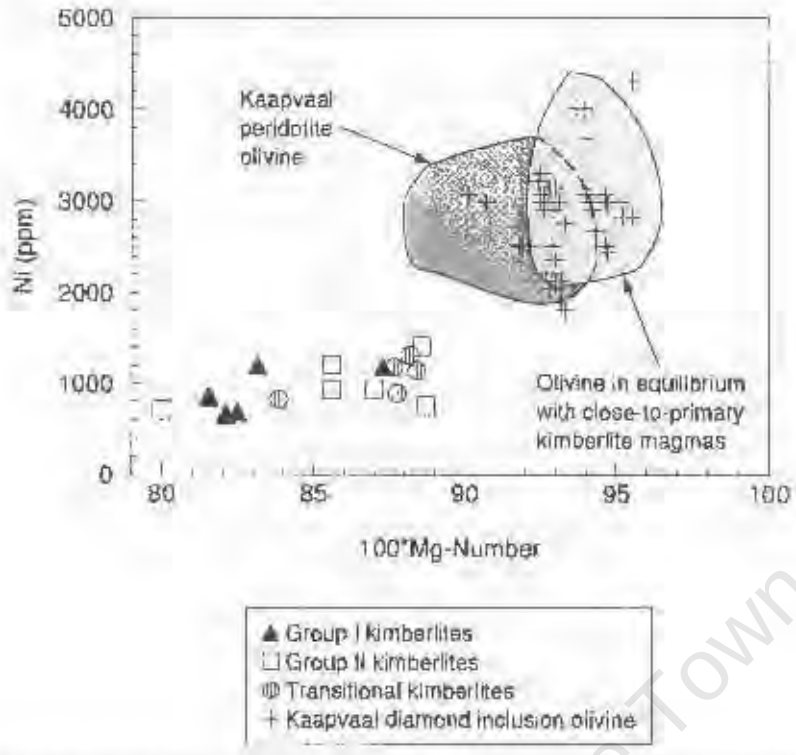

Figure 8.16: Ni content of close-to-primary group I, group II and transitional kimberlite magmas. Light shaded field represents the calculated composition of residual olivine in equilibrium with the kimberlites. Analyses of olivine inclusions from Kaapvaal diamonds (Phillips *et al.*, 2004; McKenna, 2001; Westerlund, 2000; McDade & Harris, 1999; Viljoen *et al.*, 1999) are shown, as well as the field of refractory olivine from Kaapvaal peridotite xenoliths (Gregoire *et al.*, 2003; Menzies, 2001; Mofokeng, 1998; Griffin *et al.*, 1989). Residual olivine compositions are calculated with $K_D^{Fe\text{-}Mg}$ = 0.34-0.36 from Hertzberg and O'Hara (2002) and D_{Ni} from Beattie *et al.* (1991).

Geochemical studies of peridotite xenoliths from the Kaapvaal craton and surrounding Proterozoic mantle have recognised that the subcontinental lithospheric mantle beneath southern Africa has a depleted or infertile character, deficient in Fe, Ca and Al in comparison to oceanic mantle, although the Archean mantle is more refractory than the younger Proterozoic mantle (Boyd *et al.*, 2004; Boyd & Mertzman, 1987; Boyd & McCallister, 1976). This lithospheric mantle is thought to have been depleted by ancient melting events such as komatiite extraction (Parman *et al.*, 2004; Walter, 1998). Given the initial depleted character of kimberlite sources, le Roex *et al.* (2003) and Tainton and McKenzie (1994) have argued that they are more likely to be located within the subcontinental lithosphere, since the convecting asthenosphere would be not be expected to preserve these heterogeneities over millions of years.

8.8.2 Enrichment of the source region

Calculated sources compositions of group I and group II kimberlites are all enriched in the light REE and other incompatible elements and are consistent with previous metasomatism. The incompatible element enriched metasomatising melt/fluid is postulated to have been characterised by a relative depletion in Rb, K, Tl and Sr, possibly due to the early crystallisation of phlogopite ± calcite, that was subsequently transferred to the source regions of group I, group II and transitional kimberlites (Coe, 2004; Harris *et al.*, 2004; le Roex *et al.*, 2003; Wyllie, 1980). Other differences between sources of

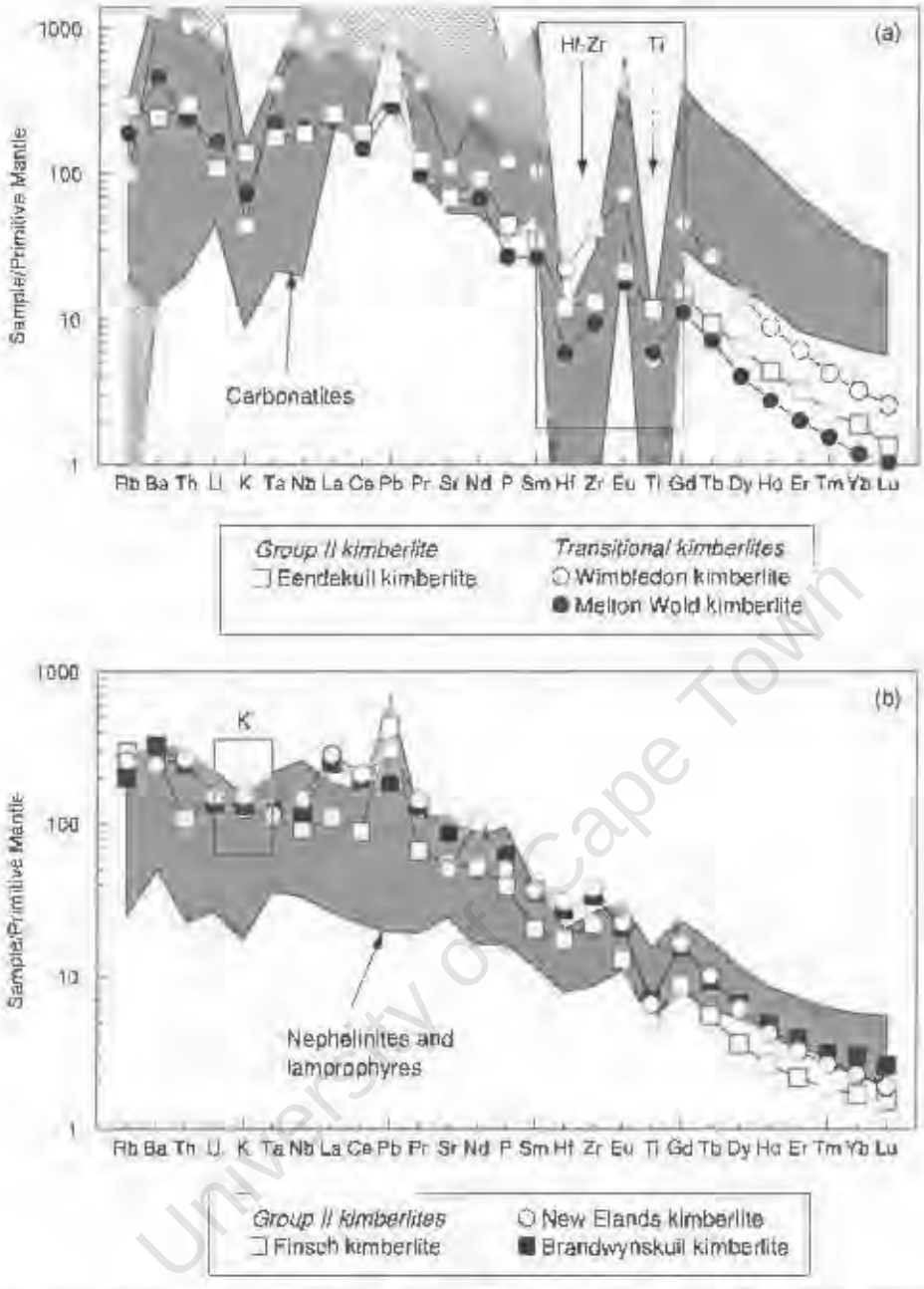

Figure 8.17: Primitive mantle normalised diagrams of (a) kimberlites characteristically depleted in the HFS elements similarly to carbonatites (although not likely to be pure liquid compositions), shown here as a proxy for carbonate metasomatism (Bizimis *et al.*, 2003; le Roex & Lanyon, 1998) (b) kimberlites showing characteristic enrichment in the alkalis as well as the lack of large negative Zr-Hf and Ti anomalies similarly to nephelinites and lamprophyres, shown here as a proxy for alkali metasomatism (Yang *et al.*, 2003; le Roex & Lanyon, 1998; Clague *et al.*, 1990; Clague & Frey, 1982). Primitive mantle normalising values are from Sun and McDonough (1989).

kimberlite varieties, for example the relative depletion of group II kimberlite source regions in Nb and Ta, are also thought to be features of the metasomatic melt/fluid.

Comparison of close-to-primary kimberlite magmas with carbonatites and other alkaline magmas show characteristic differences and similarities, suggesting that kimberlite source regions have been metasomatised by melts/fluids that are either carbonate or alkaline in character, or possibly of some

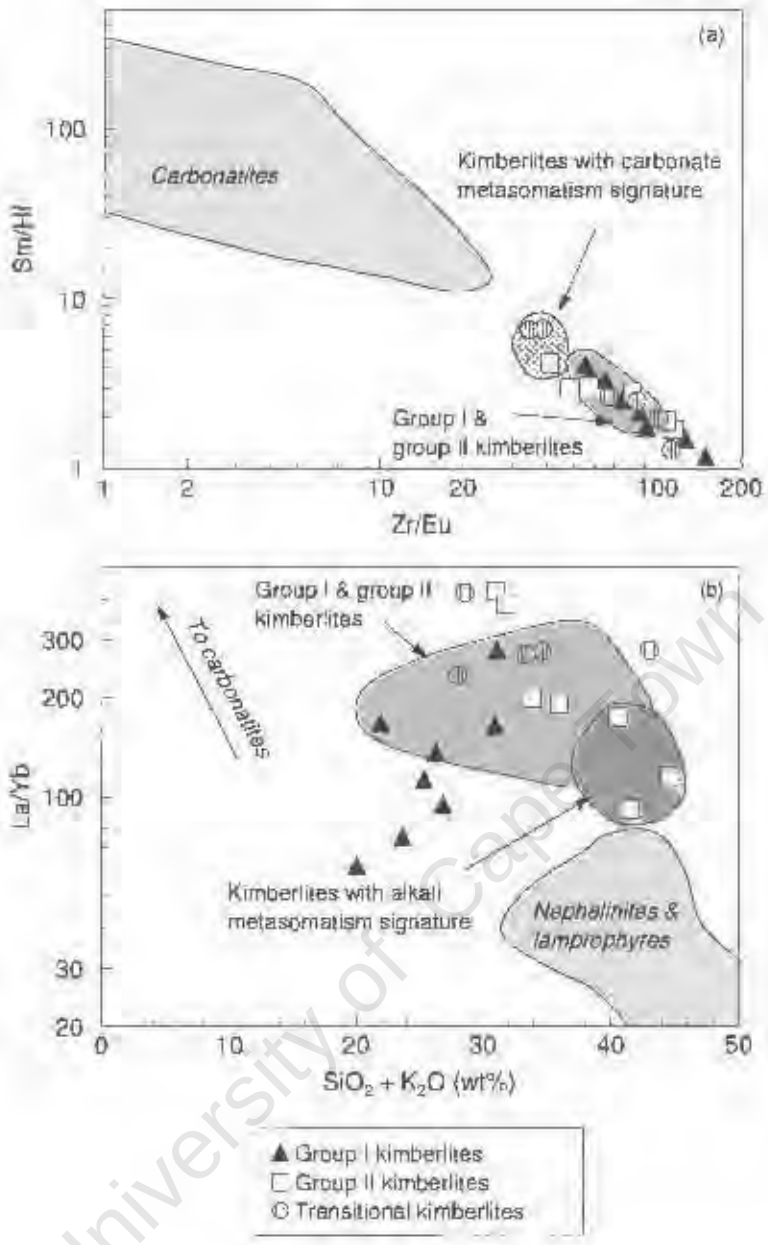

Figure 8.18: Identification of (a) the alkali and (b) the carbonate metasomatism signature in group I, group II and transitional kimberlites. Shaded fields represent group I and group II kimberlites (Coe, 2004; Harris *et al.*, 2004; le Roex *et al.*, 2003), carbonatites (Bizimis *et al.*, 2003; le Roex & Lanyon, 1998; Simonetti *et al.*, 1997), as well as nephelinites and lamprophyres (Yang *et al.*, 2003; le Roex & Lanyon, 1998; Clague *et al.*, 1990; Clague & Frey, 1982).

intermediate composition depending on the CO_2/H_2O ratio. In particular, the close-to-primary group II kimberlite magmas show similarities with nephelinites and lamprophyres, whereas the group II Eendekuil and transitional Melton Wold and Wimbledon kimberlites show many similarities to carbonatites (Figure 8.17). Carbonate metasomatism has been recognised in both continental and oceanic environments (e.g. Xu *et al.*, 2003; Dawson, 1999; Hauri *et al.*, 1993; Rudnick *et al.*, 1993) and is consistent with experimental evidence that suggests escaping carbonate melts may metasomatise the lithosphere (Yaxley & Brey, 2004; Green & Wallace, 1988). Similarly, alkali metasomatism has also been well-documented in continental and oceanic environments (Neumann & Wulff-Pedersen, 1997; Harte, 1983; Frey & Prinz, 1978; Frey & Green, 1974).

Carbonatites are characterised by depletion in alkali elements and HFS elements and are generally strongly light REE enriched (Nelson *et al.*, 1988). Rudnick *et al.* (1993) inferred high La/Yb, Ca/Al, Zr/Hf and low La/Nb, Ti/Eu as characteristics of the carbonatite melt which metasomatised xenoliths from Tanzania. The Melton Wold, Wimbledon and Eendekuil kimberlites are characterised by large negative Zr and Hf anomalies, as well as negative Ti anomalies on primitive mantle normalised diagrams (low Zr/Eu and high Sm/Hf; Figure 8.17a, 8.18a), suggesting possible carbonate metasomatism of their sources. In contrast, alkali metasomatism is characterised by high SiO_2, K_2O and Na_2O with lower La/Yb ratios and no large negative Ti and Zr anomalies on primitive mantle normalised diagrams (Coltorti *et al.*, 2000), features similar to the group II Finsch, New Elands and Brandewynskuil kimberlites (Figure 8.17b, 8.18b). Calculated sources of group IIb kimberlites however, show very distinct depletion in Rb, K and Ti more similar to group I kimberlites, suggesting metasomatism by a melt/fluid which had previously fractionated phlogopite.

8.8.3 Age of enrichment

Group I kimberlites are characterised by isotope signatures depleted relative to present day Bulk Earth and minimum Nd model ages calculated with respect to CHUR, suggest recent enrichment of their source regions, possibly just prior to the Jurassic-Cretaceous activity of group I kimberlites (Figure 8.19; Smith, 1983a). However, model ages relative to CHUR of some group I kimberlites (Goedehoop, Hebron and Klipsgatsfontein kimberlites) are younger than the age of kimberlite intrusion and indicate that CHUR may not be a suitable model for their source. Model ages of group I kimberlites calculated with respect to Depleted Mantle are significantly older (500-700Ma; Figure 8.19). It is therefore likely that the source regions of group I kimberlites had a character intermediate between Depleted Mantle and CHUR, with metasomatic enrichment event at some time less than 700Ma ago.

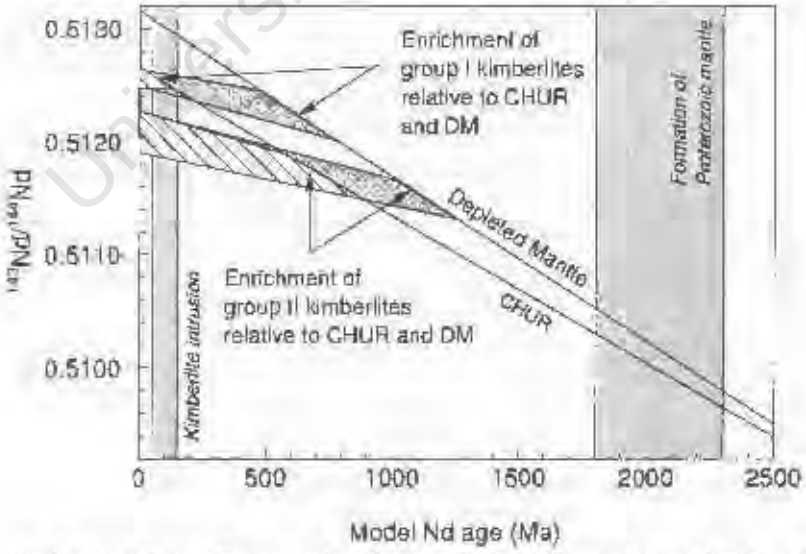

Figure 8.19: Minimum Nd model ages for group I and group II kimberlites calculated relative to Depleted Mantle (DM) and CHUR. Minimum Nd model ages of transitional kimberlites are not shown, but are intermediate to those illustrated for group I and group II kimberlites. Shaded fields represent the period of Jurassic to Cretaceous kimberlite intrusion in South Africa and the Re depletion model ages of off-craton peridotite xenoliths from the Namaqua-Natal belt (Janney *et al.*, 1999; Pearson *et al.*, 1998). Present day $^{143}Nd/^{144}Nd$ = 0.512638 and $^{147}Sm/^{144}Nd$ = 0.1966 for CHUR, whereas present day $^{143}Nd/^{144}Nd$ = 0.51315 and $^{147}Sm/^{144}Nd$ = 0.222 for depleted mantle. $^{147}Sm/^{144}Nd$ ratios of sources are derived using REE contents of calculated kimberlite sources.

Group II kimberlites are characterised by high time integrated Rb/Sr and Sm/Nd ratios indicative of ancient light REE source region enrichment (Coe, 2004; Tainton, 1992; Fraser *et al.*, 1985/86; Smith, 1983a). Calculated model ages of group II kimberlites suggest enrichment of their sources 600-900Ma ago relative to CHUR, or 1000-1300Ma ago relative to Depleted Mantle (Figure 8.19), but most importantly, indicate that the source regions of group II kimberlites were metasomatically enriched at an earlier time than group I kimberlites. It is noteworthy that according to the calculated minimum model Nd ages, sources of both on- and off-craton group II kimberlites were enriched after the formation of the mantle lithosphere underlying the Proterozoic Namaqua-Natal mobile belt (1.8-2.3Ga, Figure 8.19; Janney *et al.*, 1999; Pearson *et al.*, 1998) and prior to Gondwana breakup (180-130Ma; Storey, 1995). Calculated model ages of transitional kimberlites are intermediate to the age of enrichment for group I and group II kimberlite sources and are consistent with the interpretation that transitional kimberlites represent mixed source regions.

8.9 Geodynamics of kimberlite petrogenesis

8.9.1 Location of kimberlite source regions: Subcontinental lithosphere or asthenosphere

Isotope studies of kimberlites have provided the most substantial evidence in constraining the location of kimberlite source regions (e.g. Smith, 1983a). Since group I kimberlites have unradiogenic Sr and radiogenic Nd isotope ratios, similar to Depleted Mantle as well as OIB (Figure 8.20), their sources are likely to contain an asthenospheric component. Group II kimberlites however, have radiogenic Sr and unradiogenic Nd ratios (Figure 8.20), that require ancient enrichment of the source regions and subsequent isolation from the convecting mantle (Smith, 1983a) in which to develop their more extreme isotopic compositions. Consequently, the sources of group II kimberlites are inferred to be located in the subcontinental lithospheric mantle (Coe, 2004; Tainton, 1992; Fraser & Hawkesworth, 1992; Smith, 1983a). Karoo flood basalts have similar isotopic signatures to group II kimberlites, that also require ancient light REE enriched sources and are postulated to be located within the subcontinental lithospheric mantle (Hawkesworth *et al.*, 1984), perhaps suggesting that they share common source regions.

Trace element geochemistry can also provide insight into the origin of group I and group II kimberlites especially with incompatible trace element ratios that illustrate source characteristics. le Roex (1986) showed the relationship of group I kimberlites to the Bouvet and Marion ocean island basalts, according to the similarities in Sr and Pb isotopes, as well as various trace element ratios (Zr/Nb, Ba/Nb, La/Nb). Group II kimberlites were also argued to shown an affinity towards OIB similar to Tristan, Gough and Discovery (le Roex, 1986). More recently, both le Roex *et al.* (2003) and Harris *et al.* (2004) have shown the correspondence of diagnostic group I kimberlite trace element ratios to MORB and OIB (Nb/U = 47± 10; Ce/Pb = 25 ± 5; Hofmann *et al.*, 1986). These authors argued that the OIB trace element and isotopic character of the group I Kimberley and Uintjiesberg kimberlites was due to the upward percolation of plume melts/fluids that subsequently metasomatised the overlying lithospheric mantle. It was further shown that the age of intrusion of the Uintjiesberg kimberlite

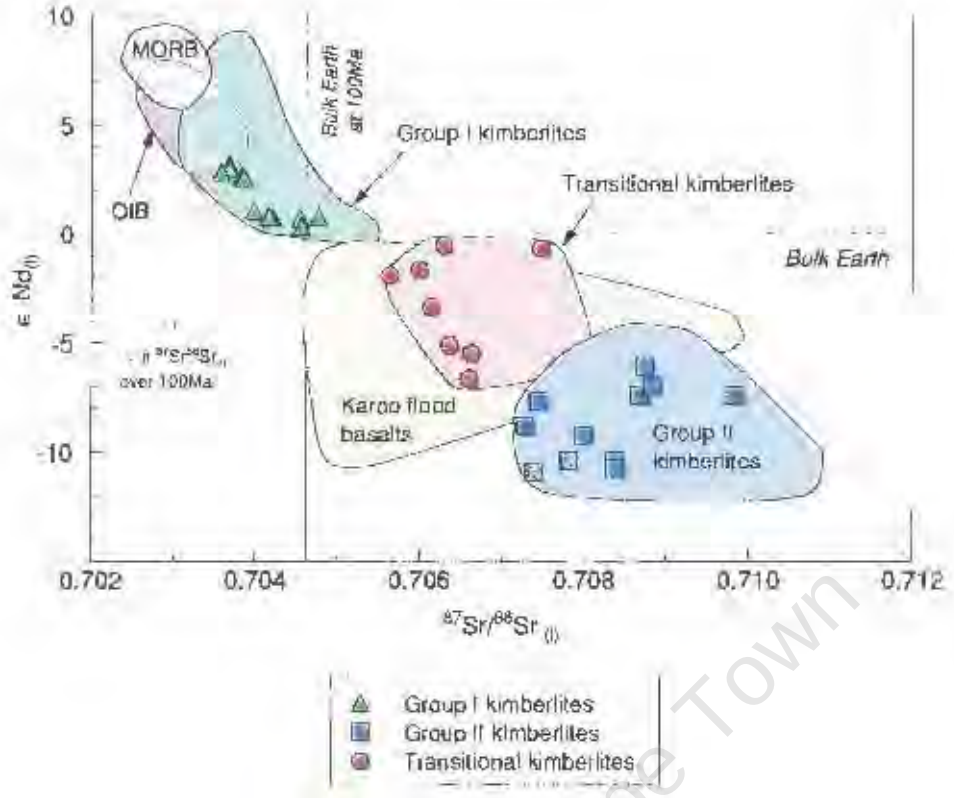

Figure 8.20: Variation of the initial εNd and $^{87}Sr/^{86}Sr$ isotope ratios for group I, group II and transitional kimberlites. Symbols for the group II kimberlites include analyses from the Finsch and New Elands kimberlites (Fraser & Hawkesworth 1992; Smith, 1983a). Initial isotope ratios are calculated according to the age/inferred age of intrusion and two-sigma errors of isotope ratios are less than the symbol size. Labelled shaded fields represent the respective kimberlite groups as well as other southern African kimberlites (Coe, 2004; Nowell *et al.*, 2004; Nowell *et al.*, 1999; Clark, 1994; Fraser & Hawkesworth, 1992; Lainton, 1992; Smith, 1983a). Compositional fields for MORB (Kurz *et al.*, 1998; Mahoney *et al.*, 1992; le Roex *et al.*, 1989), OIB (Douglass *et al.*, 1999; Mahoney *et al.*, 1992; Hart, 1988; O'Nions *et al.*, 1977; O'Nions & Pankhurst, 1974) and Karoo continental flood basalts (Hawkesworth *et al.*, 1984) are also shown for comparison.

correlated well with the paleo-track of the Shona plume and therefore the subcontinental lithospheric hosted source region of the Uintjiesberg kimberlite was most likely metasomatised by upward rising melts/fluids associated with the passage the continental lithosphere over the Shona mantle plume (Harris *et al.*, 2004). However, only the paleo-tracks of the Shona and Bouvet mantle plumes pass over southern Africa and may possibly have interacted with the subcontinental lithosphere. The paleo-track of the Tristan plume is too far north and is unlikely to have influenced kimberlite source regions (le Roex, 1986; Hartnady & le Roex, 1985).

Group I kimberlites in this study not only have Ce/Pb and Nb/U ratios similar to OIB and MORB but also Ba/Nb, La/Nb, Th/Nb and Ba/Th ratios (Figure 8.21) and thus, the lithospheric hosted sources of group I kimberlites are interpreted to show the influence of metasomatism by plume-related melts/fluids. Incompatible element ratios of group II kimberlites are different to OIB since Nb/U = 47± 10 and Ce/Pb < 25 ± 5 (Hofmann *et al.*, 1986) whereas La/Nb, Ba/Nb, Ba/Th and ThNb ratios are all greater than the ratios of OIB (Figure 8.21). Diagnostic ratios of group II kimberlites however, show good overlap with those of the Karoo flood basalts (Figure 8.21), since both rock types are depleted in

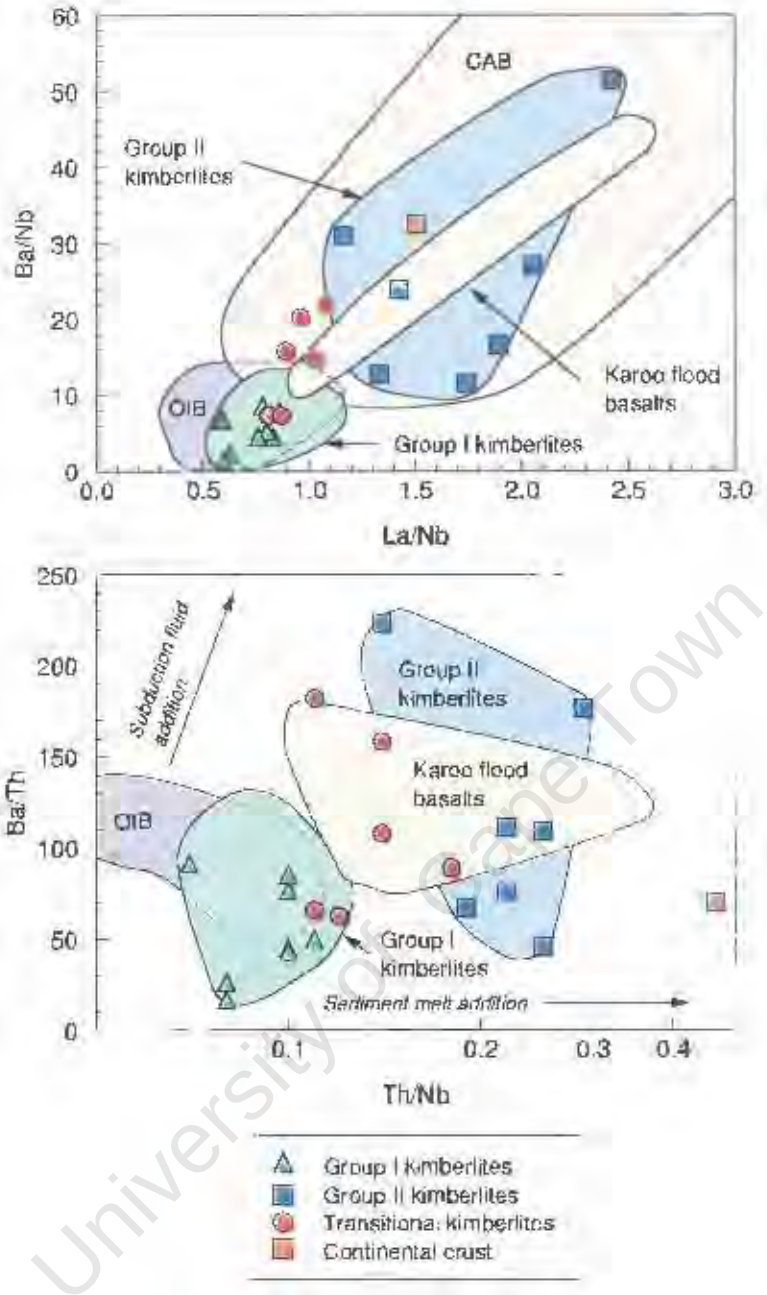

Figure 8.21: Variation of selected incompatible trace element ratios for the close-to-primary magmas of group I, group II and transitional kimberlites. Shaded fields represent group I kimberlites (Harris *et al.*, 2004; le Roex *et al.*, 2003), group II kimberlites (Coe, 2004), Karoo flood basalts (Marsh *et al.*, 1997), ocean island basalts (compilation from PetDB,) and calc-alkaline basalts (compilation from PetDB). Average continental crust is from Rudnick and Fountain (1995). See text for further explanation.

in Nb and hence are characterised by high Ba/Nb, La/Nb and Th/Nb ratios, suggesting the same processes have affected the source regions of group II kimberlites and Karoo flood basalts. Depletion in Nb and other HFS elements is considered a classic subduction zone signature of calc-alkaline basalts (CAB, e.g. Woodhead *et al.*, 1998), and since group II kimberlites and Karoo basalts have similar incompatible element ratios to CAB, it suggests that they too, have interacted with a subduction component (Figure 8.21). Although it cannot be resolved whether a subduction fluid or sediment melt (high Ba/Th and high Th/Nb, respectively, Figure 8.21b; le Roux *et al.*, 2002; Woodhead *et al.*, 1998;

Elliott *et al.*, 1997) has metasomatised the source regions of group II kimberlites (and Karoo basalts), since group II kimberlites trend to both high Ba/Th and Th/Nb ratios, it is still evident that enrichment by a subduction component has taken place. This is consistent with the model of Helmstaedt and Gurney (1984) who suggested that the sources of kimberlites were metasomatised by volatiles squeezed off the subducted slab. The similarity of Karoo basalts to calk-alkaline basalts is not a new concept either, since the depletion of Nb and Ta as well as Ti and the possibility that the Karoo basalt source may have been metasomatised by a subduction zone component has previously been commented upon Duncan (1987) and Duncan *et al.* (1984).

The source regions of group II kimberlites are inferred to be located within the subcontinental lithospheric mantle, isolated over millions of years and where their extreme isotopic characteristics and compositional heterogeneities were preserved. McKenzie and O'Nions (1983) have argued that the sources of mantle plumes may be delaminated subcontinental lithosphere, but this is not thought to be the case for source regions of group II kimberlites, since no OIB within the South Atlantic or South Indian Oceans show depletion in Nb or isotopic signatures similar to group II kimberlites (Weaver, 1991; Hart, 1988). Although the Tristan, Gough and Discovery OIB have high Ba/Nb ratios similar to group II kimberlites, this is a feature of high Ba in EM-1 OIB, thought to reflect a sediment subduction component in the mantle plume rather than depletion in Nb (Weaver, 1991; Sun & McDonough, 1986).

8.9.2 Significance of varying characteristics between on- and off-craton kimberlites

In Chapter 7, different trends in the geochemistry between on- and off-craton kimberlites were identified and now it will be assessed whether any of these similarities or differences can be placed into a geodynamic perspective, in relation to characteristics of inferred garnet lherzolite source regions. Firstly, the need for residual garnet in on- and off-craton source regions has already been mentioned (Section 8.7.2) and indicates that off-craton kimberlites are not derived from within the spinel stability field, but rather from the garnet stability field, similarly to on-craton kimberlites. The absence of any significant differences between on- and off-craton group II kimberlites suggests that both Proterozoic and Archean mantle sources have experienced similar evolutionary histories. Differences between on- and off-craton transitional kimberlites however, are more likely to be functions of the varying characteristics between the sources of group I and group II kimberlites (Section 8.7.1).

It has been noted that off-craton group I kimberlites tend to fall towards the low SiO_2 and MgO, but high FeO*, TiO_2, CaO and CO_2 ends of the compositional fields of their on-craton counterparts, although still generally falling within the range of on-craton group I kimberlites (Section 7.2). Variations in these oxides are potentially controlled by the following parameters:

(i). Degree of depletion: Off-craton peridotite xenoliths are generally more fertile have not been depleted in basaltic components FeO, CaO, Al_2O_3 and TiO_2, as much as refractory peridotites from the Kaapvaal craton (Boyd *et al.*, 2004; Janney *et al.*, 2001; Boyd & McAllister, 1976).

(ii). Pressure and depth of melting: As the depth/pressure of melting decreases, melts become progressively more SiO_2, MgO-poor but more FeO, Al_2O_3 and CaO-rich (e.g. Dalton & Presnall, 1998b; Hertzberg, 1992). Similarly, the partition coefficient for Ti is pressure dependent and increases with decreasing pressure (Adam & Green, 1994).

(iii). Degree of melting: Melts become progressively richer in SiO_2 and MgO as the degree of melting increases (e.g. Dalton & Presnall, 1998a; Hertzberg, 1992).

It is considered here that a combination of the first two parameters is most likely the cause of the variations in on- and off-craton group I kimberlite geochemistry. Recognising that on-craton group I kimberlites are likely to be derived from variably depleted sources within a range of pressures (hence the broad ranges in on-craton compositional fields), it appears that off-craton kimberlites may be derived from the less depleted sources, with melting taking place at lower pressures. Therefore it would still be possible for on- and off-craton kimberlites to be derived from similarly depleted sources at equivalent pressures, but only if the source regions are not very depleted and melting takes place within the lower pressure range. This is consistent with the experimental study of Gudfinnsson and Presnall (2003) who showed that the lower MgO, but higher CaO and CO_2 contents of an average off-craton group I kimberlite composition, are due to melting at lower pressures (~5-6GPa) than for an average on-craton group I kimberlite (~10GPa). The more SiO_2 and MgO-rich character of on-craton kimberlites is unlikely to be related to higher degrees of melting in comparison to off-craton kimberlites, since the reverse has been shown with La/Yb and Gd/Yb ratios in Section 8.7.3.

8.9.3 Significance of varying characteristics between group I and group II kimberlites

Significant similarities and differences in geochemical characteristics between the calculated sources of group I and group II kimberlites can also potentially relate to varying geodynamical processes. Group II kimberlites in particular, tend towards higher SiO_2 and K_2O, but lower TiO_2 than group I kimberlites. Consistent with the potassic nature of group II kimberlites, is their greater enrichment in the LIL elements and Pb, as well as their more radiogenic $^{87}Sr/^{86}Sr$ character, in comparison to group I kimberlites. The former also tend to be more light REE enriched with lower $^{143}Nd/^{144}Nd$ ratios and higher La/Sm, but lower Gd/Yb ratio than the latter, characteristics that have been shown to be likely related to mineralogical differences in their sources and not partial melting effects (Section 8.7.2). Both group I and group II kimberlites have similar $CaO/(CaO + Al_2O_3)$ ratios, suggesting segregation from similar pressures or depths (Sweeney & Winter, 1999; Hertzberg, 1992). Consequently, the role of metasomatism in causing these varying geochemical characteristics between source regions is investigated.

Metasomatised peridotites entrained by kimberlites show evidence for progressive metasomatism with the more highly metasomatised peridotites having a greater modal proportion of metasomatic phlogopite, ± K-richterite, but with lower proportions of garnet (Waters & Erlank, 1988; Erlank *et al.*, 1987). Textural and geochemical evidence indicates that not only has metasomatic phlogopite grown at the expense of garnet, but so has clinopyroxene and Cr-spinel (Gregoire *et al.*, 2003; Simon *et al.*, 2003b; van Achterberg *et al.*, 2001; Erlank *et al.*, 1987). These metasomatic reactions are consistent

with the argument that varying REE ratios between kimberlite varieties and the more Si, K and LIL-element enriched character of group II kimberlites, are due to their sources having more clinopyroxene and phlogopite formed by metasomatism at the expense of garnet, than those of group I kimberlites. Therefore, the mantle sources of group II kimberlites can be considered to be more highly metasomatised than group I kimberlites, although it must be emphasised that even though there may be more phlogopite present in the former, this phase is thought to be entirely consumed during partial melting.

Group II kimberlites also have lower absolute TiO_2 concentrations with larger negative Ti anomalies than group I kimberlites, consistent with the interpretation that the source regions of group II kimberlites have been metasomatised by a subduction zone fluid/melt depleted in Nb, Ta and Ti. It is of interest to note that Gregoire *et al.* (2003) identified two different geochemical signatures in clinopyroxenes from metasomatised xenoliths from the Kaapvaal craton, with both types of clinopyroxene showing enrichment in the light REE and LIL elements, and depletion in Ti, Nb and Ta. However, one of the types of clinopyroxene is more light REE enriched and shows a greater relative depletion in Nb and Ta than the other, leading Gregoire *et al.* (2003) to suggest a possible genetic relationship of the two types of clinopyroxenes with group I and group II kimberlites.

Since it has been argued that the source regions of group II kimberlites are more highly metasomatised than those of group I kimberlites, perhaps a more exotic source mineralogy, corresponding to the "clinopyroxene and mica rich-vein" model of Foley (1992b) might be plausible instead of a metasomatised garnet lherzolite. The main arguments behind the model of Foley (1992b) is that the sources of ultrapotassic rocks are completely free of olivine, due to the absence of olivine as a liquidus phase in various experimental studies (e.g. Girnis *et al.*, 1995; Foley, 1992a) and that the resulting magmas are hybrids of vein and wall rock components. Foley (1992b) suggests that, if for example, the unmelted mineralogy of the source region comprises veins of clinopyroxene, phlogopite with other accessory phases (e.g. apatite, spinel, rutile), and the wall rock of olivine, orthopyroxene, clinopyroxene and garnet, then the first stages of melting would be confined to the metasomatic veins. At some high degree of vein melting, the melt would start interacting with the wall rock consuming clinopyroxene and garnet and the resulting liquid would be a hybrid of vein and wall rock components.

In order to evaluate Foley's (1992b) suggestions, the source composition of the close-to-primary group II Markt kimberlite magma has been calculated assuming partial melting of a clinopyroxene - phlogopite vein, with no melt - wall rock interaction. Given that the vein is predominantly composed of hydrous metasomatic minerals with low melting temperatures, large degrees of melting with minimal wall rock interaction would be expected. The Markt kimberlite source region, calculated for 20% vein melting, is very enriched in the light REE (230 times chondrite) with a composition intermediate to the actual kimberlite and that of hypothetical vein (Figure 8.22). The composition of this hypothetical vein comprising 50% clinopyroxene and 50% phlogopite, was calculated using analyses of metasomatised

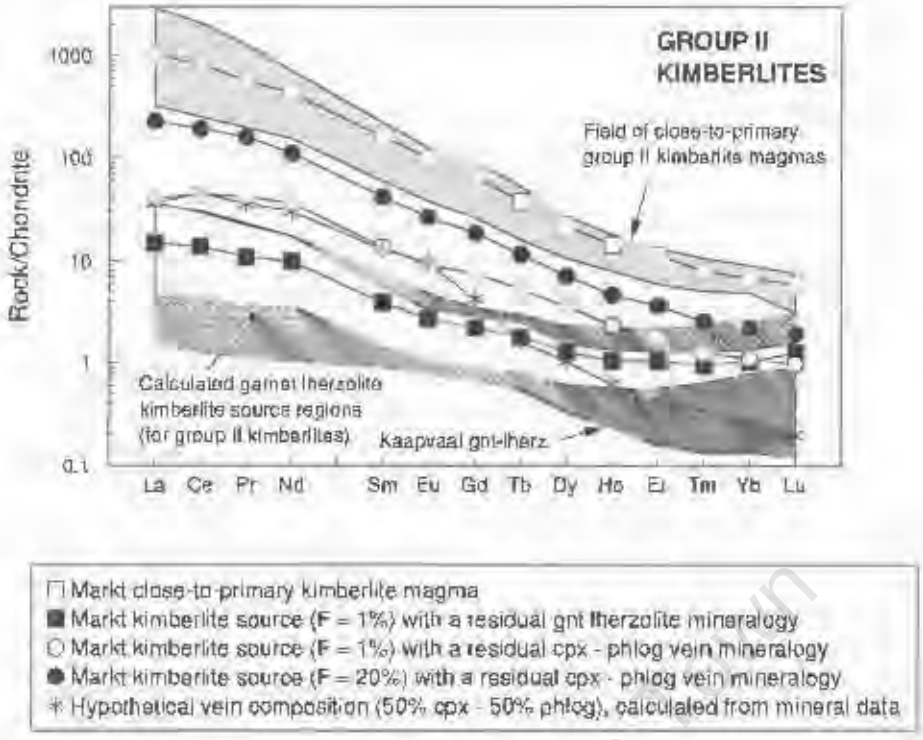

Figure 8.22: Predicted REE source compositions of the group II Markt kimberlite calculated by semi-quantitative forward modelling for 1% and 20% partial melting of a metasomatic vein (50% clinopyroxene and 50% phlogopite). The preferred Markt kimberlite source, calculated in Section 8.7.3 is also illustrated, as well as the composition of a hypothetical vein (50% clinopyroxene and 50% phlogopite), calculated using mineral analyses from Gregoire *et al.* (2003). Partition coefficients are from Table 8.3 except for D_{Phlog}, which is interpreted from Gregoire *et al.* (2003) and La Tourette *et al.* (1995). Dark shaded field represents garnet lherzolites from the Kaapvaal craton (Gregoire *et al.*, 2003). Chondrite normalising values are from Sun and McDonough (1989).

minerals from Gregoire *et al.* (2003), in order to better constrain the degree of vein melting. Only when the kimberlite source is calculated for 1% vein melting does it resemble the composition of the hypothetical clinopyroxene - phlogopite vein, in its light REE concentrations (Figure 8.22). The refractory characteristics of the kimberlite are also transferred to the vein and consequently, chondrite normalised patterns of the vein are steep with low heavy REE concentrations suggesting that the original source of the melt/fluid forming the metasomatic vein contained residual garnet.

It has been argued earlier that various lines of evidence indicate the necessity that group II kimberlites were in equilibrium with olivine at some stage during their petrogenesis, namely the high Mg-numbers and concentrations of compatible elements Ni and Cr in close-to-primary magmas. Similarly, Re-Os isotopes and Os population studies imply that group II kimberlites are derived from melting of olivine-rich sources (Pearson *et al.*, 2003; Pearson *et al.*, 1995). This would suggest that either the precursor vein was derived from partial melting of a refractory source, or that considerable wall rock interaction took place during vein melting, giving the kimberlites their refractory character. Since the calculated source only resembles the hypothetical vein at very low degrees of melting (F = 1%, Figure 8.22), minimal wall rock interaction would have taken place and therefore the refractory character of the vein would more likely be a feature inherited from its metasomatic precursor. In addition, it is hard to

envisage that kimberlites could be derived from only 1% partial melting of a metasomatic vein (assuming the composition of the hypothetical vein is representative).

However, accepting that metasomatic veins do occur within the mantle (e.g. Erlank *et al.*, 1987), garnet lherzolites entrained by kimberlites have also been extensively documented (e.g. Gregoire *et al.*, 2003; Erlank *et al.*, 1987; Boyd & Mertzman, 1987) and begs the question of why more exotic sources would be required, when it has been argued than group II kimberlites can be produced by partial melting of metasomatised garnet lherzolite sources. Secondly, the semi-quantitative modelling method used in this study is based on the residual mineralogy that the kimberlite is in equilibrium with at the time of melt segregation (e.g. metasomatised garnet lherzolite), not the mineralogy of the source region at the initiation of melting (e.g. vein mineralogy, since only at some higher degree of partial melting would the melt start interacting with the more refractory wall rock). Since the modelling technique used is unable to discriminate to this level of detail, it is still argued that group II kimberlite magmas were derived from partial melting of garnet lherzolites characterised by disseminated metasomatism.

Key differences between the sources of group I and group II kimberlites therefore appear to be related to the timing and degree of enrichment as well as the source of the metasomatising melts/fluids, since both source regions have been previously depleted and subsequently enriched. Karoo continental flood basalts and group II kimberlites are similar in some geochemical characteristics such as the depletion in Nb, Ta and Ti, and enriched isotope signatures (Duncan *et al.*, 1984; Hawkesworth *et al.*, 1984), suggesting they may have been derived from common source regions located within the subcontinental lithosphere. The relative depletion of Nb in group II kimberlites and Karoo basalts is inferred here to have been caused by the metasomatism of source regions by melts/fluids derived from a subduction zone. Minimum Nd model ages of on- and off-craton group II kimberlites suggest ancient light REE enrichment, prior to Mesozoic Gondwana break-up and after the formation of the Proterozoic mantle underlying the Namaqua-Natal belt. Since no differences have been recognised between the isotopic signatures of these kimberlites (Section 7.2), both Archean and Proterozoic kimberlite source regions must have been enriched by the same metasomatic event. During subduction, melts or fluids released from the subducted slab typically percolate upwards into the overlaying mantle wedge. Simple geometry indicates that only if multiple subduction and accretion events occurred during the 1.2-1.0Ga formation and metamorphism (Thomas *et al.*, 1994) of the Namaqua-Natal belt, similar to that imaged by the Lithoprobe study in Canada (e.g. Cook *et al.*, 1999), would the upward percolating melts/fluids have affected both Proterozoic and Archean mantle source regions.

It is postulated that after the massive outpouring of greater than 140000km^2 (present day aerial exposure, Eales *et al.*, 1984) of Karoo continental flood basalts at 180Ma (Marsh *et al.*, 1997), and the eruption of group II kimberlites from 200-110Ma (Allsopp, 1989; Allsopp Unpubl. in Skinner, 1989), the more highly metasomatised source appears to have been largely exhausted. Therefore, on- and off-

craton group I kimberlites in this study erupted from ~110-70Ma (Smith *et al.*, 1994; Smith *et al.*, 1985b) were derived from the more recently (Mesozoic) and less enriched lithosphere carrying a plume signature. Similarly, the off-craton group I East Griqualand kimberlites erupted at ~150Ma (Smith *et al.*, 1985; Davis, 1977) have geochemical characteristics in common with OIB, that may likely have been derived from melts/fluids associated with the Bouvet mantle plume that was underlying East Griqualand at this time (le Roex, 1986). However, the formation of group II kimberlites is not in anyway a prerequisite for the formation of group I kimberlites, since group I kimberlites exist that are significantly older than group II kimberlites (e.g. Proterozoic Kuruman kimberlites; Bristow *et al.*, 1986). In addition, although the geochemistry of group II kimberlites shows no evidence for a plume component, it does not preclude the possibility that the Mesozoic mantle plumes associated with Gondwana break-up, may have provided a heat source for partial melting and production of group II kimberlites.

Transitional kimberlites appear to tap mixed group I and group II kimberlite sources and for the off-craton transitional kimberlites erupted at (~174-143Ma; Smith *et al.*, 1994), the group II kimberlite source signature appears to be more predominant (Section 7.2, 7.3). In contrast, for the on-craton transitional kimberlites erupted at ~92Ma (Davis, 1978), the group I kimberlite source signature appears to dominate (Section 7.2, 7.3). The on-craton Frank Smith kimberlite has also previously been termed transitional, since although it has a $^{143}Nd/^{144}Nd$ isotopic ratio only slightly lower than most group I kimberlites, it has a typical group II kimberlite age and petrography as well as a transitional megacryst assemblage (Bell & Mofokeng, 1998; Smith *et al.*, 1985a; Smith, 1983b; Wagner, 1914), suggesting that the petrogenetic processes giving rise to transitional kimberlites are not necessarily isolated in time and space. However, the transitional kimberlites that show the strongest group II kimberlite signature (e.g. off-craton transitional kimberlites) are older than the kimberlites that show a stronger affinity to group I kimberlites (e.g. Wimbledon and Leicester kimberlites). This observation is consistent with the eruption of group II kimberlites prior to group I kimberlites during the Jurassic and Cretaceous.

CHAPTER 9

SUMMARY

9.1 Overview

Eighteen Jurassic to Cretaceous South African kimberlites representative of group I, group II and transitional varieties, from both on-craton and off-craton tectonic environments were selected for study aimed at characterising their geochemistry and source region compositions, as well as understanding the petrogenetic processes that have affected them. The petrography and geochemistry of these kimberlites was described and characterised and the effects of alteration, crustal contamination, fractional crystallisation and macrocryst entrainment on the geochemistry of the close-to-primary kimberlite magmas evaluated. Subsequently, semi-quantitative modelling of inferred close-to-primary kimberlite magmas has been used to characterise the geochemistry of their respective source regions and to investigate the effect of degree of melting and residual mineralogy on predicted source compositions. Thereafter, the evolution of the kimberlite source regions was explored with reference to their physical location, nature of depletion and enrichment events, and extent of the contributions from lithospheric and asthenospheric sources. Finally, observed differences or similarities between kimberlite varieties and their source regions were placed in a geodynamical perspective.

9.2 Petrography

Hypabyssal kimberlite samples from group I, group II and transitional kimberlites analysed in this study are all variably macrocrystic (10-45 volume % macrocrysts), with olivine as the dominant macrocryst phase and lesser phlogopite, opaque oxides and garnet. Olivine macrocrysts are typically subhedral to anhedral in habit and variably serpentinised, whereas tabular phlogopite macrocrysts are often kink banded and deformed and show calcite stringers along cleavage planes. Similarly, olivine occurs as the dominant phenocryst phase in all kimberlite groups, whereas, phlogopite phenocrysts and microphenocrysts, rimmed by tetraferriphlogopite, are largely restricted to the group II and transitional kimberlites. Kimberlite varieties show essential differences in the nature of their groundmass phases, with group I kimberlites characterised by matrix serpentine and calcite, often occurring in well developed irregular shaped segregations, whereas group II kimberlites are characterised by stubby interlocking groundmass phlogopite lathes (rimmed by tetraferriphlogopite), with interstitial calcite, serpentine and minor diopside. Accessory opaque oxides and perovskite in the groundmass of group I kimberlites are generally fairly common and fine-grained (100-300μm), in comparison to group II kimberlites that are characterised by very fine-grained (20-50μm) rare opaque oxides and perovskite. Trace apatite needles have been recognised in all kimberlite varieties. Variations in petrography between on- and off-craton kimberlites are limited to the transitional kimberlite group, with on-craton transitional kimberlites showing greater similarity to group I kimberlites and off-craton transitional kimberlites, similarity to group II kimberlites.

9.3 Geochemistry of kimberlites

The analysed group I kimberlites tend to have lower SiO_2, but with roughly comparable MgO and FeO* concentrations (23.5-33.3 wt% SiO_2, 23.0-30.3 wt% MgO, 7.3-11.8 wt% FeO*) to group II kimberlites (25.2-43.0 wt% SiO_2, 10.1-36.2 wt% MgO, 6.4-10.7 wt% FeO*), and with the transitional kimberlites showing similarity to both group I and group II kimberlites. The majority of kimberlites also tend to have Mg-numbers greater than 0.80. Al_2O_3 contents are generally comparable, although some of the high Al_2O_3 concentrations (> 6 wt% Al_2O_3) recognised in a few group II and transitional kimberlites are likely due to crustal contamination. Group I kimberlites have higher TiO_2 (2.2-3.4 wt%) and lower K_2O (0.2-1.4 wt%) contents than group II kimberlites (0.6-3.1 wt% TiO_2, 0.5-4.0 wt% K_2O), with the transitional kimberlite group characterised by intermediate TiO_2 and K_2O. All three kimberlite varieties show good negative correlations between CaO and SiO_2, and positive correlations between CO_2 and CaO (e.g. 3.2-17.2 wt% CaO, up to 15.0 wt% CO_2). Differences in on- and off-craton kimberlite geochemistry have been identified for the group I kimberlites, with off-craton group I kimberlites tending to lower SiO_2, MgO, but higher FeO*, TiO_2, CaO and CO_2 contents than on-craton kimberlites, although still broadly falling within the field of on-craton group I kimberlites. Similarly, on-craton and off-craton transitional kimberlites show more affinity to group I and group II kimberlites, respectively.

All kimberlites groups are enriched in the compatible elements (e.g. 300-1600ppm Ni, 500-2200ppm Cr), which show good positive correlations with MgO and Mg-number. All the analysed kimberlites are also highly enriched in the incompatible elements, with the more immobile elements showing good inter-element correlations. LIL element concentrations are variable (e.g. 10-210ppm Rb, 200-7700ppm Ba) and group II kimberlites tend to be more enriched in Rb, Ba and Pb than group I kimberlites. HFS element concentrations are generally comparable (e.g. 80-650ppm Zr), except for Nb and Ta, which are significantly depleted in the group II kimberlites (60-220ppm Nb), in comparison to group I and transitional kimberlites (100-520ppm Nb). Consequently, group II kimberlites are characterised by La/Nb > 1.1, Ba/Nb > 12, Th/Nb > 0.15, whereas values of these key ratios are lower for group I and transitional kimberlites. All three kimberlite groups are extremely enriched in the light REE and moderately enriched in the heavy REE relative to chondrite (La = 300-2200 and Lu = 2.2-8.5 times chondrite). Group II and transitional kimberlites tend to have higher absolute light REE concentrations with steeper light REE slopes (higher La/Sm), but flatter heavy REE slopes (lower Gd/Yb), than group I kimberlites. Off-craton group I kimberlites also tend to lower La/Sm, La/Yb and Gd/Yb in comparison to on-craton group I kimberlites.

Primitive mantle normalised patterns of the analysed kimberlites show steep negative profiles, upon which there are superimposed moderate negative K, Ti and Rb anomalies and more subdued negative Sr and Hf anomalies. Group II kimberlites also show subdued negative Nb and Ta ($(La/Nb)_N$ > 1.1), and positive Pb ($(Ce/Pb)_N$ < 0.9) anomalies. Magnitudes of anomalies are variable between kimberlite groups, with the group I, group IIb (a subset of enriched group II kimberlites characterised by very large negative Rb, K and Ti anomalies as well as low absolute K_2O contents (< 1.9 wt%), more similar to group I kimberlites) and on-craton transitional kimberlites showing the greatest relative depletion in

K (K/K* < 0.3). In contrast, group I kimberlites and off-craton transitional kimberlites show the least relative depletion in Ti (Ti/Ti* = 0.3-1.0), compared to other kimberlite groups (Ti/Ti* < 0.6). Some kimberlites are also characterised by large well-developed negative Zr and Hf anomalies (Melton Wold, Wimbledon and Eendekuil kimberlites).

Isotope ratios of the analysed group I kimberlites vary from $^{87}Sr/^{88}Sr_{(i)}$ = 0.7036-0.7048 and $^{143}Nd/^{144}Nd_{(i)}$ = 0.51249-0.51271, and show distinct similarity to ocean island basalts, with low Rb/Sr and high Sm/Nd ratios. Group II kimberlites are characterised by radiogenic $^{87}Sr/^{86}Sr_{(i)}$ =0.7074-0.7084 and unradiogenic $^{143}Nd/^{144}Nd_{(i)}$ = 0.51191-0.51205 ratios with time integrated Rb/Sr and Sm/Nd ratios indicative of ancient metasomatic enrichment. Transitional kimberlites provide a continuum to the kimberlite isotope array with intermediate $^{87}Sr/^{86}Sr_{(i)}$ = 0.7056-0.7075 and $^{143}Nd/^{144}Nd_{(i)}$ = 0.51208-0.51249 ratios. Distinct differences can be recognised within the transitional kimberlite group, with the on-craton transitional kimberlites (e.g. εNd = -0.5 to -1.9) showing more similarity to group I kimberlites, whereas off-craton transitional kimberlites are characterised by enriched isotope ratios (εNd = -3.4 to -6.7) more comparable to group II kimberlites.

All kimberlite groups show broad variation in their geochemistry and some of this variation has been attributed to secondary processes given the hybrid nature of these rock types. The effects of alteration (e.g. degree of serpentinisation and carbonatisation, correlation of mobile and immobile elements) and crustal contamination (e.g. high C.I., flattened heavy REE, raised Zr and Hf concentrations) on kimberlite bulk-rock geochemistry were identified and samples thought to be severely affected were discarded. Similarly, the effect of peridotite entrainment (trends to high MgO, SiO_2 and Ni) and fractional crystallisation (trends to low MgO, SiO_2 and Ni, but high CaO, CO_2 and light REE) were investigated. The compositions of close-to-primary kimberlite magmas for nearly all kimberlite localities were thus constrained by the selection of one or more representative samples (the least affected by the above-mentioned processes and corrected for lherzolite entrainment where necessary). Inferred close-to-primary magma compositions of the group I kimberlites analysed in this study have Mg numbers = 0.82-0.87 and ~22-27 wt% MgO, ~21-30 wt% SiO_2, ~10-17 wt% CaO, ~5.0-14 wt% CO_2, ~0.2-1.7 wt% K_2O and 660-1190ppm Ni. Close-to-primary magma compositions of group II kimberlites tend to higher SiO_2 (~28-36 wt%), MgO (~23-29 wt%), Mg-number (~0.86-0.89), Ni (590-1410ppm) and K_2O (1.6-4.6 wt%), but lower TiO_2 (0.9-1.4 wt%). Although close-to-primary magma compositions of the transitional kimberlites are generally comparable to group I and group II kimberlites for most major elements (24-29 wt% MgO, Mg-number = 0.84-0.88; 27-39 wt% SiO_2), for some elements they are intermediate (e.g. 1.0-3.7 wt% K_2O). This intermediate character of the transitional kimberlites, more apparent in isotope and trace element ratios (e.g. La/Nb, Ba/Nb, Th/Nb, $^{87}Sr/^{86}Sr_{(i)}$ and εNd), suggests they derived from mixed group I and group II kimberlite source regions.

9.4 Geochemistry of kimberlite source regions

Following experimental evidence that suggests kimberlites are derived from low degrees of partial melting of a carbonated garnet peridotite, semi-quantitative forward modelling of non-modal equilibrium melting was used in order to calculate the composition of source regions in equilibrium with close-to-primary group I and group II kimberlite magmas. It was assumed that kimberlites are produced by very low degrees of partial melting, with the residual mineralogy of the source comprising a metasomatised garnet lherzolite similar to those entrained by kimberlites located both on- and off- of the Kaapvaal craton. Prior to calculating source compositions of kimberlites using equations for non-modal batch melting, the effects of varying the above mentioned parameters were explored. As the assumed degree of partial melting is increased (e.g. F = 0.5-2%), so the light REE composition of the source becomes more enriched (e.g. 10 to 25 times chondrite). Similarly, as the residual proportion of modal clinopyroxene (e.g. 3 to 7%) and garnet (e.g. 3 to 7%) in the source is increased, so the light and heavy REE concentrations of the calculated source become more enriched, respectively. Modal estimates of on- and off-craton peridotite xenoliths show no significant differences and therefore, the residual source mineralogy for on- and off-craton kimberlites was assumed to be the same. However, varying REE ratios between kimberlites suggested that the higher La/Sm, but lower Gd/Yb ratio of group II kimberlites, was likely due to the effect of more residual clinopyroxene and less residual garnet in the source of group II kimberlites, in comparison to group I kimberlites.

Source compositions for all close-to-primary kimberlite magmas were subsequently calculated assuming 1% partial melting and with the residual source of a group I kimberlite (65% olivine, 25% orthopyroxene, 3% clinopyroxene and 7% garnet), having less clinopyroxene but more garnet than for a group II kimberlite (65% olivine, 25% orthopyroxene, 7% clinopyroxene and 3% garnet). All predicted source regions are more enriched in the light REE (4-36 times chondrite) than the heavy REE (0.9-3.6 times chondrite), with the sources of group II kimberlites being more light REE but less heavy REE enriched ($(La/Sm)_N$ = 3.2-7.0; $(La/Yb)_N$ = 7.7-28) than group I kimberlites ($(La/Sm)_N$ = 2.3-3.6; $(La/Yb)_N$ = 1.9-8.6). The lower La/Sm, La/Yb and Gd/Yb ratios of off-craton group I kimberlites in comparison to on-craton group I kimberlites, is shown to be a partial melting effect suggesting that off-craton kimberlites are slightly higher degree melts.

Predicted source regions of kimberlites are enriched in the more incompatible elements (e.g. light REE, Th, Nb), but depleted in the less incompatible elements (e.g. heavy REE, Zr) relative to primitive mantle. The large negative Rb, K and Ti anomalies as well as subdued negative Sr, Hf and Nb (group II kimberlites) anomalies on primitive mantle normalised diagrams, shown to be unrelated to crystal fractionation of phlogopite, ilmenite or any phase but are rather features of the close-to-primary kimberlite magmas, are subsequently transferred to the predicted source regions of kimberlites due to the absence of any residual accessory phase during partial melting capable of fractionating these elements. It is argued that these relative negative anomalies in close-to-primary magmas are unlikely due to residual K-phases (phlogopite, K-richterite), Ti-phases (ilmenite, rutile, armalcolite) or Zr-phases (e.g. zircon, zirconalite), but rather are intrinsic features of kimberlite source regions.

9.5 Evolution of kimberlite source regions

The characteristic compatible trace element enrichment, high Mg-numbers (Mg # = 0.80-0.89) and depleted heavy REE concentrations of group I, group II and transitional close-to-primary kimberlite magmas relative to typical MORB, suggests that kimberlites were in equilibrium with a previously melt-depleted source region, consistent with the refractory character of mantle xenoliths derived from Proterozoic and Archean mantle within southern Africa. The strongly enriched character of calculated source regions require subsequent enrichment in the light REE and other highly incompatible elements by metasomatic melts/fluids. These metasomatising melt/fluids appear to have been characterised by relative depletion in Rb, K, Ti and Sr, possibly due to the early crystallisation of phlogopite ± calcite. The characteristic depletion of alkali elements and HFS elements, as well as strongly light REE enriched character of the Wimbledon, Melton Wold and Eendekuil kimberlites, suggest that the metasomatic melt/fluid that enriched their source regions was more carbonate-rich, whereas the higher SiO_2 and K_2O, absence of large negative Ti, Zr and Hf anomalies, as well as shallower REE patterns of the Finsch, New Elands and Brandewynskuil kimberlites, suggests that the metasomatic melt/fluid was more alkali-rich in character.

Fractionated heavy REE patterns of kimberlites indicate that partial melting occurred within the garnet stability field for all on- and off-craton kimberlites. Differences in the geochemistry between on- and off-craton group I kimberlites (off-craton kimberlites tend to lower SiO_2, MgO and higher FeO*, TiO_2, CaO and CO_2, even though still broadly falling within the on-craton kimberlite field) are possibly due to partial melting of slightly less depleted source regions at lower pressures for off-craton kimberlites, although recognising that this does not necessarily imply that on-craton kimberlites cannot be derived from similarly depleted sources at equivalent pressures. Since no significant geochemical differences between on- and off-craton group II kimberlites have been identified, this suggests that both the Proterozoic (off-craton) and Archean (on-craton) lithospheric mantle sources of group II kimberlites, have experienced a similar evolutionary history. Although on- and off-craton transitional kimberlites show differences, these are more a function of the differences in geochemistry between the sources of group I and group II kimberlites, if transitional kimberlites are derived from mixed group I and group II kimberlite source regions. The more SiO_2, K_2O, LIL element and light REE-enriched character of group II kimberlites is consistent with their derivation from more highly metasomatised sources than group I kimberlites. Similarly, more highly metasomatised sources are likely to have greater proportions of phlogopite and clinopyroxene but less garnet, as suggested by varying REE ratios between kimberlite varieties. Although group II kimberlites can possibly be produced by partial melting of more exotic source regions (clinopyroxene and phlogopite veins) rather than metasomatised garnet lherzolite, various arguments suggest that a metasomatised garnet lherzolite is a more appropriate source material.

Group I kimberlites are characterised by isotopic signatures depleted relative to present day Bulk Earth that indicate recent enrichment of their sources (T_{Nd} model age = 0 - 700Ma), most likely during the Mesozoic. Isotopic signatures and selected incompatible element ratios (e.g. Ce/Pb, Nb/U, La/Nb,

Ba/Nb) of group I kimberlites are similar to ocean island basalts and consistent with the involvement of asthenospheric plume related melts/fluids in their petrogenesis. Since the depleted source of group I kimberlites is most likely located within the lithosphere, the plume signature of group I kimberlites is postulated to be caused by the upward percolation of plume melts/fluids and ensuing metasomatism of the lithospheric mantle. Group II kimberlites, however have isotopic signatures enriched relative to present day Bulk Earth and require source regions that have experienced ancient light REE enrichment (T_{Nd} model age = 600-1300Ma) and subsequent isolation from the convecting mantle in order to preserve these heterogeneities. Therefore, like group I kimberlites, the source regions of group II kimberlites are thought to be located within the subcontinental lithosphere, but with metasomatic enrichment unrelated to plume upwelling. Rather, the characteristic depletion of Nb and Ta and similarity of incompatible element ratios of group II kimberlites (e.g. La/Nb, BaNb, Th/Nb) to calc-alkaline basalts, suggests that the metasomatism of their source regions by was subduction related melts/fluids. This does not preclude the possibility that the mantle plumes beneath southern Africa during the Mesozoic provided a heat source for partial melting and group II kimberlite production. Minimum model ages of on- and off-craton group II kimberlites suggest enrichment of both Archean and Proterozoic mantle sources, prior to Gondwana break-up and after the formation of the mantle underlying the Namaqua-Natal belt. Assuming the Namaqua orogeny comprised multiple subduction and accretion episodes, then the source of the melts/fluids that metasomatised Proterozoic and Archean kimberlite source regions may have been associated with this Kibaren event.

The similarity of diagnostic geochemical characteristics suggest that group II kimberlites and Karoo basalts were derived from common source regions located within the subcontinental lithosphere. After the Jurassic eruption of the Karoo basalts and the Jurassic to Cretaceous eruption of group II kimberlites carrying a subduction signature, it appears that this highly metasomatised common source region was largely exhausted. Consequently, group I kimberlites erupted after the group II kimberlites, were derived from Mesozoic plume enriched lithospheric source regions, with enrichment possibly associated with the passage of southern Africa over the Shona and Bouvet mantle plumes. Transitional kimberlites appear to tap mixed group I and group II kimberlite source regions with the older off-craton transitional kimberlites derived from a source dominated by a group II kimberlite component, whereas the younger on-craton transitional kimberlites are derived from source regions with a stronger group I kimberlite signature.

REFERENCES

Adam, J. and Green, T. H. (1994) The effects of pressure and temperature on the partitioning of Ti, Sr and REE between amphibole, clinopyroxene and basanitic melts. *Chemical Geology* **117**, 219-233.

Allsopp, H. L. and Barrett, D. R. (1975) Rb-Sr age determinations on South African kimberlite pipes. *Physics and Chemistry of the Earth* **9**, 605-617.

Allsopp, H. L. and Roddick, J. C. (1984) Rb-Sr and ^{40}Ar-^{39}Ar age determinations on phlogopite micas from the pre-Lebombo group Dokolwayo kimberlite pipe. In: Erlank, A.J. (Ed) *Petrogenesis of the Volcanic rocks of the Karoo province*. Special Publication of the Geological Society of South Africa, Johannesburg, **13**, 267-271.

Bagai, Z. (2000) *Geochemical and geochronological investigations of the Vumba granite greenstone terrain NE of Botswana*. Unpubl. MSc, University of Durham, 170pp.

Bailey, D. K. (1993) Petrogenetic implications of the timing of alkaline, carbonatite and kimberlitic igneous activity in Africa. *South African Journal of Geology* **96**, 67-74.

Barrett, D. R. and Berg, G. W. (1975) Complementary petrographic and strontium-isotope ratio studies of South African kimberlite. *Physics and Chemistry of the Earth* **9**, 619-635.

Basaltic Volcanism Study Project (1981) *Basaltic Volcanism on the Terrestrial Planets*. Pergamon Press, New York, 1286pp.

Beard, A. D., Downes, H., Hegner, E., Sablukov, S. M., Vetrin, V. R. and Balogh, K. (1998) Mineralogy and geochemistry of Devonian ultramafic minor intrusions of the southern Kola Peninsula, Russia: Implications for the petrogenesis of kimberlites and melilitites. *Contributions to Mineralogy and Petrology* **130**, 288-303.

Beard, A. D., Downes, H., Hegner, E. and Sablukov, S. M. (2000) Geochemistry and mineralogy of kimberlites from the Arkhangelsk Region, NW Russia: Evidence for transitional kimberlite magma types. *Lithos* **51**, 47-73.

Beattie, P., Ford, C. and Russell, D. (1991) Partition coefficients for olivine-melt and orthopyroxene-melt systems. *Contributions to Mineralogy and Petrology* **109**, 212-224.

Bell, D. R. and Mofokeng, S. W. (1998) Cr-poor megacrysts from the Frank Smith Mine and the source regions of transitional kimberlites. *VIIth International Kimberlite Conference*, Extended Abstracts, 64-66.

Bell, D. R., Schmitz, M. D. and Janney, P. E. (2003) Mesozoic thermal evolution of the southern African mantle lithosphere. *Lithos* **71**, 273-288.

Berg, G. W. and Allsopp, H. L. (1972) Low $^{87}Sr/^{86}Sr$ ratios in fresh South African kimberlites. *Earth and Planetary Science Letters* **16**, 27-30.

Birch, G. F. (1981) The Karbonat Bombe: A precise, rapid and cheap instrument for determining calcium carbonate in sediments and rocks. *Transactions of the Geological Society of South Africa* **84**, 199-203.

Bizimis, M., Salters, V. J. M. and Dawson, J. B. (2003) The brevity of carbonatite sources in the mantle: Evidence from Hf isotopes. *Contributions to Mineralogy and Petrology* **145**, 281-300.

Bizzi, L. A. (1995) *Mesozoic alkaline volcanism and mantle evolution of the southwestern Saò Fransisco craton, Brazil.* Unpubl. PhD, University of Cape Town, 211pp.

Bonney, T. G. (1989) The original rock of the South African diamond. *Proceedings of the Royal Society of London* **65**, 173-182.

Boyd, F. R. (1973) A pyroxene geotherm. *Geochimica et Cosmochimica Acta* **37**, 2533-2546.

Boyd, F. R. and Nixon, P. H. (1975) Origins of the ultramafic nodules from the kimberlites of northern Lesotho and the Monastery Mine, South Africa. *Physics and Chemistry of the Earth* **9**, 431-453.

Boyd, F. R. and McCallister, R. H. (1976) Densities of fertile and sterile garnet peridotites. *Geophysical Research Letters* **3**, 509-512.

Boyd, F. R. and Mertzman, S. A. (1987) Composition and structure of the Kaapvaal lithosphere, southern Africa. In: Mysen, B. O. (Ed) *Magmatic Processes: Physicochemical Principles.* Geochemical Society Special Publication, Pennsylvania, **1**, 13-24.

Boyd, F. R., Pearson, D. G., Hoal, K. O., Hoal, B. G., Nixon, P. H., Kingston, M. J. and Mertzman, S. A. (2004) Garnet lherzolites from Louwrensia, Namibia: Bulk composition and P/T relations. *Lithos* **77**, 573-592.

Brey, G. P. and Köhler, T. (1990) Geothermobarometry in four phase lherzolites. II New thermobarometers and practical assessment of existing thermobarometers. *Journal of Petrology* **31**, 1353-1378.

Bristow, J. W., Smith, C. B., Allsopp, H. L., Shee, S. R. and Skinner, E. M. W. (1986) Setting, geochronology and geochemical characteristics of 1600 m.y. kimberlites and related rocks from the Kuruman Province, South Africa. *IVth International Kimberlite Conference*, Extended Abstracts, 112-114.

Canil, D. and Scarfe, C. M. (1990) Phase relations in peridotite + CO_2 systems to 12 GPa: Implications for the origin of kimberlite and carbonate stability in the Earth's upper mantle. *Journal of Geophysical Research* **95**, B10, 15805-15816.

Carlson, R. W., Boyd, F. R., Shirey, S. B., Janney, P. E., Grove, T. L., Bowring, W. A., Schmitz, M. A., Bell, D. R., Gurney, J. J., Richardson, S. H., Tredoux, M., Menzies, A. H., Hart, R. J., Wilson, A. H., and Moser, D. (2000) Continental growth, preservation and modification in Southern Africa. *GSA Today* **10**, 1-7.

Chalapathi Rao, N. V., Gibson, S. A., Pyle, D. M. and Dickin, A. P. (2004) Petrogenesis of Proterozoic lamproites and kimberlites from the Cuddapah Basin and Dharwar Craton, Southern India. *Journal of Petrology* **45**, 907-948.

Chazey III, W. J., Neal, C. R., Jain, J. C. and Kinman, W. S. (2003) A reappraisal of Rb, Y, Zr, Pb and Th value in geochemical reference material BHVO-1. *Geostandards Newsletter* **27**, 181-192.

Clague, D. A. and Frey, F. A. (1982) Petrology and trace element geochemistry of the Honolulu volcanics, Oahu: Implications for the oceanic mantle beneath Hawaii. *Journal of Petrology* **23**, 447-504.

Clague, D. A., Holcomb, R. T., Sinton, J. M., Detrick, R. S. and Torresan, M. E. (1990) Pliocene and Pleistocene alkalic flood basalts on the seafloor north of the Hawaiian islands. *Earth and Planetary Science Letters* **98**, 175-191.

Clark, T. C. (1994) *An integrated geochemical and isotopic study of the Prieska Province kimberlites from the Republic of South Africa.* Unpubl. MSc, University of the Witwatersrand, 237pp.

Clement, C. R. and Skinner, E. M. W. (1979) A textural-genetic classification of kimberlitic rocks. *Kimberlite Symposium II*, Abstracts, 18-21.

Clement, C. R., Skinner, E. M., Hawthorne, J. B., Kleinjan, L. and Allsopp, H. L. (1979) Precambrian ultramafic dykes with kimberlite affinities in the Kimberley area. In: Boyd, F. R. and Meyer, H. O. A. (Eds) *Kimberlites, diatremes and diamonds: Their geology, petrology and geochemistry.* American Geophysical Union, Washington D.C., **1**, 101-110.

Clement, C. R. (1982) *A comparative geological study of some major kimberlite pipes in the Northern Cape and Orange Free State.* Unpubl. PhD, University of Cape Town, 432pp.

Clement, C. R., Skinner, E. M. W. and Scott Smith, B. H. (1984) Kimberlite redefined. *Journal of Geology* **92**, 223-228.

Clement, C. R. and Skinner, E. M. W. (1985) A textural-genetic classification of kimberlites. *Transactions of the Geological Society of South Africa* **88**, 403-409.

Clifford, T. N. (1966) Tectono-metallogenic units and metallogenic provinces of Africa. *Earth and Planetary Science Letters* **1**, 241-434.

Coe, N. J. (2004) *Petrogenesis of the Swartruggens and Star kimberlite dyke swarms, South Africa.* Unpubl. MSc, University of Cape Town, 146pp.

Coltorti, M., Beccaluva, L., Bonadiman, C., Salvini, L. and Siena, F. (2000) Glasses in mantle xenoliths as geochemical indicators of metasomatic agents. *Earth and Planetary Science Letters* **183**, 303-320.

Cook, F. A., van der Velden, A. R., Hall, K. W. and Roberts, B. J. (1999) Frozen subduction in Canada's Northwest Territories: Lithoprobe deep lithospheric reflection profiling of the western Canadian Shield. *Tectonics* **18**, 1-24.

Cornell, D. H., Hawkesworth, C. J., van Calsteren, P. and Scott, W. D. (1986) Sm-Nd study of Precambrian crustal development in the Prieska-Copperton region, Cape Province. *Transactions of the Geological Society of South Africa* **89**, 17-28.

Crough, S. T., Morgan, W. J. and Hargraves, R. B. (1980) Kimberlites: Their relation to mantle hotspots. *Earth and Planetary Science Letters* **50**, 260-274.

Dalton, J. A. and Presnall, D. C. (1998a) The continuum of primary carbonatitic - kimberlitic melt compositions in equilibrium with lherzolite: Data from the system CaO-MgO-Al_2O_3-SiO_2-CO_2 at 6GPa. *Journal of Petrology* **39**, 1953-1964.

Dalton, J. A. and Presnall, D. C. (1998b) Carbonatitic melts along the solidus of model lherzolite in the system CaO-MgO-Al_2O_3-SiO_2-CO_2 from 3-7GPa. *Contributions to Mineralogy and Petrology* **131**, 123-135.

Davies, G. R., Spriggs, A. J. and Nixon, P. H. (2001) A non-cognate origin for the Gibeon kimberlite megacryst suite, Namibia: Implications for the origin of Namibian kimberlites. *Journal of Petrology* **42**, 159-172.

Davis, G.L. (1977) The ages and uranium contents of zircons from kimberlites and associated rocks. *IInd International Kimberlite Conference*, Extended Abstracts.

Davis, G. L. (1978) Zircons from the mantle. *U.S. Geological Survey, Open File Report* **78-701**, 86-88.

Dawson, J. B. (1980) *Kimberlites and their xenoliths.* Springer-Verlag, Berlin, 252pp.

Dawson, J.B. (1999) Metasomatism and melting in spinel peridotite xenoliths from Labait, Tanzania. In: Gurney, J. J., Gurney, J. L., Pascoe, M. D. and Richardson, S. R. (Eds) *Proceedings of the VIIth International Kimberlite Conference*, Red Roof Design, Cape Town, **1**, 164-173.

de Beer, J. H. and Meyer, R. (1983) Geoelectrical and gravitational characteristics of the Namaqua-Natal mobile belt and its boundaries. In: Botha, J. V. (Ed) *Namaqualand Metamorphic Complex*, Geological Society of South Africa Special Publication, Johannesburg, **10**, 91-100.

de Paolo D. J. and Wasserburg G. J. (1976) Nd isotopic variations and petrogenetic models. *Geophysical Research Letters*, **3**, 249-252.

de Wit, M. J., Roering, C., Hart, R. J., Armstrong, R. A., de Ronde, C. E. J., Green, R. W. E., Tredoux, M., Peberdy, E. and Hart, R. A. (1992) Formation of an Archean continent. *Nature* **357**, 553-562.

Deer, W. A., Howie, R. A. and Zussman, J. (1992) *An introduction to the rock-forming minerals.* Longman, Harlow, 696pp.

Douglass, J. and Schilling, J.-G. (1999) Plume-ridge interactions of the Discovery and Shona mantle plumes with the southern Mid-Atlantic Ridge (40^0-55^0S). *Journal of Geophysical Research* **104**, B2, 2941-2962.

Dowall, D. P., Pearson, D. G., Nowell, G. M., Kjarsgaard, B. A., Armstrong, J., and Horstwood, M. S. A. (2003) Comparative geochemistry of kimberlites from the Lac de Gras Field, NWT - An integrated isotopic and elemental study. *VIIIth International Kimberlite Conference*, Extended Abstracts.

Du Toit, A. L. (1908) The kimberlite and allied pipes and fissures in Prieska, Britstown, Victoria West and Carnarvon. *Cape of Good Hope Department of Agriculture 13th Annual Report of the Geological Commission*, 112-127.

Du Toit, A. L. (1929) The Geology of the major portion of East Griqualand. *Explanation of Cape Sheet No. 35 (Matatiele).* Geological Survey of South Africa, 36pp.

Duke, J. M. (1976) Distribution of the period four transition elements among olivine, calcic clinopyroxene and mafic silicate liquid: Experimental results. *Journal of Petrology* **17**, 499-521.

Duncan, A. R., Erlank, A. J. and Marsh, J. S. (1984) Regional geochemistry of the Karoo Igneous Province. In: Erlank, A. J. (Ed) *Petrogenesis of the Volcanic Rocks of the Karoo Province*, Special Publication of the Geological Society of South Africa, Johannesburg, **13**, 355-388.

Duncan, A. R. (1987) The Karoo Igneous Province - a problem area for inferring tectonic setting from basalt geochemistry. *Journal of Volcanological and Geothermal Research* **32**, 13-34.

Eales, H. V., Marsh, J. S., and Cox, K. G. (1984) The Karoo Igneous Province: an introduction. In: Erlank, A. J. (Ed) *Petrogenesis of the Volcanic Rocks of the Karoo Province*. Geological Society of South Africa Special Publication, Johannesburg, **13**, 1-26.

Edgar, A. D. and Charbonneau, H. E. (1993) Melting experiments on a SiO_2-poor, CaO-rich aphanitic kimberlite from 5-10GPa and their bearing on sources of kimberlite magmas. *American Mineralogist* **78**, 132-142.

Eggler, D. H. (1987) Solubility of major and trace elements in mantle metasomatic fluids: Experimental constraints. In: Menzies, M. A. and Hawkesworth, C. J. (Eds) *Mantle Metasomatism,* Academic Press, London, 21-41.

Eggler, D. H. and Wendlandt, R. F. (1979) Experimental studies on the relationship between kimberlite magmas and partial melting of peridotite. In: Boyd, F. R. and Meyer, H. O. A. (Eds) *Kimberlites, diatremes and diamonds: Their geology, petrology and geochemistry*, American Geophysical Union, Washington D.C., **1**, 300-330.

Elliott, T., Plank, T., Zindler, A., White, W. and Bourdon, W. (1997) Element transport from slab to volcanic front at the Mariana arc. *Journal of Geophysical Research* **102**, B7, 14991-15019.

Erlank, A. J., Waters, F. J., Hawkesworth, C. J., Haggerty, S. E., Allsopp, H. L., Rickard, R. S. and Menzies, M. A. (1987) Evidence for mantle metasomatism in peridotite nodules from the Kimberley pipes, South Africa. In: Menzies, M. A. and Hawkesworth, C. J. (Eds) *Mantle Metasomatism,* Academic Press, London, 221-311.

Fesq, H. W., Kable, E. D. J. and Gurney, J. J. (1975) Aspects of the geochemistry of kimberlites from the Premier Mine, and other selected South African occurrences with particular reference to the rare earth elements. *Physics and Chemistry of the Earth* **9**, 686-707.

Field, M. and Scott Smith, B. H. (1999) Contrasting geology and near-surface emplacement of kimberlite pipes in southern African and Canada. In: Gurney, J. J., Gurney, J. L., Pascoe, M. D. and Richardson, S. R. (Eds) *Proceedings of the VIIth International Kimberlite Conference*, Red Roof Design, Cape Town, **1**, 214-237.

Finnerty, A. A. and Boyd, F. R. (1987) Thermobarometry for garnet peridotite xenoliths: a basis for mantle stratigraphy. In: Nixon, P. H. (Ed) *Mantle Xenoliths*, John Wiley and Sons, New York, 381-402.

Foley, S. (1992a) Petrological characterisation of the source components of potassic magmas: Geochemical and experimental constraints. *Lithos* **28**, 187-204.

Foley, S. (1992b) Vein-plus-wall-rock melting mechanisms in the lithosphere and the origin of potassic alkaline magmas. *Lithos* **28**, 435-453.

Foley, S. F., Barth, M. G. and Jenner, G. A. (2000) Rutile/melt partition coefficients for trace elements and an assessment of the influence of rutile on the trace element characteristics of subduction zone magmas. *Geochimica et Cosmochimica Acta* **64**, 933-938.

Franz, L., Brey, G. P. and Okrusch, M. (1996) Steady state geotherm, thermal disturbances, and tectonic development of the lower lithosphere underneath the Gibeon Kimberlite Province, Namibia. *Contributions to Mineralogy and Petrology* **126**, 181-198.

Fraser, K. J., Hawkesworth, C. J., Erlank, A. J., Mitchell, R. H. and Scott-Smith, B. H. (1985/86) Sr, Nd and Pb isotope and minor element geochemistry of lamproites and kimberlites. *Earth and Planetary Science Letters* **76**, 57-70.

Fraser, K. J. and Hawkesworth, C. J. (1992) The petrogenesis of group 2 ultrapotassic kimberlites from Finsch Mine, South Africa. *Lithos* **28**, 327-345.

Frey, F. A. and Green, D. H. (1974) The mineralogy, geochemistry and origin of lherzolite inclusions in Victoria basanites. *Geochimica et Cosmochimica Acta* **38**, 1023-1059.

Frey, F. A. and Prinz, M. (1978) Ultramafic inclusions from San Carlos, Arizona: Petrologic and geochemical data bearing on their petrogenesis. *Earth and Planetary Science Letters* **38**, 129-176.

Girnis, A. V., Brey, G. P. and Ryabchikov, I. D. (1995) Origin of group IA kimberlites: Fluid saturated melting experiments at 45-55kBar. *Earth and Planetary Science Letters* **134**, 283-296.

Govindaraju, K. (1994) Compilation of working values and sample description for 383 Geostandards. *Geostandards Newsletter*, **18**, 158pp.

Green, T. H. and Pearson, N. J. (1987) An experimental study of Nb and Ta partitioning between Ti-rich melts and silicate liquids at high pressure and temperature. *Geochimica et Cosmochimica Acta* **51**, 55-62.

Green, D. H. and Walllace, M. E. (1988) Mantle metasomatism by ephemeral carbonatite melts. *Nature* **336**, 459-462.

Greenough, J. D. (1988) Minor phases in the Earth's mantle: Evidence from trace and minor element patterns in primitive alkaline magmas. *Chemical Geology* **69**, 177-192.

Gregoire M., Bell, D. R. and le Roex, A. P. (2003) Garnet lherzolites from the Kaapvaal craton (South Africa): Trace element evidence for a metasomatic history. *Journal of Petrology* **44**, 629-657.

Griffin, W. L., Cousens, D. R., Ryan, C. G., Sie, S. H. and Suter, G. F. (1989) Ni in chrome pyrope garnets: A new geothermometer. *Contributions to Mineralogy and Petrology* **103**, 199-202.

Gudfinnsson, G. H. and Presnall, D. C. (2003) Continuous gradations among primary kimberlitic, carbonatitic, melilititic, and komatiitic melts in equilibrium with garnet lherzolite at 3-8GPa. *VIIIth International Kimberlite Conference*, Extended Abstracts.

Gurney, J. J. (1990) The diamondiferous roots of our wandering continent. *South African Journal of Geology* **93**, 424-437.

Gurney, J. J. and Menzies, A. H. (1998) *VIIth International Kimberlite Conference,* Small mines field excursion guide, 40pp.

Haggerty, S. E. (1987) Metasomatic mineral titanates in upper mantle xenoliths. In: Nixon, P.H. (Ed) *Mantle Xenoliths,* John Wiley and Sons, New York, 671-690.

Haggerty, S. E. (1994) Superkimberlites: A geodynamic window to the Earth's core. *Earth and Planetary Science Letters* **122**, 57-69.

Hanson, G. N. and Langmuir, C. H. (1978) Modelling of major elements in mantle-melt systems using trace element approaches. *Geochimica et Cosmochimica Acta* **42**, 725-741.

Harlow, G. E. and Davies, R. (2004) Status report on the stability of K-rich phases at mantle conditions. *Lithos* **77**, 647-653.

Harris, M., le Roex, A. P., and Class, C. (2004) Geochemistry of the Uintjiesberg kimberlite, South Africa: Petrogenesis of an off-craton, group I, kimberlite. *Lithos* **74**, 149-165.

Hart, S. R. and Brooks, C. (1977) The geochemistry and evolution of Early Precambrian mantle. *Contributions to Mineralogy and Petrology* **61**, 109-128.

Hart S. R. and Davis, S. E. (1978) Nickel partitioning between olivine and silicate melt. *Earth and Planetary Science Letters* **40**, 203-219.

Hart, S. R. (1988) Heterogeneous mantle domains: Signatures, genesis and mixing chronologies. *Earth and Planetary Science Letters* **90**, 273-296.

Harte, B. (1983) Mantle peridotites and processes – the kimberlite sample. In: Hawkesworth, C.J. and Norry, M.J. (Eds) *Continental basalts and mantle xenoliths*, Shiva, Cambridge, 46-91.

Harte, B., Winterburn, P. A. and Gurney, J. J. (1987) Metasomatic and enrichment phenomena in garnet peridotite facies mantle xenoliths from the Matsoku kimberlite pipe, Lesotho. In: Menzies, M. A. and Hawkesworth, C. J. (Eds) *Mantle Metasomatism*, Academic Press, London, 145-220.

Hartnady, C. J. H., Joubert, J. P. and Stowe, C. (1985) Proterozoic crustal evolution in southwestern Africa. *Episodes* **8**, 236-244.

Hartnady, C. J. H. and le Roex, A. P. (1985) Southern Ocean hotspot tracks and the Cenozoic absolute motion of the African, Antarctic, and South American Plates. *Earth and Planetary Science Letters* **75**, 245-257.

Hatton, C. J. (1978) *The geochemistry and origin of xenoliths from the Roberts Victor Mine.* Unpubl. PhD, University of Cape Town, 179pp.

Hauri, E. H., Shimizu, N., Dieu, J. J. and Hart, S. R. (1993) Evidence for hotspot-related carbonatite metasomatism in the oceanic upper mantle. *Nature* **365**, 221-227.

Hawkesworth, C. J., Marsh, J. S., Duncan, A. R., Erlank, A. J. and Norry, M. J. (1984) The role of continental lithosphere in the generation of the Karoo volcanic rocks: Evidence from combined Nd- and Sr-isotope studies. In: Erlank, A. J. (Ed) *Petrogenesis of the Volcanic rocks of the Karoo province*. Special Publication of the Geological Society of South Africa, Johannesburg, **13**, 341-354.

Hawkesworth, C. J., Erlank, A. J., Kempton, P. D. and Waters, F. G. (1990) Mantle metasomatism: Isotope and trace-element trends in xenoliths from Kimberley, South Africa. *Chemical Geology* **85**, 19-34.

Hawthorne, J. B. (1975) Model of a kimberlite pipe. *Physics and Chemistry of the Earth* **9**, 1-16.

Heaman, L. M., Kjarsgaard, B. A., and Creaser, R. A. (2004) The temporal evolution of North American kimberlites. *Lithos* **76**, 377-397.

Helmstaedt, H. and Gurney, J. J. (1984) Kimberlites of Southern Africa - are they related to subduction processes? In: Kornprobst, J. (Ed) *Kimberlites and Related Rocks: Kimberlites 1.* Elsevier, Amsterdam, 424-435.

Hertzberg, C. and O'Hara, M. J. (2002) Plume-associated ultramafic magmas of Phanerozoic age. *Journal of Petrology* **43**, 1857-1883.

Herzberg, C. (1992) Depth and degree of melting of komatiites. *Journal of Geophysical Research* **97**, B4, 4521-4540.

Hofmann, A. W., Jochum, K. P., Seufert, M. and White, W. M. (1986) Nb and Pb in oceanic basalts: New constraints on mantle evolution. *Earth and Planetary Science Letters* **79**, 33-45.

Hops, J. J., Gurney, J. J. and Harte, B. (1992) The Jagersfontein Cr-poor megacryst suite - towards a model for megacryst petrogenesis. *Journal of Volcanology and Geothermal Research* **50**, 143-160.

Huang, Y-M., van Calsteren, P. and Hawkesworth, C. J. (1995) The evolution of the lithosphere in southern Africa: A perspective on the basic granulite xenoliths from kimberlites in South Africa. *Geochimica et Cosmochimica Acta* **59**, 4905-4920.

Jang, Y. D. and Naslund, H. R. (2003) Major and trace element variation in ilmenite in the Skaergaard Intrusion: Petrologic implications. *Chemical Geology* **193**, 109-125.

Janney, P. E., Carlson, R. W., Shirey, S. B., Bell, D. R. and le Roex, A. P. (1999) Temperature, pressure and the Re-Os age systematics of off-craton peridotite xenoliths from the Namaqua-Natal belt, western South Africa, *IXth Annual V.M. Goldschmidt Conference*, Abstracts.

Janney, P. E., Carlson, R. W., Shirey, S. B., Bell, D. R., and le Roex, A. P. (2001) Re-Os age and thermal structure of off-craton lithospheric mantle in western South Africa. *EOS*, Transactions of the American Geophysical Union **82**, 20.

Janney, P. E., le Roex, A. P., Carlson, R. W. and Viljoen, K. S. (2002) A chemical and multi-isotopic study of olivine melilitites and associated rocks from the Western Cape, South Africa. Implications for the sources of group 1 kimberlites and the origin of the HIMU signature in Africa. *Journal of Petrology* **43**, 2339-2370.

Janse, A. J. A. (1975) Kimberlite and related rocks from the Nama Plateau of South-West Africa. *Physics and Chemistry of the Earth* **9**, 81-94.

Jaques, A. L., Lewis, J. D., Smith, C. B., Gregory, G. P., Ferguson, J., Chappell, B. W., and McCulloch, M. T. (1984) The diamond-bearing ultrapotassic (lamproitic) rocks of the West Kimberley Region, Western Australia. In: Kornprobst, J. (Ed) *Kimberlites and related rocks: Kimberlites 1.* Kornprobst, Elsevier, Amsterdam, 225-254.

Jones, A .P. and Wyllie, P. J. (1984) Minor elements in perovskite from kimberlites and distribution of the rare earth elements: An ion probe study. *Earth and Planetary Science Letters* **69**, 128-140.

Kable, E. J. D., Fesq, H. W. and Gurney, J. J. (1975) The significance of the inter-element relationships of some minor and trace elements in South African kimberlites. *Physics and Chemistry of the Earth* **9**, 709-734.

Kaminsky, F. V., Sablukov, S. M., Sablukova, L. I. and Channer, D. M. D. (2004) Neoproterozoic 'anomalous' kimberlites of Guaniamo, Venezuela: Mica kimberlites of 'isotopic transitional' type. *Lithos* **76**, 565-590.

Kelemen, P. B., Shimizu, N., and Dunn, T. (1993) Relative depletion of niobium in some arc magmas and the continental crust: partitioning of K, Nb, La, Ce during melt/rock reaction in the upper mantle. *Earth and Planetary Science Letters* **120**, 111-134.

Kennedy, C. S. and Kennedy, G. C. (1976) The equilibrium boundary between graphite and diamond. *Journal of Geophysical Research* **81**, 14, 2467-2470.

Kesson, S. E., Ringwood, A. E. and Hibberson, W. O. (1994) Kimberlite melting relations revisited. *Earth and Planetary Science Letters* **121**, 261-262.

Kinzler, R.J. and Grove, T.L. (1992a) Primary magmas of mid-ocean ridge basalts: 1. Experiments and methods. *Journal of Geophysical Research* **97**, B5, 6885-6906.

Kinzler, R.J. and Grove, T.L. (1992b) Primary magmas of mid-ocean ridge basalts: 2. Applications. *Journal of Geophysical Research* **97**, B5, 6907-6926.

Kirkley, M. B. (1987) *Aspects of the geochemistry of kimberlite carbonates*. Unpubl. PhD, University of Cape Town, 282pp.

Konzett, J., Armstrong, R. A., Sweeney, R. J. and Compston, W. (1998) The timing of MARID metasomatism in the Kaapvaal mantle: An ion probe study of zircons from MARID xenoliths. *Earth and Planetary Science Letters* **160**, 133-145.

Kramers, J. D., Smith, C. B., Lock, N. P., Harmon, R. S., and Boyd, F. R. (1981) Can kimberlites be generated from an ordinary mantle? *Nature* **291**, 53-56.

Kröner, A. and Tegtmeyer, A. (1994) Gneiss-greenstone relationships in the Ancient Gneiss Complex of southwestern Swaziland, southern Africa, and implications for early crustal evolution. *Precambrian Research* **67**, 109-139.

Kurz, M. D., le Roex, A. P. and Dick, H. J. B. (1998) Isotope geochemistry of the oceanic mantle near the Bouvet triple junction. *Geochimica et Cosmochimica Acta* **62**, 841-852.

Langmuir, C. H., Vocke, R. D., Hanson, G. N. and Hart, S. R. (1978) A general mixing equation with applications to Icelandic basalts. *Earth and Planetary Science Letters* **37**, 380-392.

Larson, L. M. and Pederson, A. K. (2000) Processes in high-Mg, high-T magmas: Evidence from olivine, chromite and glass in Palaeogene picrites from West Greenland. *Journal of Petrology* **41**, 1071-1098.

La Tourette, T., Hervig, R. L. and Holloway, J. R. (1995) Trace element partitioning between amphibole, phlogopite, and basanite melt. *Earth and Planetary Science Letters* **135**, 13-30.

Le Maitre, R. W. (Ed.) Streckheisen, A., Zanettin, B., Le Bas, M. J., Bonin, B., Bateman, P., Bellieni, G., Dudek, A., Etremova, S., Keller, J., Lameyer, J., Sabine, P. A., Schmid, R., Sørensen, H., Woolley, A. R. (2002). *Igneous Rocks: A classification and glossary of terms*. Recommendations of the International Union of the Geological Sciences Subcomission on the Systematics of Igneous rocks, Cambridge University Press, Cambridge, 236pp.

le Roex, A. P. (1986) Geochemical correlation between southern African kimberlites and South Atlantic hotspots. *Nature* **324**, 243-245.

le Roex, A. P., Dick, H. J. B. and Fisher, R. L. (1989) Petrology and geochemistry of MORB from 25^{0}E to 46^{0}E along the Southwest Indian Ridge: Evidence for contrasting styles of mantle enrichment. *Journal of Petrology* **30**, 947-986.

le Roex, A. P. and Lanyon, R. (1998) Isotope and trace element geochemistry of Cretaceous Damaraland lamprophyres and carbonatites, northwestern Namibia: Evidence for plume-lithosphere interactions. *Journal of Petrology* **39**, 1117-1146.

le Roex, A. P., Bell, D. R. and Davis, P. (2003) Petrogenesis of group I kimberlites from Kimberley, South Africa: evidence from bulk-rock geochemistry. *Journal of Petrology* **44**, 2261-2286.

le Roux, P. J., le Roex, A. P., Schilling, J.-G., Shimizu, N., Perkins, W. W. and Pearce, N. J. G. (2002) Mantle heterogeneity beneath the southern Mid-Atlantic Ridge: trace element evidence for contamination of ambient lithospheric mantle. *Earth and Planetary Science Letters* **203**, 479-498.

Lorenz, V. (1975) Formation of phreatomagmatic maar-diatreme volcanoes and its relevance to kimberlite diatremes. *Physics and Chemistry of the Earth* **9**, 17-27.

Lorenz, V., Zimanowski, B., Büttner, R. and Kurslaukis, S. (1999) Formation of kimberlite diatremes by explosive interaction of kimberlite magma with groundwater: Field and experimental aspects. In: Gurney, J. J., Gurney, J. L., Pascoe, M. D., Richardson, S. H. (Eds) *Proceedings of the VIIth International Kimberlite Conference*, Red Roof Design, Cape Town, **2**, 522-528.

Mahoney, J., le Roex, A. P., Peng, Z., Fisher, R. L. and Natland, J. H. (1992) Southwestern limits of Indian Ocean Ridge mantle and the origin of low $^{206}Pb/^{204}Pb$ mid-ocean ridge basalt: Isotope systematics of the Central Southwest Indian Ridge (17^0-59^0E). *Journal of Geophysical Research* **97**, 19771-19790.

Maaloe, S. and Aoki, K. (1977) The major element composition of the upper mantle estimated from the composition of lherzolites. *Contributions to Mineralogy and Petrology* **63**, 161-173.

Mahotkin, I. L., Gibson, S. A., Thompson, R. N., Zhuravlev, D. Z., and Zherdev, P. U. (2000) Late Devonian diamondiferous kimberlite and alkaline picrite (proto-kimberlite?) magmatism in the Arkhangelsk Region NW Russia. *Journal of Petrology* **41**, 201-227.

Marsh, J. S., Hooper, P. R., Rehacek, J., Duncan, R. A. and Duncan, A. R. (1997) Stratigraphy and age of Karoo basalts of the Lesotho and implications for correlations within the Karoo Igneous Province. In: Mahoney, J. J. and Coffin, M. R. (Eds) *Large Igneous Provinces: Continental, Oceanic and Planetary Flood Volcanism*. American Geophysical Union, Washington D.C., **100**, 247-272.

Mathias, M., Siebert, J. C. and Rickwood, P. C. (1970) Some aspects of the mineralogy and petrology of ultramafic xenoliths in kimberlite. *Contributions to Mineralogy and Petrology* **26**, 75-123.

McCandless, T. E. (1999) Kimberlites: Mantle expressions of deep-seated subduction. In: Gurney, J. J., Gurney, J. L., Pascoe, M. D., Richardson, S. H. (Eds) *Proceedings of the VIIth International Kimberlite Conference*, Red Roof Design, Cape Town, **2**, 545-549.

McDade, P. and Harris, J. W. (1999) Syngenetic inclusion bearing diamonds from Letseng-la-Terai, Lesotho. In: Gurney, J. J., Gurney, J. L., Pascoe, M. D., Richardson, S. H. (Eds) *Proceedings of the VIIth International Kimberlite Conference*, Red Roof Design, Cape Town, **2**, 557-565.

McDonough, W. F. (1990) Constraints on the composition of the continental lithospheric mantle. *Earth and Planetary Science Letters* **101**, 1-18.

McKenna, N. (2001) *A study of the diamonds, diamond inclusion minerals and other mantle minerals from the Swartruggens kimberlite, South Africa*. Unpubl. MSc, University of Cape Town, 152pp.

McKenzie, D. and O'Nions, R. K. (1983) Mantle reservoirs and ocean island basalts. *Nature* **301**, 229-231.

Menzies, A.H. (2001) *A detailed investigation into the diamond-bearing xenoliths from Newlands kimberlite, South Africa*. Unpubl. PhD, University of Cape Town, 192pp.

Menzies, M. A., Rogers, N., Tindle, A. and Hawkesworth, C. J. (1987) Metasomatic and enrichment processes in lithospheric peridotites, an effect of asthenosphere – lithosphere interaction. In: Menzies, M. A. and Hawkesworth, C. J. (Eds) *Mantle Metasomatism*, Academic Press, London, 365-313-361.

Mitchell, R. H. and Crocket, J. H. (1971) The isotopic composition of Sr in some South African kimberlites. *Contributions to Mineralogy and Petrology* **30**, 277-290.

Mitchell, R., H. (1986) *Kimberlites: Mineralogy, geochemistry, and petrology*. Plenum Press, New York, 442pp.

Mitchell R. H. (1995) *Kimberlites, orangeites, and related rocks*. Plenum Press, New York, 406pp.

Mitchell, R. H. (2004) Experimental studies at 5-12GPa of the Ondermatjie hypabyssal kimberlite. *Lithos* **76**, 551-564.

Mofokeng, S. W. (1998) *A comparison of the nickel and the conventional geothermometers with respect to the Jagersfontein and the Matsoku kimberlite peridotite xenoliths*. Unpubl. MSc, University of Cape Town, 125pp.

Moore, R. O. and Gurney, J. J. (1985) Pyroxene solid solution in garnets included in diamond. *Nature* **318**, 553-555.

Morris, D. M. (2001) Wimbledon Mine. In: *Tourism on Track: Extracts from the Official Newsletter of Kimberley Publicity*.

Naidoo, P., Stiefenhofer, J., Field, M. and Dobbe, R. (2004) Recent advances in the geology of Koffiefontein Mine, Free State Province, South Africa. *Lithos* **76**, 161-182.

Nelson, D. R., Chivas, A. R., Chappell, B. W. and McCullogh, M. T. (1988) Geochemical and isotopic systematics of carbonatites and implications for the evolution of ocean-island sources. *Geochimica et Cosmochimica Acta* **52**, 1-17.

Neumann, E.-R. and Wulff-Pederson, E. (1997) The origin of highly silicic glass in mantle xenoliths from the Canary Islands. *Journal of Petrology* **38**, 1513-1539.

Nisbet, E. G., Cheadle, M. J., Arndt, N. T. and Bickle, M. J. (1993) Constraining the potential temperature of the Archean mantle: A review of evidence from komatiites. *Lithos* **30**, 291-307.

Nixon, P. H., Boyd, F. R. and Boctor, N. Z. (1983) East Griqualand kimberlites. *Transactions of the Geological Society of South Africa* **86**, 221-236.

Nowell, G. M., Pearson, D. G., Kempton, P. D., Noble, S. R., and Smith, C. B. (1999) Origins of kimberlites: A hafnium perspective. In: Gurney, J. J., Gurney, J. L., Pascoe, M. D., Richardson, S. H. (Eds) *Proceedings of the VIIth International Kimberlite Conference*, Red Roof Design, Cape Town, **2**, 616-624.

Nowell, G. M., Pearson, D. G., Bell, D. R., Carlson, R. W., Smith, C. B., Kempton, P. D. and Noble, S. R. (2004) Hf isotope systematics of kimberlites and their megacrysts: New constraints on their source regions. *Journal of Petrology* **45**, 1583-1612.

Nyblade, A. A. and Pollack, H. N. (1993) A global analysis of heat flow from Precambrian terrains: Implications for the thermal structure of Archean and Proterozoic lithosphere. *Journal of Geophysical Research* **98**, B7, 12207-12218.

O'Brien, H. E. and Tyni, M. (1999) Mineralogy and geochemistry of kimberlites and related rocks from Finland. In: Gurney, J. J., Gurney, J. L., Pascoe, M. D., Richardson, S. H. (Eds) *Proceedings of the VIIth International Kimberlite Conference*, Red Roof Design, Cape Town, **2**, 625-636.

O'Hara, M. J. (1965) Primary magmas and the origin of basalts. *Scottish Journal of Geology* **1**, 19-40.

O'Nions, R. K. and Pankhurst, R. J. (1974) Petrogenetic significance of isotope and trace element variations in volcanic rocks from the mid-Atlantic. *Journal of Petrology* **15**, 603-634.

O'Nions, R. K., Hamilton, P. J. and Evensen, N. M. (1977) Variations in $^{143}Nd/^{144}Nd$ and $^{87}Sr/^{86}Sr$ ratios in oceanic basalts. *Earth and Planetary Science Letters* **34**, 13-22.

O'Nions, R. K., Carter, S., Evenson, W. H. and Hamilton, P. J. (1979) Geochemical and cosmochemical applications of Nd isotope analysis. *Annual Review of Earth and Planetary Sciences* **7**, 11-38.

Parman, S. W., Grove, T. L., Dann, J. C., and de Wit, M. J. (2004) A subduction origin for komatiites and cratonic lithospheric mantle. *South African Journal of Geology* **107**, 107-118.

Pearson, D. G., Rogers, N. W., Irving, A. J., Smith, C. B. and Hawkesworth, C. J. (1995) Source regions of kimberlites and lamproites: Constraints from Re-Os isotopes. *VIth International Kimberlite Conference*, Extended Abstracts, 430-432.

Pearson, D. G., Carlson, R. W., Boyd, F. R., Shirey, S. B., and Nixon, P. H. (1998) Lithospheric mantle growth around cratons: A Re-Os isotope study of peridotite xenoliths from East Griqualand. *VIIth International Kimberlite Conference*, Extended Abstracts, 658-660.

Pearson, D. G. and Nowell, G. M. (2002) The continental lithospheric mantle: characteristics and significance as a mantle reservoir. *Philosophical Transactions of the Royal Society of London* **A360**, 2383-2410.

Pearson, D. G., Nowell, G. M., Dowall, D. P., Kjarsgaard, B. A., Kopylova, M. G., and Armstrong, J. A. (2003) The relative roles of lithosphere and convecting mantle in kimberlites from the Slave Province, NWT: Constraints from Re-Os isotopes and olivine population studies. *VIIIth International Kimberlite Conference*, Extended Abstracts.

Petrological Database of the Ocean Floor (PetDB), Lamont-Doherty Earth Observatory, www.petdb.ldeo.columbia.edu.

Phillips, D., Machin, K. J., Kiviets, G. B. and Fourie, L. F. (1998) A petrographic and $^{40}Ar/^{39}Ar$ geochronological study of the Voorspoed kimberlite, South Africa: Implications for the origin of group II kimberlite magmatism. *South African Journal of Geology* **101**, 299-306.

Phillips, D., Harris, J. W. and Viljoen, K. S. (2004) Mineral chemistry and thermobarometry of inclusions for De Beers pool diamonds, Kimberley, South Africa. *Lithos* **77**, 155-179.

Potts, P. J. (1987) *A handbook of silicate rock analysis*. Blackie Academic and Professional, Glasgow, 622pp.

Price, S. E., Russell, J. K. and Kopylova, M. G. (2000) Primitive magma from the Jericho pipe, N.W.T., Canada: Constraints on primary kimberlite melt chemistry. *Journal of Petrology* **41**, 789-808.

Pretorius, D. A. (1974) The structural boundary between the Kaapvaal craton and the Sanama crustal provinces. *Information Circular of Economic Geology Research Unit*, University of the Witwatersrand, **88**, 26pp.

Pyke, J. (2000) Minerals laboratory staff develops new ICP-MS preparation method. *AGSO Research Newsletter* **33**, 12-14.

Reimold, W. U. and Gibson, R. L. (1996) Geology and evolution of the Vredefort impact structure, South Africa. *Journal of African Earth Sciences* **23**, 125-162.

Richardson, S. H., Gurney, J. J., Erlank, A. J. and Harris, J. W. (1984) Origin of diamonds in old enriched mantle. *Nature* **310**, 198-202.

Richardson, S. H. (1984) Sr, Nd, and O isotope variation in an extensive Karoo dolerite sheet, southern Namibia. In: Erlank, A. J. (Ed) *Petrogenesis of the volcanic rocks of the Karoo Province*. Special Publication of the Geological Society of South Africa, Johannesburg, **13**, 289-293.

Ringwood, A. E., Kesson, S. E., Hibberson, W. and Ware, N. (1992) Origin of kimberlites and related magmas. *Earth and Planetary Science Letters* **113**, 521-538.

Robey, J. v. A. (1981) *Kimberlites of the Central Cape Province, R.S.A.* Unpubl. PhD, University of Cape Town, 261pp.

Roeder, P. L. and Emslie, R. F. (1970) Olivine-liquid equilibrium. *Contributions to Mineralogy and Petrology* **29**, 275-289.

Rogers, N. W., Hawkesworth, C. J. and Palacz, Z. A. (1992) Phlogopite in the generation of olivine melilitites from Namaqualand, South Africa and implications for element fractionation processes in the upper mantle. *Lithos* **28**, 347-365.

Rudnick, R. L., McDonough, W. F. and Chappell, B. W. (1993) Carbonatite metasomatism in the northern Tanzanian mantle: petrographic and geochemical characteristics. *Earth and Planetary Science Letters* **114**, 463-475.

Rudnick, R. L. and Fountain, D. M. (1995) Nature and composition of the continental crust: A lower crustal perspective. *Reviews of Geophysics* **33**, 267-309.

Sato, H. (1977) Nickel content of basaltic magmas: Identification of primary magmas and a measure of the degree of olivine fractionation. *Lithos* **10**, 113-120.

Sato, K., Katsura, T. and Ito, E. (1997) Phase relations in natural phlogopite with and without enstatite up to 8GPa: Implication for mantle metasomatism. *Earth and Planetary Science Letters* **146**, 511-526.

Scott, B. H. (1979) Petrogenesis of kimberlites and potassic lamprophyres from central West Greenland. In: Boyd, F. R. and Meyer, H. O. A. (Eds) *Kimberlites, diatremes and diamonds: Their geology, petrology and geochemistry*, American Geophysical Union, Washington D.C., **1**, 190-205.

Schérsten, A., Elliott, T., Hawkesworth, C., and Norman, M. (2004) Tungsten isotope evidence that mantle plumes contain no contribution from the Earth's core. *Nature* **427**, 234-237.

Schmidt, K. H., Bottazzi, P., Vannucci, R. and Mengel, K. (1999) Trace element partitioning between phlogopite, clinopyroxene and leucite lamproite melt. *Earth and Planetary Science Letters* **168**, 287-299.

Schmitz, M. D. and Bowring, S. A. (2004) Lower crustal granulite formation during Mesoproterozoic Namaqua-Natal collisional orogenesis, southern Africa. *South African Journal of Geology* **107**, 261-284.

Sharp, W. E. (1974) A plate tectonic origin for diamond-bearing kimberlites. *Earth and Planetary Science Letters* **21**, 351-354.

Shaw, D. M. (1970) Trace element fractionation during anatexis. *Geochimica et Cosmochimica Acta* **34**, 237-243.

Shee, S. R. (1985) *The petrogenesis of the Wesselton Mine kimberlites, Kimberley, Cape Province, R.S.A.* Unpubl. PhD, University of Cape Town, 220pp.

Shirey, S. B., Harris, J. W., Richardson, S. H., Fouch, M. J., James, D. E., Cartigny, P., Deines, P. and Viljoen, F. (2002) Diamond genesis, seismic structure, and evolution of the Kaapvaal-Zimbabwe craton. *Science* **297**, 1683-1686.

Simon, N. S. C., Carlson, R. W., Davies, G. R., Nowell, G. M. and Pearson, D. G. (2003a) Os-Sr-Nd-Hf isotope evidence for the ancient depletion and subsequent multi-stage enrichment history of the Kaapvaal cratonic lithosphere. *VIIIth International Kimberlite Conference*, Extended Abstracts.

Simon, N. S. C., Irvine, G. J., Davies, G. R., Pearson, D. G. and Carlson, R. W. (2003b) The origin of garnet and clinopyroxene in "depleted" Kaapvaal peridotites. *Lithos* **71**, 289-322.

Simonetti, A., Bell, K. and Shrady, C. (1997) Trace- and rare-earth-element geochemistry of the June 1993 natrocarbonatite lavas, Oldoinyo Lengai (Tanzania): Implications for the origin of carbonatite magmas. *Journal of Volcanology and Geothermal Research* **75**, 89-106.

Skinner, E. M. W. and Clement, C. R. (1977) Mineralogical classification of South African kimberlites. *IInd International Kimberlite Conference*, Abstracts, Unpaginated.

Skinner, E. M. W. (1989) Contrasting group I and group II kimberlite petrology: Towards a genetic model for kimberlites. In: Ross, J. (Ed) *Kimberlites and Related Rocks: Their composition, occurrence, origin and emplacement*, Geological Society of Australia Special Publication, Perth, **14**, 528-544.

Skinner, E. M. W., Smith, C. B., Viljoen, K. S. and Clark, T. C. (1992) The petrography, tectonic setting and emplacement ages of kimberlites in the south western border region of the Kaapvaal Craton, Prieska area, South Africa. In: Meyer, H. O. A. and Leonardos, O. H. (Eds) *Kimberlites, Related rocks and Mantle Xenoliths*, CPRM, Brazil, 80-97.

Smith, C. B. (1983a) Pb, Sr, and Nd isotopic evidence for sources of southern African Cretaceous kimberlites. *Nature* **304**, 51-54.

Smith, C. B. (1983b) *Rubidium - strontium, uranium - lead and samarium - neodymium isotopic studies of kimberlite and selected mantle-derived xenoliths.* Unpubl. PhD, University of the Witwatersrand, 436pp.

Smith, C. B., Allsopp, H. L., Kramers, J. D., Hutchinson, G. and Roddick, J. C. (1985a) Emplacement ages of Jurassic-Cretaceous South African kimberlites by the Rb-Sr method on phlogopite and whole rock samples. *Transactions of the Geological Society of South Africa* **88**, 249-266.

Smith, C. B., Gurney, J. J., Skinner, E. M. W., Clement, C.R., and Ebrahim, N. (1985b) Geochemical character of Southern African kimberlites: A new approach based on isotopic constraints. *Transactions of the Geological Society of South Africa* **88**, 267-280.

Smith, C. B., Clark, T. C., Barton, E. S., and Bristow, J. W. (1994) Emplacement ages of kimberlite occurrences in the Prieska region, southwest border of the Kaapvaal Craton, South Africa. *Chemical Geology* **113**, 149-169.

Späth, A., le Roex, A. P. and Opiyo-Akech, N. (2001) Plume-lithosphere interaction and the origin of continental rift-related alkaline volcanism - the Chyulu Hills Volcanic Province, Southern Kenya. *Journal of Petrology* **42**, 765-787.

Storey, B. C. (1995) The role of mantle plumes in continental breakup: Case histories from Gondwanaland. *Nature* **377**, 301-308.

Sun, S.-s. and McDonough, W. F. (1989) Chemical and isotopic systematics of oceanic basalts: implications for mantle composition and processes. In: Saunders, A. D. and Norry, M. J. (Eds) *Magmatism in the ocean basins*, Blackwell Scientific Publications, Oxford, 313-345.

Sweeney, R. J., Green, D. H. and Sie, S. H. (1992) Trace and minor element partitioning between garnet and amphibole and carbonatitic melt. *Earth and Planetary Science Letters* **113**, 1-14.

Sweeney, R. J. and Winter, F. (1999) Kimberlites as high-pressure melts: The determination of segregation depth from major element geochemistry. In: Gurney, J. J., Gurney, J. L., Pascoe, M. D., Richardson, S. H. (Eds) *Proceedings of the VIIth International Kimberlite Conference*, Red Roof Design, Cape Town, **2**, 846-851.

Tainton, K. M. (1992) *The petrogenesis of group-2 kimberlites and lamproites from the Northern Cape Province, South Africa*. Unpubl. PhD, University of Cambridge, 263pp.

Tainton, K. M. and McKenzie, D. (1994) The generation of kimberlites, lamproites and their source rocks. *Journal of Petrology* **35**, 787-817.

Tankard, A. J., Jackson, M. P. A., Erikson, K. A., Hobday, D. K., Hunter, D. R. and Minter, W. E. L. (1982) *Crustal evolution of southern Africa: 3.8 billion years of earth history*. Springer-Verlag, New York, 523pp.

Taylor, W. R., Tompkins, L. A. and Haggerty, S. E. (1994) Comparative geochemistry of West African kimberlites: Evidence for a micaceous kimberlite end-member of sublithospheric origin. *Geochimica et Cosmochimica Acta* **58**, 4017-4037.

Thomas, R. J., Agenbacht, A. L. D., Cornell, D. H. and Moore, J. M. (1994) The Kibaren of southern Africa: tectonic evolution and metallogeny. *Ore Geology Reviews* **9**, 131-160.

Tompkins, L. A., Meyer, S. P., Han, Z., Hu, S., Armstrong, R., and Taylor, W. R. (1999) Petrology and geochemistry of kimberlites from Shandong and Liaoning Provinces, China. In: Gurney, J. J., Gurney, J. L., Pascoe, M. D., Richardson, S. H. (Eds) *Proceedings of the VIIth International Kimberlite Conference*, Red Roof Design, Cape Town, **2**, 872-887.

Totland, M., Jarvis, I. and Jarvis, K. E. (1992) An assessment of dissolution techniques for the analysis of geological samples by plasma spectrometry. *Chemical Geology* **95**, 35-62.

Trønnes, R. G. (2002) Stability range and decomposition of potassic richterite and phlogopite end members at 5-15GPa. *Mineralogy and Petrology* **74**, 129-148.

Turner, F. J. and Verhoogen, J. (1960) *Igneous and metamorphic petrology*. McGraw-Hill Book Company, New York, 694pp.

Ulmer, P. and Sweeney, R. J. (2002) Generation and differentiation of group II kimberlites: Constraints from a high-pressure experimental study to 10GPa. *Geochimica et Cosmochimica Acta* **66**, 2139-2153.

van Achterberg, E., Griffin, W. L., and Stiefenhofer, J. (2001) Metasomatism in mantle xenoliths from the Letlhakane kimberlites: estimation of element fluxes. *Contributions to Mineralogy and Petrology* **141**, 397-414.

Viljoen, K. S., Phillips, D., Harris, J. W. and Robinson, D. N. (1999) Mineral inclusions in diamonds from the Venetia kimberlites, Northern Province, South Africa. In: Gurney, J. J., Gurney, J. L., Pascoe, M. D., Richardson, S. H. (Eds) *Proceedings of the VIIth International Kimberlite Conference*, Red Roof Design, Cape Town, **2**, 888-895.

Wagner, P. A. (1914) *The diamond fields of southern Africa*. The Transvaal Lieder, Johannesburg, 346pp.

Walker, R. J., Carlson, R. W., Shirey, S. B. and Boyd, F. R. (1989) Os, Sr, Nd and Pb isotope systematics of southern African peridotite xenoliths: Implications for the chemical evolution of subcontinental mantle. *Geochimica et Cosmochimica Acta* **53**, 1583-1595.

Walter, M. J. (1998) Melting of garnet peridotite and the origin of komatiite and depleted lithosphere. *Journal of Petrology* **39**, 29-60.

Wass, S. Y. and Rogers, N. W. (1980) Mantle metasomatism - precursor to continental alkaline volcanism. *Geochimica et Cosmochimica Acta* **44**, 1811-1823.

Waters, F. G. and Erlank, A. J. (1988) Assessment of the vertical extent and distribution of mantle metasomatism below Kimberley, South Africa. In: Menzies, M. A. and Cox, K. G. (Eds) *Oceanic and continental lithosphere: similarities and differences*, Clarendon Press, Oxford, 185-204.

Weaver, B. L. (1991) The origin of ocean island basalt end-member compositions: Trace element and isotopic constraints. *Earth and Planetary Science Letters* **104**, 381-397.

Wedepohl, K. H. and Muramatsu, Y. (1975) The chemical composition of kimberlites compared with the average composition of three basaltic magma types. In: Boyd, F. R. and Meyer, H. O. A. (Eds) *Kimberlites, diatremes and diamonds: Their geology, petrology and geochemistry*, American Geophysical Union, Washington D.C., **1**, 300-312.

Westerlund, K. (2000) *A geochemical study of diamonds, diamond inclusion minerals and other mantle minerals from the Klipspringer kimberlites, South Africa*. Unpubl. MSc, University of Cape Town, 171pp.

Williams, H. M., Turner, S. P., Pearce, J. A., Kelley, S. P. and Harris, N. B. W. (2004) Nature and source regions for post-collisional, potassic magmas in southern and northern Tibet from geochemical variation and inverse trace element modelling. *Journal of Petrology* **45**, 555-607.

Woodhead, J. D., Eggins, S. M. and Johnson, R. W. (1998) Magma genesis in the New Britain Island Arc: Further insights into melting and mass transfer process. *Journal of Petrology* **39**, 1641-1668.

Woolley, A. R., Bergman, S. C., Edgar, A. D., Le Bas, M. J., Mitchell, R. H., Rock, N. M. S. and Scott Smith, B. H. (1996) Classification of lamprophyres, lamproites, kimberlites and the kalsilitic, melilitic, and leucitic rocks. *The Canadian Mineralogist* **34**, 175-186.

Wyllie, P. J. (1980) The origin of kimberlite. *Journal of Geophysical Research* **85**, B12, 6902-6910.

Xu, X., O'Reilly, S. Y., Griffin, W. L., and Zhou, X. (2003) Enrichment of upper mantle peridotite: petrological, trace element and isotopic evidence in xenoliths from SE China. *Chemical Geology* **198**, 163-188.

Yamashita, H., Arima, M. and Ohtani, E. (1995) High pressure melting experiments on group II kimberlite up to 8GPa: Implications for mantle metasomatism. *VIth International Kimberlite Conference*, Extended Abstracts, 669-671.

Yang, H.-J., Frey, F. A. and Clague, D. A. (2003) Constraints on the source composition of lavas forming the Hawaiian North Arch and Honolulu Volcanics. *Journal of Petrology* **44**, 603-627.

Yaxley, G. M. and Brey, G. P. (2004) Phase relations of carbonate-bearing eclogite assemblages from 2.5 to 5.5GPa: Implications for petrogenesis of carbonatites. *Contributions to Mineralogy and Petrology* **146**, 606-619.

Yu, Z., Robinson, P., and McGoldrick, P. (2001) An evaluation of methods for the chemical decomposition of geological materials for trace element determination using ICP-MS. *Geostandards Newsletter* **25**, 199-217.

Zindler, A. (1980) *Geochemical processes in the Earth's mantle and the nature of crust-mantle interactions: Evidence from studies of Nd and Sr isotope ratios in mantle derived igneous rocks and lherzolite nodules*. Unpubl. PhD, Massachusetts Institute of Technology, 263pp.

Zwane, N. (2001) *Petrographic study of the Limeacres kimberlites, Northern Cape*. Unpubl. Hons, University of Cape Town, 76pp.

APPENDIX A

DESCRIPTION OF INDIVIDUAL KIMBERLITES

A.1 Group I kimberlites

A.1.1 On-craton kimberlites

Goedehoop kimberlite

The Goedehoop kimberlite is located north of the town of Hanover in the Northern Cape Province. The group of kimberlites consists of three pipes, two blows and associated dykes (Robey, 1981). Although a dyke-like excavation, filled in pit, numerous crustal and mantle xenoliths were located during this study (30^{0}50'S, 24^{0}25'E'), no fresh kimberlite was found. The kimberlite has intruded through the Beaufort Group shales and sandstones, and if the trace of the Archean Kaapvaal craton margin of Schmitz and Bowring (2004) is extrapolated (Figure 2.2), it appears as though the Goedehoop kimberlite has been emplaced through the Kaapvaal craton. This is consistent with the occurrence of a single diamond from the nearby Andriesfontein kimberlite (Robey, 1981), situated just southeast of the Goedehoop kimberlite and suggests the Goedehoop kimberlite has intruded through Archean basement (Clifford, 1966).

Koffiefontein kimberlite

The Koffiefontein kimberlite is situated in the town of Koffiefontein in the Free State Province. The pipe measuring 11.1Ha (Naidoo *et al.*, 2004), was discovered in 1870 and although it is currently being mined, has had an intermittent mining history. The Koffiefontein kimberlite occurrence consists of a pipe with east and west precursor dykes, as well as the satellite Ebenhaezer pipe (Clement, 1982). The main pipe has been dated at 90Ma by Davis (1978) and has intruded through Archean basement granite gneiss, Dwyka shale and Karoo dolerite.

A.1.2 Off-craton kimberlites

Abbotsford East kimberlite

The Abbotsford kimberlite, a member of the East Griqualand kimberlite province, is situated just west of the town of Cedarville in the Kwazulu-Natal Province. The kimberlite consists of five dykes and two pipes (Abbotsford East and Abbotsford West) and was described many years ago by Du Toit (1929). Abbotsford East is an elongate pipe measuring approximately 35 x 20m (Nixon *et al.*, 1983). Ages for other kimberlites from the East Griqualand kimberlite province are ~150Ma (Smith *et al.*, 1985a; Davis, 1977). The kimberlite has intruded through the Namaqua-Natal mobile belt as well as Beaufort Group shale, sandstone and Stormberg lavas of the Karoo flood basalt province.

Klipgatsfontein kimberlite

The Klipgatsfontein kimberlite is located northeast of the town Loxton in the Northern Cape Province. The kimberlite occurrence consists of a southern and a northern group, each of which have two pipes and an associated fissure (Robey, 1981). The kimberlite has intruded through Beaufort shales, mudstones and sandstones underlain by the Namaqua-Natal mobile belt basement.

Hebron kimberlite

The Hebron kimberlite ($31^{0}17'S$, $22^{0}34'E$) is located on the farm Haartebeesfontein, northeast of the town of Loxton in the Northern Cape Province. This occurrence consists of five sites where kimberlite is present (Robey, 1981), as well as other recordings on the adjacent farms Leyfontein and Haartebeeskuilen. The main Hebron pipe measuring 150 x 75m (Robey, 1981) has an associated pit and numerous dumps of kimberlite concentrate, that were observed when the kimberlite was visited in the course of this study. Kimberlite analysed in this study was sampled from the main Hebron pit. Geochemical analyses (Clark, 1994) and a 76Ma Rb-Sr age (Smith *et al.*, 1994) reported for the Haartebeesfontein kimberlite may be from the same location, but due to the confusion regarding nomenclature of the kimberlite cluster, it has not been assumed that this is the same kimberlite. The kimberlite has intruded through Beaufort shales and sandstones underlain by the Namaqua-Natal belt.

Uintjiesberg kimberlite

The Uintjiesberg kimberlite ($30^{0}50'S$, $22^{0}32'E$) is situated at the foothills of the Uintjiesberg Mountain, located west of the town Carnarvon in the Northern Cape Province. The kimberlite consists of a 180 x 120m pipe, as well as a dyke (Robey, 1981) and was first described by Du Toit (1914). Although much of the kimberlite consists of yellow ground that has been pitted, abundant fresh hypabyssal facies material (geochemically analysed by Harris *et al.*, 2004) was observed when the kimberlite was visited in the course of this study. Smith *et al.* (1985a) have reported a Rb-Sr age of 101Ma for this kimberlite that has intruded through Ecca Group shales, Karoo dolerites underlain by the Namaqua-Natal belt.

Zeekoegat kimberlite

The Zeekoegat kimberlite, a member of the East Griqualand kimberlite province, is situated just west of the town of Cedarville in the Kwazulu-Natal Province. The Zeekoegat kimberlite pipe measures approximately 400m across (Du Toit, 1929) and appears to be related to the nearby Abbotsford dykes (Nixon *et al.*, 1983). Ages for other kimberlites from the East Griqualand kimberlite province are ~150Ma (Smith *et al.*, 1985a; Davis, 1977). The kimberlite has intruded through the Namaqua-Natal mobile belt as well as Beaufort Group shales, sandstones and Stormberg lavas from the Karoo flood basalt province.

A.2 Group II kimberlites

A.2.1 On-craton kimberlites

Bellsbank kimberlite

Bellsbank kimberlite dyke is one of a set of northeast striking *en echelon* dykes that form the Bellsbank (Main), Bobbejaan, and Intermediate (Water) fissures (Tainton, 1992). The kimberlites are situated northwest of the town of Barkly West in the Northern Cape Province and form part of the Barkly West kimberlite group. Three blows have developed on the Bellsbank fissure and a fourth on the adjacent Kosmos fissure. The dykes are generally less than 1m wide and strike for several kilometres (Gurney & Menzies, 1998). The kimberlite was discovered in 1952 and various small mines have been in operation since then. The 122Ma kimberlite (Smith *et al*, 1985a) has intruded through the Griqualand West Sequence, Campbell Rand dolomite and Black Reef Formation, as well as Archean crystalline basement.

New Elands kimberlite

The New Elands kimberlite is situated east of the town of Boshof in the Free State Province and forms part of the Boshof cluster of kimberlites. The kimberlite consists of two dykes that intersect to form a blow (Wagner, 1914). New Elands was discovered in 1912 and like so many other small dykes in South Africa has had a history of intermittent mining. The 126 Ma kimberlite (Smith *et al.*, 1985a) has intruded through Karoo shales and sandstones underlain by Archean basement. Isotope analyses by Smith (1983a) for the New Elands kimberlite have been utilised for some of the samples in this study.

Newlands kimberlite

Newlands kimberlite is situated northwest of the town of Barkly West and forms part of the Barkly West kimberlite group in the Northern Cape Province. Newlands kimberlite is a northeast striking dyke system with five blows developed along the *en-echelon* dykes (Gurney & Menzies, 1998). Discovered in the late nineteenth century, it has been mined during various periods since then. The Newlands kimberlite, dated at 114Ma (Smith *et al.*, 1985a), has intruded through a Tertiary Kalahari Group calcrete veneer, Karoo dolerites and shales, and Ventersdorp lavas, underlain by Archean basement.

A.2.2 Off-craton kimberlites

Brandewynskuil kimberlite

Brandewynskuil kimberlite is situated 20km southwest of the town of Vosburg in the Northern Cape Province. Fresh kimberlite was not found when the kimberlite was visited in the course of this study ($30^{0}37'$S, $22^{0}41'$E), but evidence for the presence of kimberlite, in the form of numerous crustal xenoliths, a pit and kimberlite grass, were all found together. Two kimberlite pipes measuring 180 x 120m and 90 x 130m as well as a dyke have been recorded for this kimberlite (Robey, 1981). The kimberlite has intruded through Ecca Group shales and sandstones underlain by the Proterozoic Namaqua-Natal belt (Schmitz & Bowing, 2004) and is located in an area surrounded by numerous Karoo dolerite dykes.

Eendekuil kimberlite

The Eendekuil kimberlite (32°15'S, 20°59'E) is situated just west of the Riet River on the farm Eendekuil, approximately 40km northeast of the town of Sutherland in the Northern Cape Province. A trench, pit, borehole and dumps of crushed kimberlite were observed when the kimberlite was visited during this study and within the pit, the weathered yellow ground of a 1.5m wide kimberlite dyke was clearly visible. The Eendekuil kimberlite, dated at 110Ma (Allsopp, Unpubl. in Skinner, 1989), is also the youngest known group II kimberlite occurrence in southern Africa. The kimberlite has intruded through the Beaufort Group shales underlain by the Proterozoic Namaqua-Natal belt.

Markt kimberlite

The Markt kimberlite is located northwest of the town Vosburg. The kimberlite occurrence consists of two pipes as well as a blow associated with the intersection of two fissures. (Robey, 1981) The kimberlite has been dated at 117Ma (Smith *et al*, 1994) and has intruded through Ecca shales and sandstones as well as through Proterozoic rocks of the Namaqua-Natal belt (Schmitz & Bowring, 2004).

A.3 Transitional kimberlites

A.3.1 On-craton kimberlites

Leicester kimberlite

Leicester kimberlite pipe is situated southwest of the town of Windsorton in the Northern Cape Province. Mining of the Leicester kimberlite commenced in 1896 and has been intermittent since then. The pear shaped pipe measures 300 x 200m across (J.J. Gurney, pers. comm., 2003) and has been dated at 92Ma by Davis (1978). The kimberlite has intruded through Archean crystalline basement and at its surface exposure, is surrounded by Dwyka tillite.

Wimbledon kimberlite

Wimbledon kimberlite (28°49'S, 24°43'E) occurs 15km south of the town of Kimberley in the Northern Cape Province. The existence of the Wimbledon kimberlite appears to have been known of for many years and was mined in the late 19th century as the Spytfontein mine (Wagner, 1914). Wimbledon kimberlite consists of two pipes (Morris, 2001) and recent workings in a dolerite quarry uncovered a newer pipe. Fresh hypabyssal kimberlite was sampled when the pipe was visited during this study, from a pile of kimberlite adjacent to the main pipe. No previous published geochemical analyses or dates of the kimberlite appear to exist. Wimbledon kimberlite has intruded through Dwyka shale and Karoo dolerite underlain by Archean basement.

A3.2 Off-craton kimberlites

Droogfontein kimberlite

Droogfontein kimberlite is located southwest of the town of Loxton in the Northern Cape Province. Although little is known of the details of the kimberlite dyke, the Droogfontein kimberlite does appear on Wagner's (1914) map of kimberlites in South Africa. According to Smith *et al.* (1994), the older

174Ma Rb-Sr age of the kimberlite is considered more reliable than its U-Pb age of 100-150Ma. The kimberlite has intruded through Beaufort Group shales and sandstones and Proterozoic rocks of the Namaqua-Natal belt.

Melton Wold kimberlite

Melton Wold kimberlite (31^{0}30'S, 22^{0}45'E) is situated west of the town of Victoria West in the Northern Cape Province. The kidney shaped pipe is associated with a northerly striking main fissure (Robey, 1981). Much of the kimberlite is now weathered yellow ground, but late stage hypabyssal dykes that cross-cut the kimberlite were observed when the kimberlite was visited. Accompanying fissures were also identified by bush lineations in the surrounding countryside and kimberlite sample *MLW 4*, represents one of these fissures. The kimberlite has been dated 144Ma by Smith *et al.* (1994) and intrudes through the Beaufort Group and Proterozoic Namaqua-Natal belt.

Silvery Home kimberlite

The Silvery Home kimberlite located at 31^{0}34'S, 22^{0}16'E and visited in the course of this study occurs 10km southwest of the town of Loxton in the Northern Cape Province. The Silvery Home kimberlite described by Robey (1981) is a northward striking dyke with blows developed at either end and occurs on the Silvery Home farm. The kimberlite visited and sampled in this study however, occurs on the neighbouring Nuwelande homestead, but since both petrographic varieties of kimberlite reported by Robey (1981) were present on the Nuwelande farm, it was concluded that this was likely a continuation of the Silvery Home kimberlite. At this locality a trench within the dyke, borehole, and dumps were present. Fresh black, aphanitic kimberlite as well as weathered phlogopite diopside kimberlite was found in the trench. The dyke is approximately 5m wide and a bush lineation marked the strike of the dyke that when traversed, revealed some brecciated country rock contacts. The kimberlite has intruded through Beaufort Group country rock underlain by the Namaqua-Natal mobile belt.

APPENDIX B

PETROGRAPHY OF KIMBERLITE SAMPLES

B.1 Group I kimberlites

B.1.1 On-Craton kimberlites

Kimberlite		Macrocrysts	Phenocrysts	Matrix
Goedehoop kimberlite	JAR 30012	*Olivine* (10%) – Anhedral macrocrysts, 5mm, serpentinised rims. *Phlogopite* (10%) – Subhedral outline of macrocryst, 1mm, rims carbonatised and studded with opaque oxides. Fresh phlogopite core, calcite stringers along cleavage planes.	*Olivine* (30%) – Euhedral to subhedral phenocrysts and microphenocrysts, serpentinised along fractures, some carbonatisation along rims, greater than 200µm in size.	*Calcite* (25%) – Interstitial calcite and individual crystals occur. *Serpentine* (15%) – Interstitial *Opaque oxides* (5%) – Euhedral to subhedral crystals, 100µm. Some irregular aggregates 500µm in size. *Perovskite* (2%) – Euhedral crystals, 100µm.
Classification	Serpentine calcite kimberlite			
Texture	sparsely macrocrystic			
Goedehoop kimberlite	JJG 4282	*Olivine* (10%) – Anhedral macrocrysts, 4mm serpentinised fractures. *Phlogopite* (5%) – Macrocrysts have a euhedral carbonatised rim studded with opaque oxides. Most macrocrysts replaced except one with a fresh phlogopite core.	*Olivine* (30%) – Euhedral to subhedral phenocrysts and microphenocrysts, serpentinised with carbonatised rims, some fresh cores.	*Calcite* (29%) – Interstitial *Serpentine* (20%) – Interstitial *Opaque oxides* (4%) – Euhedral to subhedral crystals, 100µm. Some irregular aggregates 500µm. *Perovskite* (2%) – Euhedral crystals, 100µm. *Apatite* (trace) – Euhedral needles, 100µm
Classification	Serpentine calcite kimberlite			
Texture	sparsely macrocrystic			

Kimberlite		Macrocrysts	Phenocrysts	Matrix
Koffiefontein kimberlite	KK 3	*Olivine* (15%) – Anhedral, heavily serpentinised macrocrysts. Some sparse patches of fresh olivine remain.	*Olivine* (30%) – Euhedral phenocrysts and microphenocrysts, completely serpentinised, greater than 200µm in size.	*Calcite* (25%) – Interstitial and segregationary. Calcite-serpentine segregations 1mm. *Serpentine* (17%) – Interstitial and segregationary. *Phlogopite* (5%) – Stubby laths, 300µm. *Opaque oxides* (5%) – Euhedral crystals, 50-100µm with atoll-spinel texture. *Perovskite* (2%) – Subhedral crystals often occuring in aggregates, 250µm. *Apatite* (1%) – Euhedral laths, 300µm.
Classification	Serpentine calcite kimberlite			
Texture	macrocrystic			

Koffiefontein kimberlite	KK 5	*Olivine* (17%) – Anhedral macrocrysts 5-6mm, almost entirely serpentinised. *Phlogopite* (3%) – Subhedral macrocrysts, 5mm, opaque oxide and perovskite studded rims.	*Olivine* (30%) – Subhedral to anhedral phenocrysts and microphenocrysts, completely serpentinised, greater than 200µm in size.	*Calcite* (20%) – Interstitial and segregationary. Segregations rimmed with perovskite. *Serpentine* (17%) – Interstitial and segregationary with calcite. *Phlogopite* (5%) – Stubby microphenocrysts, 100-200µm. *Opaque oxides* (5%) – Euhedral crystals, 50µm. *Perovskite* (2%) – Anhedral crystals, 300-500µm, often occurring in aggregates. *Apatite* (1%) – Euhedral laths, 300µm.
Classification	Serpentine calcite kimberlite			
Texture	macrocrystic			
Koffiefontein kimberlite	KK 6	*Olivine* (20%) – Anhedral macrocrysts, 10mm, completely serpentinised, rimmed with opaque oxides. *Phlogopite* (5%) – Serpentinised exteriors, calcitised interiors, some fresh cores, and opaque oxide rimmed macrocrysts.	*Olivine* (25%) – Subhedral phenocrysts and microphenocrysts, completely serpentinised, rims studded with opaque oxides.	*Calcite* (20%) – Interstitial and segregationary, 1-2mm. *Serpentine* (17%) – Interstitial and segregationary with calcite. *Phlogopite* (5%) – Equant laths, 300µm. *Opaque oxides* (5%) – Euhedral crystals, 50µm. *Perovskite* (2%) – Anhedral crystals, 200-300µm, often occurring in aggregates. *Apatite* (1%) – Euhedral needles, 100µm.
Classification	Serpentine calcite kimberlite			
Texture	macrocrystic			

B.1.2 Off-craton kimberlites

Kimberlite		Macrocrysts	Phenocrysts	Matrix
Abbotsford East kimberlite	JJG 3118	*Olivine* (10%) – Anhedral macrocrysts, serpentinised and chloritised, 5mm.	*Olivine* (10%) – Anhedral and serpentinised phenocrysts, chloritised with opaque mineral rim.	*Calcite* (45%) – Interstitial. *Serpentine* (20%) – Interstitial. *Phlogopite* (8%) – Some possible altered laths with opaque oxide rims, 150µm. *Opaque Oxides* (5%) – Euhedral crystals, 100µm. *Perovskite* (2%) – Subhedral crystals, 100µm.
Classification	Calcite kimberlite			
Texture	sparsely macrocrystic			

Kimberlite		Macrocrysts	Phenocrysts	Matrix
Hebron kimberlite	HEB 1A	*Phlogopite* (13%) – Tabular macrocrysts, 4mm, altered to calcite, opaque oxide rims. *Olivine* (7%) – Anhedral macrocrysts, 3mm, carbonatised interiors and serpentinised exteriors, poikolitically encloses opaque oxides. *Ilmenite* (5%) - Irregular and discontinuous, perovskite aggregation on macrocryst edges.	*Olivine* (15%) – Anhedral phenocrysts and microphenocrysts, serpentinised, carbonatised interiors.	*Calcite* (39%) – Interstitial and segregationary, well developed rhombohedral crystals, 100-500µm occur in 1-2mm segregations. *Serpentine* (24%) – Interstitial *Opaque oxides* (4%) – Euhedral crystals, 20-100µm, perovskite overgrowths form an atoll texture. *Perovskite* (2%) Euhedral and subhedral crystals, 100µm. *Apatite* (trace) – Euhedral needles, 100µm
Classification	Serpentine calcite kimberlite			
Texture	macrocrystic			
Hebron kimberlite	HEB 1B	*Same as HEB 1A*	*Same as HEB 1A*	Same as HEB 1A
Hebron kimberlite	JJG 4295	*Olivine* (17%) Anhedral macrocrysts, 5mm, serpentinised, some fresh cores remain, opaque oxide rims. *Ilmenite* (8%) - Euhedral to subhedral macrocrysts, 3mm. *Phlogopite* (6%) – Subhedral macrocrysts, 8mm, kink banding, calcite stringers	*Olivine* (17%) – Euhedral to subhedral phenocrysts and microphenocrysts, serpentinised, opaque oxide rims. *Phlogopite* (6%) – Subhedral phenocrysts, some with strong pleochroism	*Calcite* (20%) – Interstitial and segregationary, some well developed rhombohedral crystals in 1-2mm segregations *Serpentine* (15%) – Interstitial *Opaque oxides* (6%) Subhedral crystals, 100µm *Phlogopite* (3%) – Colourless, euhedral, skeletal crystals, 100-300µm. *Perovskite* (1%) – Anhedral crystals, 50µm.
Classification	Serpentine calcite kimberlite			
Texture	macrocrystic			

Kimberlite		Macrocrysts	Phenocrysts	Matrix
Klipgatsfontein kimberlite	JAR 31012	*Phlogopite* (13%) – Anhedral macrocrysts, 5mm bright orange in colour, kink banding, calcite stringers with opaque oxide rims. *Olivine* (7%) – Anhedral macrocrysts, 3mm, serpentinised rims and fractures. *Ilmenite* (5%) – 3mm aggregate of anhedral opaque oxides and calcite stringers.	*Olivine* (20%) – Relict euhedral outline of phenocrysts and microphenocrysts, rims and fractures are all serpentinised.	*Calcite* (30%) – Interstitial and segregationary, individual rhombohedral 500µm crystals in 1-3mm segregations. *Serpentine* (19%) –Interstitial serpentine. *Opaque oxides* (4%) – Euhedral crystals 100µm. *Perovksite* (2%) – Subhedral crystals, 100µm.
Classification	Serpentine calcite kimberlite			
Texture	macrocrystic			
Klipgatsfontein kimberlite	KGF 1	*Olivine* (7%) – Anhedral, serpentinised rims. *Phlogopite* (17%) – Elongate and irregular shaped macrocrysts, bright orange in colour, with opaque oxide rims. *Ilmenite* (5%) – Euhedral to anhedral	*Olivine* (21%) – Euhedral to subhedral phenocrysts and microphenocrysts, serpentinised rims.	*Calcite* (30%) – Interstitial and segregationary, individual rhombohedral 400µm crystals in 1-2mm segregations. *Serpentine* (14%) – Occurs as rims around calcite segregations.
Classification	Serpentine calcite kimberlite			

Texture	macrocrystic	macrocrysts, perovskite nucleation on rims.		*Opaque oxides* (5%) – Euhedral crystals, 100µm. *Perovskite* (1%) – Rounded crystals, 50µm.
Klipgatsfontein kimberlite	JJG 4323	*Phlogopite* (17%) – Anhedral macrocrysts, bight orange in colour with opaque oxide rims and calcite stringers. *Olivine* (5%) – Anhedral, 3mm, serpentinised rims and fractures. *Ilmenite* (5%) – Anhedral macrocrysts, perovskite nucleation on rims.	*Olivine* (23%) – Subhedral phenocrysts and microphenocrysts, serpentinised rims and fractures	*Calcite* (25%) – Interstitial and segregationary, individual rhombohedral 200µm crystals in 1-2mm segregations. *Serpentine* (19%) – Interstitial. *Opaque oxides* (5%) - Subhedral crystals, 100µm. *Perovskite* (1%) – Anhedral crystals, 20-50µm.
Classification	Serpentine calcite kimberlite			
Texture	sparsely macrocrystic			

Kimberlite		**Macrocrysts**	**Phenocrysts**	**Matrix**
Zeekoegat kimberlite	JJG 1906	*Olivine* (15%) – Anhedral macrocrysts, serpentinised interiors, opaque oxide rims, 8mm. Few macrocrysts have fresh cores.	*Olivine* (15%) – Anhedral phenocrysts and microphenocrysts, greater than 400µm, serpentinised interiors, opaque oxide rims.	*Calcite* (35%) – Interstitial *Serpentine* (20%) – Interstitial *Phlogopite* (5%) – Altered laths with opaque oxide rims, 150µm. *Opaque Oxides* (5%) - Euhedral crystals, 100µm. *Perovskite* (2%) - Subhedral crystals, 50-100µm.
Classification	Calcite kimberlite			
Texture	macrocrystic			

B.2 Group II kimberlites

B.2.1 On-craton kimberlites

Kimberlite		**Macrocrysts**	**Phenocrysts**	**Matrix**
Bellsbank kimberlite	JJG 4676	*Olivine* (25%) – Anhedral macrocrysts, 8mm, serpentinisation along fractures. *Phlogopite* (5%) – Tabular macrocrysts, kink banding and tetraferriphlogopite rims.	*Olivine* (10%) – Anhedral phenocrysts and microphenocrysts, serpentinised rims.	*Phlogopite* (30%) –Stubby interlocking crystals, 50µm. *Calcite* (15%) – Interstitial calcite *Serpentine* (10%) - Interstitial *Opaque oxides* (2%) – Euhedral microphenocrysts, 20µm. *Apatite* (2%) - Euhedral needles, 250µm. *Perovskite* (1%) – Anhedral crystals, 20µm.
Classification	Calcite phlogopite kimberlite			
Texture	macrocrystic			
Bellsbank kimberlite	KBEL 2	*No thin section available*	*No thin section available*	*No thin section available*

Kimberlite		Macrocrysts	Phenocrysts	Matrix
New Elands kimberlite	NE K6	*Olivine* (10%) Anhedral macrocrysts, 8mm, completely serpentinised.	*Olivine* (35%) – Subhedral phenocrysts, completely serpentinised, some calcitisation in interiors	*Phlogopite* (30%) – Euhedral, interlocking, 500µm, equant microphenocrysts, opaque oxide and perovskite inclusions. *Calcite* (22%) – Interstitial, some individual 500µm rhombs in segregations. *Opaque oxides* (1%) - Subhedral crystals, 20µm. *Perovskite* (1%) Subhedral crystals, 20µm. *Apatite* (1%) – Subhedral needles, 500µm.
Classification	Calcite phlogopite kimberlite			
Texture	sparsely macrocrystic			
New Elands kimberlite	NE K10	*Same as NE K6*	*Same as NE K6*	*Same as NE K6*
New Elands kimberlite	NE K11	*Olivine* (20%) – Anhedral macrocrysts, 8mm, serpentinised, some calcitised patches.	*Olivine* (11%) – Anhedral phenocrysts and microphenocrysts, completely serpentinised. *Phlogopite* (3%) – Subhedral laths, tetraferri-phlogopite rims.	*Phlogopite* (27%) – Interlocking, equant microphenocrysts, tetraferriphlogopite rims. *Serpentine* (20%) - Interstitial *Diopside* (15%) – Anhedral crystals, 300µm although some 1mm clusters do occur. *Opaque oxides* (1%) Anhedral crystals, 20µm. *Perovskite* (1%) – Euhedral crystals, 20µm.
Classification	Serpentine phlogopite kimberlite			
Texture	macrocrystic			

Kimberlite		Macrocrysts	Phenocrysts	Matrix
Newlands kimberlite	JJG 24	*Olivine* (19%) – Subhedral macrocrysts, 8mm, serpentinisation along fractures, opaque oxide rimmed edges. *Phlogopite* (5%) Elongate laths, strong pleochroism, green chlorite rim. *Garnet* (0.5%) – Two anhedral garnet macrocrysts, 2mm. One has a kelyphite rim and the other a chlorite rim. *Opaque oxide* (0.5%) - Single subhedral macrocryst	*Olivine* (20%) – Subhedral to anhedral phenocrysts and microphenocrysts, serpentinised fractures	*Phlogopite* (30%) - Interlocking chloritised laths, 100µm *Serpentine* (12%) – Interstitial and segregationary. *Calcite* (10%) – Interstitial and segregationary. *Opaque oxides* (2%) - Euhedral crystals, 20-100µm. *Perovskite* (1%) – Euhedral crystals, 20µm *Apatite* (trace)
Classification	Phlogopite kimberlite			
Texture	macrocrystic			
Newlands kimberlite	JJG 6198	*Olivine* (8%) - Subhedral to anhedral macrocrysts, 12mm, serpentinised fractures. *Phlogopite* (14%) – Elongate macrocrysts, 2mm, kink banding with undulose extinction, green chlorite rim. *Opaque Oxide* (1%) – Subhedral macrocrysts	*Olivine* (10%) – Anhedral phenocrysts and microphenocrysts, opaque oxide interiors, serpentine rims.	*Phlogopite* (25%) – Interlocking, chloritised crystals, 100µm. *Serpentine* (10%) - Interstitial *Calcite* (8%) - Interstitial *Opaque oxides* (2%) - Euhedral crystals, 20µm *Perovskite* (1%) – Euhedral crystals, 20um *Apatite* (trace).
Classification	Phlogopite kimberlite			
Texture	macrocrystic			

Newlands kimberlite	KN 2	*Olivine* (29%) – Anhedral macrocysts, 6mm, serpentinised fractures. *Phlogopite* (5%) - Elongate macrocysts that show undulose extinction and kink banding. *Garnet* (1%) – Single anhedral macrocyst, 8mm, serpentine rim.	*Olivine* (15%) – Subhedral phenocrysts and microphenocrysts with serpentinisation along fractures	*Phlogopite* (25%) - Equant crystals, 100µm. *Serpentine* (12%) - Interstitial *Calcite* (10%) – Interstitial *Opaque oxides* (2%) – Euhedral crystals. *Perovskite* (1%) – Sparse euhedral crystals *Apatite* (trace).
Classification	Phlogopite kimberlite			
Texture	macrocrystic			
Newlands kimberlite	KN 3	*Olivine* (25%) – Anhedral olivine macrocrysts 7-8mm in size with serpentinised fractures. *Phlogopite* (5%) - Elongate macrocrysts that show undulose extinction and green pleochroic rims.	*Olivine* (15%) – Subhedral phenocrysts and microphenocrysts with serpentinised fractures.	*Phlogopite* (30%) – Stubby interlocking crystals *Serpentine* (12%) - Interstitial *Calcite* (10%) – Interstitial *Opaque oxides* (2%) – Euhedral crystals. *Perovskite* (1%) – Sparse euhedral crystals *Apatite* (trace).
Classification	Phlogopite kimberlite			
Texture	macrocrystic			

B.2.2 Off-craton kimberlites

Kimberlite		Macrocrysts	Phenocrysts	Matrix
Brandewyns-kuil kimberlite	K6/8	*Olivine* (15%) - Anhedral macrocrysts, completely serpentinised, some phlogopite replacement in patches, aggregation of ground mass phlogopite around macrocryst rims. *Phlogopite* (10%) – Tabular, deformed macrocrysts, kink banding, tetraferriphlogopite rims.	*Olivine* (20%) – Subhedral to anhedral phenocrysts and microphenocrysts, completely serpentinised, aggregation of phlogopite around rims *Phlogopite* (5%) - Phenocrysts with tetraferri phlogopite rims.	*Phlogopite* (25%) – Acicular laths with tetraferri-phlogopite rims, 100µm *Serpentine* (15%) – Segregationary *Diopside* (5%) – Subhedral to anhedral crystals, may have lath shape, 100-400µm. *Opaque Oxides* (1%) – Equant crystals, 10µm *Perovskite* (trace) – Anhedral crystals, 10µm.
Classification	Serpentine phlogopite kimberlite			
Texture	macrocrystic			
Brandewyns-kuil kimberlite	K6/11	*Olivine* (15%) - Anhedral macrocrysts, completely serpentinised, some phlogopite replacement in patches, aggregation of ground mass phlogopite around macrocryst rims. *Phlogopite* (10%) - Tabular, deformed macrocrysts, kink banding, tetraferriphlogopite rims.	*Olivine* (20%) – Subhedral to anhedral phenocrysts and microphenocrysts, completely serpentinised, aggregation of phlogopite around rims. *Phlogopite* (5%) - Phenocrysts with tetraferri-phlogopite rims.	*Phlogopite* (25%) – Acicular laths with tetraferri - phlogopite rims, 100µm. *Serpentine* (15%) - Segregationary *Diopside* (5%) – Subhedral to anhedral crystals, may have lath shape, 100-400µm. *Opaque Oxides* (1%) – Equant crystals, 10µm. *Perovskite* (trace) – Anhedral crystals, 10µm.
Classification	Serpentine phlogopite kimberlite			
Texture	macrocrystic			

Brandewyns-kuil kimberlite Classification	K6/12 Phlogopite serpentine diopside kimberlite	*Olivine* (20%) – Anhedral macrocrysts, completely serpentinised, some phlogopite replacement in patches, aggregation of ground mass phlogopite around macrocryst rims. *Phlogopite* (10%) – Tabular, deformed macrocrysts, kink banding, tetraferriphlogopite rims. *Note: Some irregular shaped possible micro-xenoliths also occur*	*Olivine* (15%) – Subhedral to anhedral phenocrysts and microphenocrysts, completely serpentinised, aggregation of phlogopite around rims.	*Diopside* (20%) – Euhedral laths, 10-20µm. *Phlogopite* (15%) – Acicular laths with tetraferriphlogopite rims, 20µm. *Serpentine* (14%) – Interstitial. *Opaque Oxides* (1%) – Equant crystals, 10µm. *Perovskite* (trace) – Anhedral crystals, 10µm.
Texture	macrocrystic			
Brandewyns-kuil kimberlite	K6/14	Same as K6/12	Same as K6/12	Same as K6/12

Kimberlite		**Macrocrysts**	**Phenocrysts**	**Matrix**
Eendekuil kimberlite Classification	EKL 1 Calcite phlogopite kimberlite	*Phlogopite* (20%) –Deformed macrocrysts with calcite and opaque oxide mineral stringers. Tetraferriphlogopite, chloritised rims. *Olivine* (5%) – Subhedral, up to 6mm, serpentinised fractures with fresh cores remaining.	*Phlogopite* (20%) – Abundant calcite and opaque oxide mineral stringers, chloritised rims. *Olivine* (5%) – Subhedral, serpentinised fractures with fresh cores remaining. *Diopside* (5%) – Subhedral phenocrysts, heavily fractured.	*Phlogopite* (22%) – Tabular, interlocking laths, tetraferriphlogopite, 100µm. *Calcite* (20%) – Interstitial and rhombic crystals. *Opaque oxides* (2%) – Equant crystals, 50-100µm. *Perovskite* (1%) – Anhedral crystals, 50µm.
Texture	macrocrystic			
Eendekuil kimberlite Classification	K2/2 Phlogopite calcite kimberlite	*Phlogopite* (20%) –Deformed macrocrysts with calcite and opaque oxide mineral stringers. Tetraferriphlogopite, chloritised rims. *Olivine* (5%) – Anhedral macrocrysts, 3mm, completely serpentinised.	*Phlogopite* (20%) – Abundant calcite and opaque oxide mineral stringers, some chloritised rims and interiors of phenocrysts. *Olivine* (5%) – Subhedral phenocrysts, completely serpentinised.	*Phlogopite* (27%) – Tabular, interlocking laths, tetraferriphlogopite rims, some chloritisation of crystals, 100µm. *Calcite* (20%) – Interstitial. *Opaque oxides* (2%) - Equant crystals, 50-100µm. *Perovskite* (1%) – Anhedral crystals, 50µm.
Texture	macrocrystic			
Eendekuil kimberlite Classification	K2/3 Calcite phlogopite kimberlite	*Phlogopite* (20%) –Deformed macrocrysts with calcite and opaque oxide mineral stringers. Tetraferriphlogopite, chloritised rims. *Olivine* (10%) – Anhedral macrocrysts, 3mm, completely serpentinised.	*Phlogopite* (10%) – Abundant calcite and opaque oxide mineral stringers, some chloritised rims and interiors of phenocrysts. *Olivine* (5%) – Subhedral phenocrysts, completely serpentinised.	*Phlogopite* (20%) – Tabular, interlocking laths, tetraferriphlogopite rims, some chloritisation of crystals, 100µm. *Calcite* (24%) – Interstitial but also occurs in segregations up to 4mm in size. *Serpentine* (8%) Interstitial with radial texture. *Opaque oxides* (2%) - Equant crystals, 50-100µm. *Perovskite* (1%) – Anhedral crystals, 50µm.
Texture	macrocrystic			

Eendekuil kimberlite	K2/6	*Same as K2/3*	*Same as K2/3*	*Same as K2/3*
Eendekuil kimberlite	K2/9	*Same as K2/3 but slightly more altered, cross cutting quartz veins also occur.*	*Same as K2/3 but slightly more altered, cross cutting quartz veins also occur.*	*Same as K2/3 but slightly more altered, cross cutting quartz veins also occur.*
Eendekuil kimberlite	K2/13	*Same as K2/2*	*Same as K2/2*	*Same as K2/2*

Kimberlite		Macrocrysts	Phenocrysts	Matrix
Markt kimberlite	JJG 2314	*Olivine* (20%) – Anhedral macrocrysts, 3-4mm, chlorite rim, serpentinised although fresh cores still remain. Opaque oxides along fractures. *Phlogopite* (10%) – Subhedral to anhedral macrocrysts, 3mm, kink banding, undulose extinction.	*Olivine* (15%) – Anhedral phenocrysts and microphenocrysts, completely serpentinised, brown alteration rim.	*Calcite* (30%) – Brown, interstitial calcite *Phlogopite* (15%) – Stubby crystals, 200µm *Serpentine* (7.5%) – Segregations with calcite, phlogopite and apatite are 2-3mm. *Opaque oxides* (1%) - Subhedral crystals, 50-100µm. *Perovskite* (1%) – Anhedral crystals, 50µm. *Apatite* (0.5%) – Euhedral needles, 50µm.
Classification	Phlogopite calcite kimberlite			
Texture	macrocrystic			
Markt kimberlite	JJG 2336	*Olivine* (15%) – Anhedral macrocrysts, 3-4mm, serpentinised, opaque oxides along fractures. *Phlogopite* (10%) – Subhedral macrocrysts, calcite stringers, tetraferriphlogopite rims, kink banding.	*Olivine* (15%) – Anhedral phenocrysts and microphenocrysts, completely serpentinised.	*Calcite* (25%) – Brown, interstitial calcite *Phlogopite* (20%) – Stubby prisms, tetraferri-phlogopite rims, poikolitically enclose opaque oxides, 250µm. *Serpentine* (12.5%) – Segregations with calcite, phlogopite and apatite are 1-5mm. *Opaque oxides* (1%) – Euhedral crystals, 20µm. *Perovskite* (1%) – Euhedral crystals, 50µm. *Apatite* (0.5%) – Euhedral needles, 100µm.
Classification	Phlogopite calcite kimberlite			
Texture	macrocrystic			
Markt kimberlite	MRK 1	*Olivine* (20%) – Anhedral macrocrysts, 4-5mm, serpentinised although a few fresh cores remain, green chlorite rim. *Phlogopite* (10%) – Subhedral macrocrysts, 2-3mm, kink banding, tetraferriphlogopite rims. *Garnet* – A 1mm orange garnet in hand specimen	*Olivine* (15%) – Anhedral, completely serpentinised phenocrysts and microphenocrysts with chlorite rims.	*Calcite* (25%) – Brown microcrystalline calcite *Phlogopite* (20%) – Stubby phlogopite laths, 250µm, poikolitically enclose opaque oxides. *Serpentine* (7.5%) – Segregations with phlogopite, calcite and apatite are 1-5mm. *Opaque oxides* (1%) – Subhedral crystals, 20µm. *Perovskite* (1%) – Anhedral crystals, 50µm. *Apatite* (0.5%) – Euhedral needles, 50µm.
Classification	Phlogopite calcite kimberlite			
Texture	macrocrystic			

Markt kimberlite	MRK 3	*Olivine* (15%) – Anhedral, completely serpentinised macrocrysts, 6mm in size, brown carbonate rims, poikolitically encloses opaque oxides. *Phlogopite* (5%) – Subhedral macrocrysts, calcite stringers, 2-7mm, tetraferriphlogopite rims also occur.	*Olivine* (15%) – Subhedral and completely serpentinised phenocrysts and microphenocrysts, carbonatised interiors.	*Phlogopite* (25%) – Stubby prisms, tetraferri phlogopite rims. *Calcite* (20%) – Microcrystalline brown calcite. *Serpentine* (17%) – Segregations with calcite, phlogopite and apatite are 1-3mm. *Opaque oxides* (1%) – Subhedral crystals, 20µm. A few 200µm clusters occur. *Perovskite* (1%) –Anhedral crystals, 50µm. *Apatite* (1%) – Euhedral needles, 100-200µm.
Classification	Calcite phlogopite kimberlite			
Texture	macrocrystic			

B.3 Transitional kimberlites

B.3.1 On-craton kimberlites

Kimberlite		Macrocrysts	Phenocrysts	Matrix
Leicester kimberlite	JJG 4326	*Phlogopite* (16,5%) – Anhedral macrocrysts, 4mm, Calcite and opaque oxides as stringers along cleavage planes. *Olivine* (8%) – Anhedral macrocrysts, 3mm, serpentinisation along fractures. *Ilmenite* (0.5%) – A single anhedral opaque oxide macrocryst 1mm in size.	*Olivine* (20%) – Euhedral to subhedral phenocrysts and microphenocrysts, serpentinisation along fractures, patches of calcitisation. *Phlogopite* (5%) – Euhedral to subhedral phenocrysts and microphenocrsyts, variable pleochroism. Chloritisation of rims and fractures.	*Calcite* (20%) – Interstitial and segregationary. Segregations are 0.5 mm in size. *Serpentine* (13%) – Interstitial and segregationary. *Monticellite* (5%) – Granular texture, 10µm *Phlogopite* (5%) – Irregularly shape laths. *Opaque oxides* (5%) – Euhedral crystals, 50µm *Perovskite* (2%) – Subhedral crystals, 20µm.
Classification	Serpentine calcite kimberlite			
Texture	macrocrystic			
Leicester kimberlite	JJG 4328	*Phlogopite* (20%) – Subhedral macrocrysts, 3mm, undulose extinction. Calcite and opaque oxides as stringers along cleavage planes. Some euhedral 0.5mm opaque oxide inclusions occur in the macrocrysts. *Olivine* (5%) – Anhedral macrocrysts, serpentinised exteriors, calcitised interiors.	*Phlogopite* (10%) – Euhedral to subhedral phlogopite phenocrysts and microphenocrysts, serrate texture, strong pleochroism. *Olivine* (10%) – Euhedral to subhedral phenocrysts, serpentinised exteriors, calcitised interiors.	*Calcite* (25%) – Interstitial and segregationary. Some calcite replacement of unknown euhedral, tabular phenocrysts. *Serpentine* (10%) – Interstitial. *Phlogopite* (8%) – Equant crystals, strong pleochroism. *Monticellite* (5%) – Granular texture, 10µm. *Opaque oxides* (5%) – Euhedral and larger, 0.5mm anhedral crystals. *Perovskite* (2%) – Anhedral crystals.
Classification	Serpentine calcite kimberlite			
Texture	macrocrystic			
Leicester kimberlite	JJG 6054	*Olivine* (25%) –Anhedral to subhedral macrocrysts, 5mm, completely serpentinised. Macrocrysts contain inclusions with opaque oxide intergrowths.	*Olivine (14%)* – Subhedral phenocrysts and microphenocrysts, completely serpentinised. *Phlogopite (5%)* – Subhedral, tabular phenocrysts, variable pleochroism. Chloritisation on rims and fractures.	*Calcite* (15%) – Interstitial and segregationary. Serpentine–calcite segregations 2mm in size. Some calcite replacement of unknown euhedral, tabular phenocrysts.
Classification	Serpentine calcite kimberlite			

Texture	macrocrystic	*Phlogopite* (9.5%) – Anhedral macrocrysts, 4mm, strongly pleochroic, undulose extinction, chloritisation along rims. *Ilmenite* (3%) – Anhedral macrocrysts, aggregation of matrix opaque oxides around rim. *Garnet* (0.5%) – Single 2mm anhedral garnet with chloritisation along rim.		*Serpentine* (10%) – Interstitial and segregationary. *Phlogopite* (5%) – Subhedral equant phlogopite *Monticellite* (5%) – Granular texture, 10μm *Opaque oxides* (5%) – Euhedral crystals. *Perovskite* (2%) – Anhedral crystals.

Kimberlite		Macrocrysts	Phenocrysts	Matrix
Wimbledon kimberlite	WIMB 1	*Olivine* (15%) – Anhedral olivine macrocrysts up to 6mm in size that are serpentinised and carbonatised. The macrocrysts may also have opaque oxide rims *Phlogopite* (15%) – Macrocrysts are up to 8mm in length, show undulose extinction, kink banding and have calcite stringers. A slight green rim may also occur.	*Olivine* (15%) – Subhedral to anhedral phenocrysts and microphenocrysts that are serpentinised, carbonatised and have an opaque mineral rim. *Phlogopite* (5%) – Subhedral phenocrysts, strong pleochroism. Green rims on phenocrysts can envelop the entire phenocryst.	*Calcite* (20%) – Interstitial and segregationary. *Phlogopite* (10%) – Stubby crystals, pleochroism and chloritisation, 50μm. *Serpentine* (9%) – Interstitial *Opaque oxides* (5%) – Euhedral crystals, 10-50μm *Apatite* (4%) – Euhedral elongate crystals, well-developed hexagonal basal sections, up to 250μm. *Perovskite* (2%) – Euhedral crystals.
Classification	Phlogopite calcite kimberlite			
Texture	macrocrystic			
Wimbledon kimberlite	WIMB 2	*Olivine* (20%) – Anhedral macrocrysts, 3mm. Serpentinised and carbonatised. *Phlogopite* (10%) – Macrocrysts are up to 8mm in length, show undulose extinction, kink banding and have calcite stringers. A slight green rim may also occur.	*Olivine* (15%) – Anhedral phenocrysts and microphenocrysts, serpentinised and carbonatised. *Phlogopite* (5%) – Subhedral phenocrysts. Some chloritisation along rims.	*Calcite* (20%) – Interstitial and segregationary. *Phlogopite* (14%) – Stubby microphenocrysts, pleochroism and chloritisation, 50μm. *Serpentine* (10%) – Interstitial. *Opaque oxides* (5%) – Equant crystals, 10-50μm. *Apatite* (4%) – Euhedral crystals, up to 250μm. *Perovskite* (2%) – Euhedral crystals.
Classification	Phlogopite calcite kimberlite			
Texture	macrocrystic			

B.3.2 Off-craton kimberlites

Kimberlite		Macrocrysts	Phenocrysts	Matrix
Droogfontein kimberlite	K19/2	*Olivine* (15%) – Anhedral macrocrysts, completely serpentinised, 4mm. *Note: A second phase of diopside-phlogopite kimberlite occurs as xenoliths with an internal structure.*	*Olivine* (15%) – Subhedral phenocrysts and microphenocrysts, completely serpentinised *Phlogopite* (10%) – Subhedral phenocrysts, poikilitically enclosing perovskite, opaque oxides.	*Phlogopite* (25%) – Interlocking laths, poikilitically enclosing perovskite, 500μm *Serpentine* (19%) – Interstitial *Diopside* (10%) – Anhedral crystals, scattered and clustered, 50μm. *Perovskite* (4%) – Subhedral crystals, may occur in rings, 50-100μm. *Opaque Oxides* (2%) – Equant crystals, 20-50μm
Classification	Serpentine phlogopite kimberlite			
Texture	macrocrystic			

Droogfontein kimberlite	K19/3	*Olivine (15%)* – Anhedral macrocrysts, completely serpentinised, 4mm. *Note: A second phase of diopside-phlogopite kimberlite occurs as xenoliths with an internal structure*	*Olivine* (20%) – Subhedral phenocrysts and microphenocrysts, completely serpentinised. *Phlogopite* (10%) – Subhedral phenocrysts, poikolitically enclosing perovskite, opaque oxides, serpentine.	*Phlogopite* (25%) – Interlocking laths, poikolitically enclosing perovskite, 500µm. *Serpentine* (19%) – Interstitial. *Diopside* (10%) – Anhedral crystals, scattered and clustered, 50µm. *Perovskite* (4%) – Subhedral crystals, may occur in rings, 50-100µm. *Opaque Oxides* (2%) - Equant crystals, 20-50µm.
Classification	Serpentine phlogopite kimberlite			
Texture	macrocrystic			
Droogfontein kimberlite	K19/5	*Same as K19/2 and K19/3*	*Same as K19/2 and K19/3*	*Same as K19/2 and K19/3*
Droogfontein kimberlite	K19/10	*Same as K19/2 and K19/3*	*Same as K19/2 and K19/3*	*Same as K19/2 and K19/3*

Kimberlite		**Macrocrysts**	**Phenocrysts**	**Matrix**
Melton Wold kimberlite	MLW 1	*Olivine* (20%) – Anhedral macrocrysts, 3mm. Serpentinised with a few fresh patches remaining. Opaque oxide dusting.	*Olivine* (30%) – Anhedral phenocrysts and microphenocrysts completely serpentinised.	*Calcite* (25%) – Interstitial and segregationary. *Phlogopite* (15%) – Irregular shaped laths with calcite and opaque oxide stringers. *Serpentine* (7%) – Interstitial. *Opaque Oxides* (2%) – Euhedral - anhedral crystals. *Perovskite* (1%) - Subhedral crystals.
Classification	Phlogopite calcite kimberlite			
Texture	macrocrystic			
Melton Wold kimberlite	MLW 3	*Olivine* (15%) – Anhedral macrocrysts, 3mm. Serpentinised with few fresh patches remaining, opaque oxide dusting. Some calcitisation also occurs.	*Olivine* (25%) - Subhedral to anhedral phenocrysts and microphenocrysts, completely serpentinised.	*Calcite* (25%) – Interstitial and segregationary. *Phlogopite* (20%) – Interlocking laths with calcite stringers, opaque mineral inclusions. *Serpentine* (12%) - Interstitial. *Opaque oxides* (2%) – Anhedral crystals. *Perovskite* (1%) – Euhedral crystals.
Classification	Phlogopite calcite kimberlite			
Texture	macrocrystic			
Melton Wold kimberlite	MLW 4	*Olivine* (20%) – Anhedral macrocrysts, 3mm. Completely carbonatised. *Note: Two anhedral very fine-grained possible micro-xenoliths, 3mm in size also occur.*	*Olivine* (20%) – Subhedral to anhedral phenocrysts and microphenocrysts, completely carbonatised. *Phlogopite* (10%) – Tabular habit but phenocrysts now completely carbonatised.	Matrix (50%) – Fine grained and completely carbonatised with cross cutting calcite veins.
Classification	Carbonated kimberlite			
Texture	macrocrystic			

Kimberlite		Macrocrysts	Phenocrysts	Matrix
Silvery Home kimberlite	JAR 21022	*Olivine* (15%) Anhedral macrocrysts, 3mm, heavily serpentinised along fractures. Opaque oxide dusting along fractures.	*Olivine* (20%) - Anhedral phenocrysts and microphenocrysts, heavily serpentinised along fractures.	*Phlogopite* (25%) - Interlocking laths, 500 µm poikolitically enclose perovskite. *Serpentine* (19%) – Interstitial *Calcite* (18%) - Interstitial, individual rhombohedral crystals, 500µm. *Opaque Oxides* (5%) - Anhedral crystals, 20-50µm. *Perovskite* (1%) – Euhedral crystals, 100µm.
Classification	Serpentine phlogopite kimberlite			
Texture	macrocrystic			
Silvery Home kimberlite	SLH 1	*Olivine* (20%) – Anhedral macrocrysts, 2-4mm, serpentinised fractures. Opaque oxides occur on fractures.	*Olivine* (30%) – Subhedral to anhedral phenocrysts and microphenocrysts, completely serpentinised.	*Phlogopite* (18%) – Interstitial laths, 500 µm poikolitically enclose perovskite, starting to be serpentinised. *Serpentine* (16%) – Interstitial and replacing calcite, some slight chloritisation. *Calcite* (13%) – Interstitial, microcrystalline calcite. *Opaque Oxides* (5%) – Euhedral crystals, 50µm. *Perovskite* (1%) – Euhedral crystals, 50-100µm.
Classification	Serpentine phlogopite kimberlite			
Texture	macrocrystic			
Silvery Home kimberlite	SLH 3	*Olivine* (10%) – Anhedral macrocrysts, 3-4mm, completely serpentinised.	*Olivine* (25%) – Euhedral phenocrysts and microphenocrysts, completely serpentinised.	*Phlogopite* (16%) – Stubby, interlocking, euhedral laths, 300-500µm, dark reaction rims, poikolitically enclose perovskite. *Diopside* (15%) Euhedral crystals, 30-50µm. *Serpentine* (15%) – Occurs in some mini-segregations with calcite. *Calcite* (13%) – Microcrystalline calcite, individual rhombs, 300µm. *Perovskite* (4%) – Euhedral crystals, 50-100µm. *Opaque oxides* (2%) – Irregular shaped crystals, 400 µm in size.
Classification	Diopside phlogopite kimberlite			
Texture	sparsely macrocrystic			
Silvery Home kimberlite	SLH 7	*Olivine* (15%) - Anhedral macrocrysts, 4mm, remarkably fresh, opaque oxide dusting along fractures.	*Olivine* (18%) Subhedral to anhedral phenocrysts and microphenocrysts, with degree of serpentinisation varying from completely altered phenocrysts to serpentinised fractures. *Phlogopite* (12%) – Interlocking, euhedral phenocrysts with tetraferriphlogopite rims.	*Phlogopite* (20%) – Interlocking, euhedral laths, 300-500µm, poikolitically enclose perovskite. *Diopside* (15%) - Euhedral crystals, fresh appearance, 30-50µm. *Serpentine* (14%) – Interstitial *Perovskite* (4%) – Euhedral crystals, poikolitically enclosed in phlogopite, 100µm *Opaque oxides* (2%) Irregular shaped crystals, 20µm.
Classification	Diopside phlogopite kimberlite			
Texture	macrocrystic			

Silvery Home kimberlite	SLH 9	*Olivine* (15%) – Anhedral macrocrysts, 4mm, remarkably fresh, opaque oxide dusting along fractures.	*Olivine* (18%) – Subhedral to anhedral phenocrysts and microphenocrysts, remarkably fresh, opaque oxide dusting along fractures. *Phlogopite* (12%) – Interlocking, euhedral phenocrysts, sparse calcite stringers along cleavage planes, tetraferriphlogopite rims.	*Phlogopite* (23%) – Interlocking, euhedral laths, 300-500µm, poikolitically enclose perovskite. *Diopside* (21%) – Euhedral crystals, fresh appearance, up to 500µm. *Serpentine* (5%) – Interstitial. *Perovskite* (4%) – Euhedral crystals, poikolitically enclosed in phlogopite, 100µm. *Opaque oxides* (2%) – Irregular shaped crystals, 20µm.
Classification	Diopside phlogopite kimberlite			
Texture	macrocrystic			
Silvery Home kimberlite	SLH 10	*Olivine* (15%) – Anhedral macrocrysts, 2-4mm, serpentinised fractures. Some fresh olivine on macrocrysts. Opaque oxides occur on fractures.	*Olivine* (25%) – Subhedral to anhedral phenocrysts and microphenocrysts, completely serpentinised. *Phlogopite* (10%) – Interlocking laths with poikolitic texture.	*Serpentine* (19%) – Interstitial and inter-grown into phlogopite. *Phlogopite* (15%) – Interstitial laths, poikolitically enclose perovskite, form coronas around olivine macrocrysts. *Calcite* (13%) – Interstitial, microcrystalline calcite. *Opaque oxides* (5%) – Euhedral crystals, 25µm. *Perovskite* (1%) – Subhedral crystals, 25-50µm.
Classification	Phlogopite serpentine kimberlite			
Texture	macrocrystic			
Silvery Home kimberlite	SLH 11	*Olivine* (15%) – Anhedral macrocrysts, 2-4mm, opaque oxides along rims and fractures. Some fresh olivine.	*Olivine* (25%) – Subhedral to anhedral phenocrysts and microphenocrysts, opaque oxides along rims and fractures. Some fresh olivine. *Phlogopite* (5%) – Sparse euhedral phenocrysts, few calcite stringers along cleavage planes, opaque oxide dusting.	*Serpentine* (23%) – Interstitial and inter-grown into phlogopite. *Phlogopite* (19%) – Interlocking laths, poikolitically enclose perovskite. *Calcite* (10%) – Interstitial, 50µm. *Opaque oxides* (5%) – Euhedral crystals, 25µm. *Perovskite* (1%) – Subhedral crystals, 25-50µm.
Classification	Phlogopite serpentine kimberlite			
Texture	macrocrystic			

B.4 Photomicrographs of individual kimberlite samples

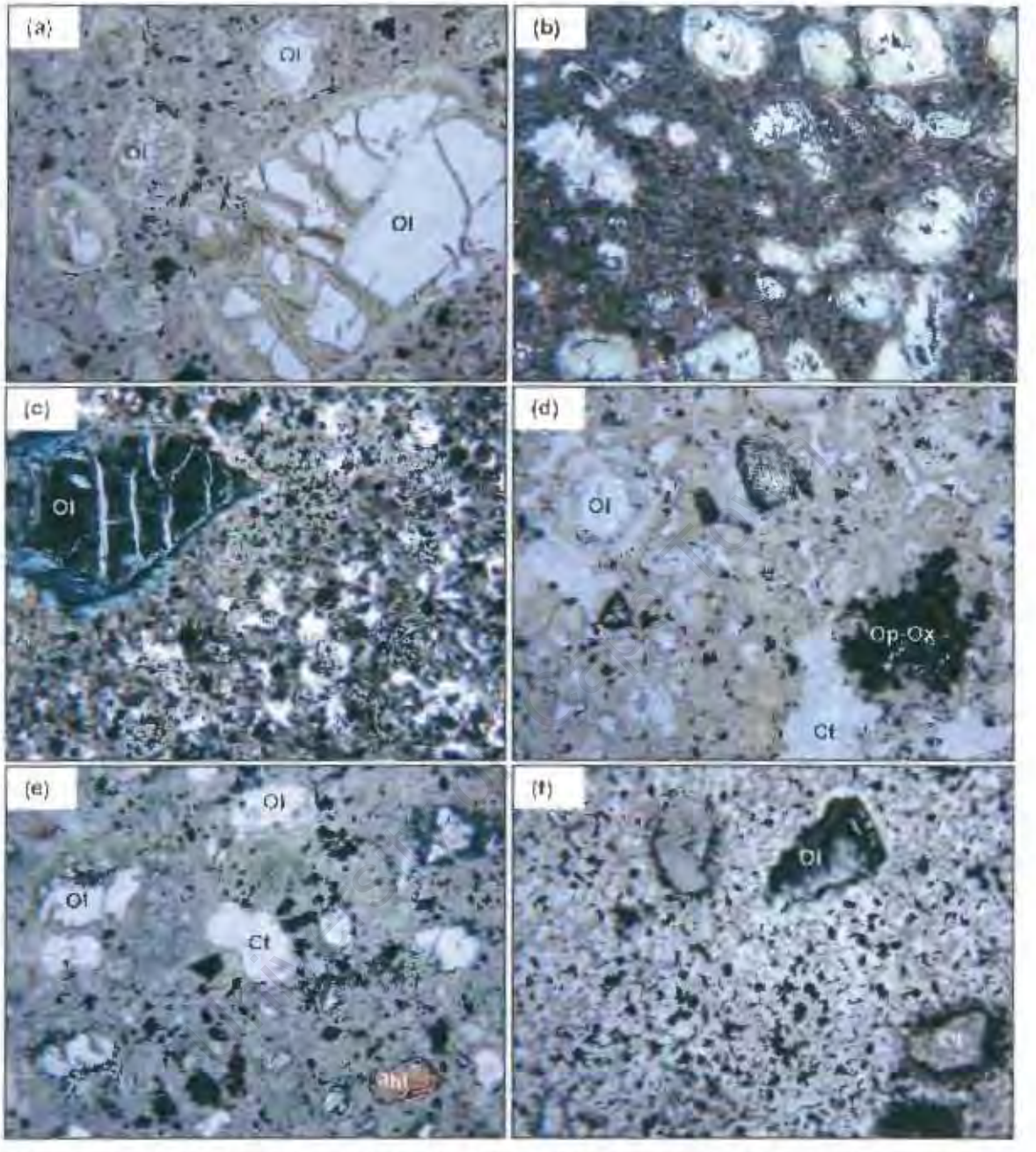

Figure B.1: Photomicrographs of group I kimberlite samples. Photomicrographs are shown in plane polarised light, field of view is 2.5mm.

(a) Goedehoop kimberlite (*JJG 4282*): Partially serpentinised and carbonatised olivine phenocrysts and microphenocrysts set in serpentine calcite matrix.
(b) Koffiefontein kimberlite (*KK 5*): Serpentinised olivine phenocrysts and microphenocrysts set in a fine grained matrix.
(c) Abbotsford East kimberlite (*JJG 3118*): Serpentinised opaque oxide-rich olivine macrocryst set in a fine grained serpentine calcite matrix.
(d) Liebron kimberlite (*HEB 18*): Serpentinised olivine phenocrysts, altered phlogopite phenocryst, an aggregation of matrix opaque oxide grains and calcite segregation are set in a serpentine calcite matrix.
(e) Klipgatsfontein kimberlite (*JAR 31012*): Serpentinised olivine phenocrysts and microphenocrysts, phlogopite macrocryst set in a serpentine calcite matrix with calcite segregations.
(f) Zeekoegat kimberlite (*JJG 1906*): Serpentinised and altered olivine macrocrysts set in a dark coloured fine-grained calcite matrix with abundant opaque oxide grains.

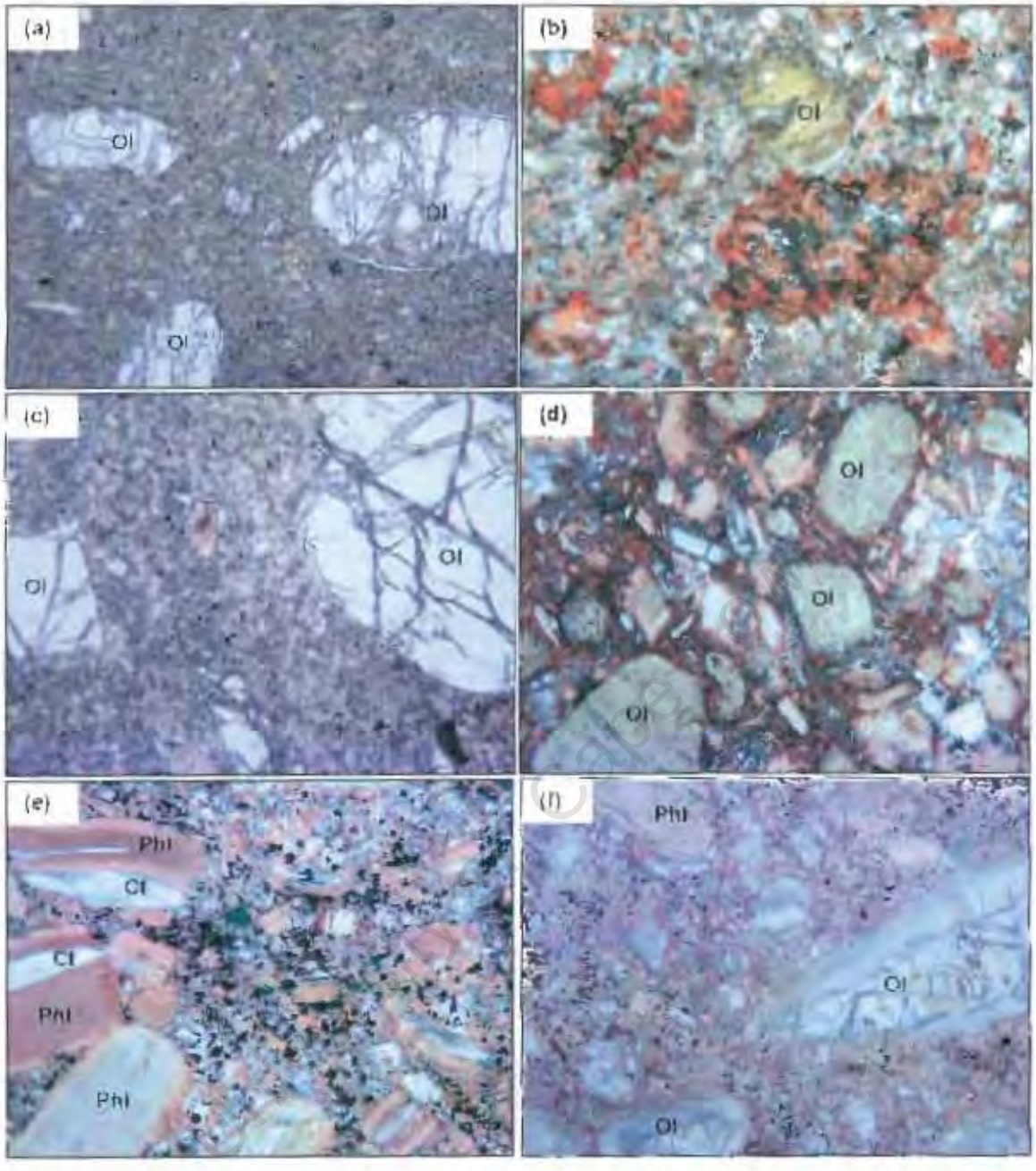

Figure B.2: Photomicrographs of group I kimberlite samples. Photomicrographs are shown in plane polarised light, field of view is 2.5mm.

(a) Bellsbank kimberlite (*JJG 4676*): Fresh olivine macrocrysts set in fine-grained phlogopite matrix.
(b) New Elands kimberlite (*NE K6*): Altered green olivine phenocrysts set in medium-grained calcite phlogopite matrix.(c) Newlands kimberlite (*KN 3*): Fresh olivine macrocrysts set in a fine-grained phlogopite matrix.
(d) Brandewynskuil kimberlite (*K6-11*): Serpentinised olivine macrocrysts and phenocrysts, tetraferriphlogopite phenocrysts set in a serpentine phlogopite matrix.
(e) Eendekuil kimberlite (*EKL 1*): Deformed phlogopite macrocrysts and some phlogopite phenocrysts/microphenocrysts with calcite stringers along cleavage planes, set in a calcite phlogopite matrix.
(f) Markt kimberlite (MRK 1): Serpentinised olivine phenocrysts and microphenocrysts, phlogopite macrocrysts, set in a calcite tetraferriphlogopite groundmass.

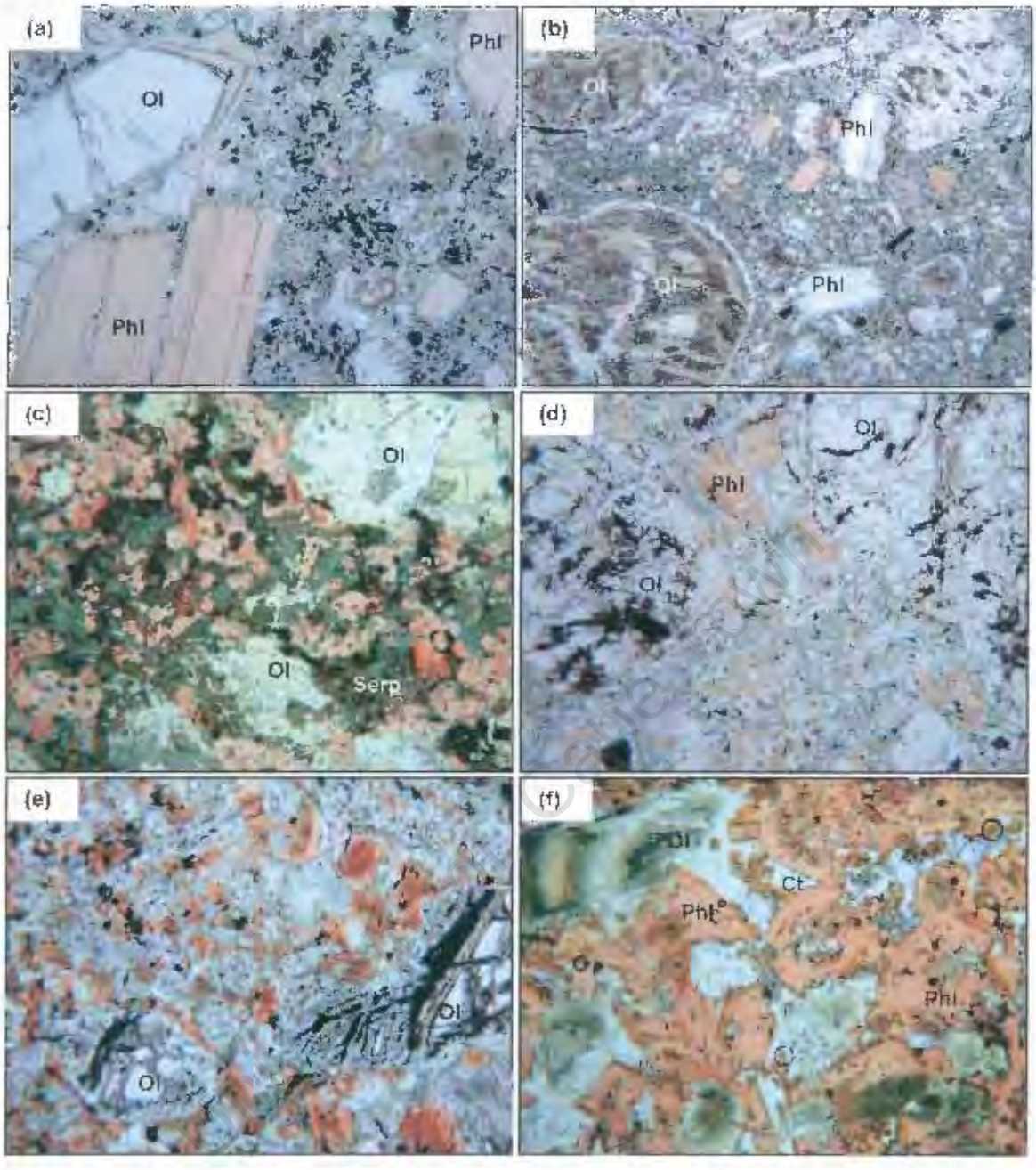

Figure B.3: Photomicrographs of transitional kimberlite samples. Photomicrographs are shown in plane polarised light, field of view is 2.5mm.

(a) Leicester kimberlite (*JJG 4326*): Fresh euhedral olivine phenocryst and phlogopite macrocryst set in an opaque-oxide rich serpentine-calcite matrix.
(b) Wimbledon kimberlite (*WIMB 1*): Serpentinised olivine macrocrysts, chloritised phlogopite phenocrysts set in a phlogopite calcite matrix.
(c) Droogfontein kimberlite (*K19/2*): Serpentinised olivine macrocrysts and phenocrysts set in a coarse-grained serpentine phlogopite groundmass. Note the coarse-grained perovskite and opaque oxides in the groundmass.
(d) Melton Wold kimberlite (*MLW 3*): Serpentinised olivine macrocrysts with an opaque oxide dusting set in a serpentine phlogopite calcite groundmass.
(e) Silvery Home kimberlite (*JAR 21022*): Serpentinised olivine phenocrysts with an opaque oxide dusting set in a coarse-grained groundmass of serpentine, phlogopite and calcite.
(f) Silvery Home kimberlite (SLH 3): Serpentinised olivine phenocrysts and microphenocrysts set in a coarse groundmass of phlogopite, calcite and fine-grained diopside.

APPENDIX C

SAMPLE PREPARATION

Once the freshest pieces of hypabyssal kimberlite from the various localities had been selected, all samples were prepared for geochemical analysis at the Department of Geological Sciences, University of Cape Town (UCT). Firstly, weathered surfaces of kimberlite, as well as any other large foreign fragments were removed using a hydraulic splitter before the sample was split into sizes suitable for passing through a jaw crusher. The jaw crush chips were then individually hand picked, with careful attention being paid to selecting kimberlite fragments free from weathering, crustal and mantle xenoliths, megacrysts and calcite veining. The 30-40g clean samples were then powdered for 1 minute using a carbon steel Sieb swing mill.

C.1 X-ray fluorescence (XRF) major element analysis

Approximately 2g of sample from each kimberlite was weighed out into clean porcelain crucibles and the weight carefully recorded. The crucibles were left to dry overnight in an oven at 110^0C and reweighed the following day. The proportion of H_2O^- present in the kimberlite samples was calculated by the mass difference of the two recorded measurements. The samples were then roasted overnight at 850^0C, followed by reweighing the next day in order to determine the percentage loss on ignition (LOI).

In order to prepare the fusion discs for XRF analysis, 0.7g of the roasted kimberlite sample was accurately weighed out with 6g of lithium tetraborate-lithium metaborate Sigma X-ray flux. The fusion discs were then prepared in the Pt-Au crucibles of the Claisse fluxy™ and stored in a dessicator prior to analysis.

C.2 X-ray fluorescence (XRF) trace element analysis

Powder briquettes were prepared using 6g of kimberlite sample and 6 drops of the binding agent, "Mowiol". The briquettes were made under a 10 ton press with boric acid as a backing. Powder briquettes were then placed in a vacuum chamber for 20-25 minutes to ensure their stability under low pressure and stored in a dessicator prior to XRF analysis. Droogfontein kimberlite samples *K19/3* and *K19/5* were particularly small in size and consequently, only 2g powder briquettes were made for these samples.

C.3 Inductively coupled plasma - mass spectrometry (ICP-MS) trace element analysis

Solutions of kimberlite samples were prepared by dissolving 50mg of sample in 4ml of a 4:1 mixture of HF and HNO_3. Sealed Teflon beakers containing the samples were left on a hot plate for 3 days to ensure maximum dissolution of the samples. Dried down samples were treated with 2ml of concentrated HNO_3 and allowed to evaporate to dryness again. This second step was repeated. After adding 4ml of stock solution (10ppb Re, Rh, In and Bi as internal standards in 5% HNO_3) to the dried down samples, the samples were placed in an ultrasonic bath for 1 hour. Finally, the samples were prepared for ICP-MS analysis by 1000 times dilution with the stock solution. One drop of HF was also added to ensure that Ta remained in solution for the duration of the analysis. Samples were then diluted another 10 times to accommodate the very high absolute concentration of certain incompatible trace elements in the kimberlites.

C.4 Thermal ionisation mass spectrometry (TIMS) isotope analysis

The first step in the preparation of kimberlite samples for Sr and Nd isotope analysis was to dissolve 100mg of each kimberlite sample in 4ml of a 4:1 mixture of HF and HNO_3 in sealed Teflon beakers for 2 days over a hotplate. After dissolution, the samples were dried down. A few millilitres of 6.2M HCl were then used to rinse the beakers of any remaining HNO_3 before the samples were evaporated to dryness again. This process was repeated a second time. The samples were then transferred into centrifuge tubes and made up into 1ml solutions with 2.5M HCl and centrifuged for approximately 15 minutes to separate any undissolved material from the solutions.

0.5ml of each sample solution was loaded onto standard primary cation exchange columns following the method and specifications of Hart and Brooks (1977) and Zindler (1980), that allows the Sr and REE fractions to be collected separately. The primary columns consisted of Dowex AG 50WX-8 (200-400 mesh) resin, were 19cm in height and 0.5cm in diameter. Once the samples had been loaded onto the columns, they were washed with three aliquots of 1ml 2.5M HCl, a further 23ml 2.5M HCl, followed by 8.5ml 2.5M HCl of which the last fraction containing the Sr was collected. The acid concentration was then changed to 6.2M HCl and the columns washed with 6ml of this acid, before 6ml aliquots that contained the REE fractions were collected. A few millilitres of HNO_3 was added to each Sr fraction to convert the aliquot to a nitrate and the solution then left to dry down on a hot plate. Primary columns were cleaned with two doses of 6.2M HCl followed by backwashing and equilibration with 2.5M HCl.

Once the REE sample aliquots had dried down, samples were dissolved in 0.25ml of 0.25M HCl and loaded onto the REE separation columns. This secondary column consisted of a round bottom flask with a built-in polyethylene fibre frit at the base of the column and supersil quartz tubing attached to the flask (Zindler, 1980). The column itself was filled with a mixture of Teflon powder and HDEHP, capped with 0.5cm of Dowex AG1-X8 (200-400 mesh) resin (Zindler, 1980). Once the samples were

loaded onto the columns, they were washed with 3 aliquots of 0.25ml 0.25M HCl, a further 1ml 0.25M HCl, followed by 3.5ml 0.25M HCl, of which the last fraction containing the Nd was collected. The Nd fraction was then dried down. Columns were cleaned with 30ml 6.2M HCl and equilibrated with 15ml 0.25M HCl.

The Sr and Nd fractions were then loaded onto single Ta and double Re/Ta degassed filaments, respectively, for thermal ionisation mass spectrometry (TIMS). The Sr fraction was loaded with a 1µl aliquot of HNO_3 and H_3PO_4, whereas the Nd fraction, with HCl and H_3PO_4.

C.5 Reagant quality and beaker cleaning

All samples prepared within the radiogenic isotope facility at UCT, utilised stringently clean Teflon beakers as well as distilled reagents for sample dissolution and column chemistry. Beakers were cleansed over a 7 day period involving several stages with Decon wash, HNO_3, HCl and aqua regia and rinsed after each step with Milli-Q water. HCl was distilled with a quartz still, whereas the two bottle process (infrared lamp and cold flask) was used for purifying HF and HNO_3. Similarly, Teflon beakers for ICP-MS analysis were cleaned over a number of days with Milli-Q water and concentrated HNO_3 before being oven dried.

C.6 Incomplete sample dissolution

Certain minerals are particularly notorious for not dissolving using standard HF/HNO_3 dissolution procedures and especially so in kimberlites (e.g. Potts, 1987). Right from the beginning of this study the problem of dissolving refractory minerals such as ilmenite, chromite and zircon and obtaining uncompromised trace element analyses was addressed. An alternative method was explored that involved dissolution of the sample by fusion with a lithium tetraborate flux, prior to solution ICP-MS analysis. This alternative technique has previously been described by various authors such as; Yu *et al.* (2001), Bagai (2000), Pyke (2000), Totland *et al.* (1992) and Potts (1987).

The method that was tested here used 0.3g of sample and 1.5g dry Claisse Scientific Corporation $Li_2B_4O_7$ flux. The sample was fused in a Pt-Au crucible over a Meker burner at 1200^0C for 20 minutes and then poured onto a graphite block and allowed to cool. The glass disc was smashed into chips, of which 50mg of chips were then dissolved in 4ml of a 5% HNO_3 internal standard solution and Teflon beakers containing the sample, were placed in an ultrasonic bath for 1 hour. The solution was made up to 50ml following the procedures described in section C.3 and then analysed by the ICP-MS standard routine.

A variety of rock types including kimberlite, basalt, gabbro and granite were used in order to determine the efficiency of the dissolution procedure. It is evident that the Uintjiesberg kimberlite trace element data shows better agreement between routine solution ICP-MS and fusion method ICP-MS, than the

Bushveld gabbro trace element analyses (Figure C.1). One of the particular problems encountered with the fusion method was that the total procedural blanks were considerably higher than those obtained for traditional solution ICP-MS using acid digestion (Table C.1; Yu *et al.*, 2001; Totland *et al.*, 1992). Total procedural blanks for the fusion method have particularly high La concentrations (913-10834ppb) that may have partly been due to contamination from the Johnson and Matthey Spectra flux used many years ago in the XRF sample preparation laboratory.

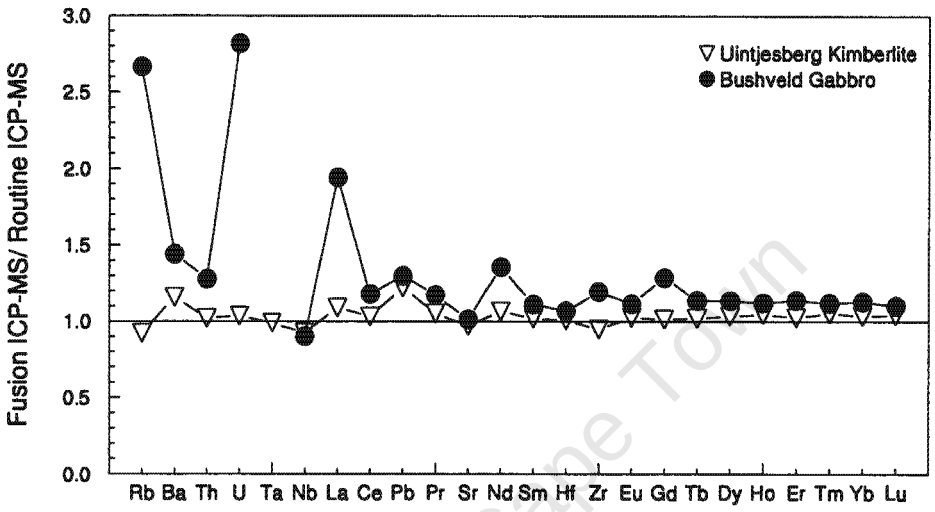

Figure C.1: Incompatible trace element concentrations of kimberlite (Uintjiesberg kimberlite) and gabbro (Bushveld Igneous Complex) samples analysed by solution ICP-MS with fusion digestion, normalised to routine solution ICP-MS analyses (with acid digestion).

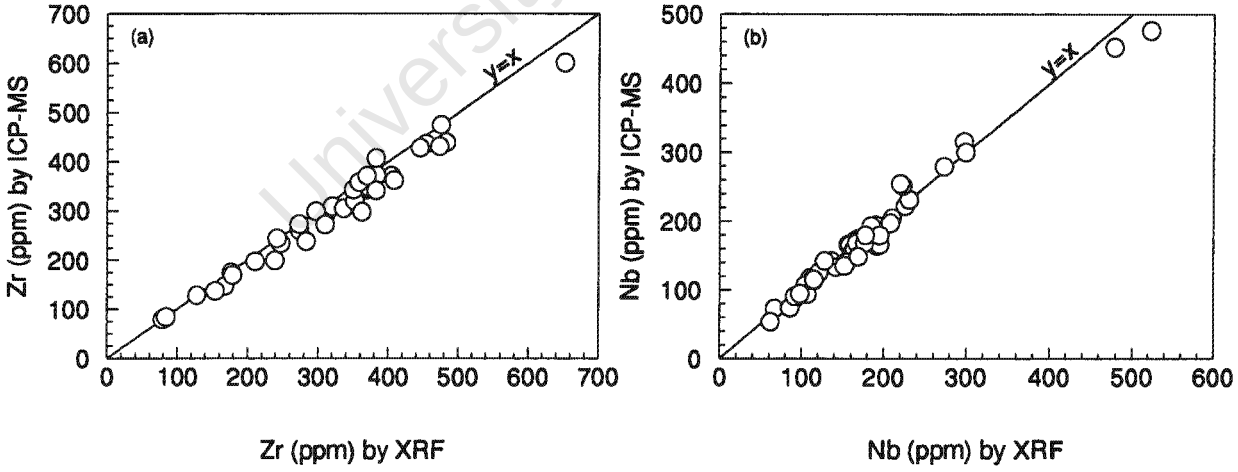

Figure C.2: Comparison of XRF and routine solution ICP-MS trace element analyses for Zr and Nb.

It was decided that conventional solution ICP-MS analysis would be chosen as the favoured method for trace element analysis, due to the considerable time that would be required to fine tune the fusion method, obtain a suitably pure flux and decontaminate the XRF sample preparation laboratory. In order to ensure maximum dissolution of the refractory minerals via acid digestion, it was decided to

leave the samples on a hot plate for 3 days instead of the 2 days used routinely at UCT. Comparison of the elements analysed by standard solution ICP-MS and XRF (Figure C.2), illustrates that the correlation between methods is generally good, except for some kimberlite samples with high Nb and Zr abundances, where ICP-MS analyses appear to have underestimated concentrations. Consequently, XRF Nb and Zr analyses (where present) were used in preference to the ICP-MS data for these two elements.

Table C.1: Total procedural blank (TPB) concentrations for routine solution ICP-MS with acid digestion, in contrast to solution ICP-MS with fusion digestion. Total procedural blanks are given for two different lithium tetraborate fluxes.

Method	**Routine ICP-MS**	**Fusion ICP-MS**	
Flux		*"Pure" Flux*	*"Ultrapure" Flux*
	TPB n=9 (ppb)	**TPB n=3 (ppb)**	**TPB n=2 (ppb)**
Sc	76.7	6950	9379
Ni	42.2	12205	6348
Rb	21.3	107	306
Sr	183	422	287
Y	8.65	151	90
Zr	97.1	569	312
Nb	81.9	2.75	53
Ba	279	987	1367
La	4.34	913	10834
Ce	6.24	196	100
Pr	2.69	20.8	13.9
Nd	10.7	410	293
Sm	3.79	22.1	17.9
Eu	1.95	2.95	2.12
Gd	4.51	92.1	18.6
Tb	1.03	2.61	2.13
Dy	3.93	14.0	11.2
Ho	0.98	1.95	1.88
Er	3.10	4.88	3.48
Tm	1.00	0.90	1.33
Yb	2.96	4.79	2.66
Lu	1.03	0.65	0.98
Hf	6.68	9.08	7.82
Ta	104	n.d.*	37.4
Pb	364	1184	1279
Th	4.45	6.39	4.08
U	1.16	43.4	21.5

* *n.d. = Not detected*

APPENDIX D

ANALYTICAL TECHNIQUES

D.1 X-ray fluorescence spectrometry (XRF)

Concentrations of the major elements and selected trace elements (Nb, Zr, Co, Cr, Ni, V) in kimberlite samples have been determined by XRF spectrometry. Analyses were run on a Philips X'Unique wavelength dispersive spectrometer housed at the University of Cape Town (UCT) and using a low dilution fusion technique. Major elements were analysed using a Mo/Sc x-ray tube, trace elements Co, Cr, Ni and V using a Au tube and high field strength elements Nb and Zr, with a Rh tube. Comparisons between analysed XRF concentrations and recommended values for certified international rock standards (*BHVO-1, SARM 48;* Govindaraju, 1994) for major (Table D.1) and trace (Table D.2) elements generally show no significant differences. The lower limits of detection for XRF major element analyses are also given for reference (Table D.1), especially since some kimberlites have very low Na_2O concentrations (LLD for Na_2O is 0.004 wt%). Two-sigma errors for trace element concentrations are less than 1.5ppm for Zr, Nb and Co and less than 3.5ppm for Cr, Ni and V (Table D.2). Ni and Cr data determined on fusion discs have been preferentially used to data obtained on pressed powder briquettes, since analyses from the latter appear to overestimate Ni and Cr contents (Figure D.1), an analytical artefact likely caused by matrix effects and lack of suitable high Ni and Cr standards.

Table D.1: Average major element concentrations obtained by XRF analysis for the international rock standard *BHV0-1*, in comparison to the recommended values reported by Govindaraju (1994). The percentage relative error (%RE) reported, is a measure of the accuracy. The lower limit of detection for XRF analysis is also given.

	BHVO-1 Recomm. (wt%)	UCT BHVO-1 (wt%)	% RE	LLD (ppm)
SiO_2	49.94	49.84	0.57	185
TiO_2	2.71	2.70	1.72	72
Al_2O_3	13.80	13.67	1.86	350
Fe_2O_3	11.40	12.14	1.04	20
MnO	0.17	0.17	6.57	20
MgO	7.23	7.40	1.80	220
CaO	11.40	11.70	2.59	14
Na_2O	2.26	2.30	3.14	40
K_2O	0.52	0.54	1.58	10
P_2O_5	0.27	0.29	2.14	38
SO_3	-	-	2.70	12
NiO	0.02	0.02	2.51	30
Cr_2O_3	0.04	0.05	4.38	46
Total	99.76	100.81	-	-

Table D.2: Comparison of elemental concentrations between recommended values (Govindaraju, 1994) and values determined in this study, for international rock standards *BHVO-1* and *SARM 48*. The 2-sigma error, lower limit of detection (LLD), as well as the root mean square parameter (RMS), a measure of the goodness of the regression, are also reported for each element.

	Standard	Recomm. Std (ppm)	UCT Std (ppm)	RMS	2-sigma error (ppm)	LLD (ppm)
Zr	SARM 48	300	293	0.00054	1.42	1.63
Nb	SARM 48	202	213	0.00015	0.96	1.10
Co	BHVO-1	45	42	0.00054	1.26	1.44
Cr	BHVO-1	289	284	0.00964	2.46	2.82
Ni	BHVO-1	121	107	0.00692	3.46	3.97
V	BHVO-1	317	322	0.00070	2.20	2.53

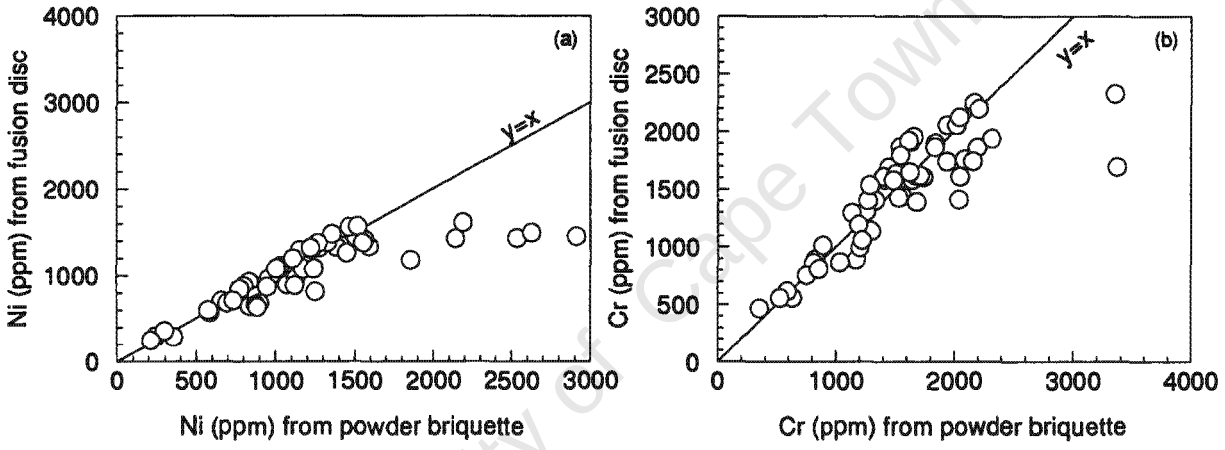

Figure D.1. Comparison of Ni and Cr concentrations of kimberlite samples on fusion discs and powder briquettes.

Powder briquettes of Droogfontein kimberlite samples *K19/3* and *K19/5* made with 2g of sample instead of 6g, could not be analysed for Nb since the sample depth did not satisfy the infinite thickness requirement, and so ICP-MS Nb analyses have been used instead for these two kimberlite samples.

D.2 The karbonat bombe

The karbonat bombe described by Birch (1981) is a simple, inexpensive instrument consisting of a plastic bucket inserted into a plexiglass cylinder, with a manometer attached to the lid. The kimberlite sample was placed in the cylinder before the little bucket was filled with 5ml concentrated HCl and the lid screwed on tightly prior to manual shaking. A reading was taken from the manometer, once the pressure gauge had stabilised, which typically took about 2 minutes. The pressure reading was used to determine the proportion of $CaCO_3$ in the kimberlite by calibration against a pure 1g $CaCO_3$ sample. The CO_2 concentration of the kimberlite was then calculated by simple stoichiometry and subsequently

the H_2O^+ concentration of the kimberlite, was determined by subtraction of the CO_2 concentration (%) from the loss on ignition (%).

Typically 3-5g of kimberlite was required to obtain a suitable pressure reading and the karbonat bombe was thoroughly washed and dried after the analysis of every sample. Calibration with pure $CaCO_3$ was carried out after every fifth sample in order to check the consistency of the bombe. New Elands kimberlite samples *NE K6* and *NE K10*, as well as Droogfontein kimberlite samples *K19/3, K19/5* and *K19/10* had insufficient sample powder to obtain a CO_2 concentration. Birch (1981) reported precision values of 2% where $CaCO_3$ is greater than 5%, and less than 4% precision at lower concentrations. Where there is greater than 10% $CaCO_3$ present in the sample, the accuracy is 2% relative (Birch, 1981).

Table D.3: Average ICP-MS total procedural blank concentrations (TPB), as well as the average concentration and relative standard deviation (RSD) obtained for the international rock standard *BHVO-1* in this study. The current in-house (UCT) average for *BHVO-1*, as well as the recommended values by Govindaraju (1994), with more recent recommended values for selected elements given in parenthesis (Chazey III *et al.*, 2003), are also shown for comparison.

		BHVO-1				
	TPB	This study		UCT		Recomm.
	n=9 (ppb)	(ppm) n=9	% RSD	UCT (ppm)	% RSD	(ppm)
Sc	76.7	29.7	2.08	30.2	3.74	31.8
Ni	42.2	121	0.86	117	4.65	121
Rb	21.3	9.19	2.90	9.54	3.40	11 (9.3)
Sr	183	401	2.61	400	3.10	403
Y	8.65	23.8	1.30	24.4	2.58	27.6 (24.4)
Zr	97.1	180	1.79	172	3.56	179 (172)
Nb	81.9	19.5	1.74	19.0	3.91	19
Ba	279	136	0.98	130	2.22	139
La	4.34	15.0	1.30	15.0	2.21	15.8
Ce	6.24	38.3	0.96	37.7	1.68	39
Pr	2.69	5.12	1.49	5.23	2.38	5.7
Nd	10.7	25.2	1.17	24.5	1.85	25.2
Sm	3.79	6.00	1.75	5.90	2.82	6.2
Eu	1.95	1.91	1.33	2.00	2.71	2.06
Gd	4.51	6.04	1.11	6.02	3.35	6.4
Tb	1.03	0.85	1.15	0.88	3.07	0.96
Dy	3.93	5.02	0.81	5.01	2.33	5.2
Ho	0.98	0.90	0.81	0.92	2.68	0.99
Er	3.10	2.37	1.00	2.37	2.51	2.4
Tm	1.00	0.31	1.20	0.31	2.97	0.33
Yb	2.96	1.87	1.35	1.85	2.51	2.02
Lu	1.03	0.25	0.96	0.26	2.96	0.29
Hf	6.68	4.09	0.95	4.11	3.99	4.38
Ta	104	1.32	3.49	1.18	6.81	1.23
Pb	364	1.99	1.30	2.17	5.92	2.6 (2.2)
Th	4.45	1.19	1.23	1.25	2.61	1.08 (1.22)
U	1.16	0.42	1.03	0.45	3.52	0.42

D.3 Inductively coupled plasma - mass spectrometry (ICP-MS)

Solution ICP-MS trace element analyses were conducted at the University of Cape Town on a Perkin-Elmer ELAN 6000 ICP-MS for the analysis of some 26 trace elements that included the REE. Artificial multi-element standards were used for external calibration and kimberlite solutions were spiked with internal standards. Trace element analyses were done in triplicate and each analysis consisted of 3 replicates of 20 sweeps, with typical peak counting times between 35ms and 50ms. Data was collected using a pulse detector, except for very high intensity signals for which an analogue detected was used instead (e.g. Sr, Zr). Repeat analyses of the international standard *BHV0-1* gave a relative standard deviation (RSD) of better than 3%, except for Ta that had a RSD of 3.5% (Table D.3). The recommended *BHVO-1* values from Govindaraju (1994), this study and the current in-house UCT average are generally comparable. (Table D.3). Total procedural blanks were run with every batch analysed and for the REE, blanks were generally less than 10ppb. Total procedural blanks for the large ion lithophile elements and Pb did however, have higher concentrations (e.g. TPB for Ba is 279ppb; Table D.3).

D.4 Thermal ionisation mass spectrometry (TIMS)

Kimberlite samples were analysed for Sr and Nd isotopes on a VG Sector 7-collector TIMS at the University of Cape Town, run in multi-dynamic mode. The routine isotope measurement procedure consisted of the analysis of 10 blocks, each consisting of 20 isotope analyses. $^{87}Sr/^{88}Sr$ isotope ratios were normalised against a $^{86}Sr/^{88}Sr$ ratio of 0.1194 and $^{143}Nd/^{144}Nd$, against a $^{146}Nd/^{144}Nd$ ratio of 0.721. International standard *NBS 987* was run for $^{87}Sr/^{86}Sr$ isotope reference and the average value obtained was 0.710260 ±17 (2σ), that falls within error of the current UCT in-house value (0.710253). Similarly, the average $^{143}Nd/^{144}Nd$ ratio measured for La Jolla was 0.511829 ±10 (2σ) that compares favourably with the UCT in-house ratio (0.511842). For all other measured isotope ratios two-sigma values are less than 20 (Table 6.1; 6.2). Duplicate isotope analyses were performed for Newlands kimberlite sample *JJG 24* and the repeat $^{87}Sr/^{86}Sr$ analyses, 0.708155 and 0.708161 ±11 are within the two-sigma standard deviation of each other.

At the beginning of the Nd isotope analysis for each sample, a test was carried out in order to check the quality of the column separation procedure. The simple test constituted measurement of the intensity of all the Nd isotopes as well the ^{147}Sm and ^{138}Ba isotopes. It was subsequently discovered that some kimberlite samples had a significant ^{138}Ba peak (up to 10V) and it was therefore likely that the ^{130}Ba + ^{16}O oxide would cause isobaric interference on ^{146}Nd. The initial solution to this isobaric interference effect was to allow the ^{130}Ba +^{16}O oxide to burn off the filament, utilising the good ionisation potential of Ba and when the ^{138}Ba isotope intensity was low enough (< 300mV), measurement of $^{143}Nd/^{144}Nd$ was initiated. However, this first order solution proved fallible and so the sample preparation was repeated for those kimberlite samples that contained a significant ^{138}Ba peak and tended to have greater than 1000ppm Ba. A refined analytical technique was devised for the kimberlite sample preparation where only those columns that showed efficient separation for Ba were

used and the size of the REE fraction collected from the primary column was reduced from 6ml to 5ml, in order to avoid sampling the tail of the eluted Ba peak. The repeat Nd analyses for these kimberlite samples showed that the intensity of the ^{138}Ba isotope was nominal and so routine $^{143}Nd/^{144}Nd$ isotope analysis continued.